

# **Adaptation Techniques in Optical Wireless Communications**

Mohammed Thamer Alresheedi

Submitted in accordance with the requirements for the  
degree of Doctor of Philosophy

University of Leeds

School of Electronic and Electrical Engineering

December 2013

The candidate confirms that the work submitted is his/her own, except where work which has formed part of jointly authored publications has been included. The contribution of the candidate and the other authors to this work has been explicitly indicated below. The candidate confirms that appropriate credit has been given within the thesis where reference has been made to the work of others.

The work in Chapter 4 of the thesis has appeared in publications as follows:

1. M. T. Alresheedi and J. M. H. Elmirghani, "Line Strip Multibeam Spot Diffusing Optical Wireless System employing Beam Delay and Power Adaptation with Angle Diversity Detection," International wireless communication and Mobile computing IEEE Conference. IWCMC'11, July 2011.

My contribution: literature review, developed the new idea of beam delay adaptation in indoor OW systems and proposed new system of beam delay and power adaptation with line strip multi-spot system (BDPA-LSMS), designed three branched angle diversity receiver and simulated system at low data rate (30 Mb/s), produced results of the proposed systems in Matlab and compared them with baseline configurations: multi-spot LSMS and CDS system.

Professor Elmirghani: Originator of the idea of beam delay adaptation algorithm, developed receiver structure design and helped with the preparation of paper.

2. M. T. Alresheedi and J. M. H. Elmirghani, "Adaptive Multibeam Spot Diffusing Optical Wireless System with Imaging receivers," IEEE International on Transparent Optical Networks (ICTON'11), July 2011.

My contribution: literature review, developed and enhanced the idea of beam delay and power adaptation with new custom imaging receiver design (200 pixels) and studied the impact of transmitter and receiver mobility. The simulation results built in Matlab and compared with basic OW systems (CDS and LSMS) when all configurations integrated with new imaging receiver.

Professor Elmirghani: developed the idea of beam delay and power algorithm, developed the new receiver design and helped with the preparation of paper.

3. M. T. Alresheedi and J. M. H. Elmirghani, "High-speed wireless infrared links with an adaptive multibeam clustering method and angle diversity detection," IEEE International on Transparent Optical Networks (ICTON'12), July 2012.

My contribution: literature review, extended and developed the adaptive beam delay and power clustering method where system employed three adaptive clusters in an indoor environment. Designed and optimised seven angle diversity receivers to overcome the impact of receiver mobility and enabled system to operate at high data rates of 2.5 Gb/s and 5Gb/s. The simulation results built in Matlab and compared with basic adaptive BDPA-LSMS and LSMS and CDS systems.

Professor Elmirghani: Developed the algorithm of new adaptive clustering techniques, developed new receiver structure and helped with the preparation of paper.

The work in Chapter 5 of the thesis has appeared in publications as follows:

4. M. T. Alresheedi and Jaafar M.H Elmirghani, "Mobile Optical Wireless Systems Employing Beam Angle and Power Adaptation with Diversity Receivers," IEEE International Conference on Wireless and Optical Communications Networks (WOCN'10), Colombo, September, 2010.

My contribution: literature review, introduced the idea of beam angle and power adaptation with three branched angle diversity receiver at low data rate (30 Mb/s), simulation of the proposed idea in Matlab and produced results and compared them with baseline configurations: multi-spot LSMS and CDS system.

Professor Elmirghani: Originator of the idea beam angle and power adaptation algorithm, developed the receiver design and helped with the preparation of paper.

5. M. T. Alresheedi and Jaafar M.H Elmirghani, "Angle and Power Adaptation in 10 Gbit/s Multibeam Mobile Optical Wireless Systems with Angle Diversity Detection," 15th IEEE International Conference on Optical Network Design and Modelling (ONDM'11), Bologna, February, 2011.

My contribution: literature review, enhanced and extended the idea of beam angle and power adaptation with three branched angle diversity receivers in order to operate at high data rates 5 Gb/s and 10 Gb/s, modelled system, simulation of proposed angle and power adaptation and performance evaluation.

Professor Elmirghani: Developed and enhanced the idea of beam angle and power adaptation with three branched angle diversity receivers, helped with development of system models and the preparation of paper.

6. M. T. Alresheedi and J. M. H. Elmirghani, "Performance Evaluation of 5 Gbit/s and 10 Gbit/s Mobile Optical Wireless Systems Employing Beam

Angle and Power Adaptation with Diversity Receivers,” Selected Areas in Communications, IEEE Journal on, vol. 29, No. 6, pp. 1328-1340, June 2011.

My contribution: literature review, improved and extended the idea of beam angle and power adaptation with angle diversity receivers where each detector associated with high concentrator gain, model APA-LSMS system, PA-LSMS, LSMS and CDS systems, simulation of the proposed system APA-LSMS at high data rates (5 Gb/s and 10 Gb/s) and enabled the system with full mobility, at a lower transmit power in an environment where eye safety is important and studied the impact of ISI of the proposed system when the third order reflection is considered.

Professor Elmirghani: Developed and enhanced the idea of beam angle and power adaptation associated with high non-imaging concentrator gains in order to support high transmission rates at low power where eye safety is important, developed system models and helped with the preparation of paper.

The work in Chapter 6 of the thesis has appeared in publications as follows:

7. M. T. Alresheedi and J. M. H. Elmirghani, “Adaptive 10 Gbit/s Mobile Optical Wireless Systems Employing Beam Delay, Angle and Power Adaptation with Imaging Receivers” IEEE GLOBECOM , December, 2011.

My contribution: literature review, developed the new idea of beam delay adaptation with angle and power adaptation algorithm, modelled new systems, designed custom imaging receiver, and studied the system with full mobility. Produced the results in Matlab and compared them when the system employed only angle and power adaptation.

Professor Elmirghani: Originator of the idea of beam delay adaptation, developed the new adaptation algorithms, new imaging receiver design and helped with the preparation of paper.

8. M. T. Alresheedi and J. M. H. Elmirghani, "10 Gbit/s Indoor Optical Wireless Systems Employing Beam Delay, Angle and Power Adaptation Methods with Imaging Detection" IEEE Journal of Lightwave Technology, vol. 30, No. 12, pp. 1843-1856, 2012.

My contribution: literature review, enhanced and developed the idea of beam delay adaptation with angle and power adaptation algorithm, modified the imaging receiver to enhanced link budget in order to support high data rates 10 Gb/s and well beyond (such as 12.5 Gb/s) under eye safety regulations, modelled BDAPA-LSMS system coupled with new imaging receiver, and developed the simulation to address new techniques and compared the results with previous adaptive systems (BDPA-LSMS, LSMS and CDS).

Professor Elmirghani: developed the idea of beam delay adaptation with angle and power adaptation to support high transmission rate of 12.5 Gb/s, developed the new imaging receiver and helped with the preparation of paper.

The work in Chapter 7 of the thesis has appeared in publications as follows:

9. M.T. Alresheedi and J. M. H. Elmirghani "High-Speed Indoor Optical Wireless Links Employing Fast Angle and Power Adaptive Computer-Generated Holograms with Imaging Receivers," to be submitted to IEEE Journal of Optical Communications and Networking.

My contribution: literature review, developed the idea new of fast angle and power adaptive Computer-Generated Holograms with imaging receivers to reduce design complexity and enhance system performance and enable system to operate at high data rates: 1.25 Gb/s, 2.5 Gb/s and 5 Gb/s. Devolved new

search algorithm based on D&C in order to reduce the time needed to select the best pre-calculated hologram. Produced results and compared them with original adaptive systems.

Professor Elmirghani: Originator of the idea of adaptive Computer-Generated Holograms, developed the system models, fast search algorithms and helped with the preparation of paper.

This copy has been supplied on the understanding that it is copyright material and that no quotation from the thesis may be published without proper acknowledgement.

*To:*

*My parents, brothers, sisters, my wife and my son*

# Acknowledgements

First and foremost, I thank Allah (subhana wa taala) for endowing me with health, patience, and knowledge to complete this work. This thesis presented here could not have been achieved without the help and encouragement of my supervisor, Professor Jaafar Elmirghani. I am grateful for his teaching, guidance and friendship. His emphasis on securing a good balance between theory and practice has been a guideline through my research. He has offered me invaluable opportunities and continuously kept faith in me. I feel very honoured to have had the chance to work with him. I would like to thank all my colleagues in the Communication Systems and Networks group at University of Leeds. I would also like to thank King Saud University for funding my studies. Finally, I would like to express my deepest gratitude to my parents, my brothers, my sisters, my wife and my son, for their love, patience, encouragement and continued prayers.

# Abstract

The need for high-speed local area networks to meet the recent developments in multimedia and video transmission applications has recently focused interest on optical wireless communication. Optical wireless systems boast some advantages over radio frequency (RF) systems, including a large unregulated spectrum, freedom from fading, confidentiality and immunity against interference from electrical devices. They can satisfy the dual need for mobility and broadband networking. However, optical wireless links are not without flaws. They are affected by background noise (artificial and natural light sources) and suffer from multipath dispersion. The former can degrade the signal-to-noise ratio, while the latter restricts the maximum transmission rate available.

The aim of this thesis is to investigate a number of techniques to overcome these drawbacks and design a robust high-speed indoor optical wireless system with full mobility. Beam delay and power adaptation in a multi-spot diffusing system is proposed in order to increase the received optical signal, reduce the delay spread and enable the system to operate at higher data rates. The thesis proposes employing angle diversity receivers and imaging diversity receivers as in order to reduce background noise components. Moreover, the work introduces and designs a high-speed fully adaptive optical wireless system that employs beam delay, angle and power adaptation in a multi-spot diffusing configuration and investigates the robustness of the link design in a realistic indoor office. Furthermore, a new adaptive optical wireless system based on a finite vocabulary of stored holograms is introduced. This method can effectively optimise the spots' locations and reduce the design complexity of an adaptive optical wireless system. A fast adaptation approach based on a divide-and-conquer methodology is proposed and integrated with the system to reduce the time required to identify the optimum hologram. The trade-off between

complexity and performance enhancement of the adaptive finite holograms methods compared with the original beam power and angle adaptation is investigated.

# Contents

<b>Acknowledgements</b> .....	<b>i</b>
<b>Abstract</b> .....	<b>ii</b>
<b>List of Figures</b> .....	<b>x</b>
<b>List of Tables</b> .....	<b>xviii</b>
<b>List of Abbreviations</b> .....	<b>xix</b>
<b>List of Symbols</b> .....	<b>xxii</b>
<b>1 Introduction</b> .....	<b>7</b>
1.1 The Advent of Optical Wireless Communications.....	7
1.2 Optical Wireless for Short Range Communication .....	9
1.3 Motivation and Research Objectives .....	11
1.4 Research Contributions.....	12
1.5 Overview of the Thesis.....	16
<b>2 Review of Optical Wireless Systems</b> .....	<b>18</b>
2.1 Introduction .....	18
2.2 Comparison between Infrared and Radio Media .....	19
2.3 An Indoor Optical Wireless (OW) System .....	21
2.3.1 Transmitter components.....	22
2.3.2 Propagation Medium and OW Transmission Links Design .....	23

2.3.3	Receiver components .....	26
2.4	Design Challenges of Indoor OW system.....	35
2.4.1	Optical Safety Regulations .....	35
2.4.2	Ambient Light .....	37
2.4.3	Multipath dispersion .....	41
2.4.4	Photodetector High Capacitance.....	43
2.5	Signal Modulation Techniques .....	44
2.5.1	IM/DD Channel.....	45
2.5.2	On-Off Keying (OOK) .....	45
2.5.3	Pulse Modulation.....	46
2.5.4	Subcarrier Modulation (SM) .....	49
2.6	Angle Diversity Receiver .....	49
2.7	Standards for Indoor OW Systems.....	50
2.8	Summary .....	51
<b>3</b>	<b>Channel Modelling of an Indoor Optical Wireless (OW) System .....</b>	<b>52</b>
3.1	Introduction .....	52
3.2	Indoor OW Communication Channel.....	53
3.3	Multipath Propagation Model.....	54
3.3.1	Ray-tracing implementation for Calculations of the Received Optical Power.....	56
3.4	Impulse Response.....	63
3.5	Delay Spread .....	64

3.6 Ambient Light Calculations.....	65
3.7 Calculations of Signal to Noise Ratio (SNR) .....	68
3.8 Simulation Package.....	71
3.9 Simulation Results.....	73
3.9.1 CDS with Single Wide FOV Receiver.....	73
3.9.2 LSMS with Single Wide FOV Receiver .....	75
3.9.3 LSMS with Angle Diversity Receiver .....	77
3.10 Summary.....	88
<b>4 Beam Delay Adaptation in Indoor Optical Wireless Systems .....</b>	<b>90</b>
4.1 Introduction .....	90
4.2 Mobile Beam Delay and Power Adaptive LSMS (BDPA-LSMS) .....	92
4.3 System Description .....	96
4.4 Performance Evaluation of BDPA-LSMS with Three-branched Angle Diversity Receptions .....	98
4.4.1 Impulse Response along with 3dB channel Bandwidth.....	98
4.4.2 Delay Spread Analysis .....	100
4.4.3 SNR Results.....	103
4.5 Mobile BDPA-LSMS coupled with seven branched angle diversity receiver.....	106
4.6 Mobile Beam Delay and Power Adaptive Multi-Beam Clustering Method (BDPA-BCM) .....	110
4.6.1 Performance assessment of BDPA-BCM.....	112
4.7 Imaging Receiver Design .....	123

4.8	Impulse Response and Delay Spread .....	127
4.9	SNR Analysis .....	130
4.9.1	SNR Results of Non-imaging and Imaging CDS diffuse Setups... ..	133
4.9.2	SNR Results of Imaging Non-adaptive LSMS and Adaptive BDPA-LSMS Configurations .....	134
4.10	Beam Delay and Power Multiple Adaptive Beam Clustering Method (BDPMA-BCM) .....	136
4.10.1	Performance Analysis and Simulation Results.....	139
4.11	Summary.....	145
<b>5</b>	<b>Performance Evaluation of 5 Gb/s and 10 Gb/s Mobile Optical Wireless Systems Employing Beam Angle and Power Adaptation with Diversity Receivers .....</b>	<b>147</b>
5.1	Introduction .....	147
5.2	Mobile Angle and Power Adaptive LSMS Configuration (APA-LSMS) .....	149
5.3	Angle Diversity Receiver Structure.....	154
5.4	Optical Wireless System Model.....	155
5.5	Performance Evaluation .....	156
5.5.1	OW 3-dB Channel Bandwidth .....	162
5.5.2	SNR Results of the APA-LSMS system .....	166
5.6	Summary.....	171
<b>6</b>	<b>Mobile Optical Wireless Systems Employing Beam Delay, Power and Angle Adaptation Methods with Imaging Detection in a Realistic Indoor Environment .....</b>	<b>173</b>
6.1	Introduction .....	173

6.2	Simulation set-up.....	174
6.3	Transmitter Configuration (BDAPA-LSMS) .....	175
6.4	Simulation Results.....	182
6.4.1	Delay Spread Distribution.....	182
6.4.2	Impulse response and 3-dB Channel bandwidth.....	184
6.4.3	SNR Results.....	188
6.5	Effect of Realistic Indoor Environment .....	190
6.6	High data rate OW communications challenges and possibilities .....	197
6.7	Summary.....	197
<b>7</b>	<b>Indoor Optical Wireless Links Employing Fast Angle and Power Adaptive Finite Vocabulary of Holograms .....</b>	<b>199</b>
7.1	Introduction .....	199
7.2	Simulation set-up.....	201
7.3	Transmitter Structures.....	202
7.3.1	Diffuse CDS and Non-adaptive LSMS Configurations .....	202
7.3.2	Adaptive Holograms Configurations.....	204
7.4	Delay Spread Assessment.....	217
7.5	SNR Results.....	219
7.6	Finite Adaptive Holograms versus Original Beam Power and Angle Adaptations.....	222
7.6.1	High-speed Mobile OW communication systems .....	228
7.7	FAPA-Holograms with 9-Angle diversity receivers .....	229

7.7.1 Delay Spread Results .....	231
7.7.2 SNR Results.....	233
7.8 Effect of Shadowing and Realistic Indoor Office on the Proposed FAPA-Holograms .....	235
7.9 Summary.....	238
<b>8 Conclusions and Future Work.....</b>	<b>242</b>
8.1 Conclusions of Research Work .....	242
8.2 Areas of Further Investigation .....	247
<b>References.....</b>	<b>249</b>

# List of Figures

Figure 1.1: OW-LAN using ceiling mounted access points to connect optical wireless devices. ....	10
Figure 2.1: A Basic Optical Wireless Terminal Block Diagram. ....	22
Figure 2.2: The main categories of OW: (a) LOS systems (b) non-LOS systems [16]: .....	25
Figure 2.3:Responsivity of a normal silicon PIN photodiode, a typical high-pass optical filter transmission and general responsivity and transmission [16], [37]. ....	28
Figure 2.4:The averaged transmission polarization of an optical band-pass filter for different incident angle $\theta$ [37], [63]. ....	28
Figure 2.5: Non-directional hemispherical lens that employs (a) planar and (b) hemispherical optical filter. ....	31
Figure 2.6: Compound parabolic concentrator (CPC) with planar filter. ....	32
Figure 2.7: Spectral power densities of natural and artificial noise sources [16]. ....	38
Figure 2.8: Basic NRZ-OOK and RZ-OOK signals [35]. ....	46
Figure 2.9: Possible waveforms of 4-PPM [16]. ....	47
Figure 2.10: Comparison of transmitted waveforms for (a) 4-PPM, and (b) 4-differential pulse-position modulation (4-DPPM) [16]. ....	48
Figure 3.1: Block diagram of IM/DD OW system. ....	54
Figure 3.2: Ray tracing set up for first and second order reflections in a diffuse link. ....	57
Figure 3.3: Calculations of direct transmitting and receiving angles. ....	58
Figure 3.4: Ray tracing for first order reflection calculation. ....	60
Figure 3.6: Modelling of the ambient light. ....	66

Figure 3.7: Eight spotlights distribution.....	68
Figure 3.8: CDS with non-imaging wide FOV receiver. ....	74
Figure 3.9: Impulse response results for CDS when the transmitter is stationary in the middle of the room and the receiver moves to two different positions (a) (1m, 1m, 1m) and (b) (2m, 4m, 1m). ....	74
Figure 3.10: OW communication system with LSMS transmitter and wide FOV receiver. ....	76
Figure 3.11: Impulse response of CDS and LSMS when the transmitter is placed at (2m, 4m, 1m) and a wide FOV receiver is placed in the room corner. ....	77
Figure 3.12: The delay spread of CDS and LSMS with a wide FOV receiver, when the transmitter is at (2m, 4m, 1m) and the receiver moves along the y axis at constant $x=1m$ . ....	78
Figure 3.13: (a) Physical structure of an angle diversity receiver, (b) single element receiver (non-imaging) that employs a concentrator coupled with a single detector. ....	80
Figure 3.14: Impulse response of the CDS and LSMS both with wide FOV receivers, and LSMS with an angle diversity receiver, transmitter at (2m, 4m, 1m), all receivers are in the corner of the room on the CP. ....	81
Figure 3.15: delay spread of CDS and LSMS with a wide FOV receiver, LSMS with angle diversity receiver, when transmitter at (2m, 4m, 1m) and the receiver moves along y axis at constant $x=1m$ . ....	82
Figure 3.16: Transmitter of an LSMS configuration placed at the room centre, where a line of spots is formed on the ceiling (b) diffusing spots on the side wall (x-z wall). ....	84
Figure 3.17: The SNR of the CDS and LSMS with wide FOV, and LSMS with angle diversity receiver when the transmitter is placed at (a) (2m, 4m, 1m) and (b) (2m, 7m, 1m) while the receiver moves along the line $x=1m$ . ....	87
Figure 4.1: Flowchart for the beam delay and beam power adaptation algorithm. ....	95
Figure 4.2: (a) Impulse response and (b) Frequency response of CDS, LSMS and BDPA-LSMS systems when the transmitter is positioned in the middle of the room and the receiver is positioned in the corner (1m, 1m, 1m). ....	102

Figure 4.3: 3-dB channel bandwidth of four arrangements: CDS, LSMS, beam power adaptation only with LSMS along with BDPA-LSMS when the transmitter is positioned at (2m, 4m, 1m) with the receiver moving along the x=1m line. ....	102
Figure 4.4: Delay spread of three arrangements: CDS, LSMS and BDPA-LSMS when the transmitter is positioned at (2m, 4m, 1m) and the receiver moves along the x=1 line. ....	103
Figure 4.5: OW CDS, LSMS along with BDPA-LSMS systems in conjugation with three angle diversity receivers, when the transmitter is located at: (a) (2m, 4m, 1m) , (b) (2m, 7m, 1m) and (c) (1m, 1m, 1m) and the receiver moves along the x=1 line in (a) and (b) and moves along the x=2m line in (c). ....	104
Figure 4.6: Spots distribution in mobile BDPA-LSMS when the transmitter is located in two locations: (a) (2m, 4m, 1m) and (b) (2m, 7m, 1m). ....	105
Figure 4.7: Physical arrangement of angle diversity detector with seven branches. ....	107
Figure 4.8: SNR of mobile diffuse CDS, multi-spot LSMS and adaptive BDPA-LSMS at different transmitter locations while the receiver moves along the line (a) x=1 and (b) x=2m on the CP. ....	109
Figure 4.9: Mobile BDPA-BCM system (a) transmitter in the middle of the room (b) transmitter near the room corner (1m, 1m, 1m). ....	112
Figure 4.10: Impulse response of the four arrangements: CDS, LSMS, BDPA-LSMS along with BDPA-BCM, with the transmitter positioned at (2m, 7m, 1m). ....	115
Figure 4.11: Delay spread of four arrangements: CDS, LSMS, BDPA-LSMS and BDPA-BCM with the emitter positioned at (2m, 7m, 1m) and (1m, 1m, 1m) while the receiver moves along the x=1m and x=2 lines. ....	117
Figure 4.12: SNR for OW CDS, LSMS, BDPA-LSMS and BDPA-BCM at 50Mbit/s, when the transmitter is positioned at (a) (2m, 4m, 1m) (b) (2m, 7m, 1m) and (c) (1m, 1m, 1m), while the receiver moves along the lines x=1m and x=2m lines. ....	119
Figure 4.13: Power penalty of BDPA-BCM when the photodetector collection area is reduced from 1 cm <sup>2</sup> to 5 mm <sup>2</sup> . ....	120
Figure 4.14: The SNR of BDPA-BCM and Beam Power adaptation BCM configurations at 2.5 Gb/s and 5 Gb/s. ....	122

Figure 4.15: Physical configuration of the imaging receiver. ....	124
Figure 4.16: The angles of reception and reception areas of the imaging receiver (200 pixels) when (a) the receiver is placed at the reference point at (2m, 4m, 1m) and (b) when it moves near to the room corner, to (1m, 1m, 1m). .....	126
Figure 4.17: Impulse response of (a) pure CDS diffuse, (b) non-adaptive multi-spot LSMS and (c) adaptive multi-spot BDPA-LSMS combined with imaging receivers when the emitter is positioned at (2m, 4m, 1m) and the receiver is moved near to the corner, at (1m, 1m, 1m). ....	128
Figure 4.18: Delay spread of the single detector and imaging CDS systems, non-adaptive LSMS and adaptive BDPA-LSMS multi-spot configurations combined imaging receivers, when the transmitter is positioned at (2m, 4m, 1m) and the receiver moves along the $x=1m$ line. ....	129
Figure 4.19: The SNR of CDS with non-imaging receiver (wide FOV receiver) and SNR of CDS with 200-pixel imaging receiver using SC and MRC when the diffuse transmitter is positioned at (a) (2m, 4m, 1m), (b) (2m, 7m, 1m) and the receiver moves along the $x=1m$ line. ....	135
Figure 4.20: the SNR of the LSMS and BDPA-LSMS with an imaging receiver when the system is positioned at (a) (2m, 4m, 1m) and (b) (2m, 7m, 1m), and the receiver moves along the $x=1m$ line. ....	137
Figure 4.21: BDPMA-BCM arrangement when the system is positioned in the middle of the room at (2m, 4m, 1m). ....	139
Figure 4.22: Delay spread of five configurations (a) CDS imaging and non-imaging receiver (b) LSMS, BDPA-LSMS and BDPMA-BCM, when the transmitter is placed in corner of the room at (1m, 7m, 1m) and the receiver moves along $x=2m$ line. ....	142
Figure 4.23: SNR of CDS, LSMS, BDPA-LSMS and BDPMA-BCM at 30 Mb/s when the transmitter is placed at (2m, 1m, 1m) while the receiver moves along the line $x=1m$ . ....	143
Figure 4.24: SNR of proposed 2.5 Gb/s and 5 Gb/s BDPMA-BCM compared with 5 Gb/s BDPA-LSMS system, when the transmitter is near the room edge transmitting 1W while the receiver moves along the $y$ -axis at $x=1m$ . ....	144
Figure 5.1: The APA-LSMS OW communication system. ....	150

Figure 5.2: The block diagram of our APA-LSMS combined with three branch angle diversity receiver.....	152
Figure 5.3: The SNR Penalty of our proposed system when the receiver moves along the y axis away from the previously optimally placed spots at (2m, 1m, 1m) and the transmitter does not update the spot locations.....	152
Figure 5.4: Impulse response of the three configurations: CDS, LSMS and PA-LSMS when the transmitter is placed at (2m, 4m, 1m) and the receiver is at (1m, 1m, 1m).....	159
Figure 5.5: Impulse response of two configurations: PA-LSMS and APA-LSMS at a transmitter-receiver horizontal separation of 6m. ....	159
Figure 5.6: Delay spread of four configurations: CDS, LSMS, PA-LSMS and APA-LSMS when the transmitter is placed at (a) (2m, 4m, 1m) and (2m, 7m, 1m) while the receiver moves along the x=1m line.....	161
Figure 5.7: Delay spread of APA-LSMS using different time bins: 0.5ns and 0.01ns. ....	162
Figure 5.8: 3-dB channel bandwidth of four configurations: CDS, LSMS, PA-LSMS and APA-LSMS when the transmitter is placed at (2m, 4m, 1m) and the receiver moves along the x=1m line.....	164
Figure 5.9: Impulse response and frequency response of CDS and APA-LSMS. ....	165
Figure 5.10: OW CDS, LSMS, PA-LSMS and APA-LSMS systems SNR at 30 Mb/s, when the transmitter is placed at (2m, 4m, 1m) and the receiver moves along the x=1m line, with a total transmit power of 1W. ....	167
Figure 5.11: OW CDS, LSMS, PA-LSMS and APA-LSMS systems SNR at 30 Mb/s, when the transmitter-receiver separation is 6m, with a total transmit power of 1 W. ....	168
Figure 5.12: OW PA-LSMS and APA-LSMS systems SNR at 5 Gb/s and 10 Gb/s, with two detection areas (0.05 cm <sup>2</sup> and 0.01cm <sup>2</sup> ), when the transmitter-receiver separation is 6m, with a total transmit power of 1 W. ....	170
Figure 5.13: The SNR of our proposed system operating at 30 Mb/s, 5 Gb/s and 10 Gb/s, with a total transmit power of 60 mW and detection area of 0.05 cm <sup>2</sup> for high data rates and 0.8 cm <sup>2</sup> for 30 Mb/s. ....	171

Figure 6.1: OW communication system architecture for our new fully adaptive BDAPA-LSMS with imaging receiver.....	178
Figure 6.2: Block diagram of the beam delay, angle and power adaptation algorithm. ....	180
Figure 6.3: Delay spread of four configurations: CDS, LSMS, APA-LSMS and BDAPA-LSMS when the transmitter is placed at (2m, 4m, 1m) and the receiver moves along the x=1m line.....	183
Figure 6.4: Delay spread of APA-LSMS using different time bins: 0.5ns and 0.01ns, when the transmitter is placed at (2m, 4m, 1m) and the receiver moves along the x=1m line.....	184
Figure 6.5: 3-dB channel bandwidth of three configurations: CDS, LSMS, BDAPA-LSMS when the transmitter is placed at (2m, 4m, 1m) and the receiver moves along the x=1m line.....	186
Figure 6.6: Impulse response and frequency response of CDS and BDAPA-LSMS when the transmitter is placed at (2m, 4m, 1m) and the receiver is at the corner of the room (1m, 1m, 1m).....	187
Figure 6.7: OW CDS, LSMS and BDAPA-LSMS systems SNR with an imaging receiver at 30 Mb/s.....	189
Figure 6.8: Schematic representation of a realistic indoor office environment with the potential of beam interruption (shadowing) .....	191
Figure 6.9: SNR of CDS, LSMS and BDAPA-LSMS systems at 30 Mbit/s, in a typical indoor office, when the transmitter is placed at (1m, 1m, 1m) and the imaging receiver moves along the x=2m line. ....	193
Figure 6.10: SNR of beam power adaptation LSMS, BDPA-LSMS, APA-LSMS, and BDAPA-LSMS systems at 10 Gbit/s and 12.5 Gbit/s, when the transmitter is placed at (2m, 7m, 1m) and the receiver moves along the x=1m line.....	196
Figure 6.11: The SNR of our proposed system operating at 30Mbit/s, 10 Gbit/s and 12.5 Gbit/s, with a total transmit power of 80 mW. ....	196
Figure 7.1 : impulse response of (a) CDS with wide FOV receiver (b) CDS with imaging receiver (c) LSMS with imaging receiver, when transmitter is placed at (1m, 7m, 1m) and receiver is moved at (2m, 1m, 1m).....	203

Figure 7.2: Our proposed OW communication system with adaptive holograms when the transmitter is placed at (3m,3m,1m) and the receiver is at (1m,3m,1m). ..... 205

Figure 7.3: (a) the desired spots intensity in far field (b) hologram phase pattern and the reconstruction intensity in the far field at iterations 1, 5, 15 and 100 using simulated annealing optimisation. Different gray levels represent different phase levels ranging from 0 (black) to  $2\pi$  (white). ..... 210

Figure 7.4: Cost function vs. the number of iterations. .... 210

Figure 7.5: Impulse response of our proposed systems with 64 and 256 Holograms: (a) FAA-Holograms, (b) FPA-Holograms and (c) FAPA-Holograms with imaging receiver, when the transmitter is placed at (1m, 7m, 1m) and the receiver is at (2m, 1m, 1m) and (2m, 2m, 1m). ..... 215

Figure 7.6: Delay spread of four configurations : (a) CDS imaging and non-imaging receiver (b) LSMS, FAA-Holograms, FPA-Holograms and FAPA-Holograms, when the transmitter is placed at (1m, 7m, 1m) and the receiver moves along the  $x=2m$  line..... 218

Figure 7.7: SNR of OW CDS, LSMS, FPA-Holograms, FAA-Holograms and FAPA-Holograms with 256-Hologram at 30 Mb/s, when the transmitter is placed at (2m, 1m, 1m) and (1m, 7m, 1m) and the receiver moves along the  $x=1m$  and the  $x=2m$  lines. .... 221

Figure 7.8: The SNR and the delay spread of the adaptive finite holograms (FPA-Holograms, FAA-Holograms and FAPA-Holograms) versus the original beam power and angle adaptive systems (PA-LSMS, AA-LSMS and APA-LSMS) when the transmitters operate at 5 Gb/s. .... 226

Figure 7.9: The SNR of APA-LSMS; and of FAPA-Holograms designed for (4m× 8m ×3m) room but used on rooms of dimensions (a) (3m× 6m ×3m) and (b) (5m×10m ×3m) when the transmitters operate at 5 Gb/s. .... 227

Figure 7.10: The SNR of our proposed FAPA-holograms system operating at 30 Mbit/s, 1.25 Gbit/s, 2.5 Gbit/s and 5 Gbit/s, with a total transmit power of 80 mW..... 229

Figure 7.11: Physical structure of 9-angle diversity receivers placed on top of octagon pyramidal faces. .... 232

Figure 7.12: Delay spread of four configurations : (a) CDS and LSMS (b) FAPA-Holograms and APA-LSMS with angle diversity receiver, when the transmitter is placed at (1m, 1m, 1m) and the receiver moves along  $x=2m$  line. .... 232

Figure 7.13: SNR of OW CDS, LSMS, FAPA-Holograms with 6400-Hologram at 50 Mb/s, when the transmitter is placed at (2m, 7m, 1m) and (1m, 1m, 1m) and the receiver moves along  $x=1m$  and  $x=2m$  lines. .... 234

Figure 7.14: SNR of CDS, LSMS, FAPA-Holograms with 6400-Hologram at 50 Mb/s, when the transmitter is placed at (1m, 1m, 1m) and (1m, 7m, 1m) and the receiver moves along  $x=2m$ . .... 237

Figure 7.15: The SNR of our proposed FAPA-holograms system operating at 2.5 Gb/s and 5 Gb/s, with a total transmit power of 80 mW. .... 238

# List of Tables

Table 2.1: Comparison between optical wireless and radio frequency systems for the indoor environment. ....	21
Table 3.1: Maximum and Minimum Delay spread, SNR and shot noise current of CDS, LSMS transmitter with wide FOV receiver as well as the LSMS coupled with a 3 detector angle diversity receiver. ....	86
Table 4.1: Simulation Parameters. ....	113
Table 4.2: Multiple Clusters, Delay and Power Adaptation Algorithm with Imaging Receivers.....	140
Table 4.3:Simulation Parameters. ....	141
Table 5.1: Simulation Parameters. ....	157
Table 5.2: Delay spread and 3 dB Channel Bandwidth of our proposed APA-LSMS. ....	166
Table 6.1: Simulation Parameters. ....	176
Table 6.2: SNR degradation of CDS imaging (MRC) and non-imaging systems in shadowed and unshadowed rooms compared with an empty room.....	193

# List of Abbreviations

AEL	Accessible Emission Limit
AM	Amplitude Modulation
AA-LSMS	Angle Adaptive Line Strip Multi-Spot System
APA-LSMS	Angle and Power Adaptive Line Strip Multi-spot diffusing System
APDs	Avalanche Photo-Diodes
BMDO	Ballistic Missile Defence Organisation
BDPA-BCM	Beam Delay and Power Adaptive Multi-spot Beam Clustering Method
BDPA-LSMS	Beam Delay and Power Adaptive Line Strip Multi-spot diffusing System
BDAPA-LSMS	Beam Delay, Angle and Power Adaptive with Line Strip Multi-spot diffusing System
BDPMA-BCM	Beam Delay and Power Multiple Adaptive Beam Clustering Method
BCM	Beam Clustering Method
BPSK	Binary Phase Shift Keying
BJT	Bipolar-Junction Transistor
BER	Bit-Error-Rate
CDMA	Code Division Multiple Access
CP	Communication Plane
CPC	Compound Parabolic Concentrator
CGH	Computer-Generated Hologram
CDS	Conventional Diffuse System
CHS	Conventional Hybrid System
DARPA	Defence Advanced Research Projected Agency
DPPM	Differential Pulse-Position Modulation
DSP	Digital Signal Processor

DBS	Direct Binary Search
DFT	Discrete Fourier Transform
DMT	Discrete Multi-tone Modulation
D&C	Divide-and-Conquer
EGC	Equal Gain Combining
FAA-Holograms	Fast Angle Adaptive Holograms
FAPA-Holograms	Fast Angle and Power Adaptive Holograms
FPA-Holograms	Fast Power Adaptive Holograms
FCC	Federal Communications Commission
FET	Field-Effect-Transistor
FOV	Field-of View
FLCB	Fluorescent Lamps with Conversion Ballast
FLEB	Fluorescent Lamps with Electronic Ballast
FEC	Forward Error Correction
FM	Frequency Modulation
hps	Half Power Semi-angle
IR	Infrared
IrDA	Infrared Data Association
IM/DD	Intensity Modulation and Direct Detection
IEC	International Electro-technical Commission
ISI	Inter Symbol Interference
LDs	Laser Diodes
LEDs	Light Emitting Diodes
LOS	Line-of-Sight
LSMS	Line Strip Multi-spot diffusing System
LC	Liquid Crystal
LANs	Local Area Networks
LPF	Low Pass Filter
MRC	Maximum Ratio Combining
MAC	Medium Access Control

MSM	Multiple Sub-carrier Modulation
NASA	National Aeronautics and Space Administration
NRZ-OOK	Non-Return to Zero
OfCom	Office of Communications
OOK	On-Off Keying
OW	Optical Wireless
OPPO	Output Plane Phase Optimisation
PCs	Personal Computers
PM	Phase Modulation
PAR 38	Philips PAR 38 Economic
PIN	Positive-Intrinsic Negative
PM	Pulse Modulation
PPM	Pulse Position Modulation
PA-LSMS	Power Adaptive Line Strip Multi-spot diffusing System
PFDR	Pyramidal Fly-eye Diversity Receiver
QoS	Quality of Service
RF	Radio Frequency
RZ-OOK	Return to Zero
rms	Root-Mean-Square
SC	Selection Combining
SNR	Signal-to-Noise Ratio
SM	Sub-carrier Modulation
VFIR	Very Fast Infrared
WLANs	Wireless local area networks

# List of Symbols

$\alpha$	Incident angle with respect to the transmitter's normal
$\alpha_1$	Angle between the first reflected ray $R2$ and the normal of the reflective element 1
$\alpha_2$	Angle between the second reflected ray $R3$ and the normal of the reflective element 2
$\alpha_i$	Transmission beam angles with respect to the transmitter normal
$A$	Photodetector area
$A'$	Exit area of the concentrator
$A_{eff}(\delta)$	Effective signal-collection area
$Az$	Azimuth angle
$\beta$	Angle between the incident ray from the transmitter and the reflective element's 1 normal
$\beta_1$	Angle between the first reflecting ray $R2$ and the normal of the reflective element 2
$BW$	Receiver Bandwidth
$c$	Speed of light
$C_d$	Detector capacitance
$C_g$	FET gate capacitance
$D$	Root mean square delay spread
$dA$	Reflection surface element area
$\delta$	Angle of incidence with respect to the receiver normal
$\Delta t$	Differential delays between beams
$dP$	Power radiated from the transmitter into a solid-angle element
$dP_{(1)}$	The received optical power by the first order reflection

$dP_{(2)}$	The received optical by the second order reflection
$d_y$	The horizontal distance separating the transmitter's normal and the diffusing spot alongside the y-axis
$El$	Elevation angle
$\eta$	Quantum efficiency of the device
$f''(x, y)$	The normalised desired object energy
$\gamma$	Angle between the normal of the reflective element 1 and the reflected ray
$\Gamma$	FET noise factor
$g(\delta)$	Concentrator gain
$g''_k(i, j)$	The scaled reconstruction energy of the $k^{\text{th}}$ iteration
$g_m$	FET transconductance
$h$	Reception area height
$h_p$	Planck's constant
$h_s$	Height of the spots
$I(t, Az, El)$	Received photocurrent at the output of the detector at a certain location
$k$	Boltzmann's constant
$K$	Total number of pixels in an imaging receiver
$\lambda$	Wavelength
$L_{Lamp}$	Total number of lamps
$M_t$	The total number of reflecting elements
$\mu$	Mean delay
$N$	Internal refractive index
$N_s$	Total number of spots
$n$	Mode number that determines the shape of the radiated beam
$\hat{n}_{e1}$	Normal of the reflective element 1

$\hat{n}_{e2}$	Normal of the reflective element 2
$\hat{n}_r$	Normal of the receiver
$\hat{n}_t$	Normal of the transmitter
$P_{bn}$	Total received background power at the receiver
$P_{Direct\ LOS}$	Direct received power
$P_e$	Probability of error
$P_{n_{direct}}$	Direct received noise power from the light source
$P_{n_{reflection1}}$	Received noise powers from the first reflecting elements
$P_{n_{reflection2}}$	Received noise powers from the second reflecting elements
$P_s$	Average transmitted optical power
$P_{s0}$	The power associated with logic 0
$P_{s1}$	The power associated with logic 1
$\psi_c$	Concentrator's FOV (semi-angle)
$P_{total\ received\ power}$	The total received optical power at the receiver
$q$	Electronic charge
$Q(.)$	Gaussian function
$R$	Photodetector responsivity
$R_d$	Direct link distance between the receiver and the transmitter
$R_f$	Feedback resistance
$R_1$	Distance between the reflective element 1 and the transmitter
$R_2$	Distance between the receiver and the reflective element 1
$R_3$	Distance between the receiver and the reflective element 2
$r_{e1}$	Position vector of the reflective element 1
$r_{e2}$	Position vector of the reflective element 2
$r_r$	Position vector of the receiver
$r_t$	Position vector of the transmitter

$\rho_1$	Reflection coefficient of the first reflective elements
$\rho_2$	Reflection coefficient of the second reflective elements
$\sigma_0$	Shot noise component associated with logic 0
$\sigma_1$	Shot noise component associated with logic 1
$\sigma_{bn}$	Background shot noise component
$\sigma_{pr}$	Preamplifier shot noise component
$\sigma_{total,i}^2$	Total noise variance
$t$	Absolute time
$t_i$	Time delay associated with the received optical power $P_{r_i}$
$T$	Absolute temperature
$T_c(\delta)$	Transmission factor of concentrator
$T_s(\delta)$	Transmission factor of filter
$x$	Distance between the receiver and the y-z wall
$x(t)$	Transmitted instantaneous optical power
$y$	Distance between the receiver x-z wall
$Y_t$	Horizontal separation distance along the y-axis between the transmitter's normal and the diffusing-spot at the new position

# 1 Introduction

## 1.1 The Advent of Optical Wireless Communications

Using light in communication, particularly to transmit information, is an old concept. In fact, optical wireless (OW) is more than a hundred years old, as semaphore, ship flags, smoke signals and fire beacons were the earliest stages of OW communication. In ancient times, holy days were announced using bonfires on the tops of mountains. Smoke and fire were used in America for communication between Indian tribes. Using mirrors to reflect sunlight is another early method of OW communication, an example being the heliograph, in which the movement of a mirror produces light flashes that can be used to send Morse code [1]. This method of communication was a simple but highly effective instrument for instantaneous optical communication over a distance of fifty miles or more, in the 19<sup>th</sup> Century. It was mostly used in the military and for forestry and survey work, and continued to be used until 1935 [1].

In 1880, Alexander Graham Bell and Sumner Trainer developed and patented the photophone, which was used to transmit sound on a beam of light [2]. It was based on electronic detection where a receiver that was comprised of a selenium crystal converted an optical signal into an electrical current. The photophone used the conductivity of selenium crystals, where the electrical conductivity depends on the intensity of the light it is exposed to [2]. The photophone is widely regarded as the precursor to modern fibre optics. Today, such technology transports more than 80% of the world's telecommunication traffic [1], with much higher data rates and with a quality of service (QoS) that exceeds the old methods [3].

The more recent history of OW communication in computer products includes calculators that use infrared (IR) links to transfer data and programmable

sequences of calculations between devices. The deployment of standard IR user models have led to many applications of IR, such as TV remote controls, payments systems, entertainment systems and Infrared Data Associated (IrDA) ports for watches, laptops, printer and mobiles.

Modern OW communication started in the 1960s when laser technologies were being developed. Back then, it was funded and promoted by government agencies: the Defence Advanced Research Projected Agency (DARPA), the Ballistic Missile Defence Organisation (BMDO) and the National Aeronautics and Space Administration (NASA). The ultimate goal was to establish communications between satellites orbiting Earth and submarines. Applications using OW communications are diverse, ranging from very short distance optical interconnects of a few centimetres, point-to-point links at 1m, local area networks (LANs) to outdoor free space optical links (in km). Indoor OW links have successfully penetrated our homes and our lives, but we have paid little attention to this vital, invisible technology. The wide availability of OW products covers personal computers, peripherals and other devices ranging from TV remote controls to IrDA ports. IrDA ports are currently installed in more than 200 million units and see an annual growth of 40% [4]. Furthermore, with the modern need for interactive multimedia applications like video conferencing, OW products offer bandwidth that cannot easily be found elsewhere, particularly where fibre optic cables are too expensive or even impossible to install.

The term 'Infrared (IR) wireless communication' refers to the use of light waves in free-space propagation in the near infrared band as a transmission medium for communication. The IR signal is electromagnetic radiation whose wavelengths are banded between those of microwaves and visible light signals. The word Infrared means "below red" and is derived from the Latin word *infra*, meaning 'below', and *red*, which is the colour at the edge of the visible spectrum. Wireless IR communication is generally used; however, the term

'wireless' can also apply to other regions of the optical spectrum. Therefore, the term 'wireless optical communication' rather than 'wireless IR communication' is used to expand the meaning of the technology across wavelengths. IR radiation has wavelengths of between 780 nm and 1550 nm [5].

## **1.2 Optical Wireless for Short Range Communication**

Optical wireless links are a good solution for short range (indoor) wireless communication because a large bandwidth is available, which assists demanding multimedia applications. IR signals cannot pass through solid objects and walls; therefore, the bandwidth can be offered (reused) in adjacent rooms without the risk of interference. OW communication does not cause electromagnetic radio frequency (RF) interference and is not affected by such interference making it ideal for hospitals and aeroplanes. However, indoor OW communication links suffer from two main problems: first, the attenuation of the transmitted signal, which reduces the signal-to-noise ratio (SNR) at the receiver; second, multipath reflections, which can spread the received pulse and thereby restrict the maximum transmission rate. These two problems may be unconnected. A high delay spread is not necessarily connected to high attenuation in the received optical power. The design of an IR link faces other problems such as natural (sunlight) or artificial (lamps) background noise, and other opaque barriers may cause shadowing and limited range, while this is not a problem for radio frequency (RF) links. The advantages and disadvantages of both IR and RF links will be considered in the next chapter.

Contemporary life and our need for multimedia and video means a big demand for ultra-broadband wireless access networks and this demand is fuelled by end users at hospitals, schools and universities and large retail stores. There is also a need for high-speed links to connect personal computers (PCs) in indoor wireless local area networks (WLANs) as inexpensively as possible, which has encouraged researchers to conduct extensive research into OW

communications. Indoor OW networks can use diffuse IR radiation. Such wireless networks can be supported and extended by a passive fibre support, which can feed diffuse infrared emitters located in the roof, and can give access to remote places and facilities within a network. Mobile users can access the network by entering a covered cell area. This system offers mobility together with reduction in the physical connections. Figure 1.1 shows a typical indoor OW network. A network of this kind would allow portable devices to communicate with multimedia servers or with other portable devices located in different rooms within the network. This optical wireless network would satisfy the dual need for both mobility and broadband networking [6]. In high-performance multimedia wireless computing environments, the portable terminals may serve as a human interface, accepting pen and keyboard input and producing full-motion video output [7].

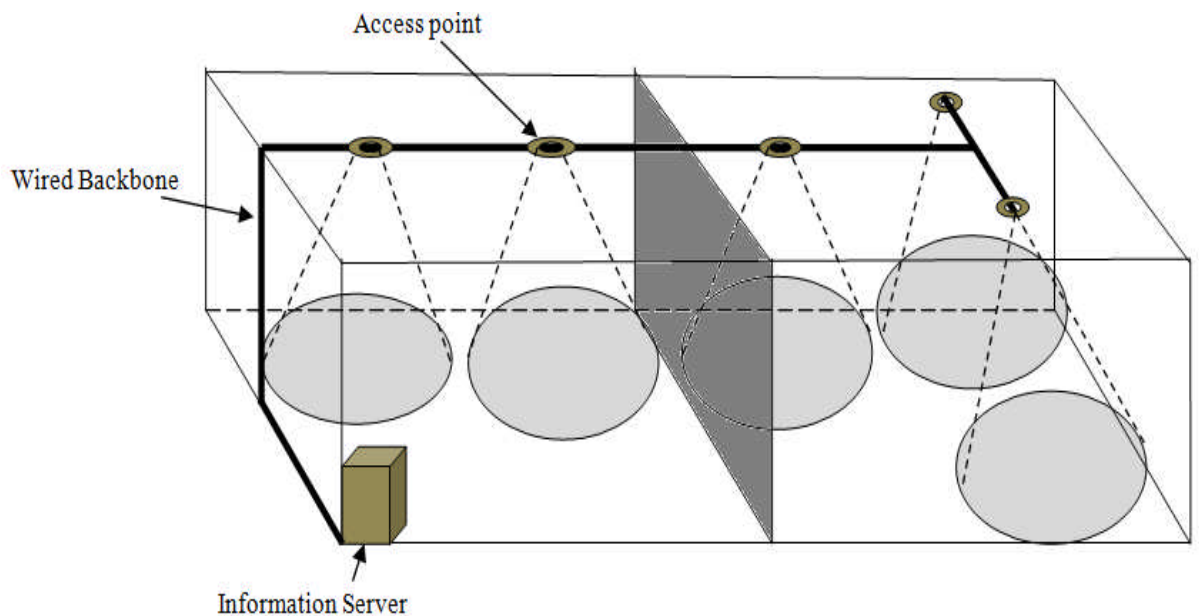


Figure 1.1: OW-LAN using ceiling mounted access points to connect optical wireless devices.

## 1.3 Motivation and Research Objectives

The performance of OW systems can be affected by several factors, including:

- Intense ambient (background) noise
- Large, variable propagation losses
- Multipath propagation, which may cause inter-symbol-interference (ISI).

The author's interest in research in this new technology has been inspired by the advantages of OW over RF communication, along with an increase in demand for mobility via wireless technologies and the expansion in the use of smart mobile phones. The recent increase in research activity in OW has encouraged further study in order to explore the challenges and to search for methods that can improve the performance of indoor OW communication systems and allow them to operate at higher data rates.

The primary objectives of this work were to:

- 1- Propose and study new mobile OW systems that perform better than the conventional diffuse system (CDS) and the basic line strip multi-spot diffusing system (LSMS) [130].
- 2- Mitigate the impact of user mobility in a realistic indoor office, especially at the weakest communication link (where the transmitter and the receiver are distant from each other).
- 3- Study the use of multiple non-imaging angle diversity receivers and imaging diversity receivers to reduce background noise components.
- 4- Devise techniques to reduce the effect of multipath dispersion and increase the 3-dB channel bandwidth and the SNR at high data rates.
- 5- Design a robust high-speed indoor OW system with full mobility under the impact of background noise sources, multipath dispersion and shadowing.

## 1.4 Research Contributions

The author in this thesis has:

- 1- Modelled and analysed the characteristics of the indoor optical wireless channel by further developing an existing ray-tracing algorithm that caters for the direct line-of-sight (LOS), first and second order reflections. This model was transformed into a comprehensive software package to carry out the simulation in *Matlab*. The outputs of the simulation are the channel impulse response, delay spread, 3-dB channel bandwidth and signal-to-noise ratio (SNR). The simulation was also developed and used to evaluate the background noise due to artificial light sources at several locations. Based on the simulation package, the author has verified the basic optical wireless systems in the literature. These systems are CDS, LSMS with a wide field-of view (FOV) receiver and LSMS in conjunction with three-branched angle diversity receivers. The results of his simulator were compared with other researchers' work. A good match was observed, giving confidence in the capability of the author's simulator to evaluate new OW systems.
- 2- Introduced a novel method of beam delay and power adaptation in indoor OW systems. Based on these adaptation techniques, the author has designed and evaluated different adaptive multi-spot OW configurations:
  - A. Beam delay and power adaptation with a line strip multi-spot diffusing system (BDPA-LSMS) in conjunction with three and seven branched angle diversity receivers.
  - B. Beam delay and power adaptive multi-beam clustering method (BDPA-BCM) coupled with seven angle diversity receivers.
  - C. Beam delay and power multiple adaptive beam clustering method (BDPMA-BCM) coupled with an imaging receiver.

He has also introduced a custom imaging diversity receiver with 200 pixels (detectors). These detectors enable the system to reduce the significant impact of background noise sources. The proposed systems were examined and compared with CDS and LSMS systems. The improvement in the SNR and delay spread enable the new systems (BDPA-BCM and BDPMA-BCM) to operate at high bit rates of 2.5 Gb/s and 5 Gb/s.

- 3- Proposed a beam angle and power adaptive line strip multi-spot diffusing system (APA-LSMS) coupled with three-branched angle diversity receivers. The main goal of the proposed system is to mitigate the impact of user mobility over the indoor environment as well as to enable the system to operate at high data rates. The author has designed, evaluated and reported for the first time a mobile OW system that operates at 10 Gb/s. The results of the proposed system APA-LSMS at high data rates are significant and have been enabled, with full mobility, at a lower transmit power in an environment where eye safety is important.
- 4- Proposed and designed a fully adaptive high-speed 10 Gb/s mobile optical wireless system that employs beam delay, angle and power adaptation with line strip multi-spot diffusing configuration (BDAPA-LSMS) coupled with imaging receivers. The author has also studied the system in a realistic indoor communication scenario where physical partitions introduce shadowing and signal blockage, window cause signal loss, and bookshelves, chairs and cabinets are present causing additional reflections. The shadowed imaging BDAPA-LSMS system was compared with imaging CDS and non-adaptive LSMS configurations. It is shown that the fully imaging adaptive BDAPA-LSMS is a suitable candidate for mobile indoor OW systems and can combat shadowing. The high data rates (5 Gb/s and 10 Gb/s) are shown to be possible

through the use of beam delay, angle and power adaptation coupled with high speed imaging receiver design.

- 5- Introduced a novel adaptive optical wireless system that employs a finite vocabulary of stored holograms. A fast adaptation approach based on a divide-and-conquer (D&C) strategy is proposed, resulting in a number of adaptation algorithms:

- A. Fast angle adaptive holograms (FAA-Holograms),
- B. Fast power adaptive holograms (FPA-Holograms) and
- C. Fast angle and power adaptive holograms (FAPA-Holograms)

and evaluated these fast algorithms in mobile optical wireless (OW) systems in conjugation with imaging reception. All the holograms are pre-calculated and stored without adding any complexity at the transmitter. Furthermore, a simulated annealing algorithm is introduced to optimise the phase of holograms. The author has investigated the trade-off between complexity and performance enhancement of the proposed systems compared with the classical beam power and angle adaptations. Moreover, he has studied nine narrow FOVs angle diversity receivers with adaptive finite vocabulary holograms system (FAPA-Holograms). The proposed system has been examined in a realistic indoor office environment, and compared with non-adaptive OW configurations.

These contributions are supported by the following publications:

### **Journals**

1. M. T. Alresheedi and J. M. H. Elmirghani, "Performance Evaluation of 5 Gbit/s and 10 Gbit/s Mobile Optical Wireless Systems Employing Beam Angle and Power Adaptation with Diversity Receivers," *Selected Areas in Communications, IEEE Journal on*, vol. 29, No. 6, pp. 1328-1340, June 2011.
2. M. T. Alresheedi and J. M. H. Elmirghani, "10 Gbit/s Indoor Optical Wireless Systems Employing Beam Delay, Angle and Power Adaptation Methods with Imaging Detection," *Lightwave Technology, Journal of*, vol. 30, No. 12, pp. 1843-1856, 2012.

3. M.T. Alresheedi and J. M. H. Elmirghani “High-Speed Indoor Optical Wireless Links Employing Fast Angle and Power Adaptive Computer-Generated Holograms with Imaging Receivers,” to be submitted to IEEE Journal of Optical Communications and Networking.

### Conferences

4. M. T. Alresheedi and J. M. H. Elmirghani,” Mobile Optical Wireless Systems Employing Beam Angle and Power Adaptation with Diversity Receivers,” in Proc. of the IEEE International Conference on Wireless and Optical Communications Networks (WOCN’10), Colombo, September, 2010.
5. M. T. Alresheedi and J. M. H. Elmirghani,” Angle and Power Adaptation in 10 Gbit/s Multibeam Mobile Optical Wireless Systems with Angle Diversity Detection,” in Proc. of the 15th IEEE International Conference on Optical Network Design and Modelling (ONDM’11), Bologna, February, 2011.
6. M. T. Alresheedi and J. M. H. Elmirghani, “Adaptive Multibeam Spot Diffusing Optical Wireless System with Imaging receivers,” IEEE International on Transparent Optical Networks (ICTON’11), July 2011.
7. M. T. Alresheedi and J. M. H. Elmirghani, “Line Strip Multibeam Spot Diffusing Optical Wireless System employing Beam Delay and Power Adaptation with Angle Diversity Detection,” International wireless communication and Mobile computing IEEE Conference. IWCMC’11, July 2011.
8. M. T. Alresheedi and J. M. H. Elmirghani, “Adaptive 10 Gbit/s Mobile Optical Wireless Systems Employing Beam Delay, Angle and Power Adaptation with Imaging Receivers,” IEEE GLOBECOM’11, December, 2011.
9. M. T. Alresheedi and J. M. H. Elmirghani, “High-speed wireless infrared links with an adaptive multibeam clustering method and angle diversity detection,” IEEE International on Transparent Optical Networks (ICTON’12), July 2012.

## 1.5 Overview of the Thesis

The next chapter provides a review of OW systems, including transmitter and receiver components. Comparison between IR and RF links is presented. Moreover, the design challenges of indoor OW systems, such as optical safety regulations, ambient noise, multipath dispersion and photodetector high capacitance, are outlined.

**Chapter 3** presents the tools that are used to model and simulate the OW channel in an indoor environment. Two major OW transmitters are studied: the CDS and the LSMS systems. Analysis of the delay spread of the received pulse is given. Moreover, background noise is explained and SNR evaluation is provided and used to analyze the impact of ambient noise on the indoor OW system's performance.

**Chapter 4** presents a novel method that employs beam delay and power adaptation in OW systems. The basic LSMS configuration is developed where beam delay and power adaptation are introduced. A new beam delay and power adaptive multi-beam clustering method (BDPA-BCM) is also proposed coupled with angle diversity receivers. Moreover, a custom design of an imaging receiver is introduced in this chapter. Furthermore, a new multiple adaptive beam clustering technique coupled with imaging diversity receivers is proposed and compared with previous adaptive systems.

**Chapter 5** proposes a 10 Gb/s mobile indoor OW system adopting four techniques: multi-spot diffusing, beam angle adaptation, beam power adaption and a simple structure of angle diversity receivers. The chapter focuses on achieving a low complexity design for a high-speed indoor OW system with full mobility, based on a combination of these methods.

**Chapter 6** introduces a fully adaptive high-speed OW system based on beam, delay, angle and power adaption with a multi-spot LSMS (BDAPA-LSMS) system coupled with imaging diversity receivers. Moreover, the proposed system is examined in a realistic indoor communication environment where physical partitions (shadowing), windows, bookshelves, chairs and cabinets all are present. The impact of shadowing and signal blockage can be sufficiently mitigated through the use of beam delay adaptation, beam angle adaptation, beam power adaption, multi-spot diffusing and imaging diversity receivers.

**Chapter 7** proposes a novel adaptive optical wireless system that employs a finite vocabulary of stored holograms. A fast adaptation approach based on a divide-and-conquer methodology is proposed, resulting in a number of adaptation algorithms: fast angle adaptive holograms (FAA-Holograms), fast power adaptive holograms (FPA-Holograms), and fast angle and power adaptive holograms (FAPA-Holograms). These systems are evaluated in mobile OW configurations in conjugation with imaging reception. Furthermore, a simulated annealing algorithm is introduced to optimise the phase of holograms. High data rates of 2.5 Gb/s and 5 Gb/s are also considered for the FAPA-Holograms system. The trade-off between complexity and performance of the proposed systems is studied and the systems are compared with beam power and angle adaptation systems proposed previously. Moreover, nine narrow FOVs angle diversity receivers have been employed with adaptive finite vocabulary holograms. The proposed system was examined in a realistic indoor office and compared with non-adaptive OW configurations.

A summary of the results and some ideas towards further research are provided in **Chapter 8**.

# 2 Review of Optical Wireless Systems

## 2.1 Introduction

The number of personal computers is significantly increasing and these are used mostly in indoor environments such as offices, homes and shopping areas. This growth has occurred in tandem with the emergence of affordable portable computing devices. The traditional physical link connection (wired network) between such devices has long been the *de facto* method of connecting one machine to another; however, this method has inherent problems involving high costs of development, reconfiguration and maintenance. The best solution to these problems is to go wireless. A wireless network can offer mobility and flexibility for its users, along with a reduction in the costs of labour and materials. Therefore, wireless transmission technology is far more favourable than a wired model. The most important issue to be decided when implementing such a system is the type of wireless medium to use. There are basically two types: the first uses radio frequency (RF) and the other employs optical frequencies. These types both have their advantages and disadvantages that need to be carefully considered.

It has nearly been three decades since Gfeller began experimenting with IR radiation and proposed a protocol for using this technology to link computers in a network [8]. Since then, a large and growing body of research in this area has emerged and in the last ten years optical wireless (OW) communication has gone from strength to strength as a leading method for local area networks, especially in situations where large bandwidth is important [8]-[18]. Furthermore, the large number of portable devices used in the indoor

environment, along with the need for low power consumption, low cost and small components, has accelerated the demands for a wireless network that can be supported by a passive optical fibre backbone.

This chapter reviews optical wireless systems and provides a comparison between Infrared and Radio media. Indoor OW transmitter and receiver components are detailed. The classifications of IR links connection are given in Section 2.3. Design challenges of indoor OW systems, such as optical safety regulations, ambient noise sources, multipath dispersion and photodetector high capacitance, are discussed in Section 2.4. Next, signal modulation techniques and angle diversity receivers are presented in Sections 2.5 and 2.6, respectively. The chapter concludes by describing standards for indoor OW systems.

## **2.2 Comparison between Infrared and Radio Media**

IR and RF are both widely used as a transmission medium, with distinguishing characteristics that make either one individually more suited to different applications than the other. Generally speaking, for applications requiring the transmission of data through walls or other large physical objects and where user mobility over wide geographic coverage is essential, RF is the preferred medium. On the other hand, OW, whose signals are as vulnerable to absorption, diffusion and reflection as visible light, is better applied in short-range network environments where the bit-rate per network link and overall system capacity must be high while keeping costs and receiver complexity to a minimum [15], [16].

IR links have some advantages over RF systems, such as larger transmission bandwidths and immunity against interference from electrical devices. Radio channels carriers typically range from a few kHz to about 60 GHz, whereas an OW channel's available spectrum starts at 300 GHz and goes upward from

there [17]. Apart from the advantages of a large potential bandwidth, optical wireless makes it possible to reuse the same wavelength in other parts of an indoor environment without facing any interference and security problems. Additionally, OW signals cannot penetrate walls or other opaque barriers and therefore will be contained in their space of origin, making them ideal for wireless local area networks. The physical size of the antennas is also a major difference between RF and OW; RF antenna sizes are typically comparable to the signal wavelengths (meters to millimetres), whereas with OW the typical dimensions of a photodetector are an area of  $1 \text{ cm}^2$  which is equal to a million wavelengths square, hence OW detectors are free from fading [15]-[22]. Freedom from fading can greatly simplify the design of OW links. OW boasts yet another advantage over RF, in that the cost of optical transceiver components, such as light emitting diodes (LEDs) and positive-intrinsic negative (PIN) detectors, is much cheaper than their radio counterparts. When it comes to regulation, OW users are free to take advantage of the entire possible spectrum, whereas the radio frequency spectrum is regulated by governments. RF transmission is monitored by the Office of Communications (OfCom) and the Federal Communications Commission (FCC) in the United Kingdom and the United States respectively [23], [24].

However, an OW system is not without drawbacks; there are two major limitations in OW links. The first is additive noise interference from natural light (sunlight) and artificial light (that is, light from fluorescent and incandescent light sources), which results in a degraded SNR ratio. The second is the spread of the received pulse due to multipath dispersion, which also degrades the SNR. Multipath dispersion is attributed to reflective surfaces such as walls, windows, doors and ceilings. Since these reflective elements act as small emitters that diffuse the signal in the form of a Lambertian pattern, the transmitted data arrives at the receiver from multiple different paths, which makes the transmitted pulses spread [16]. In addition to these drawbacks, there is a need

for a backbone in each room of the building in order to provide access points throughout the indoor environment, since optical signals cannot penetrate walls. While the spectrum itself is not regulated, restrictions on how much power an OW system may transmit are in place to comply with regulations pertaining to people’s skin and eye safety [25] – [27]. Table 2.1 provides a comparison between OW and RF systems.

Table 2.1: Comparison between optical wireless and radio frequency systems for the indoor environment.

	<b>Optical Wireless systems</b>	<b>Radio systems</b>
<b>Advantages</b>	<ul style="list-style-type: none"> <li>• Bandwidth is unlimited</li> <li>• Signals contained within the room of origin</li> <li>• Security against casual eavesdropping, as there can be no interference between links in different rooms</li> <li>• Freedom from fading</li> </ul>	<ul style="list-style-type: none"> <li>• Possibility of passing through walls, ceiling and other objects</li> <li>• High mobility and flexibility for users</li> </ul>
<b>Disadvantages</b>	<ul style="list-style-type: none"> <li>• Background noise</li> <li>• Multipath dispersion leads to ISI</li> <li>• Signal to noise ratio different according to the receiver location and ambient light (background noise)</li> <li>• Transmitted power restricted by eye and skin safety regulations</li> </ul>	<ul style="list-style-type: none"> <li>• Interference between users in different rooms</li> <li>• Multipath fading</li> <li>• Restricted bandwidth</li> <li>• Low security</li> </ul>

## 2.3 An Indoor Optical Wireless (OW) System

Figure 2.1 shows the block diagram of a standard indoor OW system. The system consists of: (1) a transmitter that uses LEDs or laser diodes (LDs), (2) a propagation medium (free space) and (3) a photodetector (avalanche photo-diodes (APDs) or PIN diodes) that acts as a receiver. Electronic circuitry

receives information (input data) in the form of digital data and modulates the transmitting light source (LED or LD). An optical system generally has an optical telescope (for long distance), an optical diffuser (for mobile short distance) or some other optical system that shapes the source beam which then propagates into the medium (free space). The received signal goes to an optical system and across to a photodetector (APD or PIN diodes). The band of wavelengths that ranges from 780nm to 950nm is considered as the better range for indoor OW systems because low-cost LDs and LEDs are available [16], [30] – [33]. This band also coincides with the peak responsivity of low cost, low capacitance silicon photodiodes. The OW system employs intensity modulation and direct detection (IM/DD). IM/DD is the *de-facto* method of implementing OW systems due to its reduced cost and complexity [8], [15], [16]. Intensity modulation (IM) can be achieved by varying the LED or LD bias current. PIN photo-diodes or APDs in a direct detection (DD) receiver produce a photocurrent proportional to incident optical power.

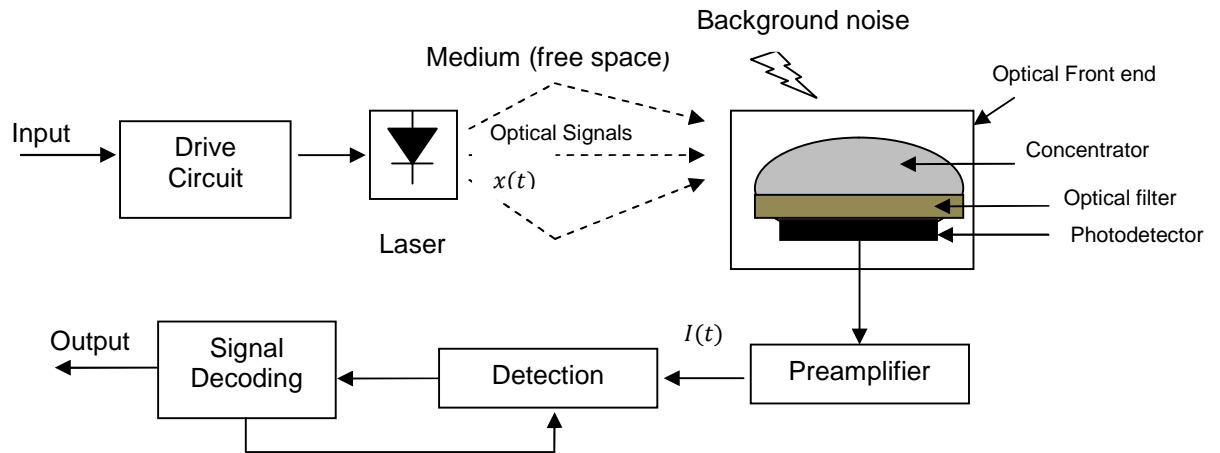


Figure 2.1: A Basic Optical Wireless Terminal Block Diagram.

### 2.3.1 Transmitter components

LDs and LEDs are the two commonly used optical sources for infrared transmission. LDs have some potential advantages over LEDs. They have higher output optical power, narrow spectral widths (from several nm to less

than 1nm), wider modulation bandwidths (from 100s of MHz to over 10 GHz) and linear electrical to optical signal conversion characteristics [16], [34]. In signal conversion, using sophisticated modulation schemes like multilevel signalling or a multi-subcarrier modulation, linearity is particularly important. However, LDs present a possible safety risk because they represent a point source which can be focused into a small area on the retina leading to high power densities and retina damage. LEDs by contrast, emit over a larger area and can therefore operate safely at higher power levels [25]. They are also more reliable and affordable. Therefore LEDs are a preferable source of light for indoor applications. However, LEDs have some drawbacks, which include: (1) in typical low cost LED devices, modulation bandwidths are limited to 10s of MHz, which limits the transmission rate of an OW system; (2) the wide spectral width, 40nm and slow response limit the modulation rate of LEDs; (3) poor electro-optic power conversion efficiency of around 10%-20%. LEDs cannot be used at higher data rates i.e. beyond 100 Mb/s typically. A data transmission rate of a few Gb/s can be achieved by employing LDs. Therefore, LD will be used in the thesis when the transmitter operates at high rates such 5 Gb/s and 10 Gb/s. More details about LEDs and LDs sources are given in [15], [16], [35], [36].

### **2.3.2 Propagation Medium and OW Transmission Links Design**

Atmospheric loss along the propagation path has a significant impact on the link budget for an OW system. Fortunately, there is no environmental degradation (i.e. fog, mist, clouds, particulate matter, etc.) in an indoor environment, but indoor OW systems experience free space loss. Free space loss refers to the amount of transmitted power that is lost due to propagation through space, or is not captured by the receiver. Around 20 dB free space loss would be average for a point-to-point OW system operating with a slightly diverging beam, whereas there can be an average free space loss of 40 dB or more with an

indoor OW system employing a wide beam angle (non line-of-sight system) [35].

Over the last three decades, indoor OW technology has attracted substantial attention. OW links use various designs to support different applications. An OW transmission can be categorised according to two criteria [16], [34] – [37]:

- 1- the transmitter and the receiver direction, and
- 2- the presence of an unobstructed direct path connecting the transmitter and the receiver.

Using these facts, two classes of OW links can be defined: line-of-sight (LOS) and non-LOS transmission configurations. In the LOS system, the receiver can always be seen by the transmitter. Furthermore, LOS systems can be divided into directed, hybrid and diffuse systems depending on the radiation pattern of the transmitter and the receiver FOV. A direct link can be created when the transmitter and the receiver are both directed, i.e. a narrow beam radiation at the transmitter and small FOV at the receiver. A hybrid link may be established either by using a transmitter with narrow beam radiation and a receiver that is non-directed, or vice versa. A diffuse link can be formed when a transmitter employs single wide beam radiation and the receiver uses a wide FOV detector. The three LOS basic links design are portrayed in Figure 2.2 (a). The LOS method relies on the degree of directionality of the transmitter and the receiver, where a direct link should be established regardless of the transmitter and the receiver beam angles. High power efficiency is obtained by an LOS system via the use of narrow beam transmitters and small FOV receivers. Additionally, direct LOS systems do not suffer from multipath dispersion or background light noise. Both of these constraints are mainly removed as a result of utilising a narrow beam transmitter as well as a small FOV receiver which can enable high transmission bit rates. The increased data rate of direct LOS systems is restricted only by the links budget rather than by multipath dispersion or

background noise. Regrettably, no LOS link is appropriate for mobile portable devices, as accurate alignment between transmitter and receiver is necessary to retain the benefits of the direct path, and they may be subject to shadowing [38] – [41]. Tracking satellite transmitters can offer the prospect of the directed LOS terminal mobility, but they nonetheless are unable to suppress the effects of shadowing [44], [45].

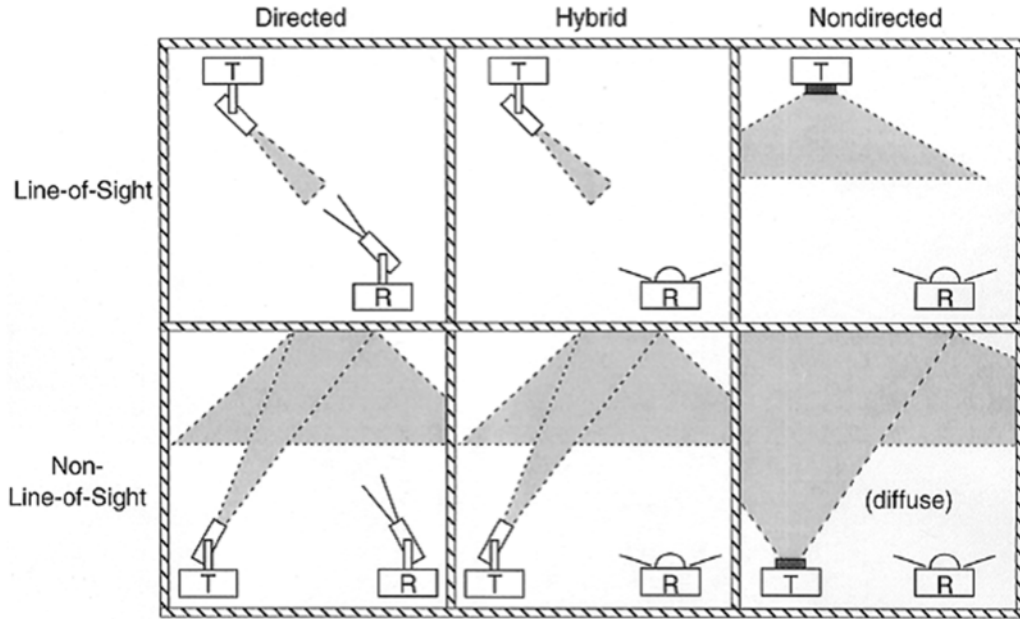


Figure 2.2: The main categories of OW: (a) LOS systems (b) non-LOS systems [16]:  
T: Transmitter, R: Receiver.

Non-LOS (diffuse) systems are dependent on reflections of light from walls and ceiling in addition to other surfaces that reflect light diffusely. They play an important role in environments where mobility is a key factor and where obstructions and the effects of shadowing are also present. This sort of arrangement permits an exceptional level of mobility inside the covered area, and mobile users may simply roam inside this area and maintain connection. This is due to the fact that a non-LOS system is not dependent on the presence of a direct path between transmitter and receiver. In a pure diffuse system, a single wide beam source (LED) is used by the transmitter, that places such a

source on the communication plane (CP) (a plane typically 1 m above ground level) up in the direction of the ceiling and the receiver makes use of a wide FOV receiver aimed vertically at the ceiling. The indirect transmitter beams normally radiate over a wide angle in addition to permitting reflection off surfaces that reflect diffusely, such as the walls, ceiling, floor and articles like bodies and furniture in a room [34], [46], [47]. As illustrated in Figure 2.2 (b), different arrangements can be obtained from the diffuse connection. For instance, pointing the receiver FOV and the transmitter beam in the direction of the same target point on a reflective diffusing surface may result in the formation of a semi-directed connection. A diffuse system has several benefits in comparison with LOS systems. Diffuse systems offer great link stability as well as providing substantial immunity to direct beam blockage near to the receiver. Furthermore, a diffuse connection permits users to immediately join and collaborate with the use of mobile computers, wireless printers, modems, and office and home networking devices. However, diffuse systems may suffer from multipath dispersion, and this may cause signal spread and ISI. The impact of multipath dispersion can be reduced through the use of angle diversity or imaging receivers and equalisation. Imaging and angle diversity receivers are studied and analysed in this thesis. Equalisation methods will not be considered here, but appear to have potential [48], [49].

### **2.3.3 Receiver components**

An optical wireless receiver converts an optical signal back to an electrical signal. It comprises a pre-amplifier receiver circuit and a photodetector that is positioned behind a front end: the front end commonly consists of an optical filter and a concentrator. Figure 2.1 shows a diagram of a standard OW receiver. In OW systems, the optical signal is received in the form of optical pulses, which represent 1 and 0 bits, and these pulses are converted into an electric current. Such an operation is a result of the IM/DD (as explained in Section 2.2). The next step after this essential conversion process is

amplification. This amplification is provided in the first instance by a preamplifier followed by a detection circuit that is controlled by a clock extracted by a clock recovery module. Optical preprocessing can be carried out on the signal before it reaches the photodetector, such as the use of an optical concentrator followed by an optical filter on the front of the photodetector. The concentrator can increase the overall optical received power at the receiver [50] – [55]. An optical filter can be used to reduce the amount of ambient light captured by removing the noise outside the signal band [42], [43], [56] – [62]. The following sections discuss the main components of OW receivers.

### 2.3.3.1 Optical Filters and Concentrators

Band-pass and high-pass optical filters are generally used in Infrared receivers in order to reduce the impact of ambient light noise sources. High-pass filters can be considered as passing light at all wavelengths beyond the cutoff wavelength. Often they are made of coloured plastic or glass and their transmission characteristics are independent of the angle of incidence. Figure 2.3, shows a typical high-pass filter [16], [37], which is superimposed onto the responsivity curve of a normal silicon photodiode. Almost all current commercial infrared systems use high-pass filters.

Band-pass filters, on the other hand, can achieve very narrow bandwidths (bandwidths lower than 1nm are now commercially available), and are usually made of a number of thin, dielectric layers [16], [37], [63]. They depend on optical interference, and can lead to superior rejection of ambient light. In order to improve the SNR, a transmitter optical spectrum must be within the filter bandwidth. Therefore, LD transmitters with a very narrow optical bandwidth should be used when the filter bandwidth is small. Figure 2.4 shows the transmission spectrum of a normal band-pass filter. The pass band is seen to shift to shorter wavelengths when the angle ( $\theta$ ), at which light strikes the filter,

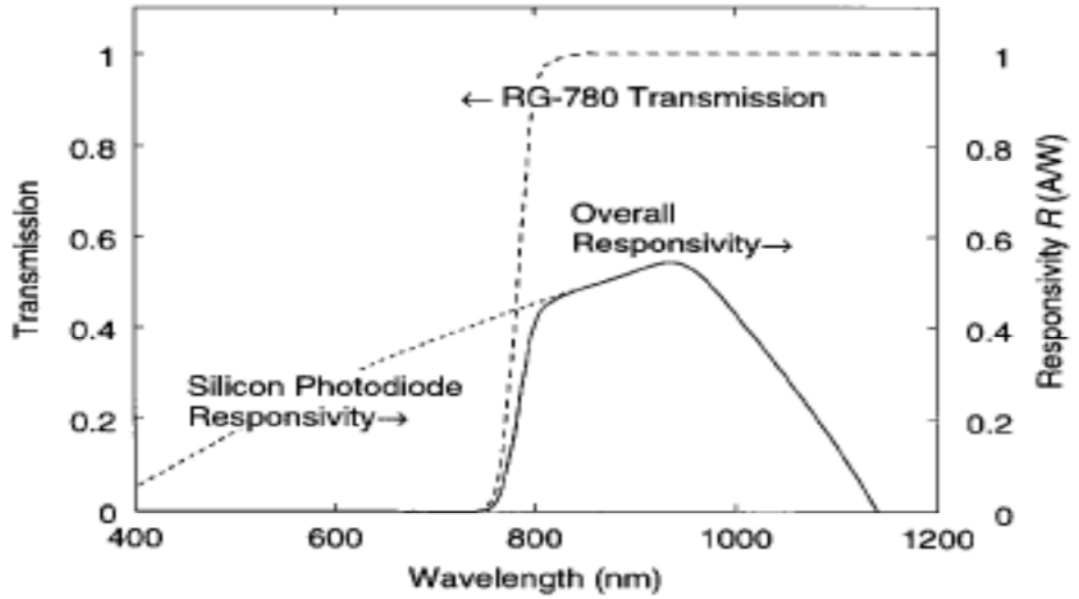


Figure 2.3: Responsivity of a normal silicon PIN photodiode, a typical high-pass optical filter transmission and general responsivity and transmission [16], [37].

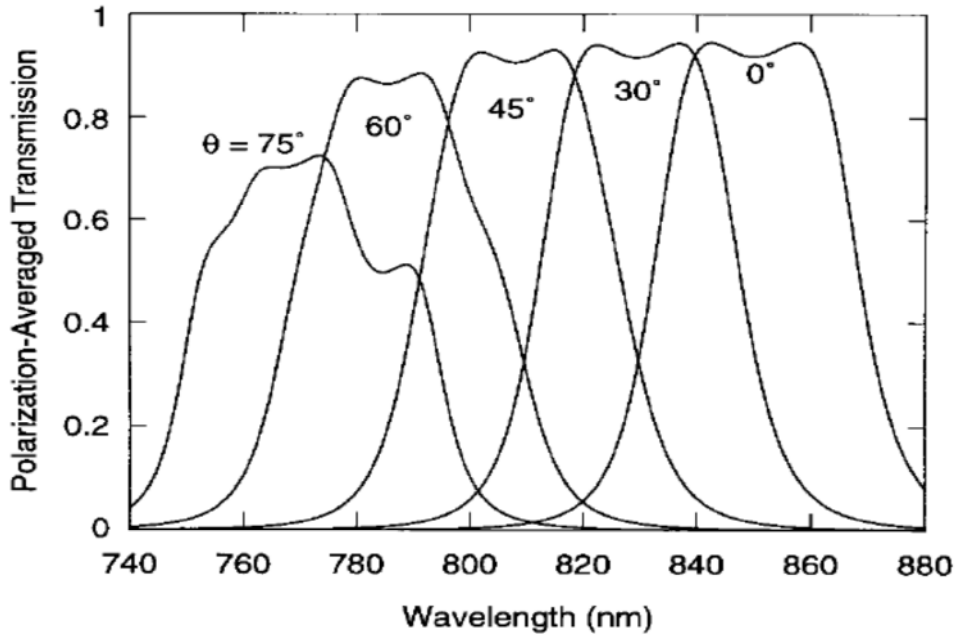


Figure 2.4: The averaged transmission polarization of an optical band-pass filter for different incident angle  $\theta$  [37], [63].

is increased. It is important to use such a filter carefully, particularly when the receiver is attempting to achieve a wide FOV [16], [63].

In an OW system, since the detected optical signal power at an infrared receiver is proportional to the photodetector's active area, increasing the active area of the photodiode results in increasing the received power, but reduces the receiver bandwidth as well as increasing the noise at the receiver, hence restricting transmission rates [28], [65] – [69]. Therefore, it is better to use an optical concentrator to augment the optical power received at the photosensitive active area while keeping the detector area small. A concentrator can be considered as a device that increases the radiant flux incident on the photodetector. Using an optical concentrator means that the requirement for a large detector is reduced as concentrators increase the effective collection area. Smaller active areas of photodetectors can therefore be used, hence decreasing capacitance, and improving receiver bandwidth. Receiver sensitivity is also improved if capacitance is small, since a given receiver bandwidth can then be achieved while using a larger receiver input impedance, the latter leads to reduced noise current and improved receiver sensitivity. Moreover, the problems with optical safety and power consumption can be avoided with the use of a concentrator which can result in a reduction in the total transmitted power.

The main function of the optical concentrator is to guide light rays incident at large area into light rays that come out of a smaller area. It is important to note that concentrators not only collect the desired optical signal power, but also collect background noise from daylight and artificial light sources. Optical filters, imaging diversity receivers and angle diversity receivers can be further employed to lower these noises, hence enhancing SNR at the receiver. OW systems may employ imaging or non-imaging concentrators. Examples of imaging concentrators can be found in the telescopes employed in longer-range, open-space optical links. Generally, most indoor OW links use non-

imaging concentrators. When we ignore reflection loss, a bare detector can achieve an effective signal-collection area of [16]:

$$A_{eff}(\delta) = \begin{cases} A \cos(\delta), & 0 \leq \delta \leq \pi/2 \\ 0 & \delta > \pi/2 \end{cases} \quad (2.1)$$

where  $A$  is the physical area of the detector and  $\delta$  is the angle of incidence with respect to the receiver normal. If we add a concentrator and filter, the effective signal-collection area becomes [16], [37]:

$$A_{eff}(\delta) = \begin{cases} AT_s(\delta) g(\delta) \cos(\delta), & 0 \leq \delta \leq \psi_c \\ 0 & \delta > \psi_c \end{cases} \quad (2.2)$$

where  $T_s(\delta)$  is the signal transmission of the filter,  $g(\delta)$  is the concentrator gain and  $\psi_c$  is the FOV of the concentrator (semi-angle). Non-imaging concentrators exhibit a relationship between FOV and gain. The maximum achievable concentrator gain in an idealised non-imaging concentrator is [70] – [72]

$$g(\delta) = \begin{cases} \frac{N^2}{\sin^2 \psi_c}, & 0 \leq \delta \leq \psi_c \\ 0 & \delta > \psi_c \end{cases} \quad (2.3)$$

where  $N$  is an internal refractive index. The above equation shows an inverse relation between the FOV and the gain of the receiver where FOV is reduced, when the gain within the FOV is increased.

The non-directional hemispherical lens is an important non-imaging concentrator [16], [73]: see Figure 2.5 (a) and (b). It is widely used in commercial infrared systems where it can achieve a wide FOV and omnidirectional gain. Therefore it is ideal for non-directed links. A hemisphere can achieve  $\psi_c = 90^\circ$  and  $g(\delta) = N^2$  over the entire FOV. A hemisphere-based receiver has an effective area of:

$$A_{eff}(\delta) = AN^2 \cos(\delta). \quad (2.4)$$

As seen in Figure 2.5 (a), when using high-pass filtering, a planar high-pass filter can be positioned between the detector and the hemisphere. When using band-pass filtering, it is not preferable to use a planar filter in this configuration. This is due to the shift in the received angle rays ( $\delta$ ) as well as  $\theta$ , the angle at which light hits the filter. This will shift the band-pass filter centre wavelength and decrease the filter transmission  $T_S(\delta)$  for some values of  $\delta$ . Instead, the band-pass filter should be bonded or deposited on to the outer surface of the hemispherical concentrator [52], [63] as shown in Figure 2.5 (b). Irrespective of the received angle ( $\delta$ ), rays reaching the detector depend on the filter at small values of the angle  $\theta$ , duly reducing the filter pass-band shift, and maximizing its transmission. Therefore, with a hemispherical filter, a narrow bandwidth and wide FOV are simultaneously achievable.

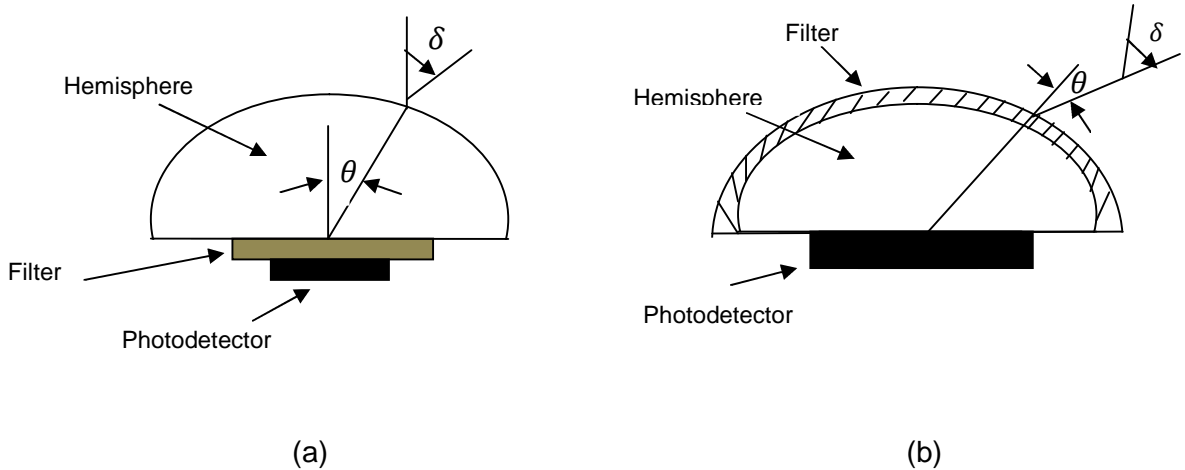


Figure 2.5: Non-directional hemispherical lens that employs (a) planar and (b) hemispherical optical filter.

Another non-imaging concentrator used widely in infrared links is the compound parabolic concentrator (CPC) [50]. It can achieve greater gain than the hemispherical concentrator, but this comes at a reduction of FOV. A CPC is particularly appropriate for directed links. A CPC with FOV  $\psi_c < 90^\circ$  can accomplish a gain near to (2.3) [53]. As Figure 2.6 shows, a high-pass or band-pass filter can be positioned on the CPC's front surface. The small FOV of a CPC is ideally suited to the restricted angular acceptance of a narrow band-

pass filter. A reduction in the background noise effect and an improvement in SNR can be achieved by using an array of CPC elements alongside an angle diversity receiver [51], [74], [75]. Additionally, techniques such as selecting or combining can be applied with this type of system in order to reduce multipath dispersion and to improve the performance of the system.

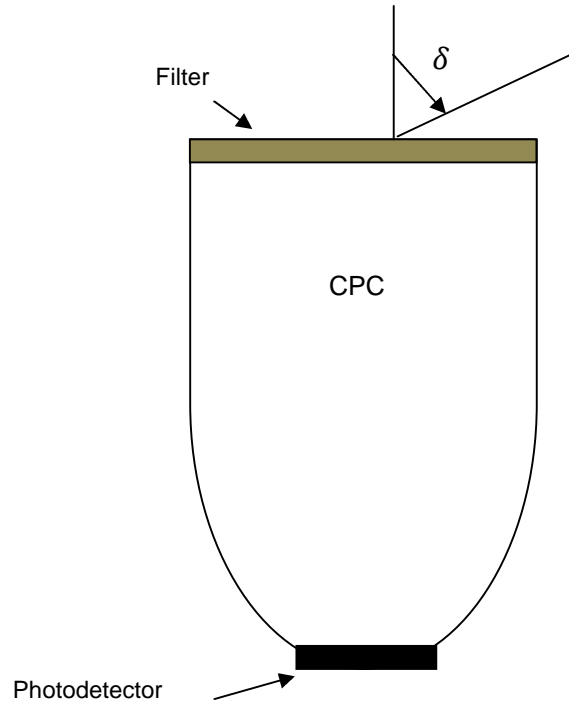


Figure 2.6: Compound parabolic concentrator (CPC) with planar filter.

### 2.3.3.2 Photodetectors and Preamplifiers

A photodetector is a square law opto-electronic device that converts the incident light into an electrical signal. There are a number of qualities that a photodetector must possess: it must be small, lightweight, reliable and cost-effective. It should also be long-lasting. Most infrared link applications use wavelengths in the 780 nm - 950nm band due to the availability of low-cost, low-capacitance, wide area silicon photodiodes operating at that wavelength band. Two main available photodiodes types are used in OW systems: positive-intrinsic-negative (PIN) photodiodes and avalanche photodiodes (APDs). These photodetectors are available with large areas which can increase the amount of

received optical power [76] – [79]. At the present time, ordinary PIN photodiodes are used in almost all commercial infrared links. PIN photodiodes are simpler to design, cheaper and require less complex biasing compared with APDs. However, PIN photodiodes are less sensitive than APDs. This disparity in sensitivity can be compensated by using a greater transmitter power and using a receiver with a larger lens diameter.

APDs can be looked upon as PIN devices which are operated with a high reverse bias. Photo-generated carriers generate secondary carriers via impact ionization, and this results in internal electrical gain. APDs are preferred in direct detection optical receivers when a small amount of background noise induces shot noise. This is due to the internal gain in APDs which can help overcome the thermal noise from preamplifiers and increases the receiver SNR. Impressive infrared link performance can be achieved from APD-based receivers when ambient light is weak [15], [16], [37], [78]. However, in situations where ambient-induced noise is dominant, APDs can result in degradation in SNR [37]. This is due to the random nature of the internal APD gain causing an increase in the variance of the shot noise by more than the signal gain.

The photodiode produces an instantaneous photocurrent ( $I$ ), when it receives an instantaneous optical power ( $P$ ) as:

$$I = R \cdot P, \quad (2.5)$$

where  $R$  is the photodiode responsivity (A/W). The responsivity represents the opto-electronic conversion factor from the optical domain to the electrical domain. The responsivity of the photodiode can be expressed as:

$$R = \frac{\eta q \lambda}{h_p c} \quad (2.6)$$

where  $\eta$  is the quantum efficiency of the device,  $q$  is the electronic charge ( $1.6 \times 10^{-19}$ ),  $\lambda$  is the wavelength,  $h_p$  and  $c$  are Planck's constant and the speed of light respectively. The internal quantum efficiency ( $\eta$ ) is the probability of the incident photon producing an electron-hole pair. Typical values of  $\eta$  range from 0.7 to 0.9. Responsivities of characteristic silicon photodiodes typically range from 0.5 A/W to 0.75 A/W within the 750nm - 950 nm wavelength bands.

Preamplifiers used for photo-receivers are classified into three types: low-impedance preamplifiers, high-impedance preamplifiers and trans-impedance preamplifiers. The low-impedance preamplifier is the most straightforward, but not necessarily the optimum design. Low-impedance preamplifiers have high noise and do not offer high receiver sensitivity. On the other hand, the high-impedance preamplifier's aim is to lower noise sources as much as possible. This is done by reducing the input capacitance by selecting a low capacitance, high frequency devices and detectors with low dark currents. The high-impedance preamplifiers provide high sensitivity, but an equalisation amplifier must be used to compensate for the poor bandwidth. In contrast, the trans-impedance preamplifier design has mostly overcome the drawbacks of high-impedance preamplifiers [77]. The main advantages of using trans-impedance amplifiers are a large dynamic range, and avoiding the need for equalisation (usually). For these reasons, the trans-impedance preamplifier is best suited to most of the applications of an infrared links; however, the noise level of the trans-impedance preamplifier is higher and its sensitivity is lower than that of the high-impedance amplifier. The noise level can be reduced using a field-effect-transistor (FET) as a front-end device instead of a bipolar-junction transistor (BJT) [77], [80]. But for power consumption, a BJT can provide better performance [80]. In this thesis, both EFT and BJT are considered and used.

### **2.4 Design Challenges of Indoor OW system**

The biggest challenge for an OW system designer is achieving a high SNR at the receiver. There are two reasons for this: first, the SNR of an IM/DD system relies upon the square of the average received optical signal power. This means that the system should transmit at a higher power level; however, the available transmit power is restricted due to skin and eye safety regulations [81]. It also means that the system should be designed to mitigate path loss and it should use a receiver with a larger collection area. The second reason is that background noise sources exist in many indoor environments, and this introduces white and low frequency cyclostationary noise into the receiver, which can degrade SNR. In addition to these limitations, OW signals are subjected to distortion due to multipath dispersion, which results in ISI, hence a restriction on the achievable bandwidth. Moreover, the bandwidth of optical wireless systems can also be restricted due to the large capacitance of a photodetector associated with its large active area. Therefore, the optical safety requirements, ambient light sources, multipath dispersion and a high photodetector capacitance can significantly limit the transmission data rate of indoor OW systems. These limitations are discussed in the following sections.

#### **2.4.1 Optical Safety Regulations**

Since OW links are limited by the need for transmitters to be safe, the laser source must emit optical power at a level that is safe [25], [82] – [84]. The main concern is that infrared light is invisible to the human eye, meaning that the eye has no internal defence against the emitted energy entering it. Eye safety is arguably the most important restriction on the emitted optical power level, and the primary hazard is that optical radiation may pass through a person's cornea and be focused on the retina by their eye's lens, at which point the risk of retinal burning is high. The level at which a person is exposed to this light, along with

the time of exposure, certain properties of the light beam, and its wavelength are all taken into consideration when trying to reduce potential hazards.

The two common sources of light in OW systems are LDs and LEDs, as explained in Section 2.3. The power emitted by LD and high-radiance LEDs in the range of 700 nm - 1400 nm is high-risk when it comes to retinal burns. Therefore, the International Electro-technical Commission (IEC) for safety standards has agreed upon a set of worldwide standards for LD / LED products and divided them into classes: 1, 2, and 3B, according to the accessible emission limit (AEL), the size of the optical source, its wavelength, and their combined potential hazards [83], [90]. Class 1 is considered inherently safe at the short wavelengths within which low cost devices operate. To eradicate the potential dangers of higher power emissions, various techniques have been proposed. For instance, light beams with large area sources are found to be much safer than those with smaller ones.

Class '2' is applicable only to visible light sources. Radiation in class 3B is considered to be dangerous. The maximum AEL output into the eye must not exceed 5 mW for a continuous wave laser [90]. This class can pose a hazard to the eye and skin in direct viewing condition. However, through diffuse reflection viewing, this class is safe. Laser sources which lie in the band of Class 3B, can have their status reduced to Class '1' by the use of an optical diffuser. It is a very important component that can be used to avoid such a hazard in laser sources. The diffuser is placed in front of the light emitter. It is used to destroy the source's spatial coherence and spread the radiation over a sufficiently extended emission aperture and emission angle to avoid potential retinal damage. Such a diffuser can achieve about 70% efficiency. Another type of diffuser that employs a computer-generated hologram (CGH) was proposed in [9], [12], [85] – [89]. This hologram physically breaks up the optical beam, scattering the image created on the retina, and is extremely efficient, with nearly a 100% success rate. This method typically yields a Lambertian radiation

pattern, which offers the designer the freedom to tailor the resulting pattern of the source radiation to the system's individual requirements. However, holograms are not without their flaws. A side-effect of their operation is that a 'hot spot' can be produced in the middle of the diffuse pattern. The intensity of the hot spot, which is higher than the rest of the pattern, can be reduced by careful manufacture.

### 2.4.2 Ambient Light

In pure fibre optic systems, the relevant light signal is kept separate from ambient light noise sources. This is not the case with OW systems where light noise sources interfere with the signal. OW receivers collect both the desired optical signal and ambient light (natural and artificial) noise sources. As shown in Figure 2.7, a photodetector captures some ambient light even with the use of a daylight filter in front of its active area, which it will convert to an electronic signal, hence generating substantial shot noise and resulting in a degraded SNR. Direct sunlight, fluorescent and incandescent lamps are the major ambient light sources in indoor environments [29], [56]. Indeed, the problem of ambient light is one of the most important factors that can degrade a receiver's sensitivity. Figure 2.7 shows the power densities of the three most common ambient light sources [16].

In OW systems, inexpensive daylight filters are widely used in order to mitigate the impact of ambient light sources. However, even with the use of such a filter the radiation emitted by incandescent light sources introduces substantial noise, compared to that introduced by daylight and fluorescent light sources, at wavelengths close to the peak sensitivity of most silicon photodiodes, as shown in Figure 2.3 and Figure 2.7 [16]. Tungsten filament and halogen lamps, for example, emit light within the pass-band of a daylight filter [60], resulting in light-induced noise that reaches the receiver and creates significant shot noise. Moreover, light from incandescent sources is directive and can lead to a burn-

out effect of the received signal, predominantly when the receiver is beneath the light source. Narrow band-pass filters may only be employed with laser diodes (LDs), and not with LEDs [91], [92].

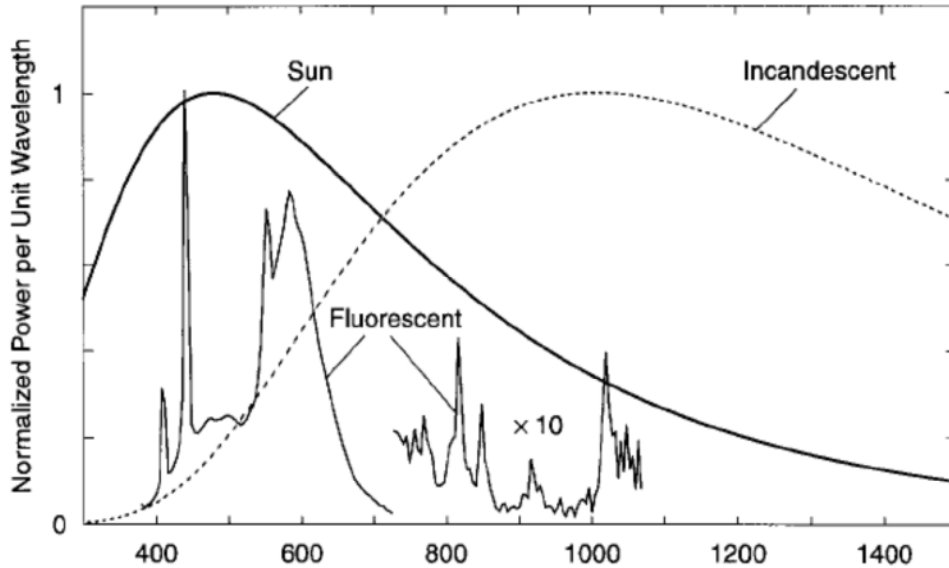


Figure 2.7: Spectral power densities of natural and artificial noise sources [16].

The properties of major light (noise) sources and their effect in OW systems have been studied in great depth in the last few years [42], [43], [56] – [61]. Some of these studies have shown that sunlight and incandescent light, such as halogen and tungsten filament lamps, produce the highest amount of noise in a system, while fluorescent light sources produces small amounts of background noise.

Fluorescent lamps can be classified into two forms: fluorescent lamps with conversion ballast (FLCB) and fluorescent lamps with electronic ballast (FLEB), and in the case of both of these, optical power is largely generated outside of a daylight filter’s pass-band [43], [57] – [61]. Although it is true that fluorescent light power when passed through a daylight filter is smaller than incandescent light power, it does not mean that the light emitted from fluorescent light has no

impact on the received optical power. Because of the coil ballast intrinsic to this kind of lamp's operation, the light flow that is produced comes in very fast pulses, and this can induce spectral lines in the resulting photodetector current [57] – [62]. Moreover, the electrical spectrum of a photocurrent generated by conventional ballast fluorescent light, has higher frequencies, going up to a few MHz [43], which may not be absorbed by the filter. Part of the solution to this is to use electric high-pass filtering and a careful choice of modulation technique [62], but this can induce a very large power penalty and lead to further ISI problems at a data rate of 10 Mb/s and beyond [62]. In an effort to combat these difficulties, differential detection [37] was introduced. After some analysis, other researchers have shown how this method may actually reduce interference from all artificial light sources [59]. Further to this, it was found that the interference of fluorescent light noise can be phased out even more via spread spectrum techniques [93].

Although light from the sun is a low-risk factor, it can nonetheless lead to a noticeably high shot noise at the receiver's end when the receiver operates close to a window. A key observation that helps in dealing with this is that sunlight is not subject to quick and random changes, which means that the irradiance it emits can be treated more or less as a steady flow of photons with very slow variations in intensity. The photodetector collects the light from the sun and from artificial sources and converts this into a photocurrent made up of two separate noise components - a Gaussian shot noise component and a DC component. The DC component is the simpler to eradicate, by using AC coupling. Therefore the shot noise induced by incandescent lamps, which cannot be removed by this process, is a major degrading factor in OW systems. This shot noise can be a further problem when the photodetector is positioned underneath incandescent lamps. This situation creates a system with a large variation in SNR; however, the source of this noise is directional (originating from ceiling or windows etc.), and therefore diversity detection techniques such

as angle diversity receivers and imaging receivers can be used to overcome this issue.

There have been many studies concentrating on different methods of reducing the effects of background noise [11] – [16], [94] – [108]. A narrow beam optical source in conjunction with a small FOV receiver was employed to reject background light. Angle diversity receivers can also be used to reduce the impact of surrounding noise, where each receiver is pointed in a different direction in order to collect the strongest possible optical signal and restrict the background noise sources [94] – [96], [102] – [109]. In this thesis, the dominant source of noise is due to background noise. Therefore, a number of systems using multiple non-imaging angle diversity receivers are studied in Chapters 4, 5 and 7 [113] – [117]. The signals received by each detector are processed using selection combining or maximum ratio combining, where the noisy signals (identified by the direction they came from) can be removed.

Another device that may substantially reduce the noise from ambient light while also improving a system's performance and reducing ISI is an imaging receiver [9], [118] – [123]. It was first proposed in [9]. Imaging receivers employ a large number of detectors that share a common concentrator with an acceptance semi-angle ( $\psi$ ), where each detector observes a small FOV associated with a single pixel in the detector array [123]. This, in turn, minimises the background light reception and multipath dispersion and maximises the SNR of the OW system. Previous work in [121] has shown that the use of multi-beam transmitters coupled with an imaging receiver can significantly reduce the total amount of power needed to drive a transmitter by at least 20 dB compared with a wide FOV non-imaging receiver. In this thesis, custom design of imaging detectors is proposed to cut down the ambient noise and multipath dispersion and also to reduce the size and cost of multiple non-imaging angle diversity receivers (Chapters 4, 6 and 7) [123] – [126].

### 2.4.3 Multipath dispersion

The main difference between RF and OW is that radio suffers from multipath fading while OW does not. This is due to the fact that the receiving photodiode spans several thousand wavelengths and also due to the square detector law where the output current of the photodiode is proportional to the squared electric field over the entire area of the photodiode surface. Spatial diversity can then prevent the impact of multipath fading [16], [37]. Freedom from fading has significantly simplified the design of OW links. Although multipath fading is not an impediment in OW links, there is still a problem with multipath propagation causing dispersion in the received signal, hence ISI.

Multipath dispersion is a big concern when designing an indoor OW system. This is attributed to the reflective properties of the OW channel. In an indoor OW diffuse channel, the transmitted signal propagates from the transmitter to the receiver, travels along multiple paths and can be reflected by walls and ceiling. These reflected signals result in time dispersion of the received pulse [108]. The signal spread in the channel causes ISI. However, in the case of directed LOS configurations, when the transmitter uses a narrow beam light source into a narrow FOV receiver, the effect of multipath dispersion can be negligible [101].

Moreover, the multipath propagation characteristics of the indoor diffuse channel rely upon the relative positions of the transmitter, the receiver and the reflectors and their optical properties. These characteristics can also be affected by the movement of people and objects. However, the movement changes are slow compared with the transmission rate. Therefore the channel can be considered stationary for specific transmitter and receiver positions. The channel impulse response can be described by the propagation of the optical signal between the transmitter and the receiver, which also relies upon the surrounding reflective surfaces. Since the transmitter, the receiver and the

reflective elements' positions are constant at a given location, the received optical power and delay can be considered deterministic for that location.

The impact of ISI induced by multipath propagation can be measured using the channel root-mean-square (rms) delay spread. In a typical indoor environment, at a data rate beyond 10 Mb/s, the ISI induced by multipath dispersion can be considered a major degrading factor [16], [37]. Different techniques have been suggested to reduce the severity of ISI. Angle diversity detection using narrow FOV detectors, which are pointed in different directions, rather than a wide non-imaging single FOV receiver, is proposed in [105] – [110]. These narrow FOV receivers can significantly reduce the impact of multipath dispersion by limiting the range of captured rays via the careful orientation and directionality of the detecting elements. Various diversity receiver structures have been proposed in the literature in attempts to find an optimum receiver structure that can significantly reduce multipath dispersion, such as the pyramidal fly-eye diversity receiver (PFDR) [11], [94], [95], [127] – [131]. In this thesis, the optimisation of three and seven angle diversity receivers with optical concentrators and filters is proposed, which lowers the impact of multipath dispersion, and also enhances the system performance [113] – [117]. Angle diversity receivers do present some drawbacks, including a large potential size and the cost of using multiple receiving elements. An alternative efficient method to overcome the limitations of ambient light noise and multipath dispersion is an imaging diversity receiver. In this work, we design a custom imaging receiver with 200 and 256 pixels, in order to enhance the overall system performance whilst reducing the effects of background noise and multipath dispersion [123] – [126].

Over the last two decades, many OW configurations have proposed, for example multi-spot diversity transmitter techniques in order to improve the OW system performance [9], [99], [134] – [144]. The concept of multi-spot transmitters was first proposed in [9]. It produces multiple diffusing spots pointing in different directions towards the reflecting surfaces (walls or ceiling).

This technique, coupled with narrow FOV receivers, has the advantage of combining both LOS and diffuse OW links, as well as reducing the impact of ambient light noise sources and multipath dispersion. A significant improvement in multi-spot diffusing systems can be achieved through the use of a line strip multi-spot system (LSMS) in conjugation with angle diversity receivers [129] – [130], [135] – [137], [140]. In [135] – [137], the authors have investigated the performance of LSMS against a conventional hybrid system (CHS) (where the transmitter is angled downward) and conventional diffuse system (CDS). The study has shown that the angle diversity LSMS performs better than CDS and CHS systems [137]. Moreover, employing line strip spot diffusing in the middle of the ceiling achieves better performance than uniform diffusing spots [135].

### 2.4.4 Photodetector High Capacitance

In an indoor environment, artificial (lamps light) and natural (sunlight) sources can produce significant background noise at an OW receiver. In addition, thermal noise can be induced by the photodetector resistance, preamplifier and amplifier or  $f^2$  noise component due to channel thermal noise of the front-end FET [141]. The other noise sources, such as shot noise induced by the received optical signal and the photodiode dark current noise, have a low impact compared with background and thermal noises.

The photodetector active area must be large enough to collect an adequate optical signal because optical transmission is restricted by eye and skin safety regulations and also because the transmitted optical signal undergoes temporal dispersion due to reflection from walls, ceiling and other objects. Unfortunately, the photodetector capacitance is directly proportional to its active area. This means that a large photosensitive area means a large capacitance, which results in a restriction on the attainable bandwidth. The capacitance at the input of the amplifier acts as a low pass filter (LPF), which limits the received high frequency components. Additionally, a large capacitance does not attenuate the

white thermal noise which occurs after the input stage, for example the thermal noise of a FET based preamplifier. This thermal noise can degrade the SNR at higher signal frequencies. When a white process following a LPF is referred back to the input of the filter, its power spectral density becomes quadratic in frequency and is known as  $f^2$  noise [141]. Because the  $f^2$  noise variance in an amplifier is directly proportional to the square of capacitance, using an array of photodetectors rather than a single photodetector can help mitigate the effect of  $f^2$  noise [141]. Furthermore, in a carefully designed receiver,  $f^2$  noise can be ignored. This is due to the insignificant amount of noise introduced in such a receiver when compared with the thermal and background noises.

An array of photodetectors, with an equivalent detection area, and with narrow FOV concentrators pointed in different directions, can be used instead of a single photodetector [68] in order to reduce the impact of a large photodetector and maximise the signal power collected. This is mainly based on diversity detection. Furthermore, a hemispherical lens can be employed to increase the effective area of the photodetector without using a large detector, as explained in Section 2.3.3.1 [16]. Additionally, the effects of the large area photodetector capacitance can be reduced by using circuit design techniques like bootstrapping [30]. In this thesis, multiple non-imaging angle diversity receivers and imaging diversity receivers are employed to improve system performance and also mitigate the impact of a large photodetector area [117], [123].

## 2.5 Signal Modulation Techniques

In OW systems, modulation occurs in two stages. In the first stage, the information to be transmitted is coded as waveforms and in the second stage these waveforms are modulated onto the instantaneous power of the carrier. Direct amplitude modulation is not preferable in practice due to the extensive amplitude fluctuations that affect optical wireless links. In the next section, we firstly define Intensity Modulation and Direct Detection (IM/DD) channels, and

then discuss the most suitable modulation schemes for IM/DD in indoor optical wireless systems: On-Off Keying (OOK), Pulse Modulation (PM) and Sub-carrier Modulation (SM).

### 2.5.1 IM/DD Channel

In OW links, intensity modulation is the most viable modulation type. The waveform is modulated onto the instantaneous power of the carrier. Direct detection is the most convenient down-conversion technique. A photodetector produces a current that is proportional to that of the received instantaneous power. Figure 2.1 shows the modelling of OW channels with IM/DD. The instantaneous optical power of the infrared emitter is shown as the transmitted waveform  $x(t)$ , while the instantaneous current in the receiving photodetector is shown as the received waveform  $I(t)$ . Multipath fading can occur where a detector is smaller than the wavelength, and this is because the received electric field can often display magnitude and phase spatial variations. However, because OW detector areas are typically millions of square wavelengths, spatial diversity occurs which helps prevent multipath fading. Therefore, no change is observed in the channel when the detector is moved commensurate with the order of the wavelength. OW channels can still be subject to multipath distortion when the transmitted optical power  $x(t)$  propagates along different paths.

### 2.5.2 On-Off Keying (OOK)

In OOK modulation, each bit is simply sent by switching the light source (LDs or LEDs) ON or OFF during its bit period. A '1' bit is encoded when the light source is ON, and a '0' bit is encoded when no signal is transmitted. It is the most common modulation scheme used in an OW system [15], [16]. There are two types of OOK modulation: Non-Return to Zero (NRZ-OOK) and Return to Zero (RZ-OOK). In NRZ-OOK, the transmission period of the transmitted pulse

is equal to the bit period ( $k=1$ ). However, RZ-OOK, with  $k=0.5$ , represents 50% of the duty cycle. A basic NRZ-OOK and RZ-OOK with a 50% duty cycle is shown in Figure 2.8. A high bit rate in the OW system can be offered using OOK modulation [54], [68]. However, at higher data rates the effect of multipath distortion is significant. Reducing the effects of multipath dispersion has been demonstrated using several equalisation techniques [48], [148] – [153].

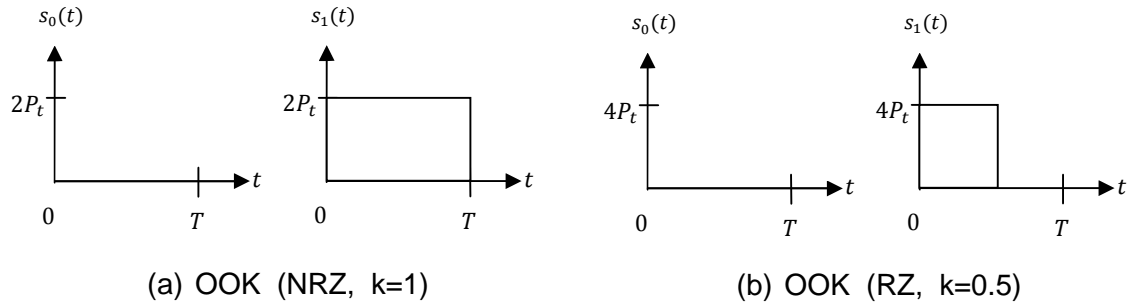


Figure 2.8: Basic NRZ-OOK and RZ-OOK signals [35].

### 2.5.3 Pulse Modulation

Modulation techniques that use minimum average transmitter power and make high-speed digital transmission achievable are required for indoor optical wireless communication. It is possible to achieve higher average power efficiency by using pulse modulation schemes where a range of time-dependent features of a pulse carrier are used to convey information. Examples of this type of modulation include pulse-position modulation (PPM) and differential pulse-position modulation (DPPM).

PPM is a technique that provides high power efficiency at the cost of relatively poor bandwidth efficiency [154], [155]. It is more susceptible than OOK to multipath dispersion. The impacts of ISI due to multipath dispersion in PPM can be reduced by using maximum-likelihood sequence detection, trellis-coded modulation and equalisation [142], [156], [157]. PPM techniques have been used widely in optical communications due to its low average power requirements [158], [159].

Furthermore, the average power efficiency of PPM can be improved by introducing L-level pulse techniques (*L*-PPM). *L*-PPM can increase the average power efficiency with an increasing order of *L*. *L*-PPM uses frames of *L* time slots. The input sequences of *M* bits are converted into the position of a pulse within the frame in PPM modulation ( $L = 2^M$ ). The frame is divided into *L* slots, each of which has duration  $T_{slot}$  and the power is only transmitted in one slot, while the other slots (*L*-1) have zero power. Figure 2.9 shows the possible waveforms of 4-PPM (*L*= 4) that represent two input bits [16]. The PPM contains a sequence of slots in which the pulse is placed. The slot number represents the binary value of the data word.

In the last two decades, various techniques have been introduced with PPM in order to improve bandwidth efficiency as well as supporting multiple users in the system [160] – [162]. Studies in [160], [161] have shown that a number of concurrent users can be supported when PPM is combined with code division multiple access (CDMA) techniques. Furthermore, a PPM scheme in which the pulses take the shape of the raised-cosine has been demonstrated in [162]. The authors have found that such a scheme can improve the bandwidth efficiency by 30% compared with the basic PPM bandwidth.

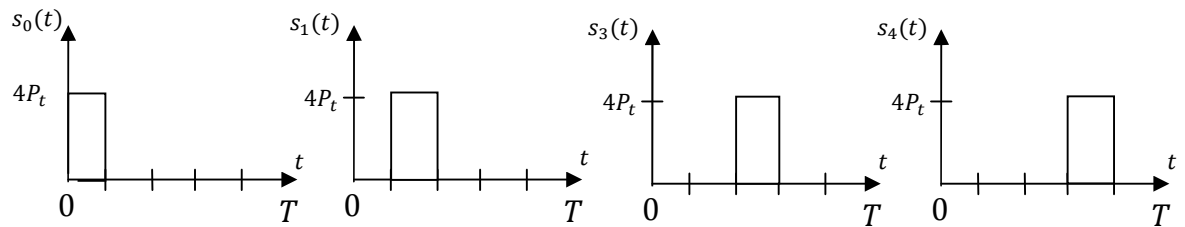


Figure 2.9: Possible waveforms of 4-PPM [16].

Differential pulse-position modulation (DPPM) can achieve better power and/or bandwidth efficiency than PPM in some applications where multipath ISI is minimal [144], [163]. It can be implemented by a simple modification of PPM.

Figure 2.10 (a) and (b) show the signal sets of 4-PPM and 4-DPPM respectively, where  $P_t$  in Figure 2.10 represents the average transmitted power,  $T$  represents the symbol duration for 4-PPM, while  $T$  in Figure 2.10 (b) represents the average symbol duration for 4-DPPM. As shown in Figure 2.10 (a), each 4-PPM symbol consists of three 'low' chips and one 'high' chip. A DPPM symbol can be obtained from the PPM symbol by removing all of the 'off' chips following the 'on' chip. The use of maximum-likelihood sequence detection is required in optimal soft decoding of DPPM, since 4-DPPM symbols remove the 'low' chips that follow the 'high' chips, and they have unequal durations and unknown symbol boundaries to detect. DPPM is easier to decode than PPM when hard decoding is employed. This is because DPPM does not require symbol-level timing recovery. Symbol synchronization is not essential with DPPM, which is considered as one of the advantages over PPM detection. In addition, DPPM can also achieve higher power and bandwidth efficiency than PPM.

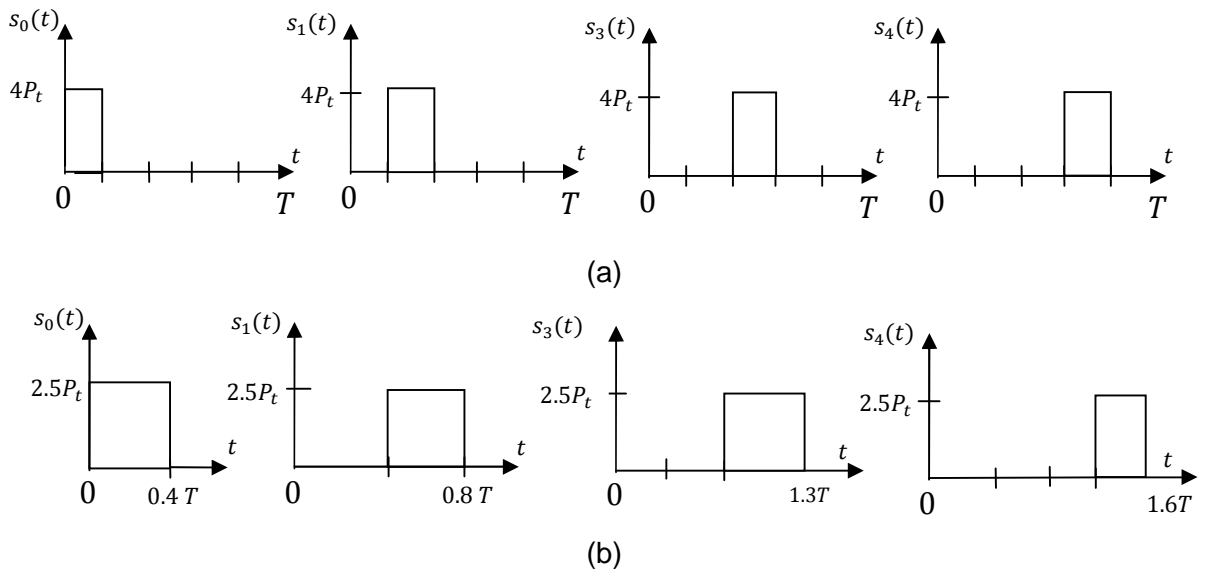


Figure 2.10: Comparison of transmitted waveforms for (a) 4-PPM, and (b) 4-differential pulse-position modulation (4-DPPM) [16].

### 2.5.4 Subcarrier Modulation (SM)

The main concern with high-speed single-carrier modulation schemes such as L-PPM and OOK is that they are wide band and suffer from ISI due to multipath dispersion especially at higher transmission rates. Single sub-carrier modulation (SSM) occurs when a bit stream is modulated onto a single radio frequency carrier which is further employed to modulate the optical signal. One such example is Binary Phase Shift Keying (BPSK). However, when bit streams are modulated into different radio frequencies (multiplexed), this type of modulation is termed multiple-sub-carrier modulation (MSM) [164]. The symbol rate of each sub-carrier in MSM is reduced relatively with the sub-carrier bearing the same total bit rate. Consequently, each sub-carrier becomes a narrow band signal. They undergo very little distortion and the receivers do not need to use equalisation.

## 2.6 Angle Diversity Receiver

As mentioned earlier, diffuse OW systems suffer from multipath dispersion due to the use of non-direct LOS transmission. The multipath dispersion can be mitigated via the use of an angle diversity receiver. This technique has been successfully used in optical wireless systems [11], [94] – [96], [127] – [131]. Angle diversity utilises multiple photodetectors with relatively small FOV which are pointed in different directions in an indoor environment. Each photodetector is oriented at a specific direction with different elevation and azimuth angles, so that light can be collected from different receiving angles [128]. Angle diversity receivers may also be used to reduce the impacts of surrounding noise sources by selecting the best photodetector that receives the strong desired optical signal with minimum background noise. Signals from the different sectors/receivers are amplified independently. The electrical signal in each branch (photodetector) can be processed using different methods, such as

Selection Combining (SC), Equal Gain Combining (EGC) and Maximum Ratio Combining (MRC) [129].

In the SC method, the receiver simply chooses the branch with the highest SNR among all branches. The way SC operates is usually based on testing the received signal components from each branch, then selecting the branch that has the best SNR. Moreover, SC can produce a significant reduction in the pulse spread, when directional narrow FOV receivers are used. However, using SC does not provide the best possible SNR among the diversity techniques. In the MRC method, the output signals of all the receiver branches are combined via an adder circuit in which each output is directly proportional to its SNR weight. In this technique, each branch is adjusted in weight independently according to its SNR in order to maximise the SNR at the output of the combiner. The purpose of this method is to reduce the dominant effect of background noise by assigning low weight values to the branch that is most affected by background noise. Hence, it improves the system performance. EGC, on the other hand, is similar to the maximum ratio combiner, but uses equal weight in all branches. Simplicity is the most attractive feature of EGC and it also avoids the need for SNR estimation, however MRC provides better performance.

## **2.7 Standards for Indoor OW Systems**

In recent years, we have witnessed the appearance of short distance optical wireless systems for a number of domestic and commercial uses: laptops, printers, palmtop computers, calculators and mobile phones. This is an exciting development. The importance of this technology has been demonstrated by the industry with the instigation of the Infrared Data Association (IrDA), which was established in 1993 [165]. The IrDA is dedicated to developing and endorsing infrared standards across a range of markets including hardware, software, components, peripherals, communications and consumer markets. In recent

years, the IrDA has established universal standards for short range, half-duplex LOS operating systems which operate at bit rates of up to 4 Mbps [26]. The IrDA has also developed a standard of Very Fast Infrared (VFIR) which provides a data rate of 16 Mb/s [166]. In the wake of this development, infrared technology can be used in applications and settings that require connectivity greater than the standard 4 Mb/s [167]. In fact, the IrDA is currently developing a standard interface which offers faster data rates beyond 100 Mb/s. In 2009, the IrDA has issued a standard for 1 Gb/s OW communications [168]. Based on these developments, a number of companies have introduced products which make use of optical wireless technology, and other such products are beginning to enter the market [169] – [171].

## 2.8 Summary

This chapter gave an overview of OW system design, including the transmitter (LEDs and LDs) and the receiver (PIN and APD) components, in addition to the classification of OW links (LOS and diffuse). It provided a comparison between OW and RF media. Moreover, design challenges of indoor OW systems, such as optical safety regulations, ambient noise, multipath dispersion and photodetector high capacitance, were addressed. Angle diversity receivers, in which each detector is pointed in a different direction, can be utilised to reduce the effect of background noise and multipath dispersion. Furthermore, optical concentrators and optical filters can be used to further enhance the performance of OW systems. Three common types of modulation schemes: OOK, PM and SM for IM/DD, were also considered in this chapter. The chapter concluded by describing standards for indoor OW systems.

# 3 Channel Modelling of an Indoor Optical Wireless (OW) System

## 3.1 Introduction

Several factors have to be considered in order to characterise indoor optical wireless systems. Firstly, an optical wireless link has to be modelled, considering the channel connecting the transmitter and the receiver. Secondly, background noise sources and multipath propagation must be modelled in an indoor setting to study their effect on the received data stream. Finally, a simulation package based on the first two steps is needed.

In an indoor OW setting, the optical signals are detected under the effect of surrounding noise sources, mobility, receiver noise and multipath dispersion. These aspects impair the performance of the OW system. In this chapter, tools are presented that are used to simulate the OW channel in an indoor environment. Two key OW transmitters are evaluated, namely the pure diffuse system (CDS) and the multi-spot diffusing configuration. The diffuse scheme does not depend on a direct path linking the transmitter and the receiver. The diffuse transmitter can be substituted by multi-spot diffusing transmitters, resulting in considerable improvement in the performance of the optical wireless system. The merits of both direct LOS and non-LOS are present in multi-spot diffusing transmitters. Important enhancement can be introduced through the use of a line strip multi-spot diffusing system (LSMS) [130], [135], [140]. Additionally, multipath dispersion and background noise can be further minimised through the use of angle diversity receivers [94] – [96], [110] – [117]. As a result of multipath propagation, a mathematical formulation and ray tracing are employed to compute the received optical power due to reflection elements.

The multipath propagation model is discussed in Section 3.3. Analysis of the delay spread of the received pulse is given in Section 3.5. Background noise is explained in Section 3.6 and the SNR evaluation is provided in Section 3.7 and used to analyse the impact of ambient noise on the indoor OW system's performance. Computations and simulations in this thesis were carried out using *Matlab*. The simulations results are summarised in Section 3.9 for a pure diffuse (CDS) configuration and multi-spot diffusing system (LSMS) coupled with angle diversity receivers. At the end of the chapter, a summary is provided.

## 3.2 Indoor OW Communication Channel

In indoor optical wireless communication, intensity modulation with direct detection (IM/DD) is thought to be the most suitable method as a result of its reduced cost and complexity [15]. As shown in Figure 3.1, at the transmitter side, the desired signal is modulated into the instantaneous optical power by varying the intensity of the optical source. The receiver makes use of a detector that produces a photocurrent  $I(t)$  which is proportional to the received instantaneous optical power. The typical detector area contains tens of millions of very short wavelengths of the received optical signal, and hence allows spatial diversity and prevents fading. The indoor optical wireless IM/DD channel can be completely investigated via its impulse response  $h(t)$ . It can be modelled as a linear baseband system [174], described by

$$I(t, Az, El) = \sum_{m=1}^{M_t} R x(t) \otimes h_m(t, Az, El) + \sum_{m=1}^{M_t} R n_m(t, Az, El), \quad (3.1)$$

where  $t$  is the absolute time,  $El$  and  $Az$  represent the direction of the arrival in elevation and azimuth angles respectively.  $M_t$  is the total number of reflecting elements,  $x(t)$  is the transmitted instantaneous optical power,  $\otimes$  denotes convolution,  $R$  is the detector responsivity and  $I(t, Az, El)$  is the received

photocurrent at a certain location resulting from  $M_t$  reflecting surfaces. Lastly,  $n_m(t, Az, El)$  represents the background light noise due to  $m^{th}$  reflecting elements at the receiver. In OW IM/DD, background shot noise and the receiver thermal noise can be modelled as white and Gaussian, and independent of  $x(t)$  [16], [85]. In (3.1), it should be observed that  $x(t)$  represents power and not amplitude. This implies that the signal should be non-negative. The total average transmitted power in (3.1) is provided by the average values of  $x(t)$  and not an integral of  $|x(t)|^2$  as is the case with electrical channels.

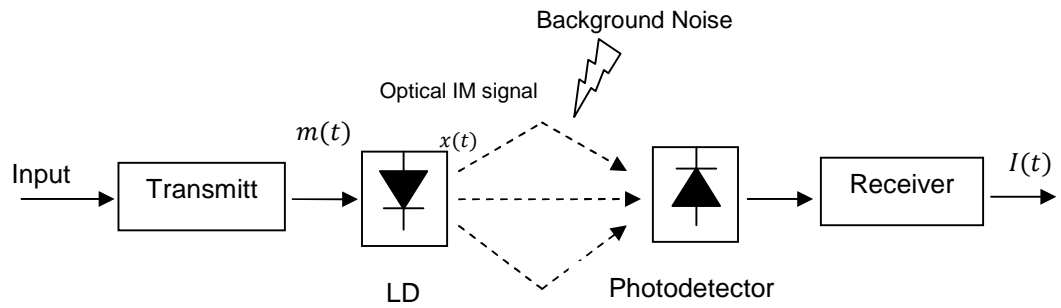


Figure 3.1: Block diagram of IM/DD OW system.

### 3.3 Multipath Propagation Model

The propagation characteristics of an indoor optical wireless channel depend on the relative positions of the transmitter, reflectors and receiver in addition to their patterns. These characteristics are also subject to the movement of objects and people. However, those changes are slow in comparison with the transmission rate. Therefore, the channel can be treated as stationary for particular transmitter and receiver locations. Multipath propagation results in the spread of the transmitted signal and the consequently ISI limits the attainable transmission rates. As the dimensions of the room increase, multipath dispersion increases as a result of the increase in the difference in paths length separating the longest and shortest paths in the room. Measurements to study

the reflection coefficients for a number of materials normally used in indoor settings were taken by Gfeller and Bapst [8]. They have shown that the reflection coefficients (ratio of reflected power to incident power) ranged from 0.4 to 0.9 and additionally with white plaster walls the reflection coefficients varied between 0.7 and 0.85 based on the surface consistency and angle of incidence. They also observed that the power reflected by either the walls or the ceiling is in a form similar to that of a Lambertian pattern. Thus, the reflecting elements for the walls, floor and ceiling were treated in their work and in this thesis as small emitters that diffuse the received signal in multiple paths from transmitter to receiver, which renders the diffuse channel more robust against shadowing. The power radiated from the transmitter into a solid-angle element  $d\Omega$  can be written as [34],

$$dP = \frac{n + 1}{2\pi} \times P_s \times \cos^n(\alpha) \times d\Omega, \quad (3.2)$$

where  $(n + 1)/2\pi$  assures that integrating  $dP$  over a hemisphere surface results in the total average transmitted optical power ( $P_s$ ) radiated by the laser source,  $\alpha$  is the angle of incidence with respect to the transmitter's normal and the parameter  $n$  represents the mode number that determines the shape of the radiated beam. The  $n$  mode number of the transmitted beam is related to the half-power semi-angle ( $hps$ ) according to

$$n = \frac{-\ln(2)}{\ln(\cos(hps))}. \quad (3.3)$$

Sources with a narrow beam have a higher value of  $n$  in order to concentrate the power at an area of interest, while  $n = 1$  corresponds to an ideal Lambertian source. As all surfaces are presumed to be rough, it is suitable to use  $n = 1$  which agrees with experimental measurements [8]. In this work, we

assume that the reflecting elements in a plaster surface have  $hps$  that is equivalent to  $60^\circ$ , which corresponds to  $n = 1$ .

#### 3.3.1 Ray-tracing implementation for Calculations of the Received Optical Power

As a result of multipath propagation, more than one path may be present between the transmitter and the receiver. Temporal dispersion is a result of these multiple paths. In order to compute the received optical power at the receiver, a ray-tracing algorithm can be used. The reflected optical rays from different reflectors are traced following all potential paths to the detector or other reflectors. Thus, for the implementation of ray-tracing, the reflective surfaces on the ceilings and walls are segmented further into small square-shaped reflecting surfaces where optical rays are reflected from such elements in a Lambertian pattern ( $n = 1$ ). The selection of a small size for these elements improves the accuracy of the impulse response determination, although at the cost of time spent in the ray tracing process. Therefore, a suitable selection is a compromise, i.e. a reasonable level of accuracy and an acceptable evaluation time. Previous researchers [8], [34], [140] have shown that the majority of the transmitted optical power is received within the first two reflections and the reflections beyond the second order were very small. Therefore, in this thesis up to second order reflections were considered in modelling the optical wireless channel and ambient light noise sources. Figure 3.2 shows the ray tracing set-up for a diffuse channel. The impulse response of the OW channel can be computed by tracing all potential light rays connecting the transmitter and the receiver.

The total received optical power ( $P_{total\ received\ power}$ ) at the receiver, considering the direct LOS component ( $P_{Direct\ LOS}$ ), first order reflections ( $dP_{(1)}$ ) and second order reflections ( $dP_{(2)}$ ) can be expressed as:

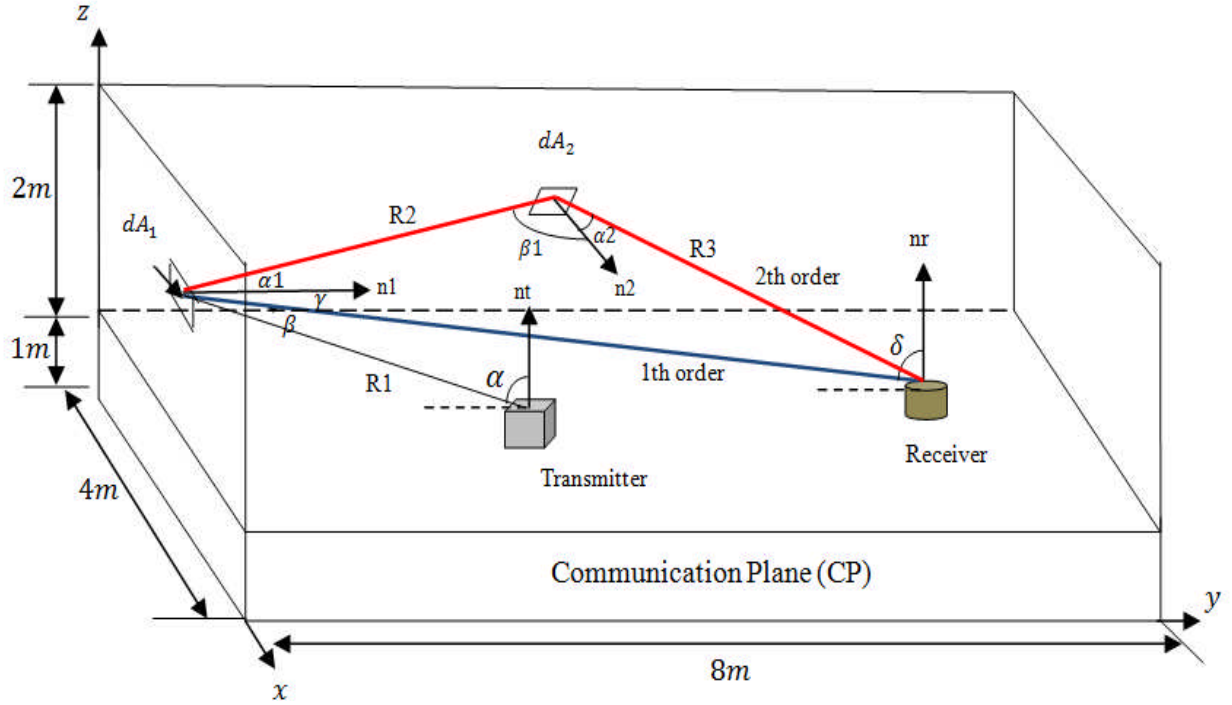


Figure 3.2: Ray tracing set up for first and second order reflections in a diffuse link.

$$P_{total\ received\ power} = P_{Direct\ LOS} + \sum_{i=1}^M dP_{(1)} + \sum_{i=1}^N dP_{(2)}, \quad (3.4)$$

where  $M$  and  $N$  are the total number of reflecting surfaces for the first and second order reflections in the room, respectively.

### 3.3.1.1 Direct Line-of-Sight (LOS) Calculation

A direct LOS link exists when a direct path connects the transmitter and the receiver. For instance, when the transmitter is placed on the ceiling facing downwards at a  $-90^\circ$  elevation angle in a down link channel, and the OW receiver faces upwards at an elevation angle of  $90^\circ$ , as shown in Figure 3.3, the direct received power ( $P_{Direct\ LOS}$ ) component can be expressed as:

$$P_{Direct\ LOS} = \begin{cases} \frac{n+1}{2\pi R_d^2} \times P_s \times \cos^n(\alpha) \times A_{eff}(\delta), & 0 \leq \delta \leq \psi_c, \\ 0, & \delta > \psi_c \end{cases} \quad (3.5)$$

where  $P_s$  represents the average optical power of the light source (LD or LED),  $\delta$  is the angle between the normal of the photodetector and the incident ray.  $A_{eff}$  is the effective area which can be founded from (Section 2.2, Chapter 2),  $\alpha$  is the angle between the normal of the transmitter and the incident ray.  $R_d$  is the direct link distance between the receiver and the transmitter. If the received angle ( $\delta$ ) is larger than the acceptance semi-angle ( $\psi_c$ ), then the direct LOS received power is reduced to zero. Light is only gathered by the receiver within the concentrator FOV ( $\psi_c$ ). Therefore, altering the FOV of the receiver can minimise the effect of unnecessary signals.

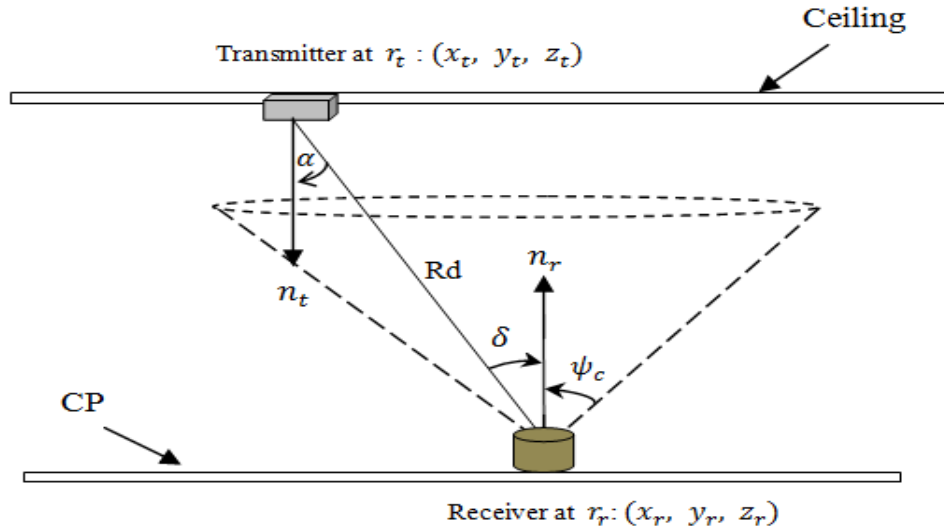


Figure 3.3: Calculations of direct transmitting and receiving angles.

As shown in Figure 3.3, the reception angle ( $\delta$ ) is first checked against the receiver's FOV. The incident ray on the receiver's photodetector is inside the detector's FOV if the reception angle is smaller than or equivalent to the

detector's FOV. The receiving and transmitting angles ( $\delta, \alpha$ ) are computed as follows:

$$\cos(\alpha) = \frac{\hat{n}_t \cdot (r_r - r_t)}{R_d}, \quad \cos(\delta) = \frac{\hat{n}_r \cdot (r_t - r_r)}{R_d}, \quad (3.6)$$

where the normal of the transmitter at location  $r_t$  is  $\hat{n}_t$  and  $\hat{n}_r$  is the normal of the receiver at locations  $r_r$ , respectively.  $R_d$  is the direct distance between the transmitter and the receiver. The subsequent link distance ( $R_d$ ) is used to calculate the vector length or distance linking two points:

$$R_d = \|r_r - r_t\| = \sqrt{(x_r - x_t)^2 + (y_r - y_t)^2 + (z_r - z_t)^2}, \quad (3.7)$$

where  $x_r, y_r, z_r$  and  $x_t, y_t, z_t$  are the receiver and the transmitter coordinates  $x, y, z$  respectively. The vector length joining the receiver and transmitter is utilised to calculate the time delay taken by the direct ray ( $R_d$ ) to reach the receiver. The speed of light rays travelling through air is  $3 \times 10^8$  m/s. The time delay is the ratio of the link length ( $R_d$ ) and the speed of light. It should be observed that both angles in (3.6) are equal if the receiver and transmitter are placed in parallel planes. This is relevant to the case when the transmitter is placed on the ceiling whereas the receiver is on the communication plane (CP). But, if the walls which are at  $90^\circ$  to the communication plane are considered or a different elevation angle of the receiver with respect to the communication plane is considered, then the transmitting and receiving angles are different. Both situations were considered when computing these angles.

#### 3.3.1.2 First Order Reflection Calculation

Figure 3.2 illustrates the ray tracing setup for first and second order reflections in the case of a fully diffuse system, where the receiver and the transmitter are situated on the CP. Third order and higher reflections are ignored as a result of

their minor contribution [16]. Supported by the findings of Gfeller and Bapst [8] that reflecting surfaces in the form of plaster walls can be considered as Lambertian reflectors ( $n_{reflector}=1$ ), with a reflector area  $dA_1$ , the received optical power of the first order reflections  $dP_{(1)}$  can be computed through the use of the Lambertian equation (3.2) twice, first from the source to the reflective surface and then from the reflective surface to the receiver as shown in Figure.

3.4:

$$dP_{(1)} = \begin{cases} \frac{n+1}{2\pi^2 R_1^2 R_2^2} \times P_s \times \rho_1 \times dA_1 \times \cos^n(\alpha) \times \cos(\beta) \times \cos(\gamma) \times A_{eff}(\delta), & 0 \leq \delta \leq \psi_c \\ 0, & \delta > \psi_c \end{cases} \quad (3.8)$$

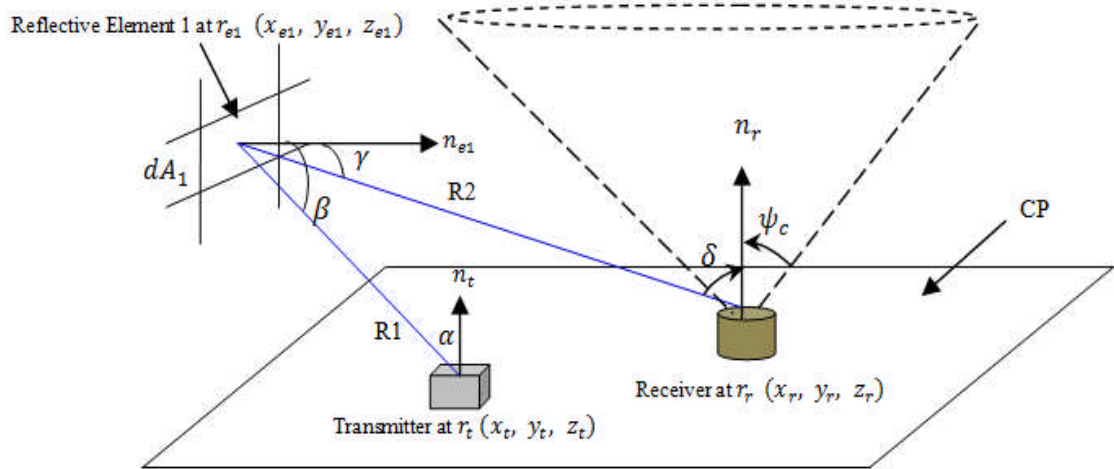


Figure 3.4: Ray tracing for first order reflection calculation.

where  $R_1$  is the distance between the reflective element and transmitter,  $R_2$  is the distance between the receiver and reflective element,  $\beta$  is the angle between the incident ray from the transmitter and the reflective element's normal,  $\gamma$  is the angle between the reflective element's normal and the reflected ray and  $\delta$  is the angle that joins the normal of the receiver and the

incident ray, as shown in Figure 3.4. The reflective surface turns into a secondary small transmitter where its retransmitted power is determined by its reflection coefficient  $\rho_1$  and the received optical power. Equation 3.8, above, illustrates that four angles are required, as seen in Figure 3.4, which can be computed as:

$$\left\{ \begin{array}{l} \cos(\alpha) = \frac{\hat{n}_t \cdot (r_{e1} - r_t)}{R_1}, \quad \cos(\beta) = \frac{\hat{n}_{e1} \cdot (r_t - r_{e1})}{R_1} \\ \cos(\gamma) = \frac{\hat{n}_{e1} \cdot (r_r - r_{e1})}{R_2}, \quad \cos(\delta) = \frac{\hat{n}_r \cdot (r_{e1} - r_r)}{R_2}, \end{array} \right. \quad (3.9)$$

where the normal of the reflective element 1 at location  $r_{e1}$  is  $\hat{n}_{e1}$ .

#### 3.3.1.3 Second Order Reflection Calculations

Broadening the reflection to additional surfaces and utilising the Lambertian model once more, the second order reflection is computed in three stages:

- 1- Calculation of the amount of incident optical power to the reflective element from the transmitter, which resembles the method used to calculate the direct power.
- 2- Calculation of the amount of incident optical power to the second reflective element from the first reflective element.
- 3- Calculation of the reflected power emitted from the second reflective element to the receiver.

Observe that the input power for the second reflective element is received from the first reflective element. Second order reflections use the same evaluation method as first order reflections, but they require more processing time. As shown in Figure. 3.5, considering first order reflection computations, the received optical by the second reflection ( $dP_{(2)}$ ) is given as:

$dP_{(2)}$

$$= \begin{cases} \frac{n+1}{2\pi^3 R_1^2 R_2^2 R_3^2} \times P_s \times \rho_1 \times \rho_2 \times dA_1 \times dA_2 \times \cos^n(\alpha) \times \cos(\beta) \times \\ \cos(\alpha_1) \times \cos(\beta_1) \times \cos(\alpha_2) \times A_{eff}(\delta), & 0 \leq \delta \leq \psi_c \\ 0, & \delta > \psi_c \end{cases} \quad (3.10)$$

where  $dA_2$  is the area of the second reflective element,  $\rho_2$  is the reflection coefficient of the second reflective elements,  $R_1$  is the distance between the transmitter and the reflective element 1.  $R_2$  is the distance between the reflective element 1 and the reflective element 2.  $R_3$  is the distance between the receiver and reflective element 2. The angle between the normal of the reflective element 1 and the incident light from the transmitter is  $\beta$ .  $\alpha_1$  is the angle that joins the first reflected ray  $R_2$  and the normal of the reflective element 1. The angle between the first reflecting ray  $R_2$  and the normal of the reflective element 2 is represented by  $\beta_1$ .  $\alpha_2$  is the angle between the second

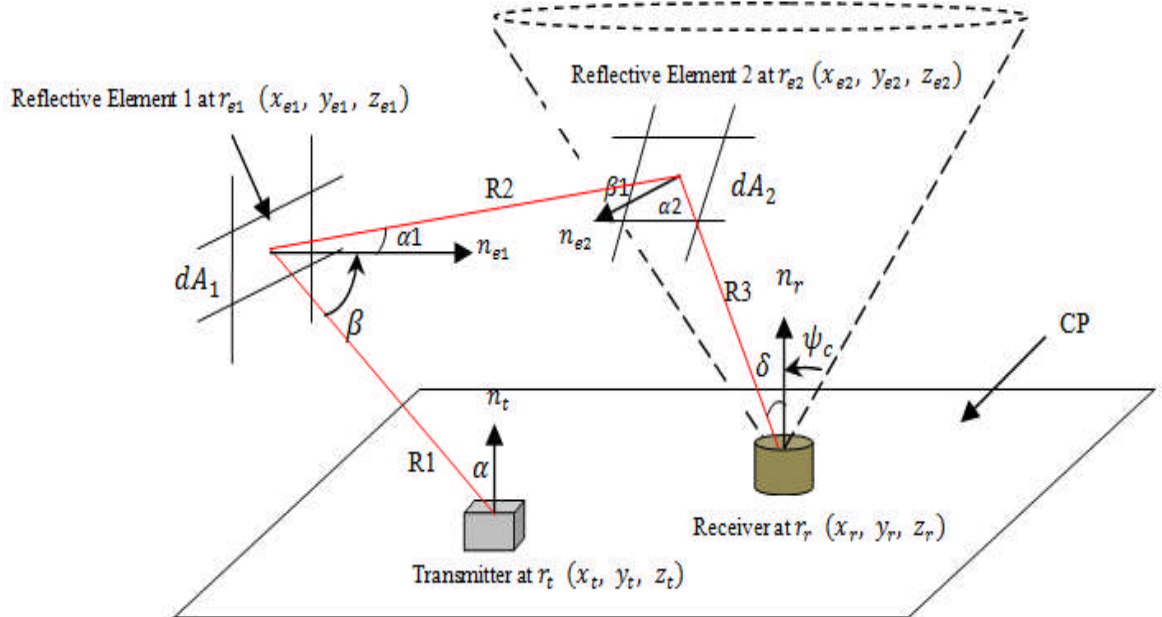


Figure 3.5: Second order reflected power analysis.

reflected ray  $R_3$  and the normal of the reflective element 2, and  $\delta$  is the angle between the normal of the receiver and the second reflected ray  $R_3$ .

As seen in Figure. 3.5, in second order reflection, six angles are required and can be computed similar to the calculation of the first order reflection and direct power by tracing the ray from transmitter to receiver as:

$$\left\{ \begin{array}{ll} \cos(\alpha) = \frac{\hat{n}_t \cdot (r_{e1} - r_t)}{R_1}, & \cos(\beta) = \frac{\hat{n}_{e1} \cdot (r_t - r_{e1})}{R_1}, \\ \cos(\alpha1) = \frac{\hat{n}_{e1} \cdot (r_{e2} - r_{e1})}{R_2}, & \cos(\beta1) = \frac{\hat{n}_{e2} \cdot (r_{e1} - r_{e2})}{R_2}, \\ \cos(\alpha2) = \frac{\hat{n}_{e2} \cdot (r_r - r_{e2})}{R_3}, & \cos(\delta) = \frac{\hat{n}_r \cdot (r_{e2} - r_r)}{R_3}, \end{array} \right. \quad (3.11)$$

where the normal of the reflecting element 2 at location  $r_{e2}$  is  $\hat{n}_{e2}$ .

## 3.4 Impulse Response

Practically, the impulse response of an OW wireless system is continuous; however, the model segments the reflecting surfaces (walls, floor and ceiling) into discrete elements. Therefore the impulse response displays the received optical power at the receiver within time intervals, i.e. 'time bins' based on the time taken by each ray to arrive at the receiver. As a result of successively tracing rays from the centres of different reflective elements, the time bin value was synchronized to the time taken by light to travel between neighbouring reflecting elements. A suitable suggestion for the time bin width is thus provided by [34], [175]:

$$time\_bin = \sqrt{dA}/c, \quad (3.12)$$

where  $dA$  is the reflection element area and  $c$  is the speed of light. Rays received within similar time intervals are assembled and stored for a particular transmitter-receiver position. An exact histogram of the practical impulse response is achieved as  $dA$  approaches zero. It should be observed that reduction of  $dA$  results in improved resolution in impulse response assessment together with an increase in the computation time. Thus the reflective element size  $dA$  has to be selected so as to maintain the computation time within acceptable limits [34], [94], [95]. The indoor optical wireless channel can be completely analysed via its impulse response  $h(t)$ . A number of parameters may be calculated from the impulse response such as delay spread and SNR, where the latter calls for determination of the receiver and ambient background noise.

### 3.5 Delay Spread

In indoor environments, the OW system is affected by multipath dispersion due to non-directed radiation. This causes spread of the received pulse signal and results in ISI. The channel spread can be quantified using the root mean square (rms) delay spread [85], [133]. The delay spread of an impulse response can be expressed as:

$$D = \sqrt{\frac{\sum (t_i - \mu)^2 P_{r_i}^2}{\sum P_{r_i}^2}}, \quad (3.13)$$

where  $t_i$  is the time delay associated with the received optical power  $P_{r_i}$  ( $P_{r_i}$  reflects the impulse response  $h(t)$  behavior within time bin interval) and  $\mu$  is the mean delay, which is given by:

$$\mu = \frac{\sum t_i P_{r_i}^2}{\sum P_{r_i}^2}. \quad (3.14)$$

The delay spread is deterministic, when the location of the transmitter, reflecting surfaces and receiver are unchanged (fixed). In this chapter, for every location, the delay spread is computed as the impulse response is calculated. In practice the delay spread may change for a given transmitter and receiver location if the reflecting elements in the room move, for example people entering and leaving and fans rotating. These effects are not considered here and have not been quantified by other researchers to the best of our knowledge.

## 3.6 Ambient Light Calculations

As opposed to fibre optic systems, an indoor OW communication system is impaired by natural as well as artificial light sources, which induce shot noise in the receiver. The main sources of ambient light are daylight, incandescent light and fluorescent light sources. These light sources induce a considerable amount of shot noise in silicon detectors in the wavelength range of operation and can saturate the detector if their power is high [56]. Even though ambient light sources can emit stronger optical power (noise) than the desired transmitted data, an optical filter may be utilised to reduce their effect.

Ambient light sources such as incandescent lamps can be modelled as a Lambertian sources based on the studies in [60], [176]. Therefore the total undesired received optical power at the receiver generated by an ambient light source ( $l$ ) can be generally expressed as:

$$P_{total\ noise,l} = \left( P_{n_{direct}} + P_{n_{reflection1}} + P_{n_{reflection2}} \right)_l, \quad (3.15)$$

where  $P_{n_{direct}}$  is the direct received noise power from the light source.  $P_{n_{reflection1}}$  and  $P_{n_{reflection2}}$  are the total received noise powers from the first and second reflecting elements respectively, over the room as illustrated in Figure 3.6.

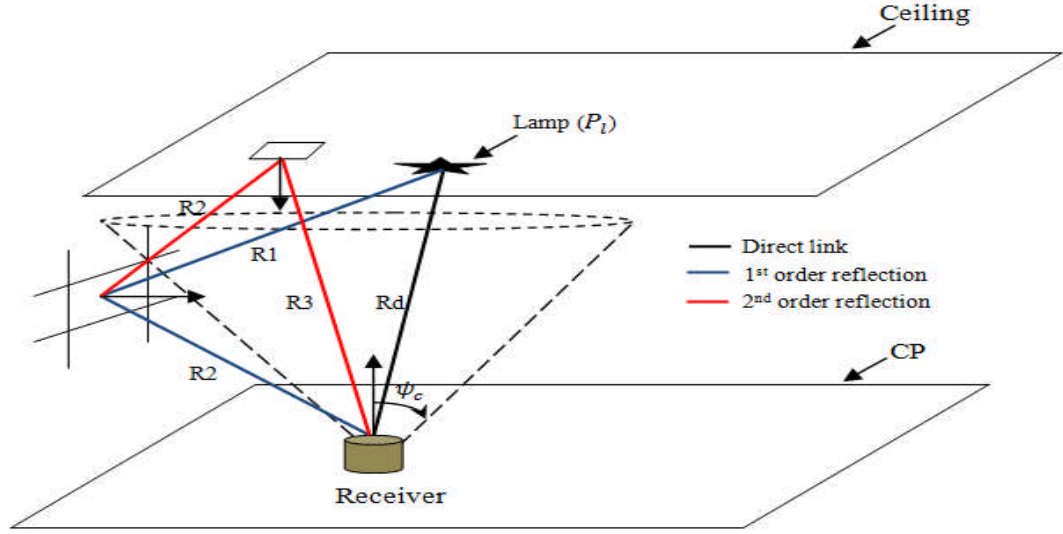


Figure 3.6: Modelling of the ambient light.

Subsequent to the direct and reflected assessment of the received optical signal previously provided in Section 3.3,  $P_{n_{direct}}$ ,  $P_{n_{reflection1}}$  and  $P_{n_{reflection2}}$  can be written as:

$$P_{n_{direct}} = \begin{cases} \frac{n_{Lamp} + 1}{2\pi R_d^2} \times (P_{lamp})_l \times \cos^{n_{Lamp}}(\alpha) \times A_{eff}(\delta), & 0 \leq \delta \leq \psi_c, \\ 0, & \delta > \psi_c \end{cases} \quad (3.16)$$

$$P_{n_{reflection1}} = \begin{cases} \frac{n_{Lamp} + 1}{2\pi^2 R_1^2 R_2^2} \times (P_{lamp})_l \times \rho_1 \times dA1 \times \cos^{n_{Lamp}}(\alpha) \times \cos(\beta) \times \\ \cos(\gamma) \times A_{eff}(\delta), & 0 \leq \delta \leq \psi_c \\ 0, & \delta > \psi_c \end{cases} \quad (3.17)$$

$$P_{n_{reflection2}} =$$

$$\begin{cases} \frac{n_{Lamp} + 1}{2\pi^3 R_1^2 R_2^2 R_3^2} \times (P_{lamp})_l \times \rho_1 \times \rho_2 \times dA1 \times dA2 \times \cos^{n_{Lamp}}(\alpha) \times \\ \cos(\beta) \times \cos(\alpha1) \times \cos(\beta1) \times \cos(\alpha2) \times A_{eff}(\delta), & 0 \leq \delta \leq \psi_c \\ 0, & \delta > \psi_c \end{cases} \quad (3.18)$$

The total noise power ( $P_{total\ noise\ power}$ ) reaching the receiver at a particular location is the summation of noise power reaching the photodetector from all the ambient light sources from various rays and can be expressed as:

$$P_{total\ noise\ power} = \sum_{l=1}^{L_{Lamp}} (P_{n_{direct}})_l + \sum_{l=1}^{L_{Lamp}} \sum_{m=1}^M (P_{n_{reflection1}})_l + \sum_{l=1}^{L_{Lamp}} \sum_{m=1}^N (P_{n_{reflection2}})_l \quad (3.19)$$

where  $L_{Lamp}$  is the total number of lamps employed in an indoor setting.  $M$  and  $N$  are the total amount of the first and second order reflective elements respectively. For the purpose of assessing the ambient light noise sources in the indoor office eight lamp lights, which cause strong optical spectral corruption of the received signal at the detector, have been selected. These were halogen lights, Philips PAR 38 type, which emit an optical power of 65 W transmitted in the form of a narrow beam with the prorogation mode  $n_{Lamp} = 33.1$  (based on the study reported in [60]), which correspond to a semi-angle of  $11.7^\circ$ . These lamps, spot lights, cause strong noise corruption for a receiver under their beam due to their high directionality. The lamps were situated on the ceiling with a distance of 1m separating them from all walls and identical separation distances of 2m between lamps, see Figure 3.7. Thus the initial four lamps are situated on the  $x=1m$  line at  $y=1m, 3m, 5m,$  and  $7m$ , and the other four lamps are situated along the  $x=3m$  line at the same  $y$  coordinates. The location of these sources is shown in Figure 3.7, in which the Cartesian points of these lamps are  $(1m, 1m, 3m), (1m, 3m, 3m), (1m, 5m, 3m), (1m, 7m, 3m), (3m, 1m, 3m), (3m, 3m, 3m), (3m, 5m, 3m), (3m, 7m, 3m)$ .

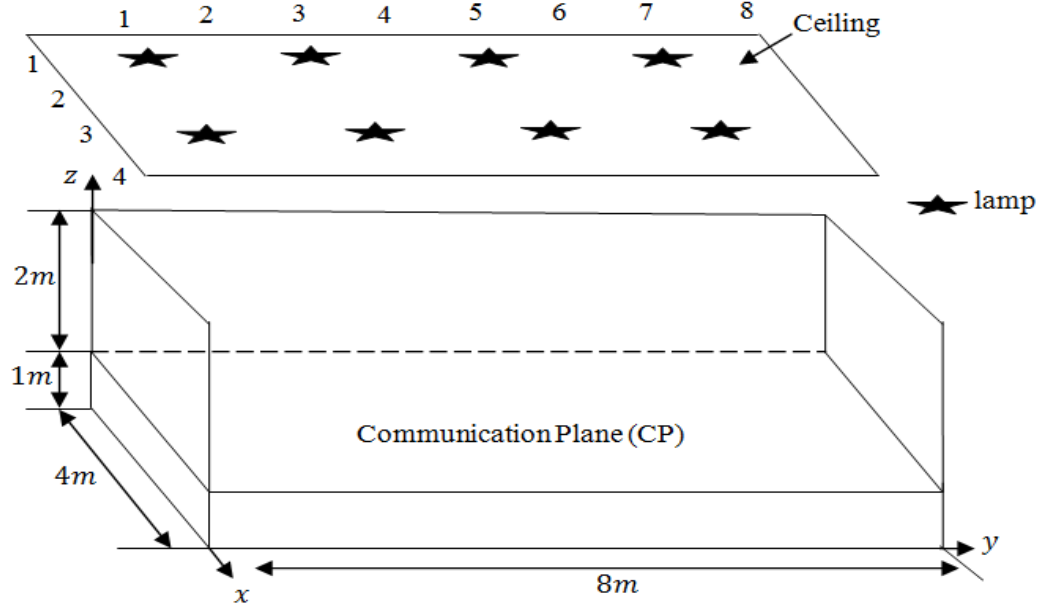


Figure 3.7: Eight spotlights distribution.

### 3.7 Calculations of Signal to Noise Ratio (SNR)

The OW system's performance is best evaluated using the SNR, which provides due consideration to the noise and signal spread (eye opening). The probability of error is expressed as:

$$P_e = Q(\sqrt{SNR}), \quad (3.20)$$

where  $Q(\cdot)$  is the Gaussian function and can be approximated as

$$Q(x) = \frac{1}{2} \operatorname{erfc} \left( \frac{x}{\sqrt{2}} \right) \approx \frac{1}{\sqrt{2\pi}} \frac{e^{-(x^2/2)}}{x} \quad (3.21)$$

The function has the value  $x=6$  at probability of error of  $10^{-9}$ . Hence,  $SNR = 36$  (15.6 dB) is needed for a  $10^{-9}$  probability of error.

In OOK the SNR associated with the received signal can be calculated by considering  $P_{s1}$  and  $P_{s0}$  (the powers associated to logic 1 and 0 respectively).

These powers ( $P_{s1}$  and  $P_{s0}$ ) determine the eye opening at the sample instant, thus ISI. The SNR is given by [77], [177]

$$SNR = \left( \frac{R(P_{s1} - P_{s0})}{\sigma_0 + \sigma_1} \right)^2, \quad (3.22)$$

where  $R$  is the photodetector responsivity ( $R = 0.54 \text{ A/W}$ ),  $\sigma_0$  and  $\sigma_1$  are the noises associated with the signal and can be calculated using

$$\sigma_0 = \sqrt{\sigma_{pr}^2 + \sigma_{bn}^2 + \sigma_{s0}^2}, \quad (3.23)$$

$$\sigma_1 = \sqrt{\sigma_{pr}^2 + \sigma_{bn}^2 + \sigma_{s1}^2}, \quad (3.24)$$

where  $\sigma_{s0}$  and  $\sigma_{s1}$  are the shot noises associated with the received signal  $P_{s0}$  and  $P_{s1}$  respectively. The signal-dependent noise ( $\sigma_{si}^2$ ) is small due to the weak received signal (in comparison to background light induced shot noise and receiver noise) and can be neglected based on the experimental findings presented in [56].  $\sigma_{bn}$  is the background shot noise component and can be computed from its relevant associated power level ( $P_{bn}$ ) as

$$\sigma_{bn} = \sqrt{2RqP_{bn}BW}, \quad (3.25)$$

where  $q$ ,  $R$ ,  $P_{bn}$  and  $BW$  represent the electron charge, the detector responsivity, the received background power and receiver bandwidth respectively.  $\sigma_{pr}$  in (3.23) and (3.24) represents the preamplifier noise. In this chapter, the preamplifier used is the 70 MHz PIN-BJT design by Elmirghani *et.al.* [30]. This receiver has a noise spectral density of  $2.7 \text{ pA}/\sqrt{\text{Hz}}$ . It relatively large bandwidth introduces minimal distortion at a data rate of 50 Mb/s, which is the data rate used. The preamplifier shot noise can be written as:

$$\sigma_{pr} = 2.7 \times 10^{-12} \times \sqrt{70 \times 10^6} = 0.023 \text{ } \mu\text{A}. \quad (3.26)$$

Substituting equations (3.23) and (3.24) in (3.22), the SNR can be expressed as

$$SNR = \left( \frac{R(P_{s1} - P_{s0})}{\sqrt{\sigma_{pr}^2 + \sigma_{bn}^2 + \sigma_{s0}^2} + \sqrt{\sigma_{pr}^2 + \sigma_{bn}^2 + \sigma_{s1}^2}} \right)^2. \quad (3.27)$$

In the angle diversity receiver, two schemes are considered: selection combining (SC) and maximum ratio combining (MRC). SC is a straightforward diversity method. The receiver merely chooses the branch with the largest SNR among the branches. The SC SNR is given by

$$SNR_{SC} = \max_k \left( \frac{R(P_{s1} - P_{s0})}{\sqrt{\sigma_{pr}^2 + \sigma_{bn}^2 + \sigma_{s0}^2} + \sqrt{\sigma_{pr}^2 + \sigma_{bn}^2 + \sigma_{s1}^2}} \right)_k^2, 1 \leq k \leq J \quad (3.28)$$

where  $J$  represents the total number of detectors used in the angle diversity method. Unlike the SC method, MRC makes use of all the branches. All the output signals from the branches are combined through an adder circuit. Each input to the circuit is weighed in proportion to the SNR of the relevant branch so as to maximise the output SNR. The weight of every branch is obtained as [129]:

$$w_k = \frac{R(P_{s1k} - P_{s0k})}{(\sigma_{0k} + \sigma_{1k})^2}, 1 \leq k \leq J. \quad (3.29)$$

The SNR at the output of the MRC is

$$SNR_{MRC} = \frac{(\sum_{k=1}^J R(P_{s1k} - P_{s0k})w_k)^2}{\sum_{k=1}^J (\sigma_{0k} + \sigma_{1k})^2 w_k^2} \quad (3.30)$$

Resulting in,

$$\begin{aligned}
SNR_{MRC} &= \frac{\left(\sum_{k=1}^J R(P_{s1k} - P_{s0k}) \frac{R(P_{s1k} - P_{s0k})}{(\sigma_{0k} + \sigma_{1k})^2}\right)^2}{\sum_{k=1}^J (\sigma_{0k} + \sigma_{1k})^2 \left(\frac{R(P_{s1k} - P_{s0k})}{(\sigma_{0k} + \sigma_{1k})^2}\right)^2} \\
&= \sum_{k=1}^J \left(\frac{R(P_{s1k} - P_{s0k})}{\sigma_{0k} + \sigma_{1k}}\right)^2 = \sum_{k=1}^J SNR_K. \tag{3.31}
\end{aligned}$$

This SNR analysis will be used in Section 3.9 to evaluate baseline systems (CDS and LSMS) and will also be employed to analyse new systems, as will be clarified in the next chapter.

### 3.8 Simulation Package

For the purpose of assessing the OW system performance under the impact of multipath propagation, user mobility and background noise, the channel impulse response of the OW system has to be evaluated and the background noise has to be determined. In this chapter, the impulse response and background noise evaluations are based on the mathematical formulation presented and a ray tracing algorithm built in *Matlab*. A simulation tool comparable to that in [34] is developed and employed to obtain the received optical power and generate the impulse response (the tool in [34] was developed for a simple diffuse transmitter).

Simulations were run in a typical rectangular room that was unfurnished, with dimensions of 4m width, 8m length and 3m height. The walls and ceiling were segmented into small reflective elements. The reflective elements were treated as small secondary emitters that diffuse the received signal in the shape of a Lambertian pattern, with reflectivity of 0.8 for walls and ceiling and 0.3 for the floor [8]. In this chapter reflections from windows and doors were considered to be similar to those from the walls. A realistic indoor environment is considered in Chapter 6. The accuracy of the received impulse response profile evaluated is controlled by the size of the reflective elements. Therefore,  $5\text{cm} \times 5\text{cm}$  and

$20\text{cm} \times 20\text{cm}$  surface element sizes for first and second order reflections, respectively, are utilised for all systems in this thesis. These values keep the calculation time within acceptable limits and the accuracy is not significantly improved for smaller element sizes as these element sizes (especially for first order reflections) capture the important feature sizes in the room [95]. Previous research has found that the majority of the transmitted power is inside the first and second reflections and that the power within third and higher order reflections are very small [8], [16], [34]. Therefore, reflections up to the second order are taken into account in our simulator. We compared the results of our simulator in the case of the CDS with experimental as well as theoretical results detailed in [8], [16], [34], and with the results for the LSMS reported by other researchers in [129], [130], [135], [140]. All the comparisons showed close agreement between the simulator used in the work reported in this thesis and the published theoretical and experimental results above giving confidence in the ability of our simulator to assess new optical wireless systems.

In order to assess the OW systems under the mobility, transmitters were positioned upright at two different positions on the communication plane, 1m above the floor, i.e. (2m, 4m, 1m) and (2m, 7m, 1m) for the fully diffuse system (CDS) as well as multi-spot configuration (LSMS). Both configurations transmitted 1 W optical power. In the case of the LSMS arrangement, a computer generated hologram (CGH) is assumed at the transmitter, resulting in the generation of multiple diffusing spots. The researchers in [179] have shown that the diffuse transmitter (CDS) can employ an integrating sphere as a diffuser to produce optical power from 100 mW to 1W. Furthermore, 1 W transmission power can also be handled by the use of CGHs [133]. The reduction in the total transmit power below 1W will be considered later in our new adaptive OW systems in Chapters 4, 5, 6, and 7 in order to comply with eye safety requirements. In order to evaluate the effect of mobility, the receiver was relocated at seven different positions along the  $x=1\text{m}$  line which scan the peaks and troughs of background noise sources. The receiver detector had a

photosensitive area of  $1\text{cm}^2$ . Eight spotlights are used, as explained in Section 3.6 to illuminate the room and this form background noise. In this work, we assume that signals underneath the communication plane (1m above the floor) are totally blocked. Moreover, we do not take into account the noise power of daylight from the windows.

## 3.9 Simulation Results

The purpose of our simulator was to assess the capability of the OW system under the influence of multipath dispersion, user mobility, background noise and receiver noise. In this chapter, the simulator was used to assess two indoor OW arrangements: a fully diffuse system (CDS) and a multi-spot diffusing configuration (LSMS). There are two main reasons for assessing the CDS and LSMS systems. The first is to ensure that our simulator is functioning and able to assess new OW systems. The second is to use these arrangements as a baseline reference for new OW configurations. The results of the simulation are reported in the form of impulse response, delay spread and SNR.

### 3.9.1 CDS with Single Wide FOV Receiver

The CDS is the basic optical wireless system. It has been thoroughly examined by many researchers in the field [8], [16], [34], [46], [47], [85], [141], [147]. For the CDS, the simulation of the channel impulse response was performed using a single detector with a wide angle of reception ( $\text{FOV}=90^\circ$ ) and an active area of  $1\text{cm}^2$ , and employing a fully diffuse source ( $n_{source} = 1$ ) as shown in Figure 3.8. The transmitter is placed in the middle of the room at (2m, 4m, 1m), whereas the receiver is located at two different positions: (a) near to the room corner at (1m, 1m, 1m) and (b) close to the transmitter at the centre of the room (co-located with the transmitter). These two positions of the receiver represent the weakest and strongest path of the diffuse system when the transmitter is

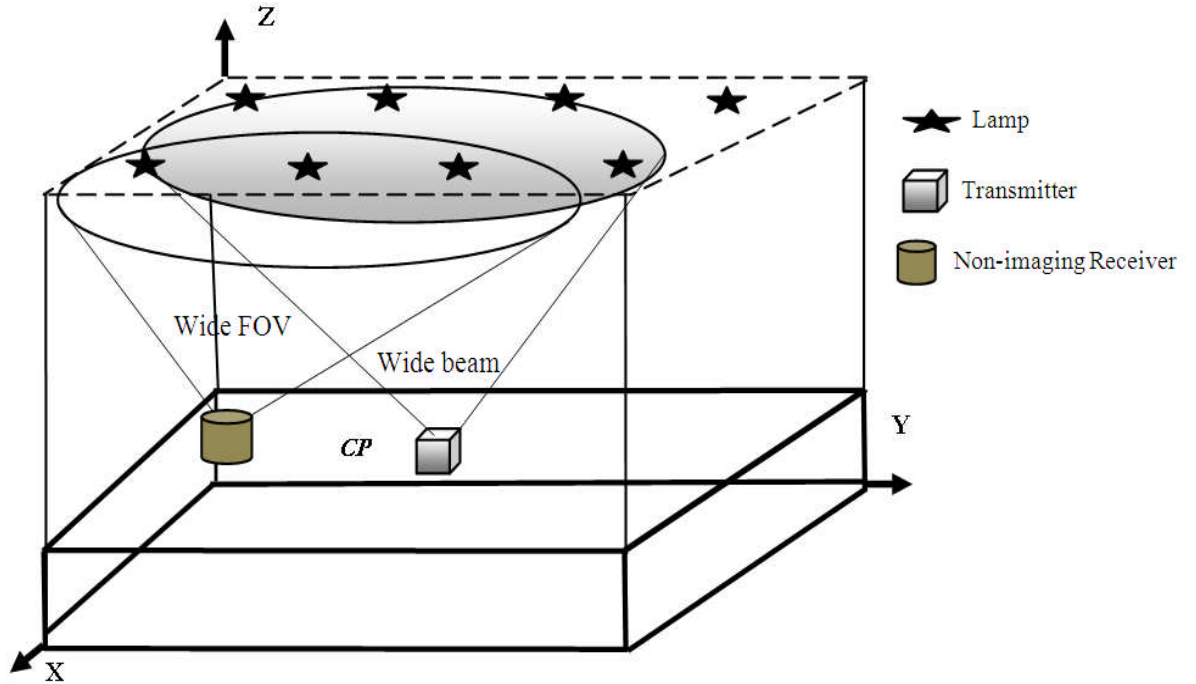
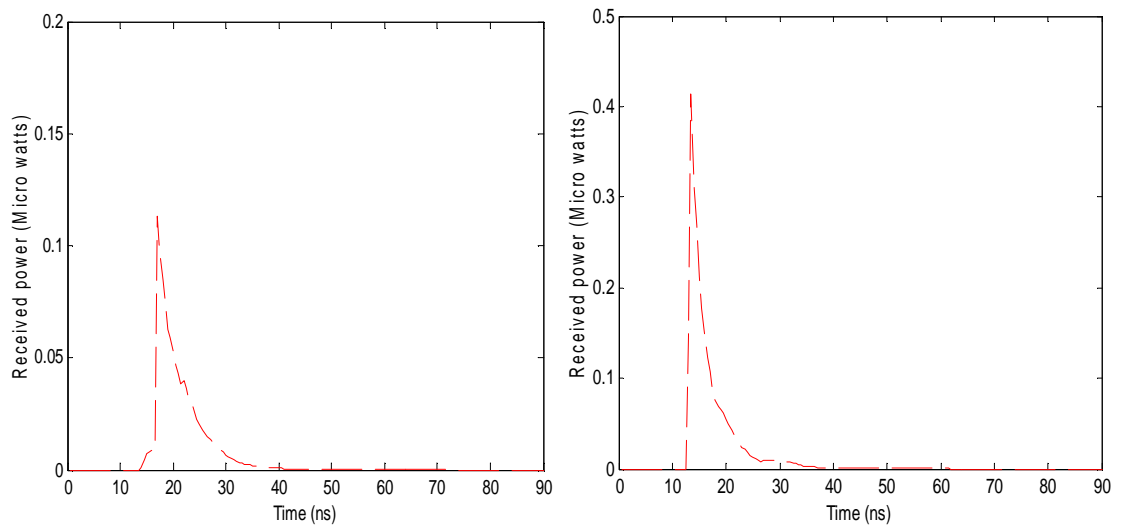


Figure 3.8: CDS with non-imaging wide FOV receiver.



(a) Receiver is placed at (1m, 1m, 1m)

(b) Receiver is placed at (2m, 4m, 1m)

Figure 3.9: Impulse response results for CDS when the transmitter is stationary in the middle of the room and the receiver moves to two different positions (a) (1m, 1m, 1m) and (b) (2m, 4m, 1m).

immobile at the centre of the room. The channel impulse response of the pure diffuse system is plotted in Figure 3.9. The results show that the shape of the channel impulse response is a function of the position of the transmitter and the receiver in the room. When the receiver is at the corner of the room at (1m, 1m, 1m), the received optical power is reduced in comparison with other receiver positions. When the receiver is co-located with the transmitter at the centre of the room, the received optical power is to  $0.413 \mu W$  compared with  $0.113 \mu W$ , (when the receiver is moved to the corner of the room). This improvement in the received CDS power is due to minimum distance between the transmitter and the receiver. For about 3m displacement between the transmitter and the receiver in CDS system, the indoor propagation of the transmitted signal results in a reduction in the received power by a factor more than 3 at the receiver. The impact of multipath propagation on the received signal is observed to result in temporal dispersion, hence potentially ISI.

### **3.9.2 LSMS with Single Wide FOV Receiver**

As opposed to the previous arrangement (CDS), performance enhancement can be achieved by the use of multiple beams (diffusing spots) in OW configurations. A simple structure of diffusing spots, LSMS, coupled with a wide FOV receiver was proposed and reported in [130], [135]. Such a configuration merges the benefits of OW LOS systems and diffuse systems. A LSMS transmitter provides multiple diffusing spots with equal intensities,  $80 \times 1$  beams, aimed at the centre of the ceiling in the shape of a line strip with a space of 10 cm separating adjacent spots, when the transmitter is placed in the middle of the room, as illustrated in Figure 3.10. The total optical power emitted by the LSMS transmitter was 1 W, which remains unchanged for the purpose of comparison with the CDS system; therefore, each spot has  $12.5 mW$ . Diffusing spots on the ceiling can be accomplished by using a holographic diffuser on the front of the emitter or by employing multiple laser sources to produce collimated beams [46], [89]. Furthermore, an alternative method of creating multiple spots

is by employing a CGH beam-splitter at the transmitter as in [85], [133]. This technique can produce an accurate power distribution overall the spots. These diffusing spots on the reflective surface (ceiling) act as secondary transmitters which emit Lambertian transmission. [9], [85], [129] – [137], [88], [89], [181], [182]. As the beams emerging from the transmitter in the multi-spot channel are nearly collimated, we neglect the path loss between the transmitter and the ceiling based on the practical findings in [9]. In an indoor environment, the walls and ceiling are considered as Lambertian reflectors for first and second order reflections, as clarified earlier. A LSMS arrangement performs better than a uniform multi-spot diffusing structure [181].

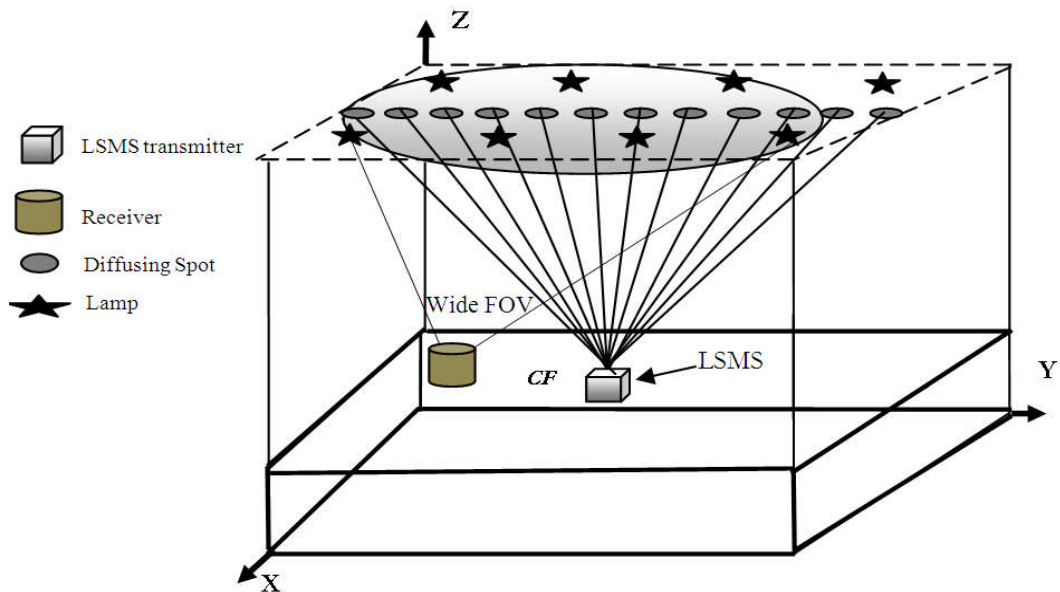


Figure 3.10: OW communication system with LSMS transmitter and wide FOV receiver.

Figure 3.11 compares the channel impulse response of the CDS and LSMS systems employing a wide FOV receiver, when the receiver is moved near to the room corner at (1m, 1m, 1m) and the transmitter is stationary in the middle of the room. The multi-spot LSMS system performs better than the CDS system. This is attributed to the fact that the channel impulse response of the LSMS contains many peaks associated with different direct LOS components between the diffusing spots and the receiver, hence increasing the received

optical power. The result of the delay spread distribution of these systems is portrayed in Figure 3.12. The transmitter is positioned in the middle of the room (2m, 4m, 1m) and the receiver is moved across the  $x=1\text{m}$  line. It is observed that the delay spread associated with the LSMS transmitter is much lower than that of the CDS configuration. In the case of the diffuse system, it is clearly visible that there is a direct relation between the delay spread and the transmitter receiver separation where the delay spread increases when the receiver moves away from the transmitter, i.e., near to the room corner. The LSMS with a single wide FOV receiver can reduce the delay spread from 2.4 ns associated with the diffuse system to 1.3 ns. This significant reduction in delay spread can help reduce ISI and hence reduce the bit-error-rate (BER).

### 3.9.3 LSMS with Angle Diversity Receiver

The effect of pulse spread as well as directional surrounding light noise sources can additionally be minimised by the use of an angle diversity receiver. Unlike the wide FOV receiver, the angle diversity receiver employs multiple non-imaging detectors that point in different directions. The small FOVs of these

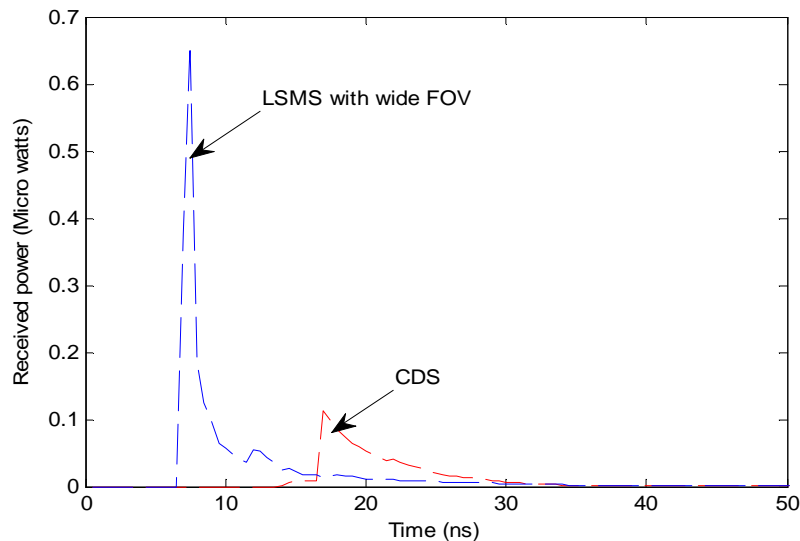


Figure 3.11: Impulse response of CDS and LSMS when the transmitter is placed at (2m, 4m, 1m) and a wide FOV receiver is placed in the room corner.

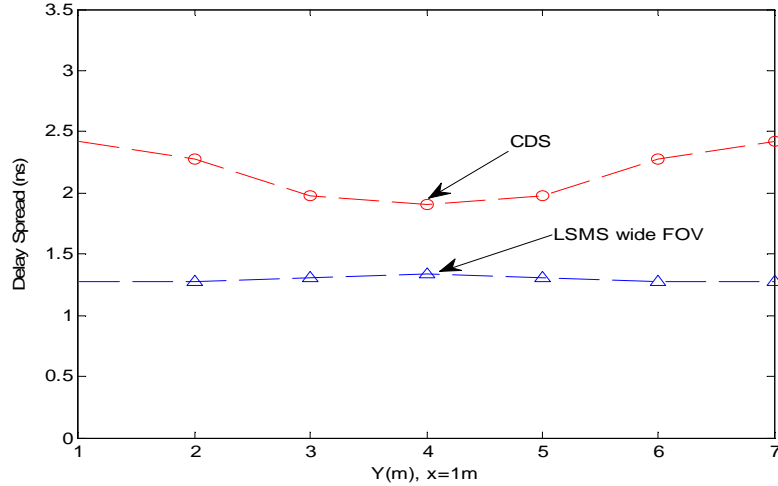


Figure 3.12: The delay spread of CDS and LSMS with a wide FOV receiver, when the transmitter is at (2m, 4m, 1m) and the receiver moves along the y axis at constant  $x=1m$ .

detectors are chosen in order to collect a strong optical signal and restrict the background noise sources. The photocurrents at each detector can be amplified separately and processed using different techniques such as SC and MRC. These techniques can enhance the system performance. The square pyramid-like diversity detection system considered comprises three detectors, mounted on three pyramid faces, as illustrated in Figure 3.13 (a). Each receiver direction can be described by two angles: Azimuth ( $Az$ ) and elevation ( $El$ ) angles. The  $El$  of two photodetectors stays at  $35^\circ$  and the detector that faces upwards is set at  $90^\circ$ . The  $Az$  angles of the branches are  $0^\circ$ ,  $180^\circ$  and  $0^\circ$ . The FOV of these branches is set in the following way: two are limited to  $35^\circ$ , while the detector facing upwards is set at  $20^\circ$ . The values of  $El$ ,  $Az$  and FOV were chosen using an optimisation that resembles that used in [94], [95], in order to achieve the highest SNR.

The CDS and LSMS with a wide FOV receiver described in Sections 3.9.1 and 3.9.2, use a detector that faces upwards, but this is not the case for angle diversity receivers and therefore modifications in the calculation of the reception angle ( $\delta$ ) are required. In the angle diversity receiver, the calculation of the

reception angle has to consider the  $El$  and  $Az$  angles and the reflecting element by using the analysis in [94]. Considering Figure 3.13 (b), in order to calculate the reception angle ( $\delta$ ) for any detector pointing at  $(x_r, y_r, z_r)$  over the CP, a point  $P$  was defined, positioned on the detector's normal, 1m over the detector. A triangle may be created by linking the middle of a reflecting element  $E$ , the middle of the detector and point  $P$ . Thus, the angle of reception from surface element  $E$  onto a detector of angle diversity is given by [94]

$$\cos(\delta) = \frac{|PR|^2 + |ER|^2 - |EP|^2}{2 |PR| |ER|}, \quad (3.32)$$

where  $|RP|$  is the distance between the receiver and a common point  $P$ ,  $|ER|$  represents the distance between the receiver and the reflective element  $E$  and  $|EP|$  is the distance between the reflective element  $E$  and the point  $P$ . These distances are given by:

$$|PR|^2 = 1 + \left(\frac{1}{\tan(El)}\right)^2. \quad (3.33)$$

$$|ER|^2 = (x_r - x_E)^2 + (y_r - y_E)^2 + (z_r - z_E)^2. \quad (3.34)$$

$$|EP|^2 = \left[ \left( \left( \frac{\cos(Az)}{\tan(El)} \right) + x_r \right) - x_E \right]^2 + \left[ \left( \left( \frac{\sin(Az)}{\tan(El)} \right) + y_r \right) - y_E \right]^2 + [(z_r + 1) - z_E]^2. \quad (3.35)$$

The angle diversity receiver was implemented in conjunction with a multi-spot diffusing transmitter (LSMS). This physical structure of the angle diversity receiver is able to observe the spots over the communication plane when the transmitter is at the centre of the room. The channel impulse responses of the CDS, LSMS with wide FOV and LSMS coupled with an angle diversity receiver

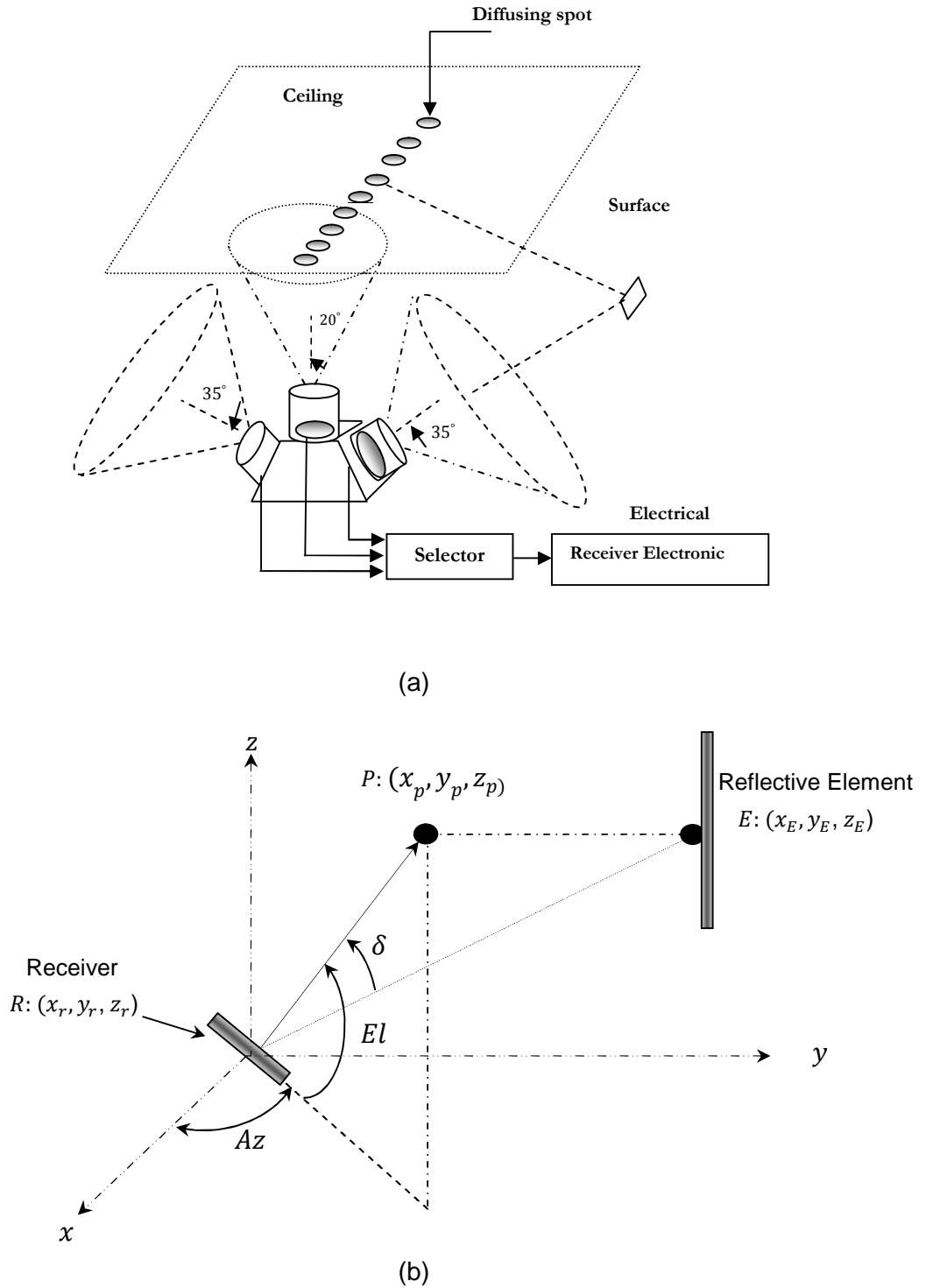


Figure 3.13: (a) Physical structure of an angle diversity receiver, (b) single element receiver (non-imaging) that employs a concentrator coupled with a single detector.

are shown in Figure 3.14. The transmitter is located in the middle of the room and the receiver is moved near to the room corner. It is obvious that the LSMS integrated with angle diversity receivers operates better than the CDS and the LSMS with a wide FOV receiver. The angle diversity LSMS system minimises the pulse spread of the received optical signal compared with wide FOV spot-diffusing arrangement. This is attributed to the small FOVs of the diversity receivers. These FOVs restrict the number of reflected rays captured in addition to the number of diffusing spots' contributions, hence maintaining the high power component from spots (LOS equivalent) and minimising the contribution from reflective elements. The enhancement in impulse response can reduce the delay spread and improve the SNR of the angle diversity LSMS configuration. Note that a single narrow FOV receiver employed with the LSMS can achieve comparable delay spread, but is not able to select spatial orientations (as the diversity receiver is able to) to reject background noise.

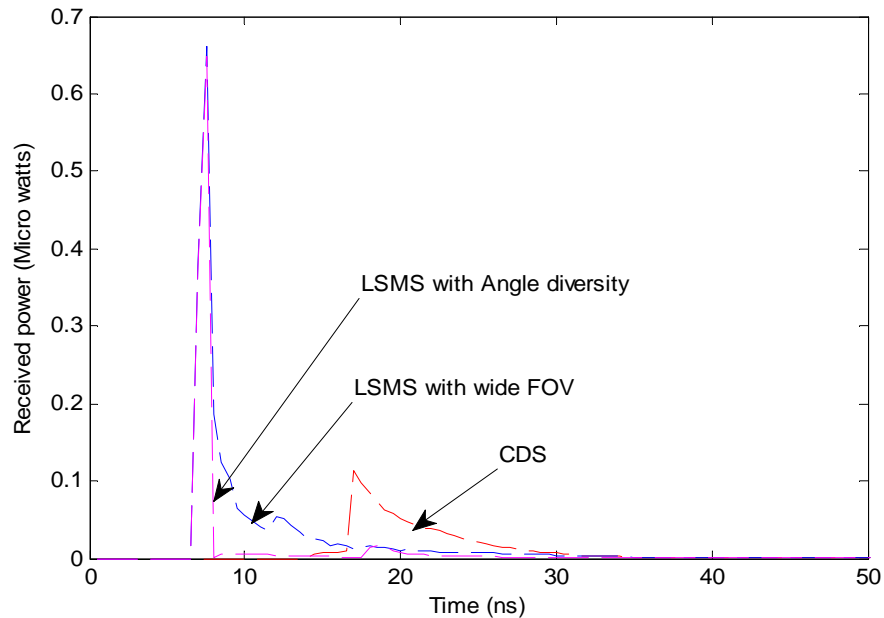


Figure 3.14: Impulse response of the CDS and LSMS both with wide FOV receivers, and LSMS with an angle diversity receiver, transmitter at (2m, 4m, 1m), all receivers are in the corner of the room on the CP.

The result of delay spread for all three arrangements (CDS, LSMS with wide FOV receiver and LSMS with angle diversity receiver), when the transmitter is positioned in the middle of the room and the receiver is moved across the  $x=1\text{m}$  line above the CP, are plotted in Figure 3.15. The LSMS integrated with the angle diversity receiver has the smallest delay spread in comparison with the other arrangements. This is due to the restricted FOV of the diversity receivers. The LSMS coupled with angle diversity reduced the delay spread by more than a factor of 3 in comparison with the CDS. Furthermore, Figure 3.15 shows that the diversity receivers reduced the delay from 1.3 ns for the wide FOV LSMS to about 0.7 ns. The impulse response and delay spread results for the CDS and LSMS systems are closely matched with previous work reported in [16], [86], [34], [135], [140].

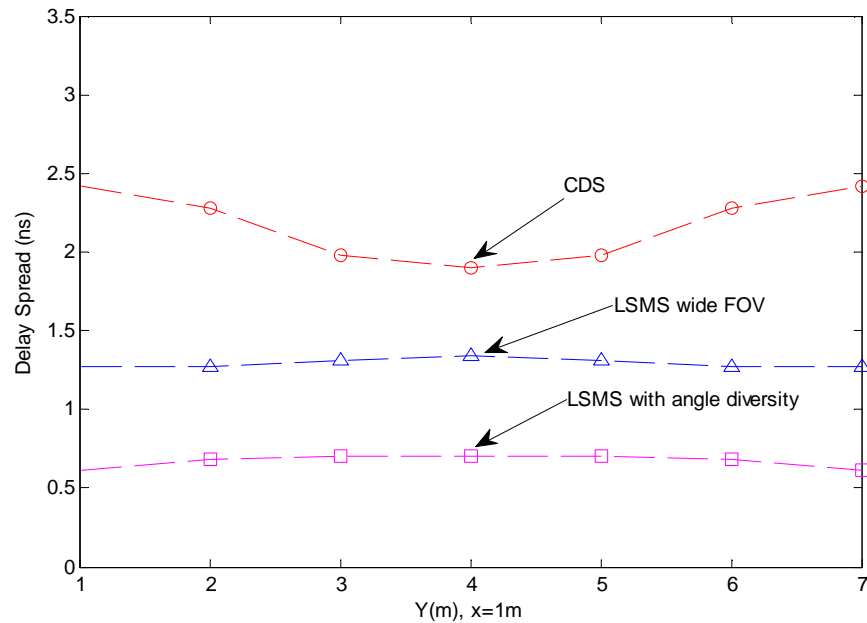


Figure 3.15: delay spread of CDS and LSMS with a wide FOV receiver, LSMS with angle diversity receiver, when transmitter at (2m, 4m, 1m) and the receiver moves along y axis at constant  $x=1\text{m}$ .

In order to assess the performance of the multi-spot diffusing configuration (LSMS) and the diffuse system (CDS) under mobility, transmitters are positioned upright in two different positions on the CP, 1m above the floor i.e.,

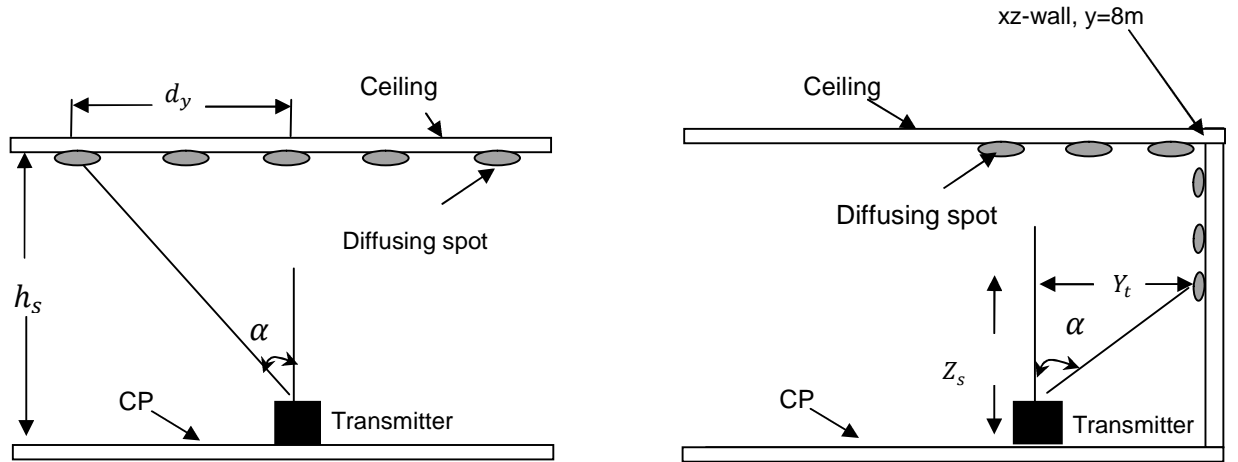
(2m, 4m, 1m) (2m, 7m, 1m), whereas the receiver moves across  $x=1m$ . The movement of the LSMS configuration on the CP, however, causes alterations to the positions of diffusing-spots but does not alter the angles of the beams with respect to the transmitter normal. Therefore, the new coordinates of the spots as a consequence of the transmitter mobility over the CP can be recalculated with respects to the reference location of the transmitter in the middle of the room. To aid visualisation of the mobile LSMS arrangement, Figure 3.16 shows the transmitter in two different positions. The LSMS transmitter in the middle of the room (2m, 4m, 1m) was considered as a reference for comparison with other transmitter positions in the room. So as to encompass spot mobility, the transmission beam angles ( $\alpha_i$ ) with respect to the transmitter normal can be computed by utilising the trigonometry of rectangular triangles, whereby spot angles are determined at the reference point and taken into account for each transmitter movement. The beam angles of the spots are provided by

$$\alpha_i = \tan^{-1}\left(\frac{d_y}{h_s}\right), \quad 1 \leq i \leq N_s \quad (3.36)$$

where  $d_y$  represents the horizontal distance separating the transmitter's normal and the diffusing spot alongside the y-axis and  $h_s$  is the height of the spots and  $N_s$  is the total number of the spots. These angles are fixed for all transmitter positions. Subject to user mobility, the spot positions and height change accordingly. When the transmitter is relocated from (2m, 4m, 1m) to (2m, 7m, 1m), some spots begin to emerge on the  $xz$ -wall, as seen in Figure 3.16. The new spot height ( $Z_s$ ) on the wall can be computed by considering the reference beam angle related to each spot as follows:

$$Z_s = \frac{Y_t}{\tan(\alpha_i)}, \quad (3.37)$$

where  $Y_t$  is the horizontal separation distance along the y-axis between the transmitter's normal and the diffusing-spot at the new position. Thus, our computations are performed for all the spots to determine the new spot locations based on the reference point when the transmitter is in the middle of the room.



(a) Transmitter at (2m, 4m, 1m)

(b) Transmitter (2m, 7m, 1m)

Figure 3.16: Transmitter of an LSMS configuration placed at the room centre, where a line of spots is formed on the ceiling (b) diffusing spots on the side wall (x-z wall).

From the evaluation of SNR in Section 3.7, Figure 3.17 shows the detected SNR for three transmitter configurations, namely the CDS and the LSMS with wide FOV and the LSMS in conjunction with angle diversity reception, when the system operates under the impact of surrounding noise sources (eight spotlight lamps with  $n=33.1$ , shot noise), receiver noise, mobility and multipath dispersion. The transmitter is located at two different positions: (2m, 4m, 1m) and (2m, 7m, 1m), operating at 50 Mb/s while the receiver is moved underneath the spotlights along  $x=1\text{m}$  line. In order to compare the SNR results with the work of other researchers in the literature, both optical concentrators and optical filters were neglected in this chapter. Optical concentrators and filters associated with angle diversity receivers will be employed in the following chapters. Figure 3.17 (a) illustrates that the peak SNR of CDS and LSMS

structures occur when the receiver was placed near to the middle of the room at (1m, 4m, 1m). This is due to the fact that the distance between the receiver and the transmitter is very small, ensuring a strong received optical signal. Furthermore, the directive ambient light noise has small values at the positions (1m, 2m, 1m), (1m, 4m, 1m) and (1m, 6m, 1m), where the receiver is not beneath a spotlight which can further improve the SNR at these positions. Additionally, Figure 3.17 (a) illustrates that background noise has a substantial effect on the performance of the OW system when only a single wide FOV detector is utilised for CDS as well as LSMS, where the SNR curves illustrate the peaks and troughs related to background noise. The multi-spot diffusing system has improved the optical signal reception at poor connections like the corner of the room. When the transmitter is stationary in the middle of the room and the receiver is moved near to the room corner, the LSMS system with a wide FOV receiver accomplishes about 6 dB SNR gain over the wide CDS system. Moreover, the multi-spot LSMS coupled with angle diversity receivers attains a constant 22 dB SNR under the impact of background noise present and multipath dispersion. This is attributed to: (1) adopting spot diffusing where the receiver can collect a strong signal through use of the direct LOS component, and (2) employing diversity receivers which can substantially minimise the ambient noise. The result is well matched with previous work in [135], [140]. The angle diversity receiver produces a uniform SNR above the CP when the transmitter is stationary at the room's centre. This is due to the capability of the angle diversity receiver structure, which can select the best branch that has a strong received signal (direct LOS component), with minimum background noise. The values of the highest and lowest SNR and the delay spread detected by the receiver as well as the related shot noise current for the configurations above are given in Table 3.1 when the transmitter is placed at the centre of the room.

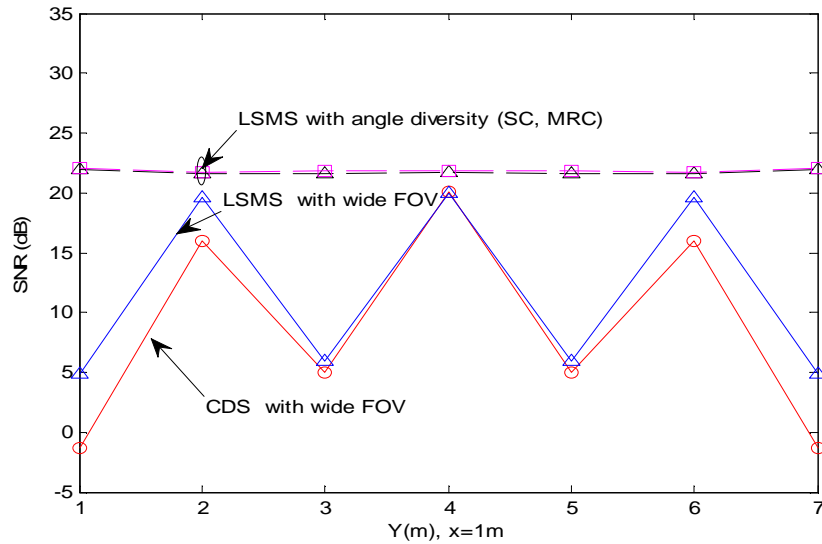
Table 3.1: Maximum and Minimum Delay spread, SNR and shot noise current of CDS, LSMS transmitter with wide FOV receiver as well as the LSMS coupled with a 3 detector angle diversity receiver.

Transmitters	Maximum Delay Spread (ns)	Maximum Shot noise current ( $\mu A$ )	Minimum SNR (dB)
CDS with wide FOV Receiver	2.42	0.3143	-1.3
LSMS with wide FOV Receiver	1.33	0.3143	4.8
LSMS with 3-Angle Diversity Receivers	0.7	0.009583	22.1

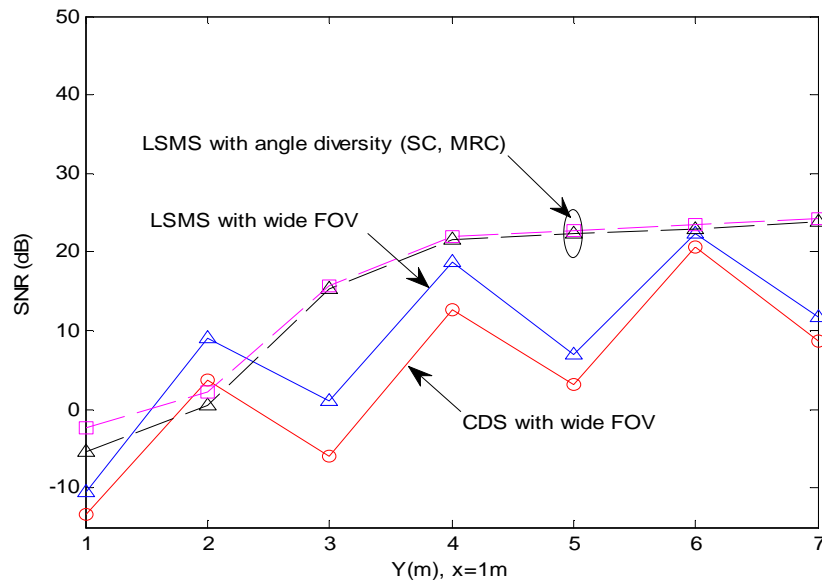
However, performance degradation in the conventional diffuse system as well as multi-spot configuration is observed during transmitter motion, as seen in Figure 3.17 (b). At the most unsuitable path considered, of 6 m receiver-transmitter horizontal separation, the LSMS with a wide FOV receiver achieves around 3 dB SNR gain above the CDS. Additional SNR enhancement of 8 dB can be obtained when the LSMS angle diversity receiver replaces the wide FOV receiver. Mobility can induce substantial SNR degradation in the basic OW system (pure diffuse and multi-spot diffusing configurations). Despite the mobility of the transmitter, the SNR enhancement of the multi-spot LSMS, coupled with three-branched angle diversity receivers, is significant for the given receiver position across  $x=1$  line in comparison with the wide FOV CDS system. The three-branched angle diversity LSMS enhances the SNR result by over 11 dB above the CDS structure.

The findings for the CDS, LSMS with wide FOV receiver and LSMS coupled with angle diversity receivers have been compared against the practical and theoretical findings for the simple CDS presented in [16], [34], [86] and the findings for the LSMS presented by other researchers in [135, 140]. Good

agreement was observed, providing confidence in the ability of our model to assess new systems.



(a) Transmitter at (2m, 4m, 1m)



(b) Transmitter at (2m, 7m, 1m)

Figure 3.17: The SNR of the CDS and LSMS with wide FOV, and LSMS with angle diversity receiver when the transmitter is placed at (a) (2m, 4m, 1m) and (b) (2m, 7m, 1m) while the receiver moves along the line  $x=1m$ .

## 3.10 Summary

Background noise, mobility, multipath dispersion as well as receiver noise can substantially impair the performance of OW systems in an indoor setting, especially in the case of pure diffuse systems that are dependent on the diffuse reflections from the ceiling and walls rather than direct LOS. This chapter presented tools that can be used to simulate the OW channel in an indoor environment. Moreover, ambient noise sources in an indoor environment were also modelled. A ray-tracing algorithm and analytical details were presented for multipath propagation and ambient noise sources. Simulation was done with the use of *Matlab*. Two major OW transmitters (CDS and multi-spot LSMS) were studied. The CDS does not rely on a direct LOS, which permits the OW CDS system to operate even when the receiver is obstructed from the transmitter. However, a pure diffuse system coupled with a wide FOV is subject to multipath dispersion, which may result in pulse spreading and extreme ISI. The multiple spot diffusing technique (LSMS) can be used to further enhance the performance of an indoor OW system. It merges both LOS and non-LOS features. Furthermore, three angle diversity detectors were integrated with the LSMS configuration to reduce the effect of multipath dispersion and background noise. The proposed systems were assessed using impulse response, delay spread and SNR. The findings show that the multi-spot LSMS with a wide FOV receiver offers about 6 dB SNR gain over the pure diffuse CDS system. Significant SNR improvements of about 23 dB can be achieved over the CDS system when three-branch angle diversity techniques (SC and MRC) are integrated with a multi-spot LSMS configuration. Furthermore, there is a significant reduction in the delay spread of the angle diversity LSMS system by more than a factor of 3 compared with the CDS configuration. The results of the CDS and LSMS, associated with the wide FOV receiver, as well as the LSMS, combined with angle diversity detectors, have been compared with other researchers' results in the literature. These systems will be considered as a

baseline to enable comparison with the new systems described later in the thesis.

# 4 Beam Delay Adaptation in Indoor Optical Wireless Systems

## 4.1 Introduction

Multimedia communication and mobile computing have recently focused on OW technology where huge bandwidth is available [54], [102] – [105], [132] – [134], [172], [174]. However, in practice, the performance of a diffuse OW system (CDS), along with a basic multi-spot diffusing configuration (such as LSMS), is affected by user mobility; consequently, there is considerable drive for finding techniques to reduce the impact of user mobility on optical wireless connections. The most important issues that OW multi-spot diffusing system designers have to take into account are the arrival time and the amount of received optical power that comes from each spot. Even though signal reception can be improved through the use of angle diversity detection (as explained in Chapter 3), a considerable quantity of the transmitter's power might be wasted in a number of diffusing spots (that are not within the receiver FOV) due to transmitter mobility. In addition, the direct LOS components of the spots arrive at the receiver at different times which results in pulse spread and causes ISI. Therefore, this chapter introduces new adaptive approaches (novel methods of beam delay and power adaptation) to improve the OW multi-spot diffusing transmitters during user mobility. The proposed method uses adaptive techniques that introduce a range of differential delays between the beams as well as allocating high intensity to the spots located closest to the receiver position, in order to improve the SNR as well as reduce the ISI at the receiver.

In this chapter, we model an optical wireless system that employs beam delay and power adaptation in a line strip multi-spot diffusing system (BDPA-LSMS) coupled with angle diversity detectors. The proposed system is studied, at 50 Mb/s, in order to simplify the comparisons with research in the field. The simulations show that the BDPA-LSMS configuration, where three-branched angle diversity detectors are used, produces around 13 dB SNR improvement over the non-adaptive LSMS system. In order to further strengthen the signal reception, a new beam delay and power adaptive multi-beam clustering method (BDPA-BCM) is proposed. The proposed BDPA-BCM configuration is evaluated at 50 Mb/s, in order to compare its results with non-adaptive and adaptive multi-spot configurations (LSMS and BDPA-LSMS), and is also analysed at high bit rates of 2.5 Gb/s and 5 Gb/s.

Angle diversity is normally looked at as a way of minimising the fading effects in radio frequency wireless communication systems by obtaining independent replicas of the transmitted signal [184]. Optical wireless configurations are free from fading [16]; therefore, diversity can be used as a solution for mitigating multipath dispersion, SNR variation and combating shadowing. Although the enhancements were obtained, the angle diversity detectors need a dedicated optical concentrator for each detector, which can be heavy and expensive. Another design that might significantly reduce the noise from the surrounding light and simultaneously enhance a setup's performance is an imaging receiver [9], [118] – [124]. In this chapter, a custom design of an imaging receiver is proposed in Section 4.7 [123] – [126]. The basic diffuse CDS setup, the multi-spot LSMS arrangement as well as the adaptive BDPA-LSMS configuration are reassessed and studied using an imaging reception technique. Furthermore, a new beam delay and power multiple adaptive beam clustering method (BDPMA-BCM) coupled with imaging detection is proposed, to further improve the performance of the OW system and to enhance the links budget while the system operates at high bit rates of 2.5 Gb/s and 5 Gb/s.

## 4.2 Mobile Beam Delay and Power Adaptive LSMS (BDPA-LSMS)

A novel beam delay and power adaptation method is introduced here with a multi-spot diffusing system (BDPA-LSMS), in order to enhance the received power, minimise the impact of multipath dispersion and reduce the degradation of the system due to user mobility. Unlike the traditional LSMS proposed in [134], [135], [140], [181] (and also verified in the previous chapter), where the transmitter distributes the total power (1W) among 80 beams equally (12.5 mW per beam) as well as switches ON all the beams at the same time, the BDPA-LSMS here is based on adaptive approaches that adapt the delay between the beams as well as adjusting the distribution of the transmitter power among the beams. Beam delay adaptation helps minimise the delay spread, hence increasing the 3-dB channel bandwidth and the SNR at higher data rates. Instead of turning on all the beams simultaneously and increasing the delay spread, beam delay adaptation switches on the beam that has the longest journey to travel first, and then switches on the other beams with different differential delays ( $\Delta t$ ) so that all the beams reach the receiver at the same time. Beam power adaptation operates in a similar way to the water filling algorithm in the case of a single user scenario which allocates more power to the best spots' channel at each given location, hence increasing SNR at the receiver. For example, if the BDPA-LSMS transmitter is moved near to the corner of the room and the receiver is located in the opposite corner in the same line, then the spots located near to the receiver (facing the receiver) will emit more power. The flowchart of our beam delay and power adaptation algorithm is illustrated in Figure 4.1. The adaptive algorithm of the proposed BDPA-LSMS system adapts the transmission power and the delay among the beams for a single user setup as below:

- 1- Switch on a line strip (LSMS),  $N_s \times 1$  beams, with  $l$  cm spacing between adjacent spots. Equally distribute the total power among the beams and compute the received power as well as the SNR at the angle diversity detectors.
- 2- The transmitter individually turns on each spot, the receiver computes the received power and the SNR at each detector (three branches) and the SNR after combining the signals through maximum ratio combining (MRC) and also calculates the time delay of the maximum received power ( $t_i$ ).
- 3- The receiver considers the time delay and the SNR in step 2 as the time delay and the SNR associated with the spot.
- 4- The transmitter and the receiver repeat step 2 and step 3 for all the spots (80 spots in our BDPA-LSMS system).
- 5- The receiver sends a signal, at a low rate, back to the transmitter conveying the information about the time delay and the SNR weight associated with each spot.
- 6- The transmitter redistributes the transmission optical power ( $P_s$ ) among the beams according to the ratio of SNRs as:

$$\text{new power of the spot} = \left( \frac{\text{SNR of the spot}}{\text{Total SNR of the spots}} \right) \times P_s \quad (4.1)$$

- 7- The transmitter calculates a differential delay ( $\Delta t$ ) between the beams:

$$\Delta t_i = \max(t_{i_{max}}) - t_i \quad 1 \leq i \leq N_s \quad (4.2)$$

to compensate the spread in channel due to the time delays as seen by the receiver. It is worth noting that the majority of the power is collected by the receiver through the line of sight with each spot (significantly lower power through reflections). Therefore, adjusting the differential beam delays helps reduce the delay spread at the receiver.

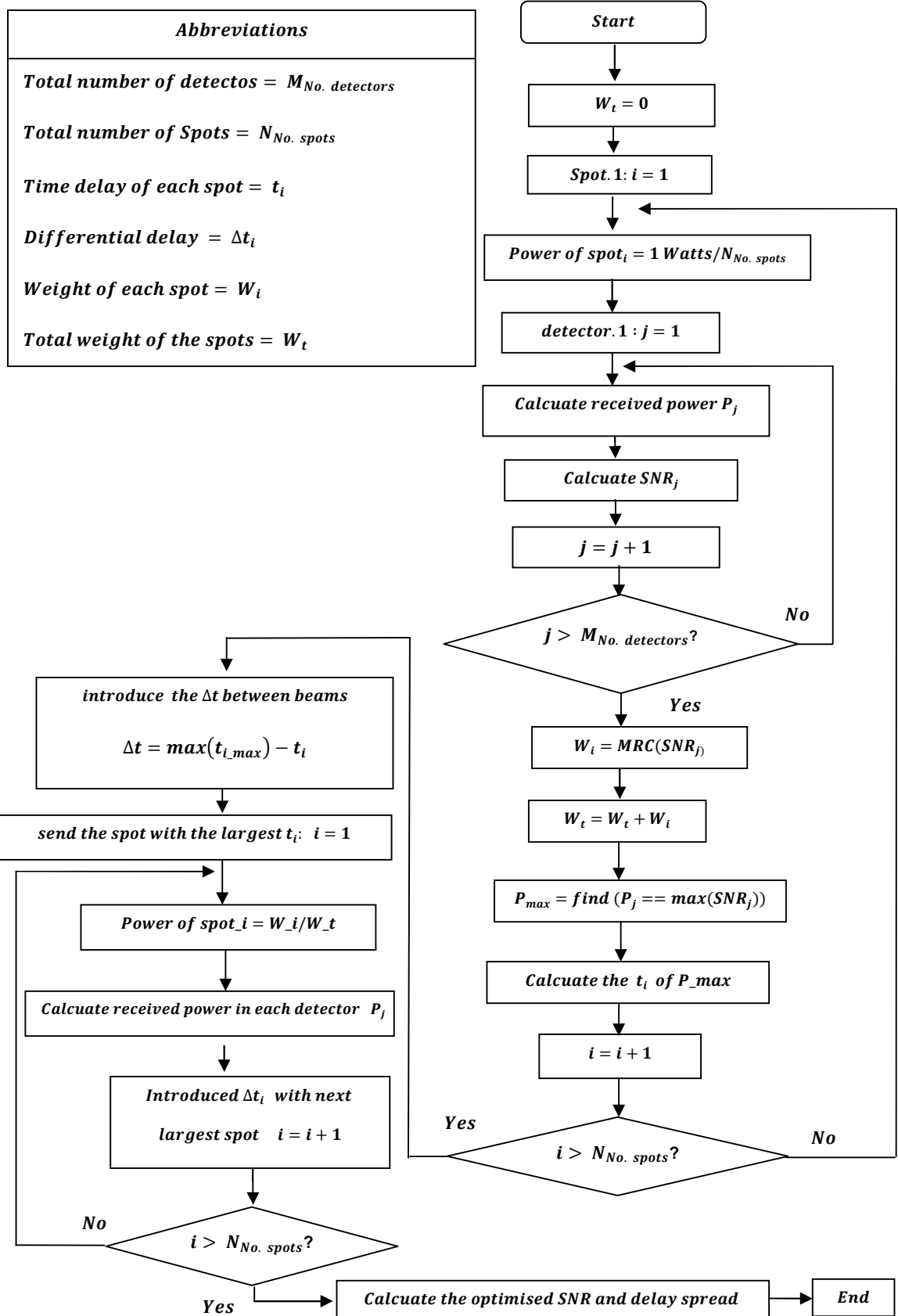


Figure 4.1: Flowchart for the beam delay and beam power adaptation algorithm.

- 8- The transmitter switches on the beam with the longest journey first, and then switches on the other beams with differential delays so that all the beams reach the receiver at the same time. It should be noted that beams with the same delay (due to room symmetry) are switched ON simultaneously.

The link assumes a medium access control (MAC) protocol, which provides time to estimate the noise levels, the received optical signal and the time delay of the spots. After estimating the delay and the SNR weight for all the spots, the receiver communicates with the transmitter at a low rate signal for reliability, conveying the delay and the SNR ratio associated with each spot. This signal might be a diffuse channel, perhaps set up using one of the beams or a separate beam. Our adaptive approaches are designed for a single transmitter and receiver setup where a high power level is allocated to the spots located closest to the receiver position. When multiple transceivers (emitters/receivers) are used within an indoor environment, an opportunistic arrangement [183] might be utilised to enhance the overall throughput of the system if there are time varying channels and interference. This deserves additional research.

The adaptive algorithm can be practically implemented using a liquid crystal (LC) device which is used as a holographic diffuser. The device drive voltage can be electronically varied to dynamically control the turning on of specific beams shaped by the holographic diffuser as well as the power in individual beams. It has to be noted that the adaptation of the delay and power of the beams is carried out at the rate at which the indoor setting changes, such as human movement, not at the system bit rate. Pedestrian speed is around 1 m/s. The LC devices have a response time from microseconds to milliseconds [185]. Moreover nanosecond response times of electroclinic liquid crystals have been demonstrated in [190], [197]. Beam delay adaptation can also be implemented

through the use of multiple sources and delayed switching (hence the switching speed limitations are reduced or removed).

Our adaptive multi-spot diffusing transmitter (BDPA-LSMS) transmits  $80 \times 1$  beams targeting the middle of the ceiling with different delays and intensities among the beams when the transmitter is stationary in the centre of the room. The beam spots on the ceiling turn into secondary emitters, producing Lambertian radiation. The spot allocation arrangement in the proposed BDPA-LSMS configuration is like that of LSMS (see Figure 3.10), but with different delays and powers among the beams. Moreover, the spots' locations of our proposed system are changed according to the transmitter's mobility. The calculations of the new location of spots can be worked out following the equations given in (3.36) and (3.37). Our new mobile system (BDPA-LSMS) shows a considerable improvement in the SNR, delay spread and 3-dB channel bandwidth compared with basic CDS and LSMS systems.

## 4.3 System Description

The characteristics of the optical wireless channel produced from the adaptive BDPA-LSMS system coupled angle diversity receivers are analysed. Moreover, the proposed system is compared with a basic CDS diffuse system and a non-adaptive multi-spot LSMS configuration. Propagation simulations were undertaken in a setting like that in the previous chapter: an unfurnished room (empty) with a size of  $(4\text{m} \times 8\text{m} \times 3\text{m})$  (width  $\times$  length  $\times$  height). Up to second order reflections were taken into consideration. The room is split into surface reflectors where the size of the first and second order reflectors are  $5\text{cm} \times 5\text{cm}$  and  $20\text{cm} \times 20\text{cm}$  respectively. Walls, ceilings and floors are modelled as Lambertian emitters for the first and second order reflections with reflectivity coefficients of 0.3 for the floor and 0.8 for walls and ceiling. The reflections from windows, doors and other objects on the walls are looked at in a completely

identical manner to the reflections from the walls. The adaptive BDPA-LSMS transmitter emits  $N_s \times 1$  beams on the ceiling with different delays and intensities among the beams. Static spot intensities might be generated using CGHs, such as those proposed in [85], [138]. Beam delay and power adaptation can be implemented by LC devices, as explained in the previous section. To study the performance of an adaptive multi-spot diffusing transmitter under user mobility, three configurations were assessed: a pure CDS diffuse system (with wide FOV detector), a non-adaptive LSMS and adaptive BDPA-LSMS multi-spot configurations combined with three-branched diversity detectors. The proposed transmitters were set at three places on the CP: room centre (2m, 4m, 1m), room corner (1m, 1m, 1m) and room edge (2m, 7m, 1m), producing 1W total transmission optical power. The simulation was undertaken by placing the receiver at fourteen different locations across the  $x=1\text{m}$  and  $x=2\text{m}$  lines, down to the  $y$ -axis, over the CP. The angle diversity receivers described in the previous chapter, Section 3.9.3 (using three detector branches with collection areas of  $1\text{ cm}^2$  each and responsivity of  $0.54\text{ A/W}$ ) are used for multi-spot LSMS and adaptive BDPA-LSMS systems to mitigate the impact of multipath dispersion and artificial background noise in an indoor setting. As mentioned in the previous chapter, the direction of a detector is based on its azimuth ( $Az$ ) and elevation ( $El$ ) angles. The  $El$  of a pair of detector is fixed at  $35^\circ$ , while the upward facing detector is set at  $90^\circ$ . The  $Az$  angles of the detectors are  $0^\circ$ ,  $180^\circ$  and  $0^\circ$ . Two of the detectors' FOVs are set at  $35^\circ$ , while the upward facing detector is restricted to  $20^\circ$ . In this work, our BDPA-LSMS and LSMS coupled three angle diversity receivers use optical concentrators with typical concentrator gains of 13.9 dB and 9.4 dB corresponding to  $20^\circ$  and  $35^\circ$  FOVs respectively [72]. A hemispherical lens is employed for the pure CDS system coupled wide FOV receiver which has a gain of 4.6 dB [16]. Furthermore, band-pass filter can be used reduce the impact of background noise.

Along with the high reflectivity surfaces, and to examine the performance of our proposed adaptive BDPA-LSMS configuration in a reasonable scenario, the room illumination from the previous chapter was used (Section 3.6): eight spotlight lamps of 65 W power equally spaced on the ceiling (Figure 3.7). For our purpose, these lamps are considered as artificial ambient noise sources.

### **4.4 Performance Evaluation of BDPA-LSMS with Three-branched Angle Diversity Receptions**

The performance of the adaptive BDPA-LSMS transmitter is evaluated in the form of impulse response, 3-dB channel bandwidth, delay spread and SNR. The proposed configuration is examined and compared with a pure CDS diffuse system and a non-adaptive LSMS system coupled with angle diversity receivers, in order to find the best configuration geometry for indoor optical wireless during user mobility. All the configurations are evaluated under the influence of multipath dispersion, transmitter-receiver mobility, receiver noise and background noise.

#### **4.4.1 Impulse Response along with 3dB channel Bandwidth**

The impulse response of a wide FOV diffuse CDS system, a multi-spot LSMS and an adaptive BDPA-LSMS coupled with angle diversity receivers, when the transmitter is positioned in the room's centre at (2m, 4m, 1m) and the receiver is placed in the corner of the room over the CP, is given in Figure 4.2 (a). The channel impulse response results in Figure 4.2 (a) show the received power levels ( $\mu\text{W}$ ) versus time (ns). The multi-spot LSMS system performed better than the CDS. This is due to the direct power links between multiple diffusing spots on the ceiling and the receiver. These direct link components are significantly enhanced by the use of optical concentrators associated with narrow FOVs receivers. The findings also show that an adaptive multi-spot

BDPA-LSMS transmitter combined with angle diversity receivers can increase the power levels while noticeably reducing the signal spread compared with the CDS and non-adaptive LSMS systems. The direct LOS power level of BDPA-LSMS increases by a factor of four compared with the LSMS system. This is attributed to allocating high power levels to spots located close to the receiver position as well as introducing delay between the beams, which significantly increases the direct power and reduces the delay spread hence increasing channel bandwidth.

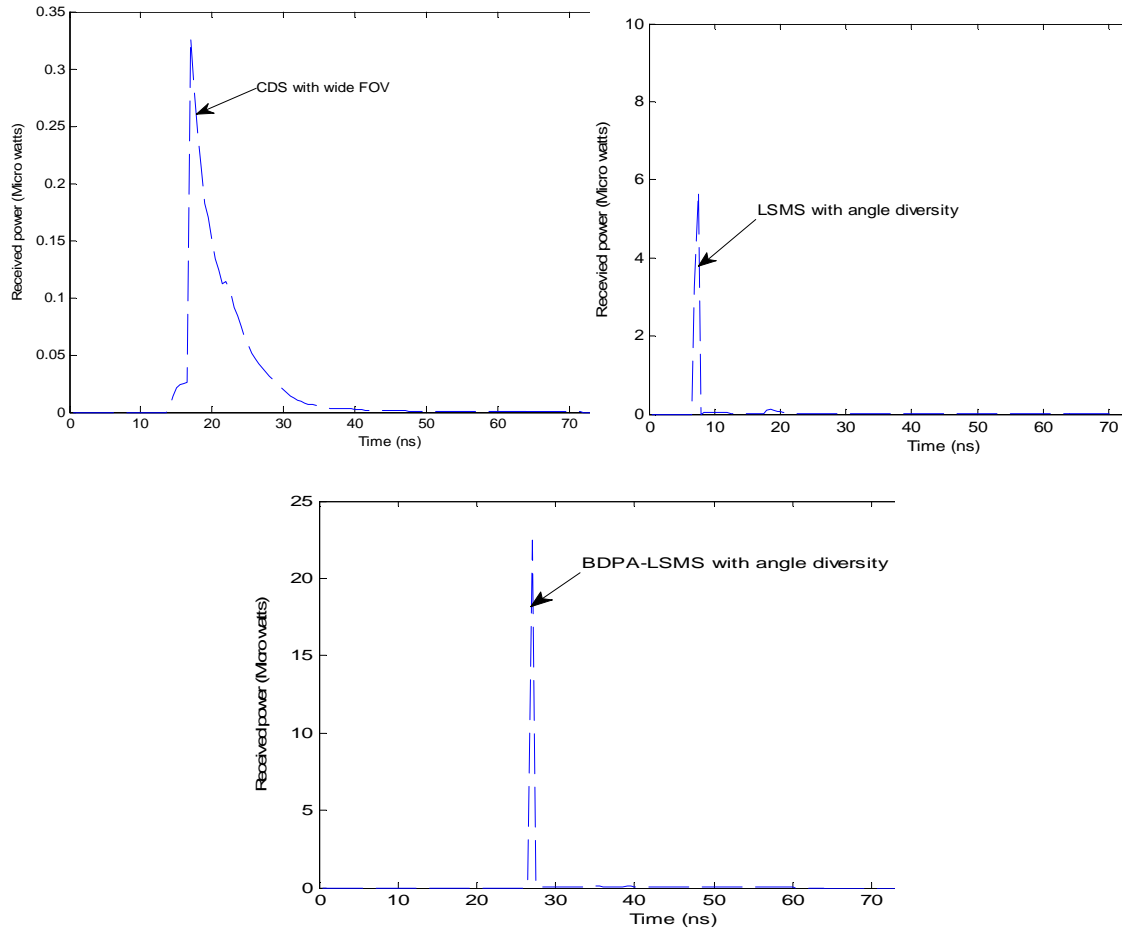
The 3-dB channel bandwidth of the adaptive angle diversity BDPA-LSMS and only beam power adaptation with LSMS systems, compared with pure CDS and LSMS configurations, when the transmitter is placed near to the middle of the room and the receiver is moved down the y-axis along the  $x = 1\text{m}$  line, is shown in Figure 4.3. The CDS system is considered as a baseline to which the majority of researchers compare their new systems. We have compared our findings to the experimental and simulation study of the CDS system reported in [8], [16], [86] and also to the multi-spot diffusing angle diversity receivers published in [132] – [138], [140]. The results in Figure 4.2 (b) and Figure 4.3 show that the pure diffuse system achieves around 36 MHz, which is in agreement with that in [16], [86]. Previous research has shown that using uniform diffusing spots geometry can increase the channel bandwidth to as high as 236 MHz [86]. Moreover, using a simple multi-spot LSMS setup coupled with angle diversity receivers may give up to 638 MHz, as in Figure 4.2(b), which is in agreement with earlier findings in [140]. Recent research has shown an experimental 1 Gb/s OW setup employing spot-diffusing associated with a single receiver in an indoor environment [54]. The same group in [132] has also found that employing multi-spot diffusing coupled with narrow FOVs angle diversity receivers for instance, an  $\text{FOV}=7^\circ$  may achieve 3-dB channel bandwidths exceeding 2.5 GHz. However, these studies do not use beam delay and power adaptations coupled with angle diversity detectors. When only beam

power adaptation replaces the conventional LSMS, there is considerable bandwidth improvement to roughly 4.2 GHz (see Figure 4.3). Additional improvement can be achieved by using beam delay and power adaptation with angle diversity detectors which may increase the 3-dB channel bandwidth from the 36 MHz of CDS to 5.2 GHz (see Figure 4.2(b) and Figure 4.3). This is due to four factors: (1) employing multi-spot diffusing, which provides strong direct LOS links between the receiver and the multi-spot transmitter, (2) introducing delay between the beams, which considerably reduces the delay spread, hence increasing the channel bandwidth, (3) allocating high power to the spots located near to the receiver position, hence increasing the direct received power and (4) using angle diversity detectors with small FOVs, considerably reducing the influence of multipath dispersion and background noise.

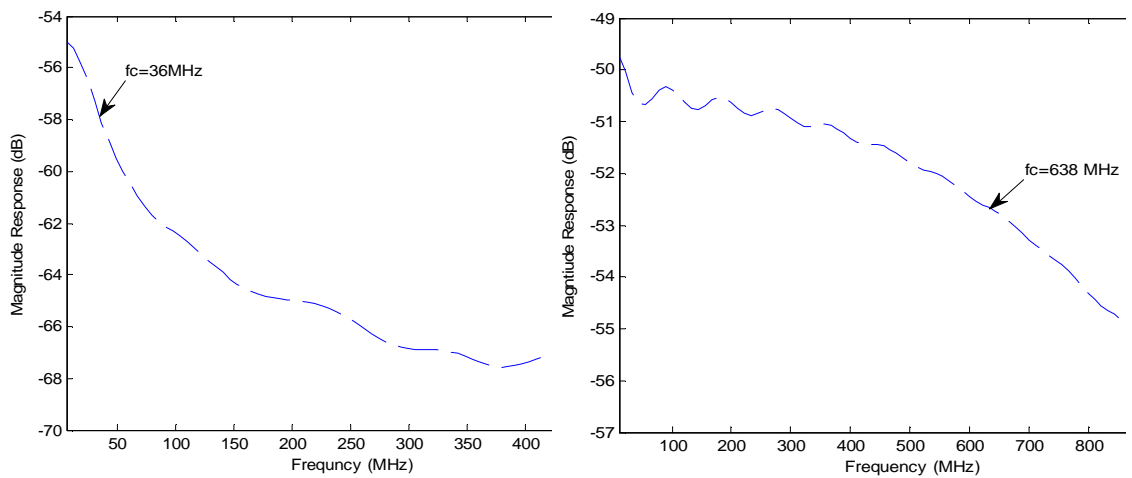
#### **4.4.2 Delay Spread Analysis**

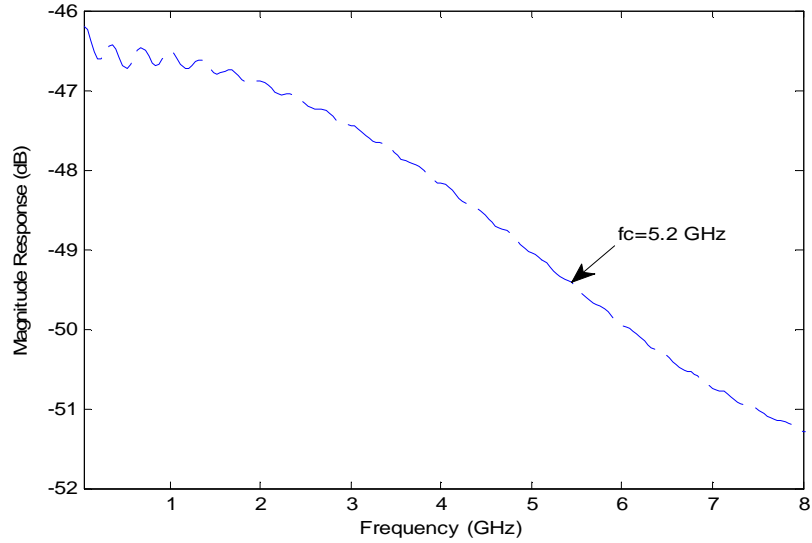
Figure 4.4 illustrates the delay spread results for adaptive BDPA-LSMS and non-adaptive LSMS multi-spot transmitter arrangements combined with three-branched angle diversity detectors. The pure CDS diffuse system is also considered for comparison purposes. The transmitters are placed in the middle of the room while the receiver is moved down the y-axis along the  $x=1\text{m}$  line. The results show that the pure CDS system provides a high delay spread. This is due to diffuse transmission ( $n=1$ ) of the CDS system and the large FOV ( $90^\circ$ ) detector. The delay spread results decrease from 2.4 ns to 0.7 ns if the multi-spot angle diversity LSMS configuration substitutes the diffuse transmitter and wide FOV receiver. Additional reduction in delay spread up to 0.4 ns can be obtained when only power adaptation algorithm is implemented in LSMS. Furthermore, our new BDPA-LSMS (beam delay and power adaptation) significantly reduces the delay spread from the 0.4 ns associated with the power adaptive multi-spot LSMS system to 0.1 ns. This improvement in delay spread is due to introducing a differential delay between the beams which can significantly reduce the signal pulse spread at the receiver.

#### 4.4 Performance Evaluation of BDPA-LSMS with Three-branched Angle Diversity Receptions



(a)





(b)

Figure 4.2: (a) Impulse response and (b) Frequency response of CDS, LSMS and BDPA-LSMS systems when the transmitter is positioned in the middle of the room and the receiver is positioned in the corner (1m, 1m, 1m).

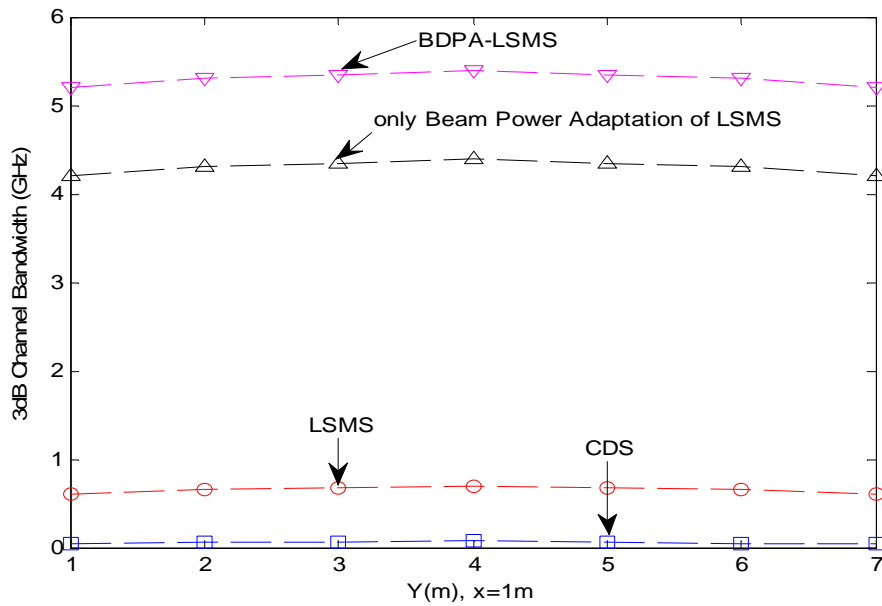


Figure 4.3: 3-dB channel bandwidth of four arrangements: CDS, LSMS, beam power adaptation only with LSMS along with BDPA-LSMS when the transmitter is positioned at (2m, 4m, 1m) with the receiver moving along the x=1m line.

The delay spread in our proposed BDPA-LSMS is due to the diffusing of the spots on the ceiling ( $n=1$ ) as well as the spread in the channel from the spots that not seen by the best receiver.

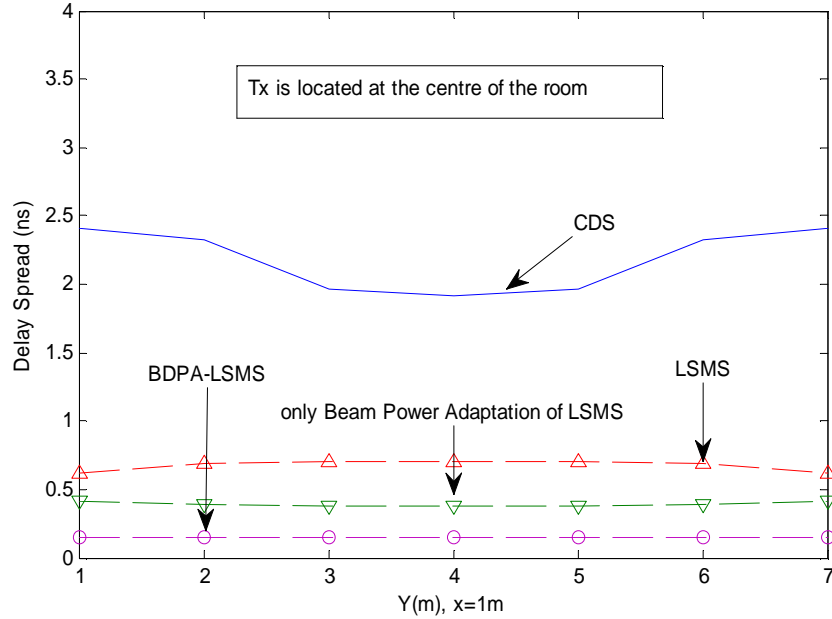
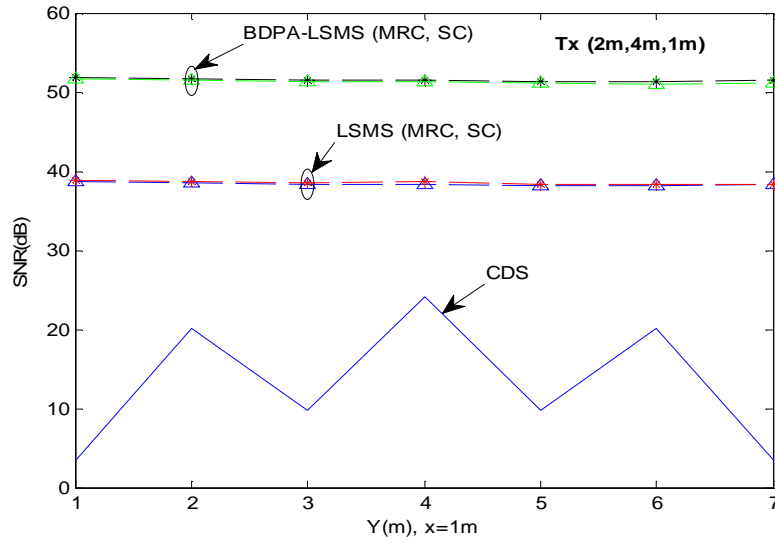


Figure 4.4: Delay spread of three arrangements: CDS, LSMS and BDPA-LSMS when the transmitter is positioned at (2m, 4m, 1m) and the receiver moves along the  $x=1$  line.

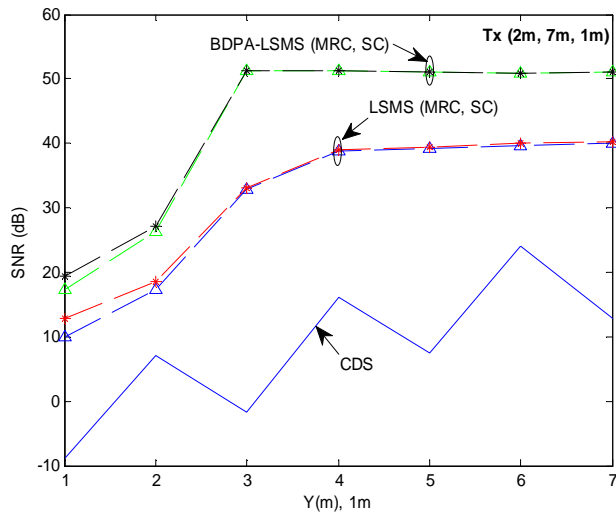
### 4.4.3 SNR Results

The SNR evaluation of an optical wireless system employing BDPA-LSMS coupled with angle diversity receivers is studied using two processing techniques: selection combining (SC) and maximum ratio combining (MRC). The proposed BDPA-LSMS system is compared with the pure diffuse system and the non-adaptive multi-spot configuration (CDS and LSMS). The SNR result (MRC and SC) of the proposed systems, operating at 50 Mb/s, is plotted in Figure 4.5. The  $x$  and  $y$  values in the figure stand for the associated cartesian coordinates on the CP. At 50 Mb/s, we used the preamplifier design proposed in [30]. SNR calculations were undertaken when the proposed systems were located near to the room centre, room's corner and room's edge at: (2m, 4m,

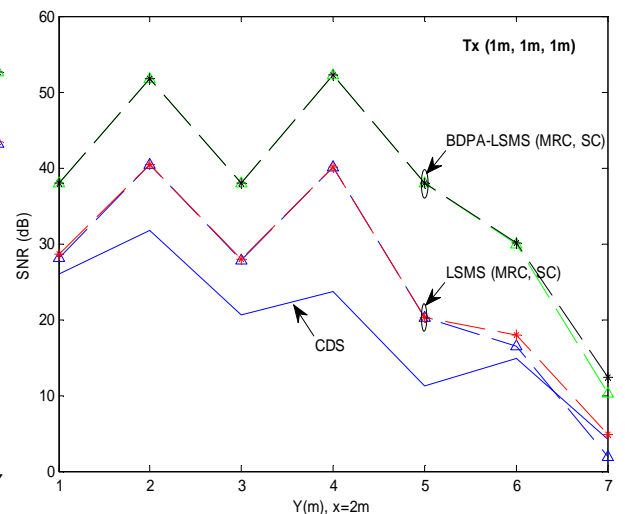
1m), (1m, 1m, 1m) and (2m, 7m, 1m) respectively, while the receiver is moved down the y-axis along the lines:  $x=1m$  and  $x=2m$ , which are lines that scan the maximum and minimum levels of artificial background noise. Figure 4.5 (a)



(a)



(b)



(c)

Figure 4.5: OW CDS, LSMS along with BDPA-LSMS systems in conjugation with three angle diversity receivers, when the transmitter is located at: (a) (2m, 4m, 1m) , (b) (2m, 7m, 1m) and (c) (1m, 1m, 1m) and the receiver moves along the  $x=1$  line in (a) and (b) and moves along the  $x=2m$  line in (c).

shows that the effect of multipath dispersion and artificial ambient light noise can be significantly reduced, when LSMS coupled with three-branched diversity detectors is employed. The angle diversity LSMS system offers around 32 dB SNR gain over the CDS configuration. This significant enhancement is due to adopting multiple diffusing spots (LOS components) as well as employing a high concentrator gain of 9.4 dB associated with a small FOV ( $35^\circ$ ) receiver compared with 4.6 dB with a wide FOV ( $90^\circ$ ) receiver: see Figure 4.5 (a). Furthermore, a significant improvement is obtained by using BDPA-LSMS, which offers 13 dB of SNR improvements above LSMS. This is due to (1) assigning more power to the spots closest to the receiver (increasing the received optical power) and (2) introducing delay between the beams, hence reducing the delay spread. However, the performance of the pure diffuse system and the multi-spot configuration can be degraded if the transmitter is mobile. Figure 4.6 illustrates the multi-spot diffusing spot locations of the mobile LSMS and BDPA-LSMS arrangements in two different transmitter locations: room's centre (2m, 4m, 1m), and room's edge (2m, 7m, 1m). The SNR of the BDPA-LSMS during the transmitters' mobility are given in Figure 4.5 (b) and (c). At the worst communication link (6m transmitter-receiver separation), the proposed BDPA-LSMS with three-branched diversity reception offers nearly 28

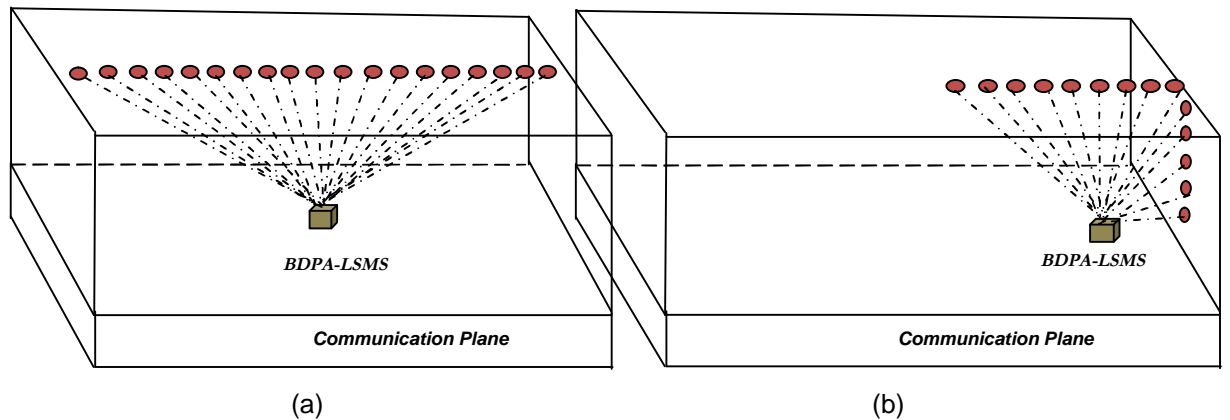


Figure 4.6: Spots distribution in mobile BDPA-LSMS when the transmitter is located in two locations: (a) (2m, 4m, 1m) and (b) (2m, 7m, 1m).

dB and a 8 dB SNR improvement over the CDS diffuse and non-adaptive LSMS multi-spot systems, respectively. Even though the adaptive techniques improve the performance of the multi-spot transmitter, considerable degradation occurs due to transmitter movement, specifically if the transmitter is moved near to the corner of the room (where the spots and the ambient noise sources are in the same line or close to each other) and the receiver is moved down the  $x=2\text{m}$  line. In this case, the best branch will collect both background noise and spot-power due to the three-branched angle diversity receiver structure, spot locations and noise sources locations hence degradation of 10 dB in SNR is observed compared with the case where the transmitter is located near the edge of the room at (2m, 7m, 1m); see Figure 4.5 (b) and (c). This degradation can be reduced and the performance of the proposed BDPA-LSMS system might be further improved if the total number of diversity receivers is increased, i.e., if a seven angle diversity structure replaces the three angle branches.

## **4.5 Mobile BDPA-LSMS coupled with seven branched angle diversity receiver**

In contrast to the aforementioned section, where only three-branched diversity receivers were employed, here seven detectors are considered to improve the multi-spot OW system's performance due to transmitter-receiver mobility. Figure 4.7 illustrates the physical structure of the seven diversity receivers. The  $El$  angle of six detectors is set at  $20^\circ$ , while the detector facing up has an  $El$  of  $90^\circ$ . The  $Az$  angles for the seven branches are set to  $0^\circ$ ,  $45^\circ$ ,  $90^\circ$ ,  $135^\circ$ ,  $225^\circ$ ,  $270^\circ$  and  $315^\circ$  respectively. In addition, their FOVs are restricted to  $24^\circ$ ,  $30^\circ$ ,  $25^\circ$ ,  $30^\circ$ ,  $30^\circ$ ,  $25^\circ$  and  $30^\circ$ . The top FOV receiver ( $24^\circ$ ) has been selected to be smaller than the angle of the direct ray from a side lamp when the receiver is placed midway between and underneath two lamps, hence the top receiver's FOV is given by:  $FOV < \tan^{-1}(1/2)$ . The rest receivers' FOVs have been optimised by changing the  $El$ ,  $Az$  and FOV of each receiver in 5 degree step.

The values ( $EL$ ,  $Az$  and FOV) are selected to achieve an optimal result (highest SNR), similar to an optimisation used in [94] – [95], taking into account the system mobility. The FOVs were selected to ensure that seven or more spots can be viewed by their corresponding detectors if the transmitter is mobile, even directly under the spotlights at the  $x=1\text{m}$  line.

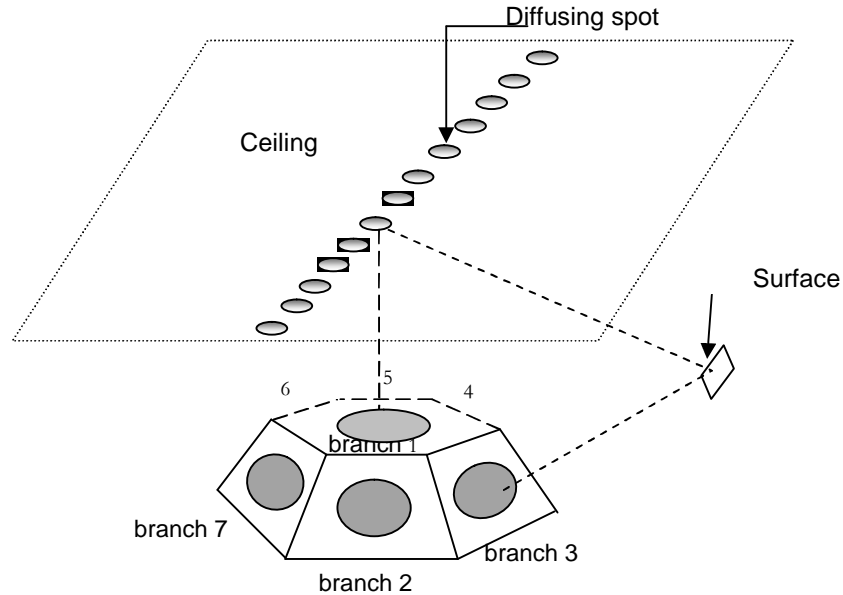
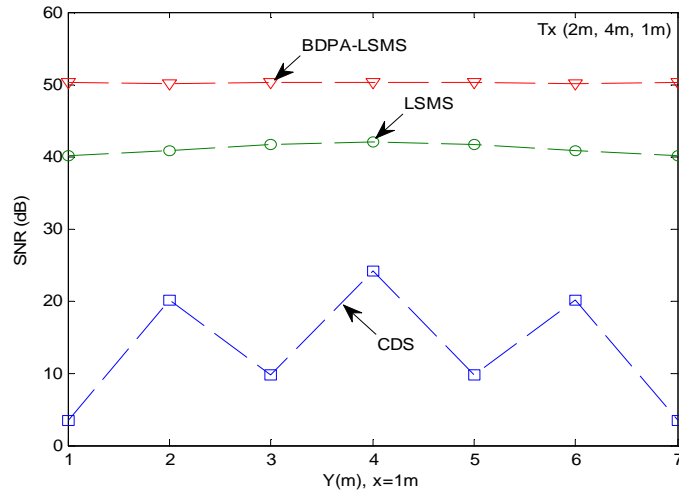


Figure 4.7: Physical arrangement of angle diversity detector with seven branches.

Figure 4.8 shows the MRC SNR distribution of the proposed configurations coupled with seven detectors at different transmitter positions: (2m, 4m, 1m), (1m, 1m, 1m) and (2m, 7m, 1m) while the receiver moves along the  $x=1\text{m}$  and 2m lines (down to the  $y$ -axis). The CDS with a wide FOV receiver is also plotted for comparison purposes. The systems operate under constraints of multipath dispersion, user mobility artificial background noise sources and receiver noise. The results show that the minimum SNR levels only occurred in the CDS system, when the transmitter was located close to spotlights (eight spotlights are considered with different locations in an indoor environment in our study, see Figure 3.7 in Chapter 3), while for the multi-spot LSMS and adaptive BDPA-LSMS configurations, the effect of the ambient noise sources from the

spotlights is almost insignificant over the entire room through the use of seven-branched angle diversity detectors. The minimum noise levels and the strong desired signals are always seen and selected by the best detector, even if the transmitter is underneath the ambient lights or is mobile. Our seven angle diversity detectors have typical concentrator gains of 12.4 dB, 12.1 dB and 10.6 dB corresponding to  $24^\circ$ ,  $25^\circ$  and  $30^\circ$  FOVs respectively [50], [72]. The results show that the LSMS with seven diversity detectors offers about 23 dB SNR gain over three-branched angle diversity detectors: see Figure 4.5 and 4.8. This is for two reasons: firstly, seven diversity detectors may constantly preserve direct LOS links between the receiver and the multi-spot transmitter, even with a large separation distance and secondly, high optical concentrators associated with narrow FOVs, can add additional improvement to the system performance.

Moreover, Figure 4.8 shows that the maximum SNR occurs when the receiver is moved close to the transmitter, for instance, if the transmitter is positioned near the corner of the room (1m, 1m, 1m) and the receiver is moved to the edge of the room close to the transmitter at: (1m , 2m , 1m). The adaptive BDPA-LSMS coupled with seven branched angle diversity detectors offers about 10 dB SNR gain over the traditional LSMS diversity receivers.



#### 4.5 Mobile BDPA-LSMS coupled with seven branched angle diversity receiver

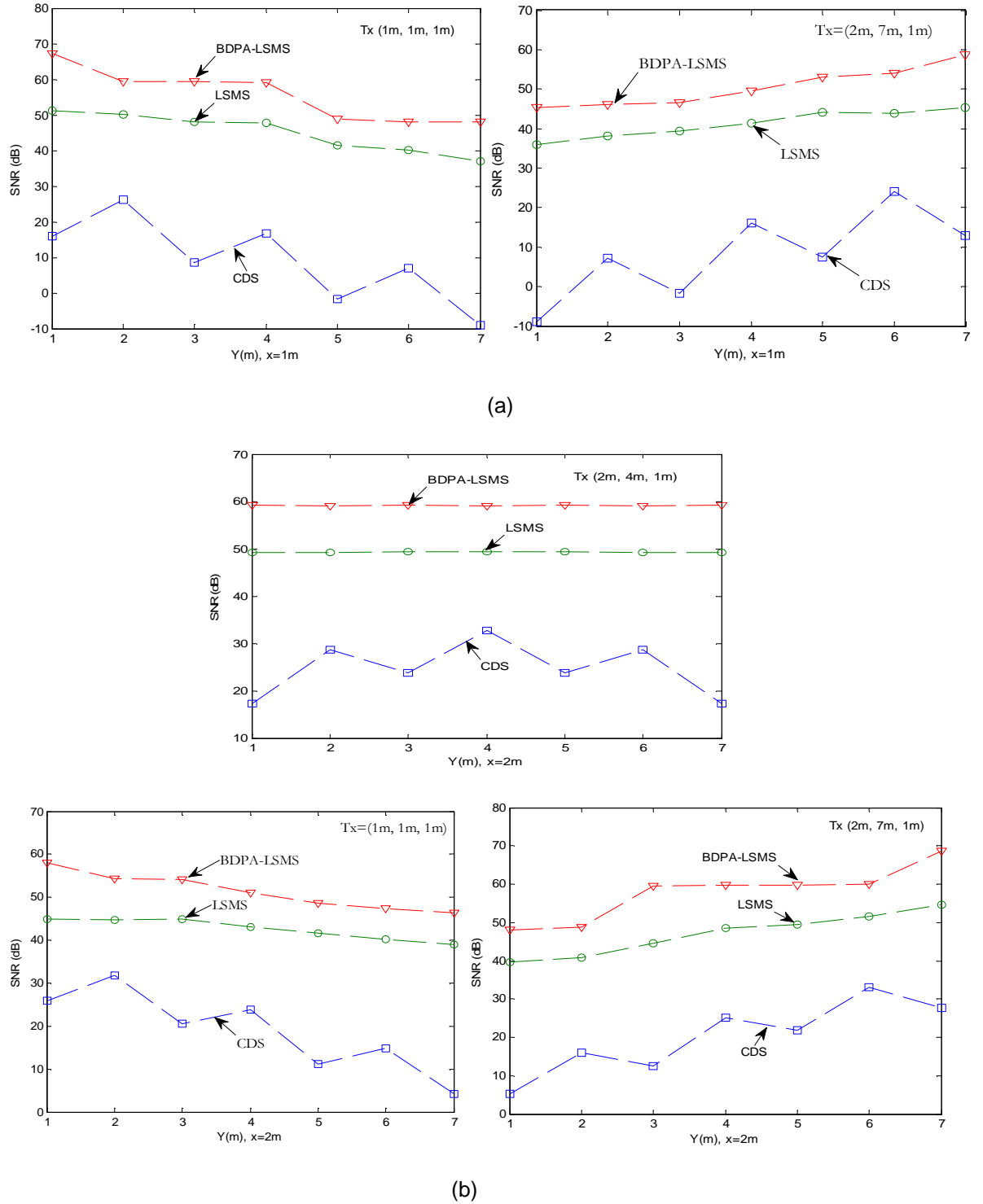


Figure 4.8: SNR of mobile diffuse CDS, multi-spot LSMS and adaptive BDPA-LSMS at different transmitter locations while the receiver moves along the line (a)  $x=1$  and (b)  $x=2m$  on the CP.

## 4.6 Mobile Beam Delay and Power Adaptive Multi-Beam Clustering Method (BDPA-BCM)

To additionally enhance the performance of the OW system, we propose a beam delay and a power adaptation multi-beam clustering method (BDPA-BCM) for use in mobile optical wireless configurations. The proposed system, coupled with seven angle diversity detectors, is evaluated and compared with our previous systems (LSMS and BDPA-LSMS). The key aim of this arrangement is to enhance the SNR of optical wireless systems during user mobility in a setting affected by multipath dispersion, artificial ambient noise sources and receiver noise. Early research on the beam clustering method (BCM) was undertaken in [172] – [173] where the concept was first introduced. Here, a novel geometry of spots' distribution based on beam delay and power adaptive multi-beam clustering techniques is introduced, and the findings show that better SNR, delay spread and impulse response can be obtained when the BDPA-BCM is compared with the LSMS, BDPA-LSMS and basic beam clustering method [117], [172] – [173]. The BDPA-BCM system uses 120 diffusing spots with the total optical power (1W) remaining the same as LSMS and BDPA-LSMS, where each spot produces 8.33 mW. The BDPA-BCM divides the diffusing spots into three clusters as follows: two-thirds of the diffusing spots (80 diffusing spots) on the ceiling, while 16.7% (20 diffusing spots) are on two walls, equidistant with 10 cm gaps between the adjacent spots, when the transmitter is stationary in the middle of the room. The optimum number of spots and the angles between the adjacent spots deserves further research. The BDPA-BCM system is able to see and cover its environment via three groups of diffusing spots, helping the receiver to gather signals from the closest spots. The beam delay and power adaptation algorithm, presented at the beginning of Section 4.2, is used where the receiver communicates with the transmitter sending the SNR weights and the delay associated with each spot. Based on the information from the receiver, the transmitter adjusts the beam

powers and introduces the delay between the beams to improve the system performance.

The BDPA-BCM produces  $120 \times 1$  spots in the form of three clusters targeting the middle of three different surfaces: one cluster on the ceiling and the two other clusters on the walls (at  $y=0$  and  $y=8\text{m}$ ) when the transmitter is in the middle of the room. To assist in visualising the mobile BDPA-BCM system, Figure 4.9 illustrates a limited number of the diffusing spots in the OW communication system. Similar to the LSMS explained in Chapter 3 Section 3.7, the reference point for calculating the spots' angles of the BDPA-BCM system is considered when the transmitter is in the middle of the room. This point is also used to calculate the locations of spots for other transmitter positions in the room during user mobility. The spots on the ceiling and walls turn into secondary distributed transmitters which produce a Lambertian pattern ( $n = 1$ ). Moreover, to include multipath propagation, the reflector surfaces from the floor, walls and ceiling were considered to be Lambertian reflectors for the 1<sup>st</sup> order and 2<sup>nd</sup> order reflections ( $n = 1$ ). To study the BDPA-BCM during user mobility, the transmitter was positioned in two positions over the communication plane at: (1m, 1m, 1m) and (2m, 7m, 1m). Furthermore, simulation calculations were undertaken for fourteen different receiver positions along the line  $x=1\text{m}$  and also the line  $x=2\text{m}$  over the CP. The receiver contains seven small FOV detectors pointed in different directions to cover a particular zone, as explained in Section 4.5. The total received optical signal is defined as the sum of all received signals (direct, 1<sup>st</sup> and 2<sup>nd</sup> reflected signals) from the spots (120 in the case of BDPA-BCM configuration) at each particular location. The received optical signals arriving into the receivers are considered at independently and processed using the MRC method. The simulation set-up is similar to the one used in Section 4.3. Table 4.1 gives more details about the simulation parameters that have been used in this study.

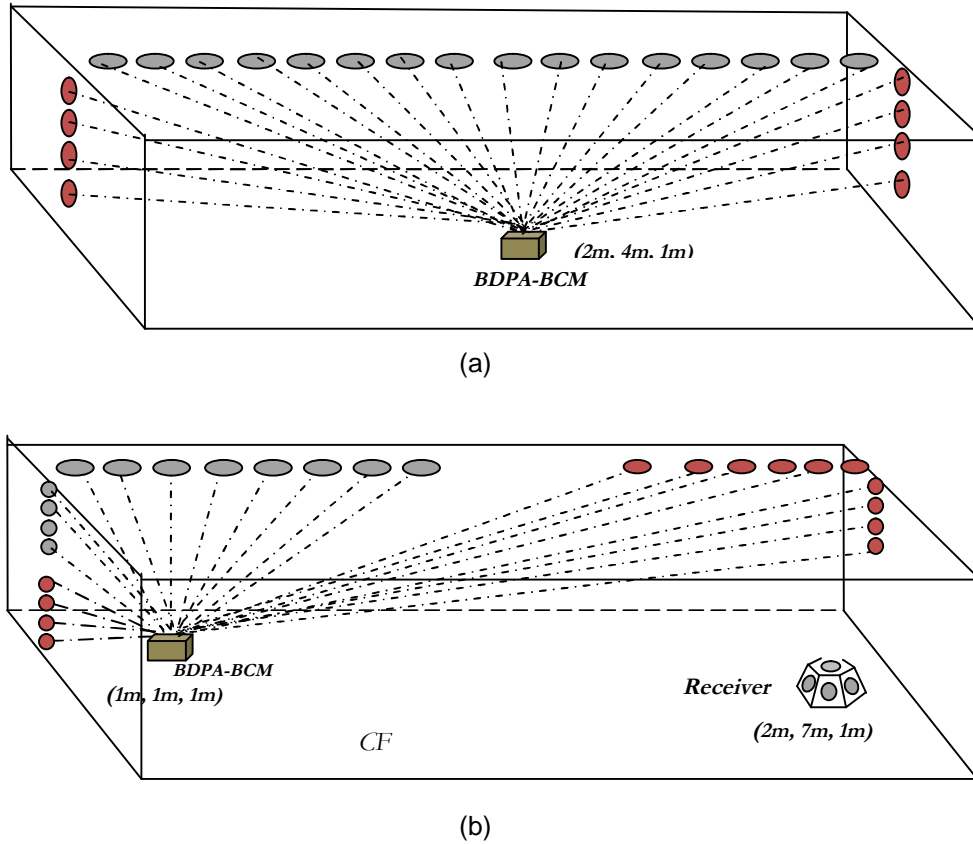


Figure 4.9: Mobile BDPA-BCM system (a) transmitter in the middle of the room (b) transmitter near the room corner  $(1m, 1m, 1m)$ .

#### 4.6.1 Performance assessment of BDPA-BCM

This section analyses our proposed BDPA-BCM system. The impulse response, delay spread and SNR results are examined. The proposed configuration is evaluated under the constraints of multipath dispersion, user mobility, artificial background noise and receiver noise. Moreover, the diffuse system (CDS) and adaptive and non-adaptive multi-spot configurations (BDPA-LSMS and LSMS), explained in the previous sections, are compared with our BDPA-BCM system.

Table 4.1: Simulation Parameters.

Parameter	Configuration						
	UPLINKS TRANSMISSION						
Length	8 m						
Width	4 m						
Height	3 m						
$\rho$ x-z wall	0.8						
y-z wall	0.8						
x-z op wall	0.8						
y-z op wall	0.8						
Floor	0.3						
	Transmitter						
Quantity	1						
Location (x,y,z)	(2m, 4m, 1m)	(2m, 7m, 1m)	(1m,1m,1m)				
Elevation	90°	90°	90°				
Azimuth	0°	0°	0°				
	Receiver						
Quantity	7						
Photodetector's area	1 cm <sup>2</sup>	1 cm <sup>2</sup>	1 cm <sup>2</sup>	1 cm <sup>2</sup>	1 cm <sup>2</sup>	1 cm <sup>2</sup>	1 cm <sup>2</sup>
Acceptance semi-angle	24°	25°	30°	30°	25°	30°	25°
Location (x,y,z)	(1m,1m,1m),(1m,2m,1m),(1m,3m,1m),(1m,4m,1m), (1m,5m,1m),(1m,6m,1m),(1m,7m,1m)						
Elevation	90°	20°	20°	20°	20°	20°	20°
Azimuth	0°	45°	90°	135°	225°	270°	315°
	Resolutions						
Time-bin duration	0.5 ns						
Bounces	1			2			
Surface elements	32000			2000			
Area of surface elements	5cm × 5cm			20cm × 20cm			
Number-of-spot lamps	8						
Locations	(1m,1m,1m), (1m,3m,1m), (1m,5m,1m), (1m,7m,1m) (3m,1m,1m), (3m,3m,1m), (3m,5m,1m), (3m,7m,1m)						
Wavelength	850 nm						
Preamplifier	PIN-BJT			PIN-FET			
Bandwidth (BW)	70 MHz			2.5 GHz		5 GHz	
Bit rate	50 Mb/s			2.5 Gb/s		5 Gb/s	

### 4.6.1.1 Impulse Response

The channel impulse response of the OW system shows the impact of multipath propagation on the received signal. The OW channel impulse response of the CDS and LSMS is given in Figure 4.10 (a). The transmitter is positioned over the CP near to the edge of the room while the receiver is placed near to the corner of the room. The multi-spot LSMS configuration combined with seven-branched diversity detectors shows better results than the diffuse CDS configuration with a single detector. This is due to (1) different direct LOS links seen by the receiver, even with a large distance between the transmitter and the receiver and (2) high optical concentrator gains associated with small FOV detectors ( $24^\circ$ ,  $25^\circ$  and  $30^\circ$ ) compared with a wide single detector ( $90^\circ$ ). Due to these factors, the direct received power of the multi-spot LSMS system increases considerably from nearly  $0.1 \mu W$  in the diffuse CDS system to about  $3 \mu W$ .

Although the LSMS system increased the received optical power, a spread in the channel and echos from first order reflections of the spots are observed; see Figure 4.10 (a). Furthermore, the results also show that when the distance between the receiver and the transmitter is increased, the received signals optical power decreases rapidly, thereby reducing the overall coverage. Moreover, distributing the total transmission power among the beams equally as well as switching all the beams at the same time will lead to a small direct received power level; approximately  $3 \mu W$  in the case of the LSMS system. The proposed adaptive multi-spot transmitter (BDPA-LSMS) may considerably increase the received power and noticeably reduce the channel spread, as illustrated in Figure 4.10 (b). BDPA-LSMS increases the direct received power from  $3 \mu W$  to  $14 \mu W$ . A further improvement in the received optical power by

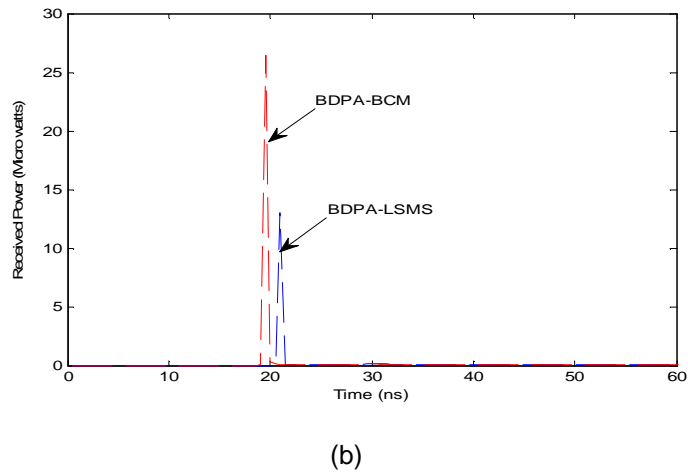
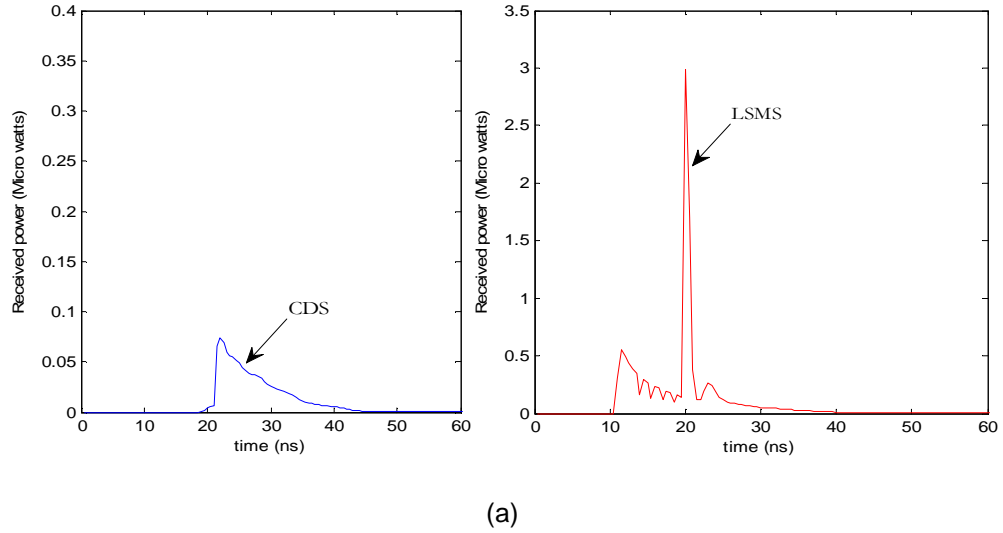


Figure 4.10: Impulse response of the four arrangements: CDS, LSMS, BDPA-LSMS along with BDPA-BCM, with the transmitter positioned at (2m, 7m, 1m).

more than a factor of two can be achieved in the BDPA-BCM link over the BDPA-LSMS. This gain improvement comes from a clustering technique (allocating the spots on different surfaces (ceiling and walls)), as well as employing our beam delay and power adaptation approach, which provides an opportunity for the receiver to pick the strongest desired signals from the closest spots.

### 4.6.1.2 Delay Spread Results

The delay spread results of the proposed configurations (CDS, LSMS, BDPA-LSMS and BDPA-BCM) are plotted in Figure 4.11. The results give a better view of how the delay spread varies with the receiver positions. The results show that the delay spread of the multi-spot LSMS system is much lower than that of the pure CDS diffuse system. There is a direct relation between the receiver-transmitter distance separation and the delay spread in both diffuse CDS and multi-spot LSMS configurations. When the separation increases, the delay spread gradually increases. For example, in the case of the LSMS system, the delay spread reaches 3.6 ns at 6m receiver-transmitter separation. Beam delay and power adaptation techniques are implemented in a multi-spot system in order to reduce the degradation induced due to user mobility. The proposed adaptive BDPA-LSMS reduces the delay spread by more than a factor of fifteen compared with the multi-spot LSMS system. A further reduction in the delay spread of BDPA-BCM by a factor of eight compared with the BDPA-LSMS is observed, because the BDPA-BCM geometry results in spot clusters (higher powers) nearer to most receiver positions as the transmitter moves.

### 4.6.1.3 SNR Results

This section studies the SNR of the mobile OW adaptive multi-beam clustering technique (BDPA-BCM) combined with seven-branched diversity detectors. The SNR results are compared with those of the adaptive BDPA-LSMS. The SNR calculations are given in equation (3.27), in Chapter 3. The proposed configuration is evaluated at 50 Mb/s. At 50 Mb/s, we used the preamplifier design proposed in [30] to allow comparison of the results with our previous systems.

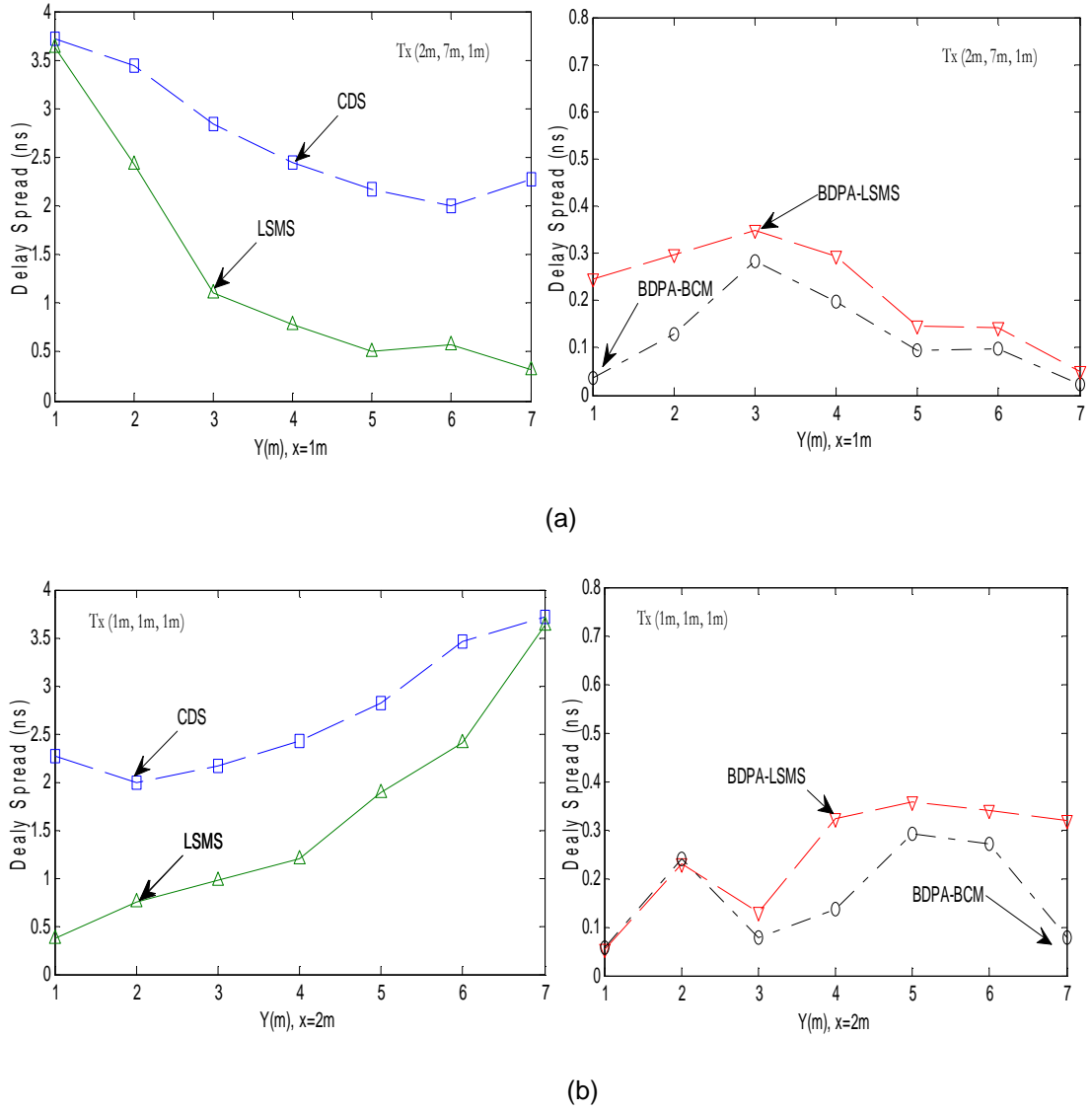


Figure 4.11: Delay spread of four arrangements: CDS, LSMS, BDPA-LSMS and BDPA-BCM with the emitter positioned at (2m, 7m, 1m) and (1m, 1m, 1m) while the receiver moves along the x=1m and x=2 lines.

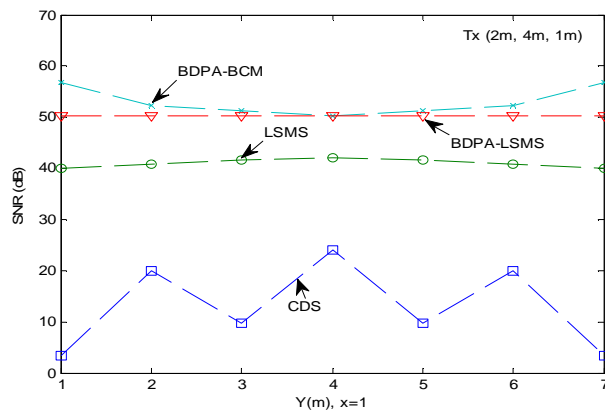
Figure 4.12 shows the MRC SNR results of the proposed mobile optical wireless systems. The performance analysis was carried out for three transmitter locations: (2m, 4m, 1m), (1m, 1m, 1m) and (2m, 7m, 1m), while the receiver is moved down to the y-axis, along the x=1m and x=2m lines at 14 different locations over the CP. When the transmitter and the receiver are placed close to the centre of the room, the SNR result of the BDPA-BCM system is almost identical to the BDPA-LSMS configuration, see Figure 4.12

(a). This is attributed to the fact that the receiver collects most of the power from the ceiling where both systems have the same distributions of spots (line strip spot diffusing from BDPA-LSMS and also one of the clusters produces line strip spot-diffusing in BDPA-BCM), see Figure 4.6 (a) and Figure 4.9 (a). When the receiver is placed near to the corner of the room at (1m, 1m, 1m), the proposed BDPA-BCM achieves about 7dB SNR gain over the BDPA-LSMS. This is due to the optimisation of the diffusing spots through the use of two clusters on the walls, which helps the receiver pick more power from the spots located near to the receiver location, see Figure 4.12 (a).

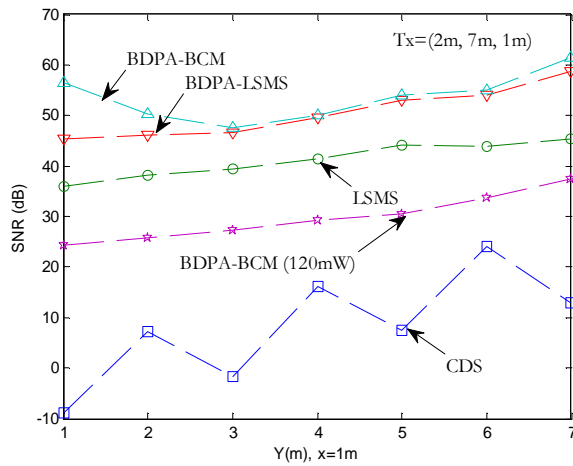
Although the BDPA-LSMS in combination with seven diversity receivers provides direct LOS signals, a large distance between the multi-spot transmitter and the receiver might still degrade the system performance. Figure 4.12 (b) and (c) show the impact of transmitter mobility on the proposed configurations. When the separation between the multi-spot cluster system and the receiver is 6 m, the proposed BDPA-BCM configuration achieves an SNR improvement of 10 dB and 20 dB over the BDPA-LSMS and LSMS configurations, respectively (see Figure 4.12). This is due to optimising the spot diffusing pattern through the clustering technique connected with beam delay and power adaptation, which may help the receiver choose the desired signals from the closest spots while moving. Additional improvement in the SNR results of the proposed BDPA-BCM system by more than 30 dB is obtained compared with the basic beam clustering techniques and other multi-spot diffusing techniques reported in [103] – [106], [172], [173].

In OOK systems, the required SNR should be at least 15.6 dB or above in order to achieve a BER of  $10^{-9}$ . By combining our techniques: multi-spot diffusing, beam clustering technique, beam delay adaptation, transmission power adaptation, and seven diversity detection, the total transmit optical power can be reduced by more than 9 dB and the system is still able to achieve  $10^{-9}$  BER. To investigate our proposed system BDPA-BCM with respect to eye safety

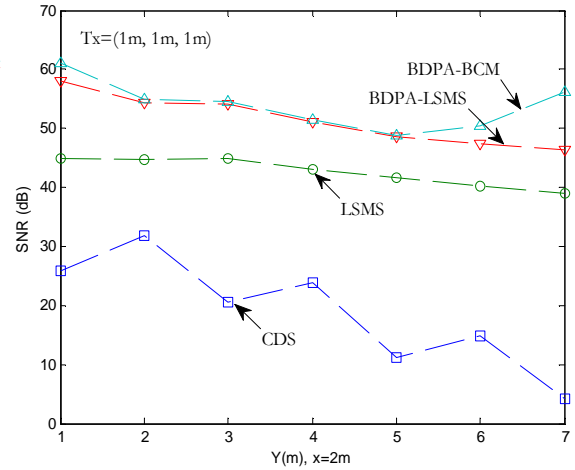
regulations, we used a total transmit power of 120 mW (1 mW per beam) and introduced a restriction in the power adaptation algorithm so that the power per beam is not allowed to increase beyond 0.5 mW (which is under OW safety regulations [54]). In this case, the SNR result obtained is about 24 dB, which is still high even without increasing the contractor gain (the latter can be achieved by reducing the receiver FOV). The degradation in the SNR is due to: (1) the reduction of the total transmission power from 1W to 120 mW and (2) a restriction on our power adaptation algorithm.



(a)



(b)



(c)

Figure 4.12: SNR for OW CDS, LSMS, BDPA-LSMS and BDPA-BCM at 50Mbit/s, when the transmitter is positioned at (a) (2m, 4m, 1m) (b) (2m, 7m, 1m) and (c) (1m, 1m, 1m), while the receiver moves along the lines  $x=1\text{m}$  and  $x=2\text{m}$  lines.

The high SNR results through the use of our BDPA-BCM system allow the system to operate at high bit rates of 2.5 Gb/s and 5 Gb/s. However, the photodetector capacitance is directly proportional to its active area. This means that if the active area of the photodetector is large, such as  $1 \text{ cm}^2$ , the photodetector capacitance will be large, which results in a restriction on the achievable bandwidth. Therefore the detector active area has to be reduced at higher data rates. The impact of reducing the area of the detector in our BDPA-BCM systems is illustrated in Figure 4.13. The active area of the detector is reduced from  $1 \text{ cm}^2$  to  $5 \text{ mm}^2$ , and the SNR is computed. Figure 4.13 illustrates the power penalty of our system that can be induced if the photodetector collection area is reduced from  $1 \text{ cm}^2$  to  $5 \text{ mm}^2$ .

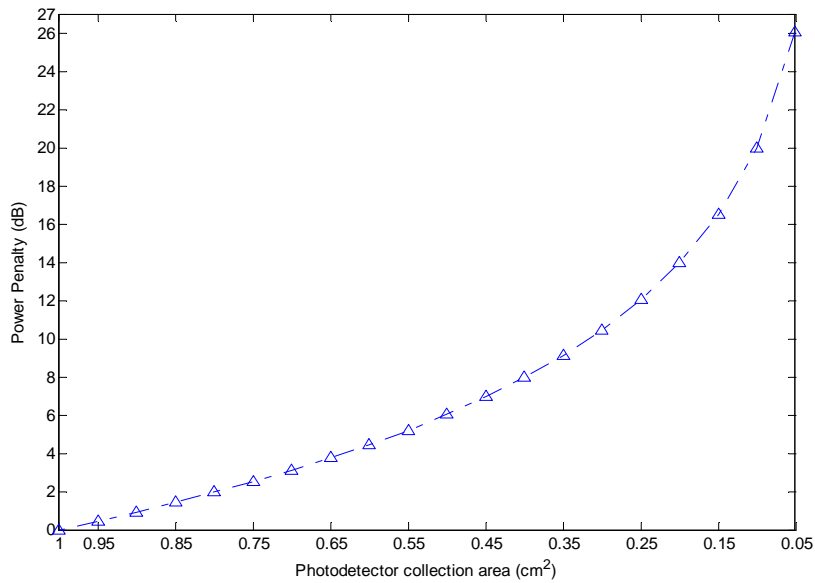


Figure 4.13: Power penalty of BDPA-BCM when the photodetector collection area is reduced from  $1 \text{ cm}^2$  to  $5 \text{ mm}^2$ .

Our proposed system at  $5 \text{ mm}^2$  will collect approximately 26 dB less power than a  $1 \text{ cm}^2$  photodetector. The use of a  $5 \text{ mm}^2$  will result in less power, but can be compensated by increasing the concentrator gain to about 20.7 dB by reducing its FOV to  $9^\circ$ . Our proposed system can use a narrower receiver FOV because our methods (beam delay adaptation, beam power adaptation, beam cluster,

angle diversity) are able to maximise the receiver SNR at each given location. We modified the  $El$ , and  $Az$  angles associated with the narrow FOV of our seven angle diversity receivers, in order to maximise the SNR within small a FOV. The FOV was restricted to  $9^\circ$ , for all the detectors. The  $El$  angles of the seven branches of the receiver are set at  $90^\circ, 50^\circ, 50^\circ, 50^\circ, 50^\circ, 50^\circ$  and  $50^\circ$ , and the  $Az$  angles are fixed at  $0^\circ, 45^\circ, 90^\circ, 135^\circ, 235^\circ, 270^\circ$  and  $315^\circ$ . Our proposed system has a typical concentrator gain of 20.7 dB corresponding to a  $9^\circ$  FOV [72]. At a high data rate, our proposed system uses detector area of  $5 \text{ mm}^2$ . We employed the preamplifier PIN-FET detector design presented in [186] for our proposed 2.5 Gb/s and 5 Gb/s BDPA-BCM systems. It should be noted that the receiver in [30] is designed specifically for OW, but the optical receiver proposed in [186] is not. There have been no receivers with such high bandwidths designed specially for mobile OW (we intend to design one, (future work)). In the optical direct detection receiver, the optimum bandwidth is 0.7 of the data rate. For example, the optimum receiver bandwidth at 5 Gb/s data rate is 3.5 GHz. This ratio comes from Personik's study reported in [77]. Although the detector area has been reduced, the receiver design in [186] has to be improved, circuit design techniques, such as bootstrapping, can be used to reduce the effect of the large area detector capacitance [30]. A smaller time bin of 0.01 ns is used at high bit rates (2.5 Gb/s and 5 Gb/s) in our proposed system, rather than the 0.5 ns used for 50 Mb/s. The impact of using a very small time bin (0.01 ns) is shown in our work in [113], [123] and will be presented in Chapters 5 and 6. The results show a very small increase in the delay spread when the 0.01 ns time bin is used compared with 0.5 ns. Figure 4.14 shows the SNR of the proposed beam power adaptation BCM and BDPA-BCM, operating at 2.5 Gb/s and 5 Gb/s when the systems operate under background noise and multipath dispersion impairments. The transmitter is located near to the edge of the room while the receiver is moved down the y-axis along the line  $x=1\text{m}$  above the communication plane. At 6m transmitter-receiver horizontal separation, the BDPA-BCM system achieves an SNR of 16

dB when operating at a bit rate of 5 Gb/s and using an active detector area of  $5 \text{ mm}^2$ . The results also show that the BDPA-BCM offers about 10 dB SNR gain in the worst case scenario over the beam clustering method that uses beam power adaptation only. This is due to the fact that beam delay and power adaptation helps reduce the delay spread and increase the 3-dB channel bandwidth, hence increasing the SNR at the higher data rates. Note that the SNR as defined in equation (3.27) (explained in Chapter 3) considers the eye opening, hence dispersion. The higher data rates (2.5 Gb/s and 5 Gb/s) in the BDPA-BCM system are achievable through the combination of beam delay adaptation, beam power adaptation, beam clustering method and  $9^\circ$  FOV angle diversity receivers. A further improvement in the link budget can be achieved by using error correction codes and this aspect warrants further study.

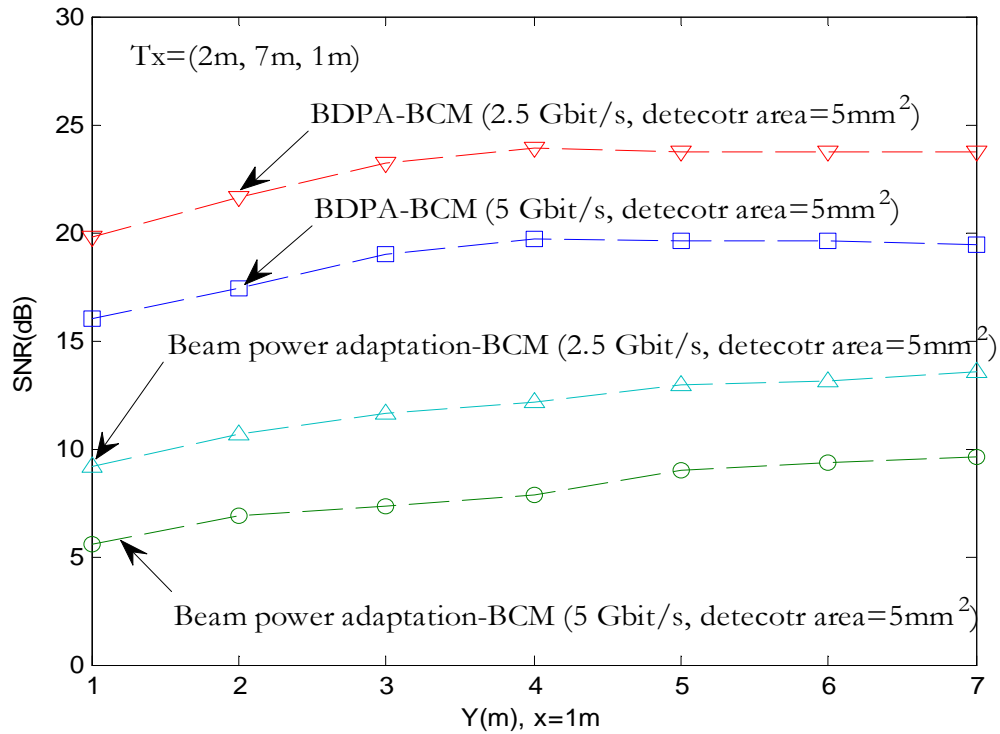


Figure 4.14: The SNR of BDPA-BCM and Beam Power adaptation BCM configurations at 2.5 Gb/s and 5 Gb/s.

## 4.7 Imaging Receiver Design

The improvements in the received optical power, delay spread, and the SNR of multi-beam OW system have been achieved through the use of our new adaptive techniques (beam delay and power adaptation) coupled with multiple angle diversity receivers. However, the main disadvantages of using angle diversity receivers are the large bulk and the high expense of the multiple non-imaging concentrators. Another design that might significantly reduce the noise and simultaneously reduce multipath dispersion is an imaging receiver [118] – [123]. The imaging receiver design offers a suitable substitute solution. It provides a number of advantages over a non-imaging receiver. Firstly, a single imaging concentrator (lens) can be used to cover all the detectors, reducing the bulk and expense compared to angle diversity receivers. Secondly, a single planar array is utilised for all of the detectors, potentially facilitating the utilisation of a large numbers of pixels, hence minimising the detector area. The received signal from each pixel can be analysed and processed using different techniques, like selection or combining methods (SC or MRC), in order to maximise the SNR of an OW system.

In an imaging receiver, all detectors are organised and filled into a planar detector array (divided into  $K$  equal sized squared pixels without gaps between them), as illustrated in Figure 4.15. Therefore, the area of an individual pixel is the detector's array area (which is equivalent to the exit area) divided by the number of pixels. In our design, 200 pixels are considered in the detector array ( $K=200$ ). We use an imaging concentrator lens that is employed in [120] – [121]. The transmission factor of the concentrator is given by:

$$T_c(\delta) = -0.1982 \delta^2 + 0.0425 \delta + 0.8778, \quad (4.3)$$

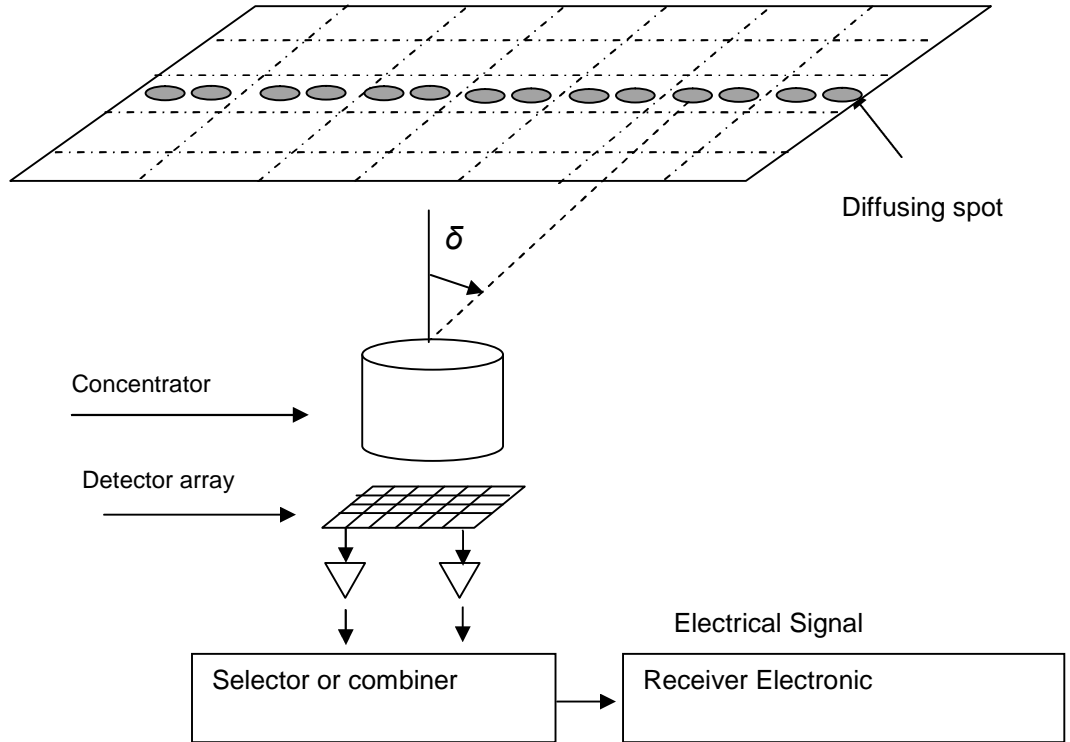


Figure 4.15: Physical configuration of the imaging receiver.

where  $\delta$  represents the reception angle calculated in radians. The imaging receiver has a refractive index  $N = 1.7$ , the entrance area is  $A = 9\pi/4 \text{ cm}^2$  and its concentrator's acceptance semi-angle is restricted to  $\psi_a = 65^\circ$  to be able to see the entire ceiling (if the receiver is in the middle of the room). The exit area of the receiver is  $A' = A \sin^2(\psi_a)/N^2$ . The receiver planar array is assumed to fit precisely into its matching concentrator's exit area. Therefore, the receiver planar array has a photosensitive area of  $2 \text{ cm}^2$  and each pixel has an individual area of  $1 \text{ mm}^2$ . It should be noted that as the total number of pixels increases, the area of each individual pixel shrinks compared to the detector array's area. The photodetector has a responsivity of  $0.6 \text{ A/W}$ .

In our calculations, when the receiver is positioned in the middle of the room (2m, 4m, 1m) it sees the entire ceiling, dividing the ceiling into 200 imaginary

reception areas, where each reception area represents the FOV of a single pixel. The FOV of the reception area can be found by calculating the reception angles  $(\alpha_{xi}, \alpha_{xj}, \alpha_{yi}, \alpha_{yj})$  with respect to the receiver's normal down the  $x - y$  directions, as illustrated in Figure 4.16 (a). These angles  $(\alpha_{xi}, \alpha_{xj}, \alpha_{yi}, \alpha_{yj})$  can be calculated as:

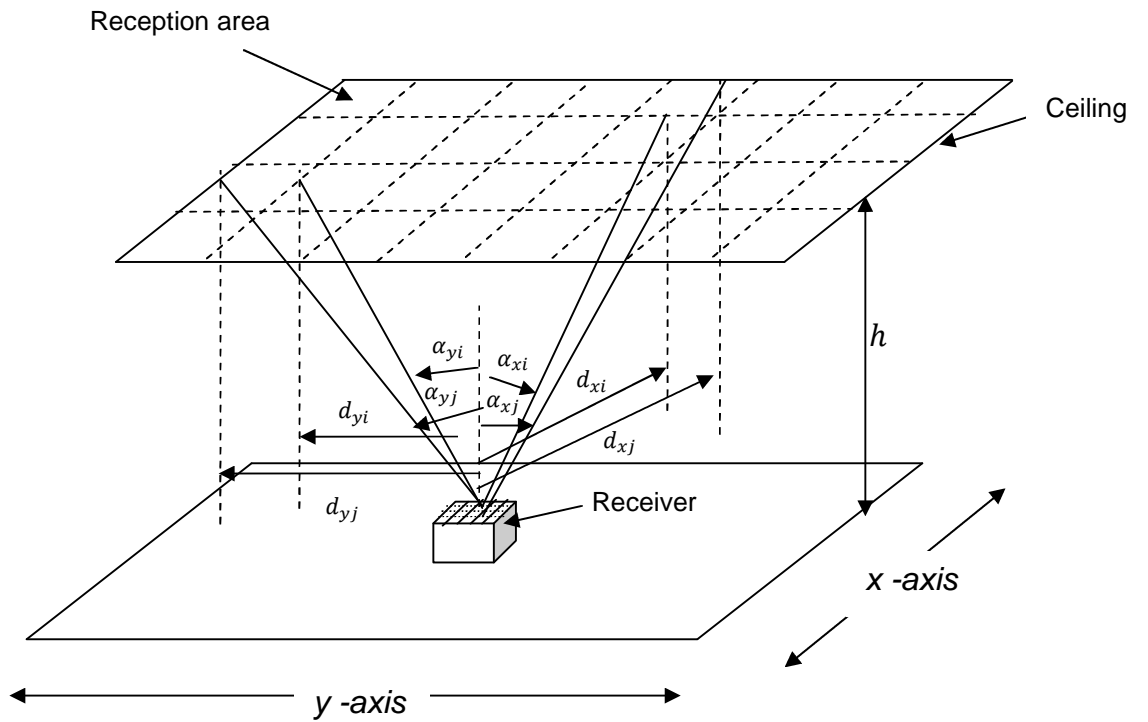
$$\begin{cases} \alpha_{xi} = \tan^{-1}\left(\frac{d_{xi}}{h}\right), \alpha_{xj} = \tan^{-1}\left(\frac{d_{xj}}{h}\right) \\ \alpha_{yi} = \tan^{-1}\left(\frac{d_{yi}}{h}\right), \alpha_{yj} = \tan^{-1}\left(\frac{d_{yj}}{h}\right) \end{cases} \quad (4.4)$$

where  $(d_{xi}, d_{xj})$  and  $(d_{yi}, d_{yj})$  are the distance separations across the  $x$ -axis and the  $y$ -axis between the receiver's normal and the reception area's boundaries respectively, and  $h$  is the reception area height. When the receiver is in the middle of the room (2m, 4m, 1m), the reception angles turn into reference points for the imaging receiver at all other locations in the indoor setting. The height of all reception areas is unchanged ( $h = 2m$ ) when the receiver is in the middle of the room.

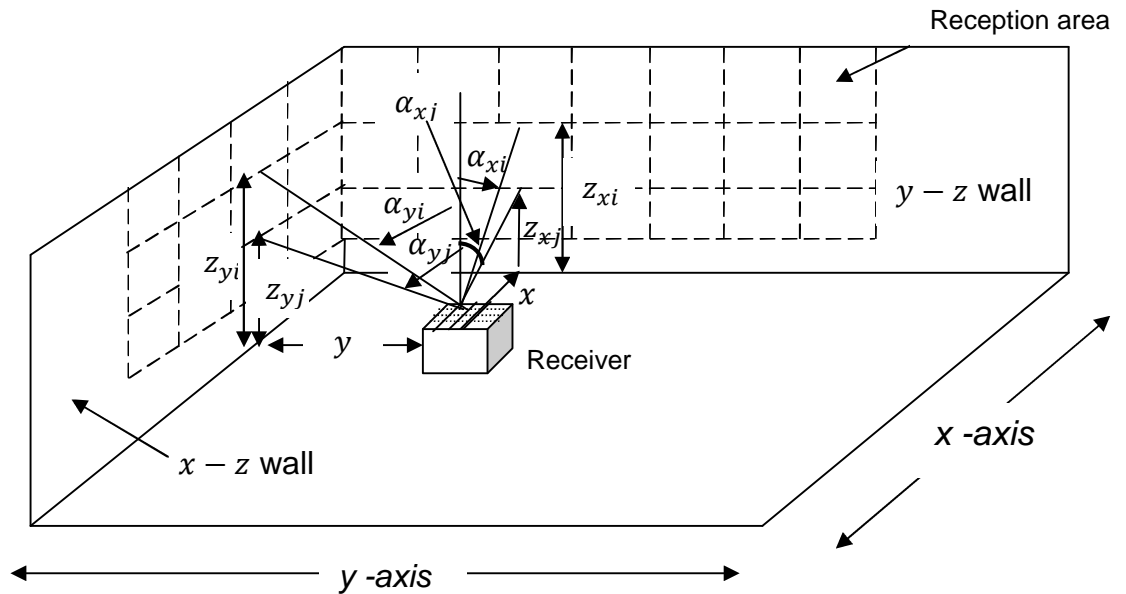
As the receiver terminal starts to move from the room centre, the reception areas will change accordingly. For example, if the receiver is shifted closer to the corner (1m, 1m, 1m), a number of the reception areas begin to fall on the walls:  $y$ - $z$  wall and  $x$ - $z$  wall as shown in Figure 4.16 (b). Therefore, the new  $(z_{yi}, z_{yj})$  or  $(z_{xi}, z_{xj})$  heights according to the new reception areas can be computed by considering the reference angles  $(\alpha_{xi}, \alpha_{xj}, \alpha_{yi}, \alpha_{yj})$  when the receiver is at the centre of the room as:

$$\begin{cases} z_{yi} = \frac{y}{\tan(\alpha_{yi})}, z_{yj} = \frac{y}{\tan(\alpha_{yj})}, x - z \text{ wall} \\ z_{xi} = \frac{x}{\tan(\alpha_{xi})}, z_{xj} = \frac{x}{\tan(\alpha_{xj})}, y - z \text{ wall} \end{cases} \quad (4.5)$$

where  $x$  and  $y$  represent the distance between the receiver and the  $y$ - $z$  wall and  $x$ - $z$  wall, respectively. In this study, during receiver mobility, the calculations of



(a) Receiver is placed in the middle of the room (2m, 4m, 1m).



(b) Receiver is moved near to the room corner (1m, 1m, 1m)

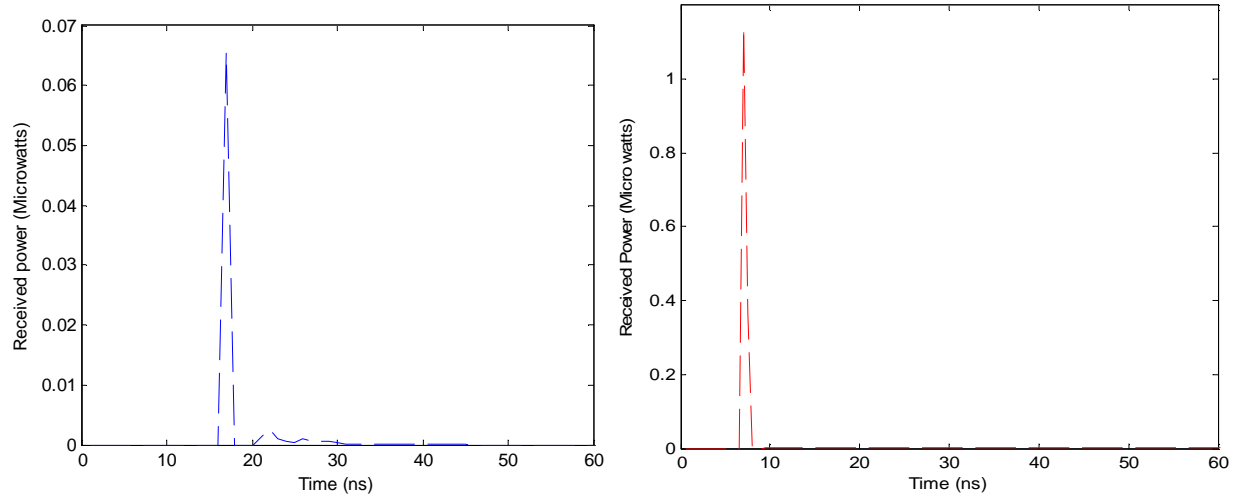
Figure 4.16: The angles of reception and reception areas of the imaging receiver (200 pixels) when (a) the receiver is placed at the reference point at (2m, 4m, 1m) and (b) when it moves near to the room corner, to (1m, 1m, 1m).

the receptions areas were undertaken following the process described above, taking into account the new receiver location and the reference points.

## 4.8 Impulse Response and Delay Spread

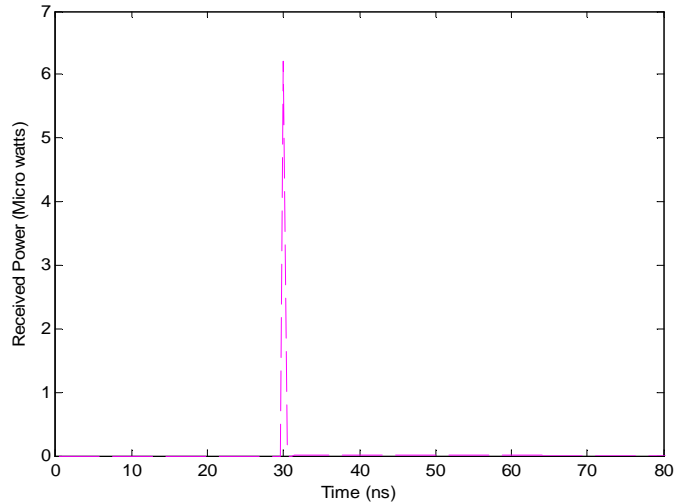
In this section, we examine the SC channel impulse response and the delay spread of the three proposed arrangements: CDS, non-adaptive LSMS and adaptive BDPA-LSMS combined with the imaging receiver (selecting the best pixel result). Figure 4.17 illustrates the channel impulse response (the received optical powers ( $\mu W$ ) as a function of time (nanoseconds)), when the transmitter is stationary in the middle of the room and the imaging receiver is positioned in the corner over the CP. A considerable drop in the received signal is seen in the diffuse channel (Figure 4.17 (a)). This is as a result of restricting the rays received by using narrow FOV pixels, where the FOV of each individual pixel is  $11.3^\circ$ . The drop in the total received signals increases when the non-adaptive LSMS multi-spot system (Figure 4.17 (b)) is used. The multi-spot LSMS configuration increases the overall received power from  $74.219 nW$  associated with the imaging CDS arrangement to around  $1.5 \mu W$ . Furthermore, the results show that the adaptive BDPA-LSMS system coupled with an imaging receiver provides notably better performance than the diffuse CDS and non-adaptive LSMS configurations. As shown in Figure 4.17 (c), the received optical power ( $\mu W$ ) of the BDPA-LSMS increases by a factor of five compared with the non-adaptive LSMS configuration. This is due to the use of beam delay and power adaptation. In practice, the channel impulse response of an OW configuration is continuous, however, the simulation ray tracing algorithm divides the reflective surfaces into discrete surfaces (small reflectors). The impact of discretisation is minimised by grouping the optical powers received within a  $0.5 ns$  time bin into a single power which smoothes the channel impulse response results.

## 4.8 Impulse Response and Delay Spread



(a) Imaging CDS system.

(b) Imaging LSMS system.



(b) Imaging BDPA-LSMS system.

Figure 4.17: Impulse response of (a) pure CDS diffuse, (b) non-adaptive multi-spot LSMS and (c) adaptive multi-spot BDPA-LSMS combined with imaging receivers when the emitter is positioned at (2m, 4m, 1m) and the receiver is moved near to the corner, at (1m, 1m, 1m).

For delay spread analysis, Figure 4.18 shows the delay spread of the CDS diffuse configuration, non-adaptive LSMS and adaptive BDPA-LSMS systems in conjunction with a 200-pixel imaging receiver. The results are presented when transmitters are placed in the room centre while the imaging receiver is moved down the y-axis along the line  $x=1m$ . Moreover, the wide FOV non-imaging

CDS link is also examined here for comparison purposes. The results show that our adaptive multi-spot BDPA-LSMS arrangement gives the lowest delay spread compared with other configurations at all receiver locations. This is due to our adaptive techniques (beam delay and power adaptations) as well as employing an imaging receiver, which limits the rays received by using 200 small FOVs ( $11.3^\circ$ ) pixels and selecting the best image result.

The results in Figure 4.18 show that the highest delay spread only occurred in a pure CDS diffuse configuration with a single wide FOV detector. When the imaging receiver substitutes a single non-imaging receiver in the diffuse CDS arrangement the delay spread is reduced from nearly 2.4 ns to about 0.35 ns. The non-adaptive LSMS configuration minimises the delay spread to nearly 0.14 ns. A further improvement in the delay spread can be obtained when our adaptive BDPA-LSMS is employed. The adaptive BDPA-LSMS combined with a 200 pixel imaging receiver reduces delay spread by a factor of three compared to the angle diversity receivers provided in the previous sections.

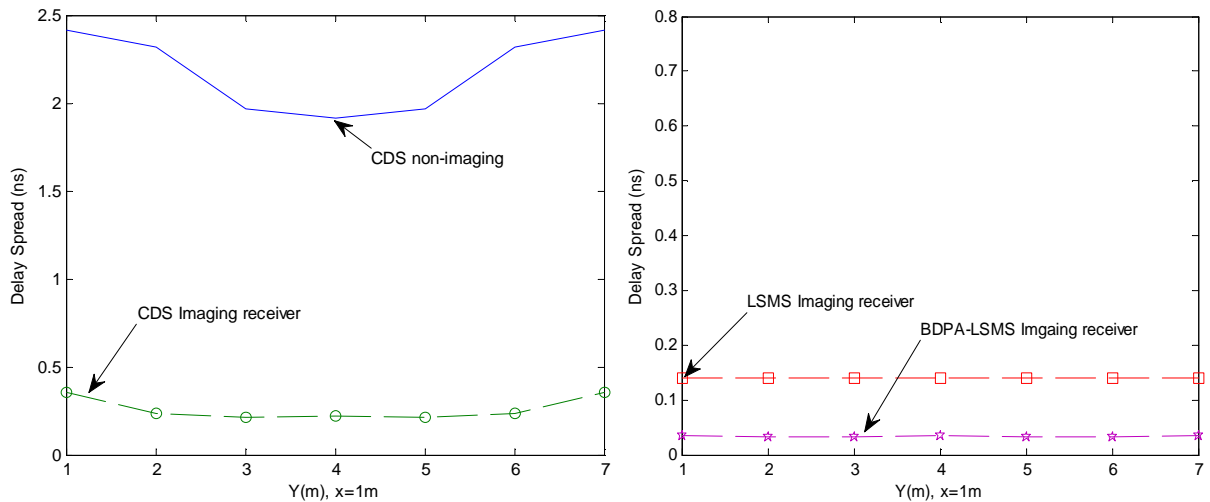


Figure 4.18: Delay spread of the single detector and imaging CDS systems, non-adaptive LSMS and adaptive BDPA-LSMS multi-spot configurations combined imaging receivers, when the transmitter is positioned at (2m, 4m, 1m) and the receiver moves along the x=1m line.

## 4.9 SNR Analysis

In this section, we study the SNR of CDS, non-adaptive LSMS and adaptive BDPA-LSMS configurations coupled with imaging receivers. All the systems operate at 30 Mb/s to help compare the results with other work in the literature [121]. Furthermore, a single large FOV non-imaging receiver with diffuse CDS setup is simulated here for comparative reasons. Higher data rates of 2.5 Gb/s and 5 Gb/s will also be considered in Section 4.10.

Indoor mobile optical wireless communication setups are negatively affected by artificial background noise sources, which can cause shot noise at the receiver. Following the SNR analysis given in Chapter 3 in (3.27), which accounts for the effect of pulse spread, in the imaging receiver, the total noise variance referring to the contribution of the  $i$ th pixel is given by:

$$\sigma_{total,i}^2 = \sigma_{0,i}^2 + \sigma_{1,i}^2, \quad (4.6)$$

in which

$$\sigma_{0,i}^2 = \sigma_{pr}^2 + \sigma_{bn,i}^2 + \sigma_{s0,i}^2 \quad \text{and} \quad \sigma_{1,i}^2 = \sigma_{pr}^2 + \sigma_{bn,i}^2 + \sigma_{s1,i}^2, \quad (4.7)$$

where  $\sigma_{pr,i}^2$  presents the preamplifier noise variance component associated with pixel  $i$ ,  $\sigma_{bn,i}^2$  refers to the background shot noise seen by the pixel  $i$ .  $\sigma_{s0,i}^2$  and  $\sigma_{s1,i}^2$  represent the shot noise signal components captured by the pixel  $i$  associated with  $P_{s0,i}$  and  $P_{s1,i}$  respectively. The signal shot noise due to  $P_{s0,i}$  and  $P_{s1,i}$  is very low and can be neglected based on the experimental findings reported in [56]. The background shot noise variance component ( $\sigma_{bn,i}^2$ ) associated with a pixel  $i$  can be calculated as [178]:

$$\sigma_{bn,i}^2 = 2qRP_{bn,i}BW, \quad (4.8)$$

where  $R$  is the detector responsivity,  $q$  is the electronic charge,  $P_{bn,i}$  is the surrounding light power detected by the  $i$ th pixel, and  $BW$  is the receiver bandwidth. In the imaging receiver design, we utilised the PIN-FET transimpedance preamplifier used in [121]. The gate leakage and  $1/f$  noise of the FET were neglected. Therefore, the preamplifier noise variance is given by [121]

$$\sigma_{pr}^2 = \frac{4kT}{R_f} I_2 B + \frac{16\pi^2 k T \Gamma}{g_m} (C_d + C_g)^2 I_3 B^3 \quad (4.9)$$

The first term in (4.9) represents thermal noise from the feedback resistor where  $k$  is Boltzmann's constant,  $T$  is absolute temperature and  $R_f$  represents feedback resistance,  $I_2=0.562$ . The second term describes thermal noise from FET resistance,  $\Gamma$  is the FET noise factor,  $g_m$  is the FET transconductance,  $C_d$  is the capacitance of each detector pixel,  $C_g$  is the FET gate capacitance, and  $I_3=0.0868$ . In order to see specifically how the two noise terms in (4.9) rely on the pixel size, we consider a fixed capacitance per unit area,  $\eta_c$ , for the detector where  $C_d = \eta_c A'$ , ( $A'$  represents the detector area). To simplify the calculations, we assume that  $C_g \ll C_d$ . We also assume that the transimpedance amplifier has a restricted open-loop voltage gain  $G$ . It is preferable to maximise  $R_f$  in order to minimise the noise. However, if the preamplifier has to obtain a 3-dB cut-off frequency equal to bit rate ( $B$ ), then we need to add the condition  $R_f = G/2\pi B C_d$ . Therefore, after all these considerations, equation (4.9) can be written as

$$\sigma_{pr}^2 = \frac{8\pi k T}{G} \eta_c A' I_2 B^2 + \frac{16\pi^2 k T \Gamma}{g_m} \eta_c^2 A'^2 I_3 B^3. \quad (4.10)$$

For modelling the noise of a single wide FOV non-imaging detector, we use (4.8) and (4.10), where all components are referred to a single non-imaging detector. The amount of shot noise in (4.8) and (4.10) is significantly reduced

when 200-pixel imaging receivers with small FOVs are used compared with a single non-imaging detector. The noise reduction in equation (4.8) is due to the use of narrow FOVs associated with 200 pixels which minimise the received background power. The terms in equation (4.10) are reduced due to a small pixel size which reduces the preamplifier input capacitance. In our calculations, we select parameter values for the preamplifier similar to those used in [121]:  $\Gamma = 1.5$ ,  $T = 295K$ ,  $R = 0.6 A/W$ ,  $G = 10$ ,  $g_m = 30ms$  and,  $\eta_c = 112pF/cm^2$ . This preamplifier is employed for a data rate of 30 Mb/s.

In the imaging receiver, we consider two signal processing techniques: SC and MRC. The imaging SC applies a simple diversity technique, where the best SNR pixel is selected among all the pixels as follows:

$$SNR_{SC,IMG} = \max_i \left( \frac{R(P_{s1i} - P_{s0i})}{\sqrt{\sigma_{pri}^2 + \sigma_{bni}^2 + \sigma_{s0i}^2} + \sqrt{\sigma_{pri}^2 + \sigma_{bni}^2 + \sigma_{s1i}^2}} \right)_i^2, 1 \leq i \leq K \quad (4.11)$$

where  $K$  represents the total number of pixels ( $K=200$ ). Considering a fixed area for the planar array, as the total number of pixels goes up the area of each pixel is reduced, which leads to a reduction in the shot noise components per pixel  $\sigma_{total,i}^2$ , hence increasing the SNR. Unlike the SC method, the MRC approach uses all the pixels, where the output signals of the pixels are combined using an adder circuit. Each input is assigned a weight (relative to its SNR ratio) to maximise the MRC SNR as

$$w_i = \frac{R(P_{s1i} - P_{s0i})}{(\sigma_{0i} + \sigma_{1i})^2}, 1 \leq i \leq K. \quad (4.12)$$

The MRC SNR is

$$SNR_{MRC,IMG} = \frac{(\sum_{i=1}^K R(P_{s1i} - P_{s0i}) w_i)^2}{\sum_{i=1}^K (\sigma_{0i} + \sigma_{1i})^2 w_i^2} \quad (4.13)$$

$$\begin{aligned}
SNR_{MRC,IMG} &= \frac{\left( \sum_{i=1}^K R(P_{s1i} - P_{s0i}) \frac{R(P_{s1i} - P_{s0i})}{(\sigma_{0i} + \sigma_{1i})^2} \right)^2}{\sum_{i=1}^J (\sigma_{0i} + \sigma_{1i})^2 \left( \frac{R(P_{s1i} - P_{s0i})}{(\sigma_{0i} + \sigma_{1i})^2} \right)^2} \\
&= \sum_{i=1}^K \left( \frac{R(P_{s1i} - P_{s0i})}{\sigma_{0i} + \sigma_{1i}} \right)^2 = \sum_{i=1}^K SNR_i.
\end{aligned} \tag{4.14}$$

It is clear that the SNR obtained from MRC is better than the SC technique, but at the cost of increased circuit complexity. The complexity is linked to the increased signal processing so as to establish the right weighting factors compared to the SC.

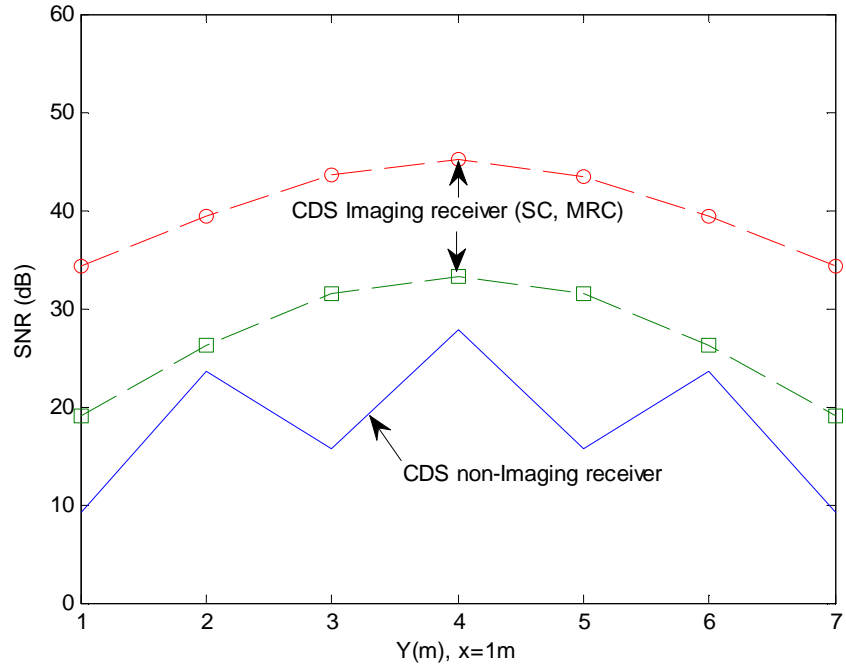
#### 4.9.1 SNR Results of Non-imaging and Imaging CDS diffuse Setups

The SC and MRC SNR results of the imaging CDS diffuse configuration under the influence of background noise sources, user mobility, multipath dispersion and receiver noise, are given in Figure 4.19. The imaging CDS results are compared with a single wide FOV detector (non-imaging). The pure CDS diffuse system was positioned in the middle of the room and also near to the room's edge, while the imaging and the non-imaging receiver were moved down to the y-axis across the x=1m line. The CDS simulation results are evaluated at a 30 Mb/s data rate, in order to allow comparison with the earlier results reported in [121]. The preamplifier employed for the imaging CDS configuration is the PIN FET transimpedance receiver explained above. At a constant x=1m line (down to the y-axis), the highest and lowest ambient noise levels are clear in the SNR of the non-imaging CDS configuration. This is attributed to the ambient light noise sources which have very directive high noise power at the certain coordinates, (x, y), on the CP: (1m, 1m), (1m, 3m), (1m, 5m) and (1m, 7m), whereas low noise power is observed at: (1m, 2m), (2m, 4m) and (2m, 6m).

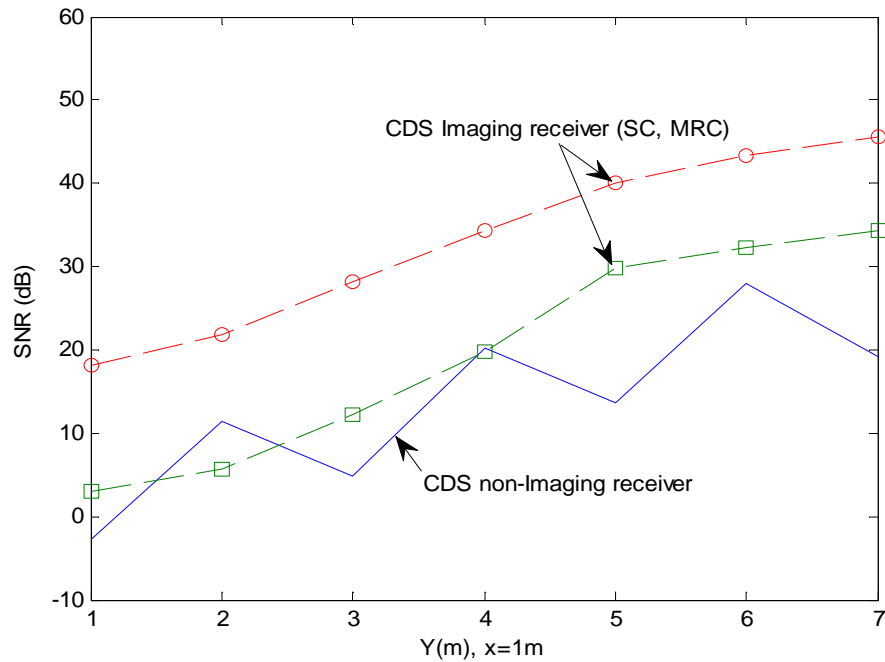
The SNR variation of the CDS diffuse system is reduced when an imaging receiver substitutes the single large FOV non-imaging detector. At the worst communication link considered, the imaging SNR MRC diffuse CDS system provides a considerable SNR gain of roughly 20 dB over a single wide FOV non-imaging CDS system. This result corresponds closely with those observed in [121]. The increase in the SNR is due to the ability of the imaging receiver which can select or combine (SC or MRC) the pixels that monitor the lowest ambient noise levels. Furthermore, a drop in the received background noise levels is observed at the receiver as a result of the small FOVs associated with 200 pixels. Although the 200-pixel imaging receiver improves the overall performance of the CDS diffuse setup, degradation is still induced due to user mobility. For example, if the CDS system moves closer to the room's edge and the receiver is located near to the room's corner on the other side, the SNR of the imaging MRC CDS setup is reduced by 15 dB. This SNR degradation is attributed to low received optical power due to a large distance separating the diffuse CDS transmitter and the imaging receiver. The performance degradation in the CDS diffuse configuration due to user motion can be reduced by substituting the imaging CDS with imaging LSMS and adaptive BDPA-LSMS arrangements.

#### **4.9.2 SNR Results of Imaging Non-adaptive LSMS and Adaptive BDPA-LSMS Configurations**

Figure 4.20 shows the SC and MRC SNR performance of a non-adaptive LSMS and adaptive BDPA-LSMS multi-spot diffusing configurations combined with an imaging receiver, when the systems operate at 30 Mb/s. The multi-spot configurations were positioned in the middle of the room as well as close to the room's edge, while the imaging receiver moved down the y-axis, along the  $x=1\text{m}$  line. The results show a steady SNR for both SC and MRC imaging LSMS setup, when the system is in the middle of the room, in comparison with



(a) The diffuse system is positioned at the room centre at: (2m, 4m, 1m).



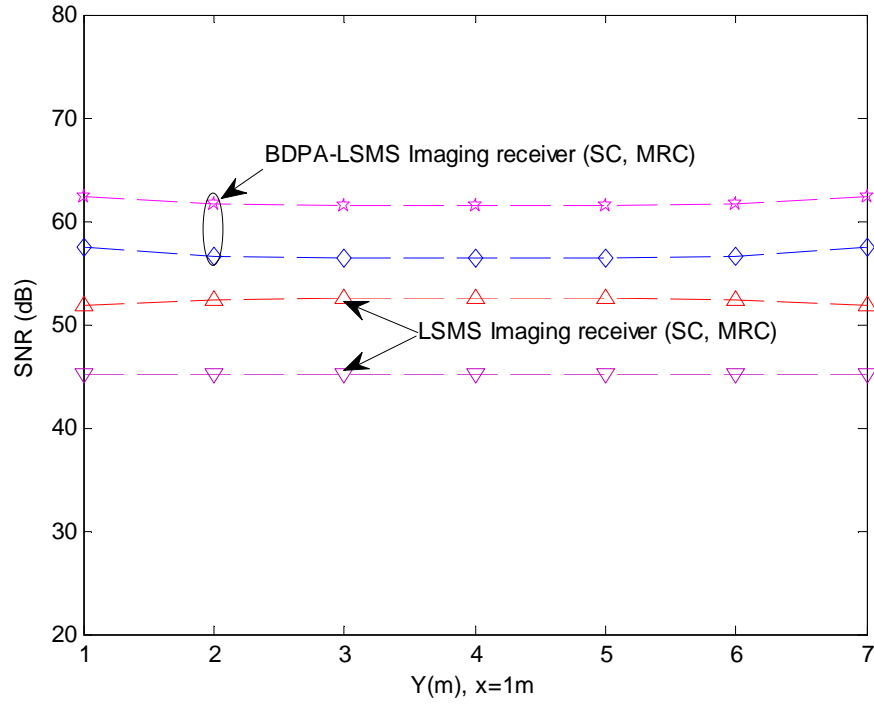
(b) The diffuse system is positioned near to the room's edge at: (2m, 7m, 1m).

Figure 4.19: The SNR of CDS with non-imaging receiver (wide FOV receiver) and SNR of CDS with 200-pixel imaging receiver using SC and MRC when the diffuse transmitter is positioned at (a) (2m, 4m, 1m), (b) (2m, 7m, 1m) and the receiver moves along the  $x=1m$  line.

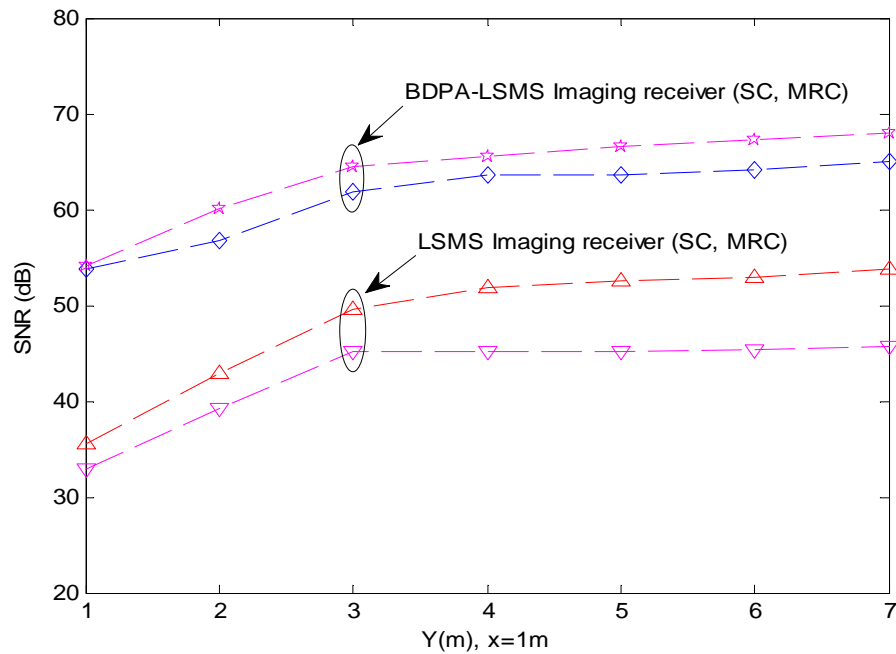
the SC and MRC SNR of the imaging diffuse CDS system given in the previous section. Along with the constant SNR, the non-adaptive LSMS configuration gives around 17 dB SNR improvement over the imaging pure CDS diffuse system. This SNR gain is attributed to the capability of the non-adaptive LSMS arrangement to more consistently cover its environment through a number of diffusing spots, giving the imaging receiver an option to select the signal from the closest spots. In Figure 4.19 (b) and 4.20 (b), at a 6m separation between the transmitter and the imaging receiver, the non-adaptive LSMS arrangement produces roughly 16 dB SNR again, above the imaging CDS diffuse setup. Additional SNR improvement of 19 dB can be obtained when the non-adaptive LSMS is substituted with our adaptive BDPA-LSMS system. This significant improvement in the SNR result is attributed to employing our new delay and power adaptive techniques coupled with an imaging receiver. The small size of the pixels associated with small FOVs results in a drop in the received ambient noise detected by each pixel, as well as reducing the preamplifier thermal noise.

### **4.10 Beam Delay and Power Multiple Adaptive Beam Clustering Method (BDPMA-BCM)**

Spot distribution based on the beam clustering method (BCM) has been shown in [172] – [173] and extended into the beam delay and power adaptive multi-beam clustering method (BDPA-BCM) combined with an angle diversity receiver in Section 4.6. Although the adaptive clustering BDPA-BCM configuration combined with angle diversity receivers improved the overall optical wireless system performance, there is a need for other techniques that may additionally be used to reduce the system degradation induced by transmitter mobility. Therefore, in this section the concept of adaptive delay and beam clustering is extended and modified to the new beam delay and power



(a) The multi-spot configuration positioned at (2m, 4m, 1m).



(b) The multi-spot configuration positioned at (2m, 7m, 1m).

Figure 4.20: the SNR of the LSMS and BDPA-LSMS with an imaging receiver when the system is positioned at (a) (2m, 4m, 1m) and (b) (2m, 7m, 1m), and the receiver moves along the x=1m line.

multiple adaptive beam clustering method (BDPMA-BCM) combined with an imaging receiver. The new concept of using multiple adaptive clusters is employed to design a new geometry that can achieve a good performance in mobile OW communications. The proposed BDPMA-BCM configuration generates three two-dimensional clusters of spots distributed as follows: 240 spots (3×80) on the ceiling and 60 spots (3×20) on each of the two end walls ( $y=0$  and  $y=8\text{m}$ ) along the lines  $x=1\text{m}$ ,  $2\text{m}$  and  $3\text{m}$ , when the transmitter is located at the centre of the room. The distance between the nearby spots is 10 cm. Each spot produces 2.77 mW. The spots on the ceiling and walls turn into secondary diffuse transmitters, which produce Lambertian emissions ( $n=1$ ). To assist in visualising the BDPMA-BCM arrangement, Figure 4.21 shows a limited number of diffusing spots when the transmitter is placed in the middle of the room. The three clusters cover the lines  $x=1\text{m}$ ,  $2\text{m}$ , and  $3\text{m}$  (Figure 4.21). Rather than turning on all of the clusters simultaneously (at the same time) and distributing the transmission power (1W) between clusters equally in the basic beam cluster method, the proposed adaptive setup switches on each spot individually and calculates the delay and the SNR weight associated with the spot at the imaging receiver. The receiver then notifies the transmitter about the detected SNR weight and the delay due to each spot through low rate feedback signals. This helps the system change the intensities and adapt the delay between the beams to increase the SNR level as well as mitigate the influence of multipath dispersion and user mobility. Beam delay adaptation helps reduce the pulse spread of the received signal, therefore reducing the delay spread and increasing the SNR. An algorithmic description of the multiple adaptive beam clustering algorithms is given in Table 4.2. More details about the parameters used in this study are provided in Table 4.3.

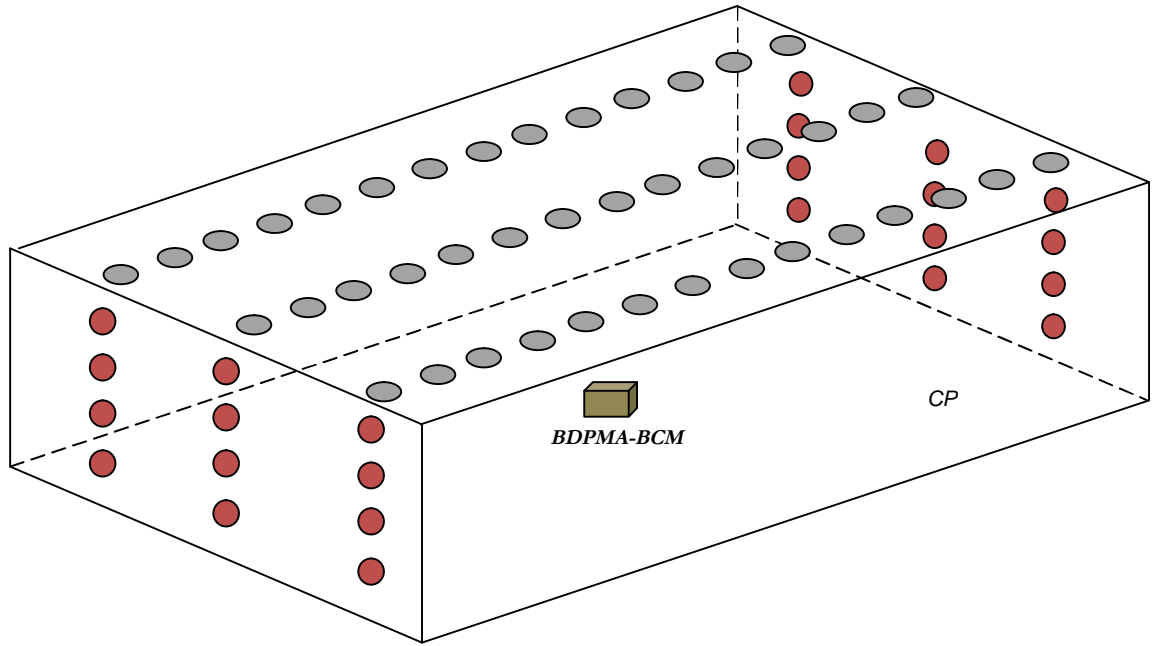


Figure 4.21: BDPMA-BCM arrangement when the system is positioned in the middle of the room at (2m, 4m, 1m).

### 4.10.1 Performance Analysis and Simulation Results

In this section, we study the delay spread and SNR of adaptive BDPMA-BCM system. The proposed system combined with a 200-pixel imaging receiver and the results are compared with our previous geometries: imaging CDS diffuse, non-adaptive LSMS and adaptive BDPA-LSMS multi-spot configurations at two different locations, when the system is located near to the edge of the room and the corner of the room while the imaging receiver moves down to the y-axis, along the lines of  $x=1\text{m}$  and  $2\text{m}$ , respectively.

#### 4.10.1.1 Delay Spread Analysis

The delay spread of our proposed adaptive BDPMA-BCM system is given in Figure 4.22. Moreover, the proposed system is compared with our previous:

Table 4.2: Multiple Clusters, Delay and Power Adaptation Algorithm with Imaging Receivers

---

1	$N_{clusters} = 3;$ (Number of Clusters)
2	$M_{spots} = 120;$ (Number of Spots in each line)
3	$J_{pixels} = 200;$ (Number of pixels in imaging receiver).
4	$p(\cdot)$ is a rectangular pulse defined over $[0, T_b]$ , $T_b = 1/B$ ; $B$ is bit rate.
5	Input $Tx(\cdot)$ ; , $Rx(\cdot)$ ; , $T(\cdot)$ ; strat of the frame.
6	Initilise the total impulse response of each pixel $h(\cdot)_t = 0$
7	For $i = 1: M_{spots} \times N_{clusters}$
8	$P_{spot} = \frac{P_{total\ transmit\ power}}{M_{spots} \times N_{clusters}};$ (Power per spot)
9	For $j = 1: J_{pixels}$
10	Calculate the received power level $P_j$ within a time bin (0.5ns duration)
11	Produce the impulse response $h(\cdot)_j$
12	compute the total impulse response $h(\cdot)_t = h(\cdot)_t + h(\cdot)_j$
13	Calculate the pulse response $h(\cdot)_t \otimes p(t - T_b)$ and $(P_{s1} - P_{s0})_t$
14	Compute $SNR_j = \left( \frac{R \times (P_{s1} - P_{s0})_t}{(\sigma_t)_j} \right)^2$
15	end
16	$W_{spot} = MRC(SNR_j);$ (weight of each spot).
17	$W_{total} = W_{total} + W_{spot};$ ( total weight )
18	$P_{max} = find(P_j == \max(SNR_j))$
19	compute $t_i$ of $P_{max}$
	End
20	introduce the $\Delta t$ between beams $\Delta t_i = \max(t_{i,max}) - t_i$
21	the total impulse response of each pixel $h(\cdot)_t = 0$
22	For $j = 1: J_{pixels}; ;$
23	For $i = 1: M_{spots} \times N_{clusters}$
24	$Tx$ sends the beam with the largest time delay first
25	$P_{spot_i} = \left( \frac{W_{spot_i}}{W_{total}} \right) \times P_{total\ transmit\ power}$
26	Calculate the received power level $P_j$
27	Produce the impulse response $h(\cdot)_i$
28	Compute the total impulse response $h(\cdot)_t = h(\cdot)_t + h(\cdot)_i$
29	$Tx$ introduces $\Delta t$ with next spot ( $i + 1$ )
30	end
31	Compute $SNR_j = \left( \frac{R \times (P_{s1} - P_{s0})_t}{(\sigma_t)_j} \right)^2$
32	End
33	$SNR_{optimum} = MRC(SNR_j)$
34	$P_{optimum}(t) = find(P_j(t) == \max(SNR_j)).$
35	$Delay\ spread_{optimum} = \sqrt{\frac{\int (t - \mu)^2 P_{optimum}^2}{\int P_{optimum}^2}}$

---

Table 4.3: Simulation Parameters.

Parameter	Configuration		
	UPLINKS TRANSMISSION		
Length	8 m		
Width	4 m		
Height	3 m		
$\rho$ x-z wall	0.8		
y-z wall	0.8		
x-z op wall	0.8		
y-z op wall	0.8		
Floor	0.3		
	Transmitter		
Quantity	1		
Location (x, y, z)	(2m, 4m, 1m) (2m, 7m, 1m) (1m, 1m, 1m)		
Elevation	90°		
Azimuth	0°		
	Imaging Receiver		
Quantity	1		
Detector array's area	2 cm <sup>2</sup>		
Number of Pixels	200		
Area of pixels	1 mm <sup>2</sup>		
Elevation	90°		
Azimuth	0°		
Acceptance semi-angle	65°		
	Resolutions		
Time bin duration	0.5 ns , 0.01ns		
Bounces	1	2	
Surface elements	32000	2000	
Number-of-spot lamps	8		
Locations	(1m,1m,1m), (1m,3m,1m), (1m,5m,1m), (1m,7m,1m) (3m,1m,1m), (3m,3m,1m), (3m,5m,1m), (3m,7m,1m)		
Wavelength	850 nm		
Preamplifier design	PIN-FET		
Bandwidth (BW)	30 MHz	2.5 GHz	5 GHz
Bit rate	30 Mb/s	2.5 Gb/s	5Gb/s

CDS, non-adaptive LSMS and adaptive BDPA-LSMS configurations when the systems are placed near to the corner of the room at (1m, 7m, 1m) and the imaging receiver moves down at a constant x=2m line, along the y-axis. In the CDS diffuse arrangement, the delay spread reduces from 3.7 ns to nearly 0.8 ns when an imaging receiver is substituted for a single wide FOV receiver (non-imaging). Moreover, the imaging non-adaptive LSMS system minimises the delay, from the 0.8 ns of the imaging CDS configurations to nearly 0.5 ns, see

Figure 4.22. This improvement in the delay spread is due to the use of the multi-spot diffusing technique (directed-LOS links) as well as restricting the rays received by using small FOV ( $11.3^\circ$ ) pixels, which reduces pulse spread, hence reducing delay spread. Significant reduction in delay spread can be achieved when our beam delay and power adaptation are implemented in LSMS. The results show that the adaptive BDPA-LSMS configuration reduces the delay spread by a factor of 5 compared with the non-adaptive LSMS system. Further reduction in delay spread by a factor of 2 can be obtained compared with the BDPA-LSMS system, when our new multiple adaptive clustering (BDPMA-BCM) system is used. This is attributed to the optimisation of the spots' distribution through the use of multiple adaptive clustering techniques.

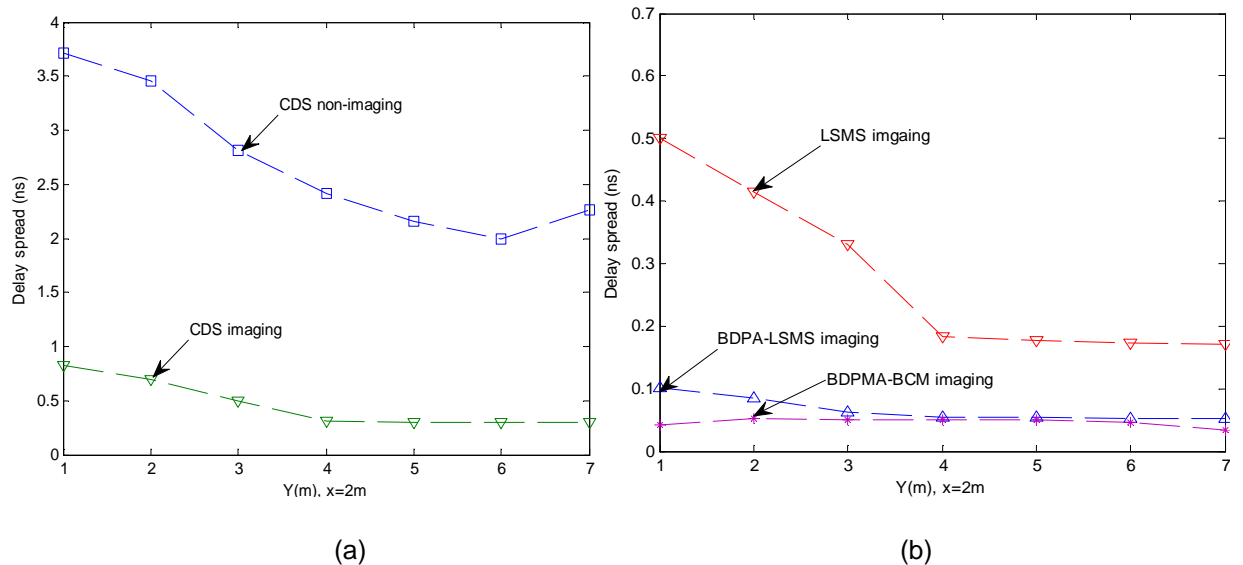


Figure 4.22: Delay spread of five configurations (a) CDS imaging and non-imaging receiver (b) LSMS, BDPA-LSMS and BDPMA-BCM, when the transmitter is placed in corner of the room at (1m, 7m, 1m) and the receiver moves along  $x=2m$  line.

#### 4.10.1.2 SNR Results

The MRC SNR result of the BDPMA-BCM system coupled with an imaging receiver operating at 30 Mb/s is plotted in Figure 4.23. The proposed configuration is compared to the imaging CDS system, non-adaptive LSMS, and adaptive BDPA-LSMS configurations. At 30 Mb/s, we used the preamplifier

design explained in Section 4.9 in order to compare the result with our previous systems. The results indicate that the CDS system replacing the single large FOV non-imaging receiver with narrow FOVs imaging receiver increases the SNR by roughly 20dB at the worst case scenario. A 16 dB SNR enhancement can be obtained over an imaging CDS diffuse system when a non-adaptive multi-spot diffusing LSMS system is employed. Moreover, SNR improvements of 19 dB and 35 dB are achieved when the adaptive BDPA-LSMS is substituted for non-adaptive LSMS and CDS configurations respectively. These SNR enhancements are due to the ability of the spot diffusing structure coupled with our adaptive techniques which can significantly increase the direct links between spots and the receiver during mobility. Furthermore, our new proposed adaptive clustering techniques coupled with an imaging receiver can enhance the system performance during mobility. At the worst communication link, the BDPMA-BCM setup coupled with narrow FOVs imaging receiver produces a considerable SNR gain of 10 dB above the BDPA-LSMS system.

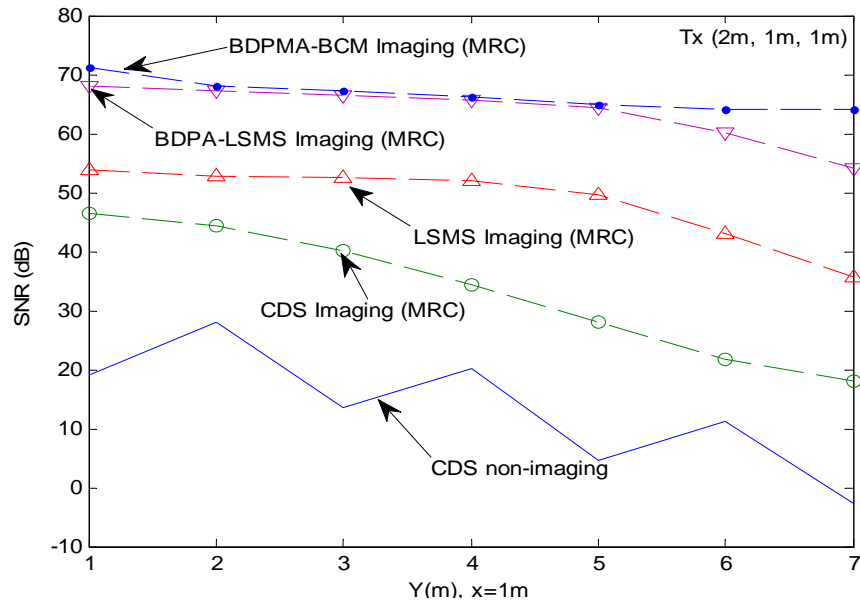


Figure 4.23: SNR of CDS, LSMS, BDPA-LSMS and BDPMA-BCM at 30 Mb/s when the transmitter is placed at (2m, 1m, 1m) while the receiver moves along the line  $x=1m$ .

The SNR and delay spread enhancements through the use of our imaging BDPMA-BCM system allow the system to increase the data rate. Figure 4.24 illustrates the MRC SNR results of BDPA-LSMS and BDPMA-BCM systems functioning at high data rates of 2.5 Gb/s and 5 Gb/s, under the impairments of multipath dispersion, transmitter mobility, ambient noise sources and receiver noise. For high data rates of 2.5 Gb/s and 5 Gb/s, we used the PIN FET receiver design proposed in [187]. As mentioned earlier, the optimum receiver bandwidth is 0.7 of the system data rate [77]. Therefore, the receiver bandwidth was restricted to 1.75 GHz and 3.5 GHz at 2.5 Gb/s and 5 Gb/s, respectively via the use of appropriate filters. At the worst link, the new 5 Gb/s imaging BDPMA-BCM, produces an MRC SNR enhancement of 10 dB over the BDPA-LSMS configuration. The high bit rates: 2.5 Gb/s and 5 Gb/s in the imaging BDPMA-BCM are therefore seen to be achievable by using multiple clusters, beam delay adaptation, transmission power adaptation and imaging detection.

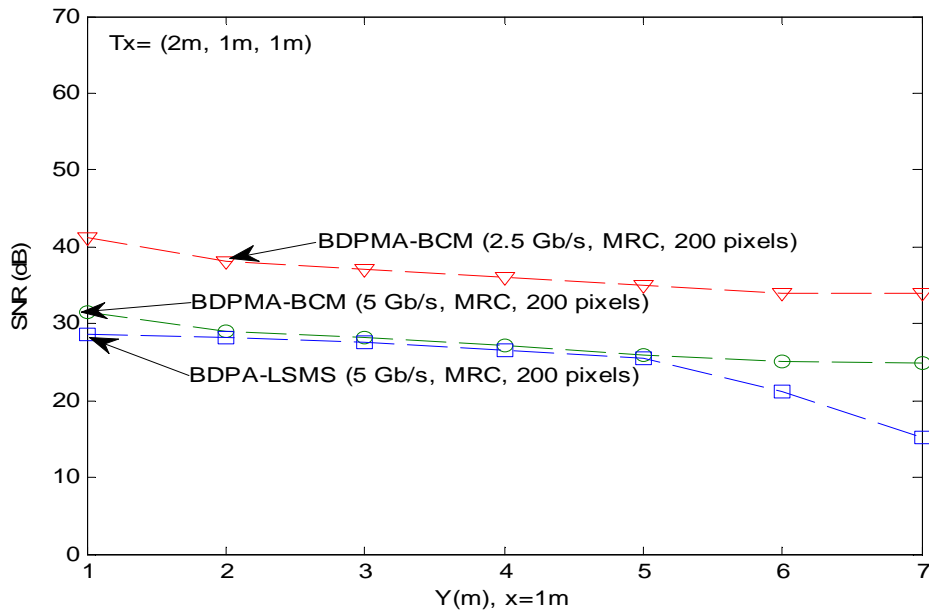


Figure 4.24: SNR of proposed 2.5 Gb/s and 5 Gb/s BDPMA-BCM compared with 5 Gb/s BDPA-LSMS system, when the transmitter is near the room edge transmitting 1W while the receiver moves along the y-axis at x=1m.

The SNR achieved using our new adaptive techniques with multi-spot diffusing enables the system to reduce the total transmit power while operating at a high data rate. A reduction in the total transmit power of OW systems at high data rates will be considered in Chapters 5, 6 and 7.

### **4.11 Summary**

The impact of transmitter mobility on the indoor OW channel was studied using the CDS and the non-adaptive multi-spot system LSMS. At a 6m separation between the transmitter and the receiver, the mobile system using a multi-spot LSMS transmitter coupled with seven-angle diversity receivers provided more than 30 dB SNR improvement over the pure diffuse CDS system. As such, given this considerable SNR improvement, the multi-spot LSMS configuration coupled with an angle diversity receiver is a candidate replacement for the CDS system for both fixed transmitter-receiver location scenarios and mobile systems. In this chapter, we designed and investigated a novel mobile OW system that uses beam delay and power adaptation in multi-spot (BDPA-LSMS) coupled with angle diversity detection. Our aim was to increase the received optical power, and enhance the SNR when the transmitter operates under the effect of ambient noise sources, user mobility, receiver noise and multipath dispersion. At 50 Mb/s, our proposed adaptive multi-spot BDPA-LSMS obtained a better SNR with an SNR gain of 10 dB over the LSMS system. Moreover, the idea of beam delay and power adaptive multi-beam clustering (BDPA-BCM) was introduced. The proposed adaptive clustering system can significantly enhance the performance of mobile non-directed OW connections. It offered a 10 dB SNR gain over adaptive multi-spot BDPA-LSMS system. The good SNR results and large channel bandwidth allowed our BDPA-BCM system to operate at high bit rates (2.5 Gb/s and 5 Gb/s).

Furthermore, in this chapter, a custom design of an imaging receiver is introduced. The CDS, non-adaptive LSMS and adaptive BDPA-LSMS

configurations are studied with our imaging receiver to enhance the mobile OW system's performance. Imaging reception can significantly help mitigate the effect of background noise sources by selecting or combining (SC or MRC) the pixels that receive the minimum noise level. A 20 dB SNR gain was achieved when a diffuse CDS system employed an imaging receiver (MRC) instead of a wide FOV receiver. Additionally, 16 dB SNR improvement was obtained over the CDS system when multiple spot diffusing coupled with an imaging receiver was employed. This enhancement is due to the utilisation of a range of multi-spot diffusing arrangement which helps provide directed-LOS links. The directed LOS received signals can be further enhanced in our imaging adaptive BDPA-LSMS configuration, by allocating high intensities to spots closest to the receiver as well as introducing differential delays between the beams. The adaptive BDPA-LSMS multi-spot configuration combined imaging receiver produces an SNR gain of 19 dB above the imaging non-adaptive LSMS system.

In this chapter, we also proposed and studied a new multiple adaptive beam clustering method (BDPMA-BCM) coupled with imaging receivers and the results have shown that it can enhance the system's performance in the presence of multipath dispersion, user mobility, receiver noise and ambient noise sources. The proposed BDPMA-BCM setup can also help reduce the impact of ISI at high data rates. High data rates of 2.5 Gb/s and 5 Gb/s are considered in our BDPA-LSMS and BDPMA-BCM configurations and the results shown that these systems are feasible. In the worst communication path considered, the 5 Gb/s BDPMA-BCM combined with the imaging receiver obtained an SNR gain of 10 dB above the imaging BDPA-LSMS.

# **5 Performance Evaluation of 5 Gb/s and 10 Gb/s Mobile Optical Wireless Systems Employing Beam Angle and Power Adaptation with Diversity Receivers**

## **5.1 Introduction**

Mobility as well as shadowing can impair the performance of an OW link; therefore, there is considerable interest in finding techniques to reduce the impact of mobility on OW configurations. Our previous research in Chapter 4 has illustrated that adaptively redistributing the power as well as introducing differential delays between the beams coupled with non-imaging or imaging diversity receivers can considerably enhance the SNR in realistic environments, where mobility, directive light noise sources and multipath dispersion are all present [116] – [117], [125]. Even though these ideas have led to considerable enhancements, the SNR is still subject to degradation as a result of transmitter movement (when the receiver and transmitter are distant from each other), beam obstruction as well as shadowing. In the previous OW systems discussed, the locations of the spots are fixed. With fixed spots angles, the locations of the spots are dictated by the transmitter location. For example, in the case of the beam delay and power adaptive line multi-spot diffusing system

(BDPA-LSMS), when the receiver and the transmitter are away from each other; the spots are particularly disseminated close to the transmitter, on the ceiling and in the corner adjacent to the transmitter. In this instance, the fixed beam angle coupled with beam delay and power adaptation does not offer full enhancement. In order to surmount this challenge, and to improve the SNR at the receiver, 'angle adaptation' is proposed here to offer an additional degree of freedom in order to optimise the location of the spots (reallocate the spots close to the receiver location despite the transmitter position) [113] – [115], [123], [124], [188]. In this chapter, the idea of beam angle adaptation is combined with beam power adaptation. Our objective is to refine the distribution of spots in the room by using an adaptive multi-spot transmitter, whose spot angles and powers can be managed and adapted using a digital signal processor (DSP). This can considerably reduce the impact of user mobility, in addition to enhancing the operation of the OW system in a realistic indoor setting (multipath dispersion, transmitter/receiver mobility and very directive background light sources).

Over the last two decades, indoor mobile OW systems have typically operated at 30 Mb/s to 155 Mb/s. In this chapter, we propose, design and report a new mobile OW system that operates at 5 Gb/s and 10 Gb/s. The enhancements in data rates and channel bandwidth are obtained by employing our methods: beam power adaptation, beam angle adaptation and angle diversity receivers. We propose a mobile OW system that employs beam angle and beam power adaptation in a line strip multi-spot diffusing system (APA-LSMS) in conjunction with three-branched angle diversity receivers. The performance of our proposed system is characterised through channel and noise modelling. Beam angle adaptation can help find the optimum spot location for the receiver. Our results demonstrate that the proposed APA-LSMS at a 30 Mb/s bit rate achieves about 45 dB signal-to-noise ratio (SNR) gain over a power adaptive line strip multi-spot system (PA-LSMS) at a 6 m horizontal separation between the transmitter and the receiver. Moreover, the simulation results show an increase in the

channel bandwidth from 36 MHz associated with the wide FOV CDS system to around 7.2 GHz in our new proposed configuration (APA-LSMS). Such significant enhancements in the SNR and 3-dB channel bandwidth can enable our system to operate at higher data rates, i.e., 5 Gb/s and 10 Gb/s.

## **5.2 Mobile Angle and Power Adaptive LSMS Configuration (APA-LSMS)**

A large distance between the closest diffusing spot on the ceiling or walls and the receiver can result in degradation in the OW system's SNR. In order to reduce the impact of this problem, we propose APA-LSMS in conjunction with three-branched angle diversity receivers. Beam angle and power adaptation help find the optimum locations of spots that maximise the SNR at the receiver. The APA-LSMS mobile OW communication system is illustrated in Figure 5.1, where the transmitter is positioned at the room edge: (2m, 7m, 1m), multi-spot angle and beam power adaptations are employed and the receiver is moved to the room corner (1m, 1m, 1m) and utilises angle diversity with three branches. The beam angle and beam power adaptations can be implemented by an adaptive hologram that produces spots whose locations and intensities can be varied with transmission angles  $(\delta_x, \delta_y)$  in the  $x - y$  directions. These angles can be varied from  $-90^\circ$  to  $90^\circ$  with respect to the transmitter's normal in  $x, y$  directions. An adaptive hologram first produces a single spot which is scanned along a range of rows and columns in the ceiling and walls to identify the best single beam location that produces the best SNR at the receiver. This location is used as the centre of the line strip of spots (80 spots in our case). This technique helps identify the strongest path between the transmitter and the receiver. The block diagram of our APA-LSMS system is given in Figure 5.2.

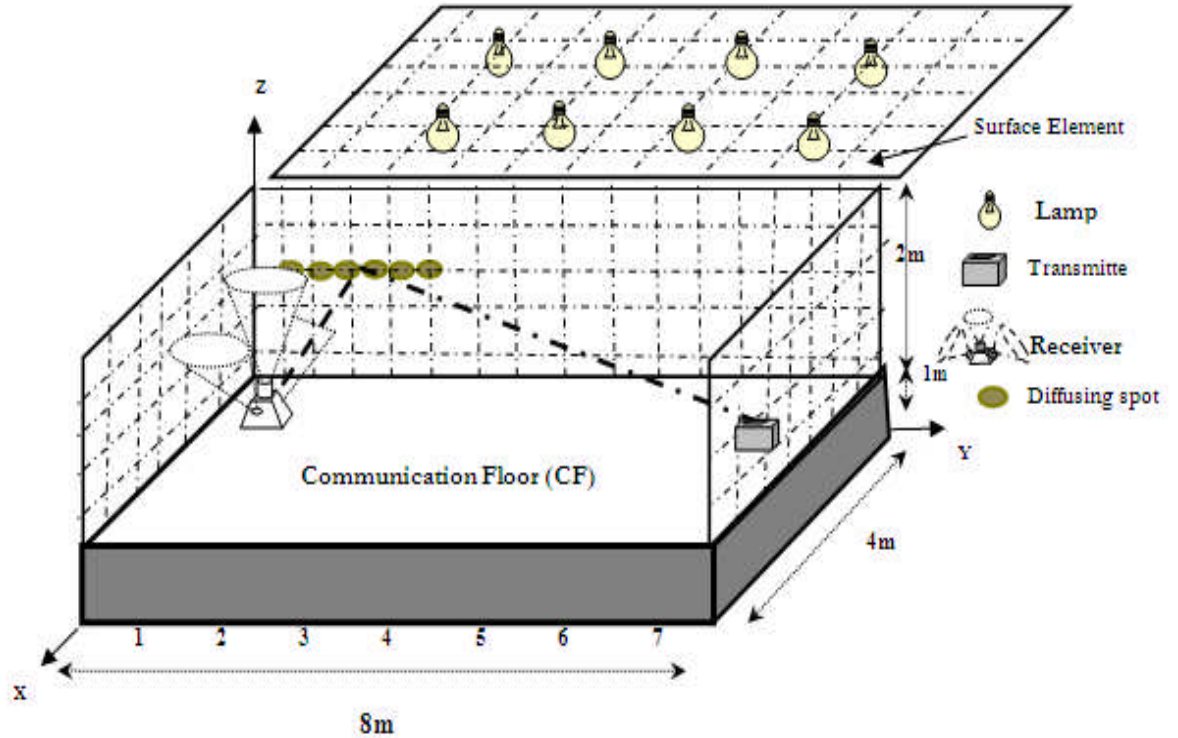


Figure 5.1: The APA-LSMS OW communication system.

The proposed system adapts the beam powers and beam angles for a single transmitter and receiver in the following way:

- 1- The adaptive hologram generates a single spot which scans the walls and ceiling by changing the beam angle associated the spot between  $-90^\circ$  and  $90^\circ$  in steps of  $2.86^\circ$  (in each step the spot moves 10 cm which results in a total of 8000 possible locations ( $40 \times 80$  locations in the ceiling,  $40 \times 20$  locations in the wall  $xz_{y=0, y=8m}$  and  $80 \times 20$  locations in the wall  $yz_{x=0, x=4m}$ ).
- 2- It computes the SNR at the receiver for each step and sends a low-rate feedback control signal to the transmitter about the SNR associated with each step.
- 3- It records the transmission angles  $(\delta_{x_c}, \delta_{y_c})$  that maximise the receiver's SNR, and determines the spot location  $(x_c, y_c, z_c)$ .

- 4- A line strip of spots is produced with uniform power distribution among the beams whose centre is  $(x_c, y_c, z_c)$  starting with an angle of  $0.28^\circ$  between the beams (all spots in the line touch each other and each spot has a diameter of 1cm).
- 5- It individually turns on each spot, and then computes the SNR associated with the spot.
- 6- A feedback control signal is sent at low-rate to the transmitter about the SNR associated with the spot.
- 7- The SNR in step 5 is used as the SNR associated with the spot.
- 8- Steps 5 to 7 are performed for all the spots.
- 9- The transmit power is redistributed among the spots based on the SNR ratio from equation (4.1) given in Chapter 4.
- 10- The angle between the beams is increased by  $0.57^\circ$  (observe that the angles between the beams are equal) and steps 5, 6,7,8 and 9 are repeated.
- 11- The algorithm ceases when the angle between the beams reaches  $2.86^\circ$ .
- 12- The transmitter is specified so that it operates at the optimum beam angles and powers.

Our proposed system firstly scans about 8000 locations in order to find the optimum spot location. If each SNR computation is carried out in  $1 \mu\text{s}$ , then the total adaption time when the receiver moves is 8 ms. Pedestrians typically move at a speed of 1m/sec. If the receiver moves by 1m, the SNR penalty (Figure 5.3) incurred as a result of using the old beam power and old beam angle is less than 3 dB. As such the holograms can adapt every 1 second (or slightly more frequently if the SNR penalty is to be reduced). The 8 ms adaptation time therefore represents an overhead of 0.8% in terms of transmission time. If an SNR penalty lower than 3 dB is desired then Figure 5.3 shows how often the system has to adapt its settings. For example for the SNR

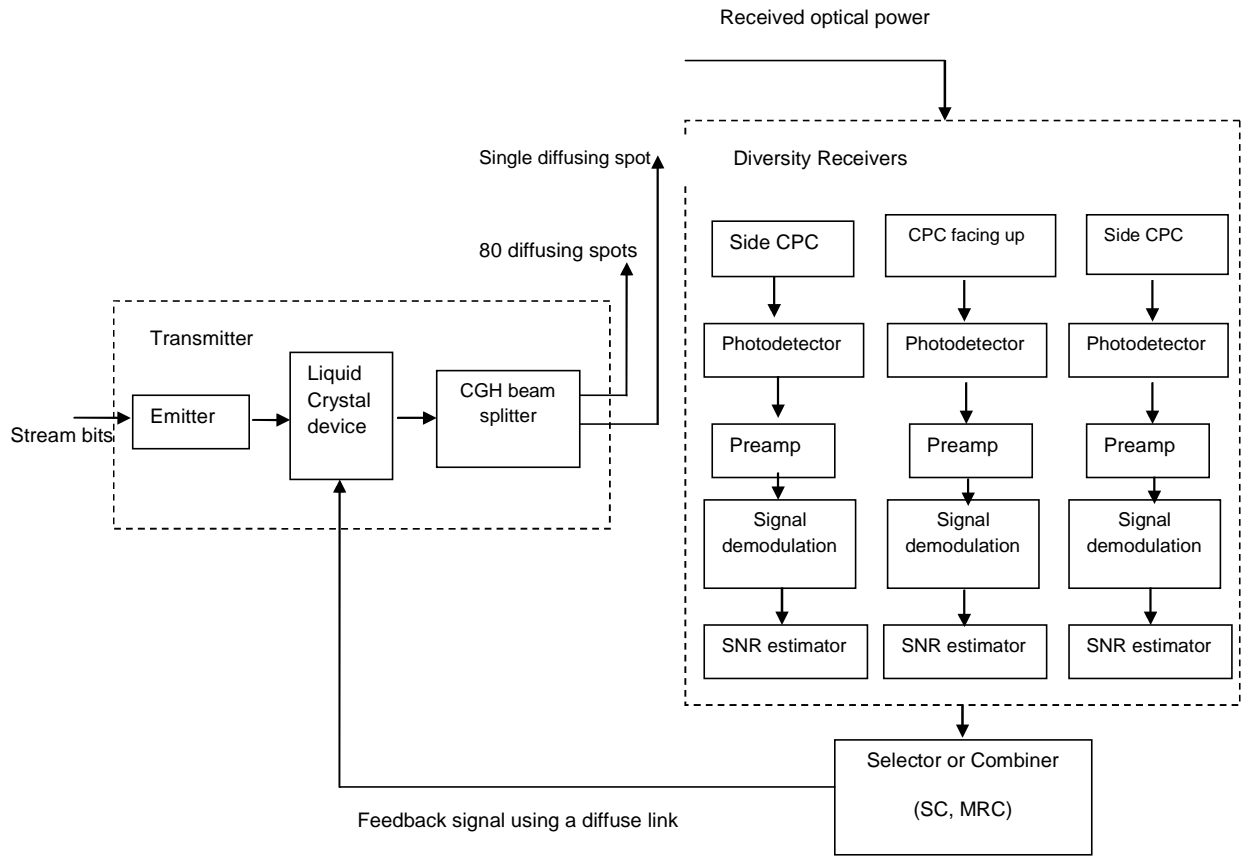


Figure 5.2: The block diagram of our APA-LSMS combined with three branch angle diversity receiver.

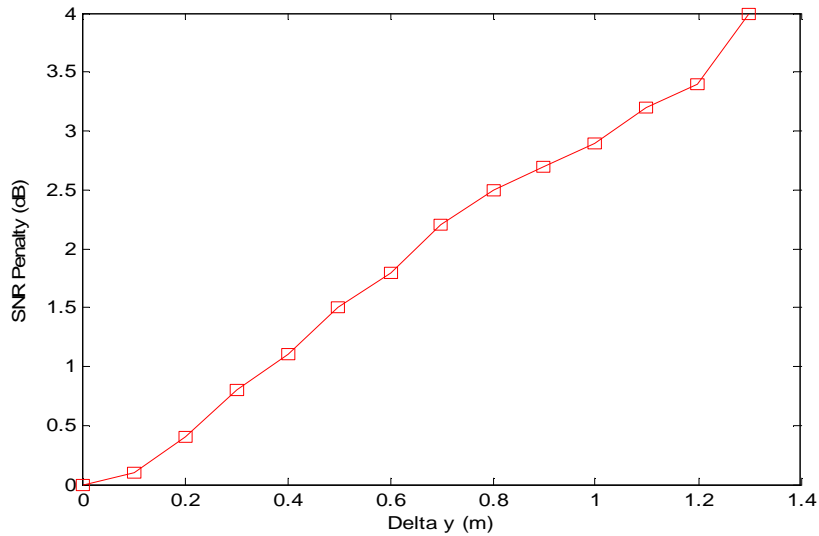


Figure 5.3: The SNR Penalty of our proposed system when the receiver moves along the y axis away from the previously optimally placed spots at (2m, 1m, 1m) and the transmitter does not update the spot locations.

penalty to be below 1 dB, the system has to adapt the beam powers every 0.4m approximately which corresponds to 0.4 second adaptation frequency, which increases the overhead to 2% which is still acceptable. It should be noted that this adaptation has been done at the rate at which the environment changes not at the system's bit rate. Holograms based on liquid crystal (LC) devices capable of adapting within ms times are feasible.

In order to carry out steps 5 to 10, a medium access control (MAC) protocol is required to provide a repetitive training time. This training is needed at the low rate at which the channel changes. The algorithm for beam angle and beam power adaptation is applied to every single transmitter and single receiver position during mobility. For beam power and angle adaptations, we propose that the receiver periodically (namely at 1 second intervals) re-evaluates its SNR and if this has changed significantly (compared to a threshold) then this change initiates transmitter adaptation. In Figure 5.3, an SNR penalty is calculated based on the transmitter using its old angle and power settings while in motion. The results show the SNR penalty incurred as a result of mobility (distance moved, x-axis) and non-adaptation of weights. The system design should allow a link margin. For example, with a link power margin of 3 dB, Figure 5.3 shows that adaptation has to be done every time the receiver moves by 1 m approximately. At a pedestrian speed of 1 m/s, this corresponds to re-adaptation every 1 second which is feasible. The transmitter and receiver orientation may affect the line strip system performance. However, during the initialisation of the proposed systems, the angle adaptation algorithm turns on one spot and scans the room to find the optimum location and orientation of the spots that maximises the SNR. The power and angle adaptation algorithms therefore offers a degree of robustness against changes in the receiver orientation however this can be investigated further.

In this chapter, a multi-spot LSMS and (only) power adaptive line strip multi-spot diffusing system (PA-LSMS) with three angle diversity receivers are

evaluated in order to find the most suitable geometry for indoor OW under mobility. For comparison, a CDS system was also modelled, establishing its channel impulse response, 3-dB channel bandwidth, delay spread and SNR.

### 5.3 Angle Diversity Receiver Structure

In this section, the three-branched angle diversity detectors discussed in Chapter 3 are considered with our new APA-LSMS configuration. As illustrated in Chapter 3, Figure 3.13 (a) shows the three detectors situated on pyramidal faces. Every branch is oriented in a particular direction, which can be described by two angles: the azimuth ( $Az$ ) angle and the elevation ( $El$ ) angle. The elevation,  $El$ , of the two detectors remains at  $35^\circ$  and the detector that faces upwards is set at  $90^\circ$ . The  $Az$  angles of the three branches are set at  $0^\circ$ ,  $180^\circ$  and  $0^\circ$ . The FOVs for the branches are determined subsequently: two are limited to  $35^\circ$ , while the one facing upwards is set at  $20^\circ$ . Furthermore, each detector employs a compound-parabolic concentrator (CPC), which can collect and concentrate the light from a large input area down into a smaller detector area. The CPC is a non-image concentrator and has an acceptance semi-angle of  $\psi_a < 90^\circ$ . When the reception angle  $\delta$  exceeds the acceptance semi-angle, the transmission factor ( $T_c$ ) of the concentrator approaches zero. The transmission factor of the concentrator is given by [121]

$$T_c(\delta) = T \left[ 1 + \left( \delta / \psi_a \right)^{2R} \right]^{-1} \quad (5.1)$$

where  $T = 0.9$  and  $R = 13$  [121]. The CPC has a refractive index of  $N = 1.7$  and the entrance area is  $A = 9\pi/4 \text{ cm}^2$ . The exit area of the CPC is  $A' = A \sin^2(\psi_a) / N^2$ . In our analysis, each detector is assumed to employ a CPC. The detector facing up employs a CPC with an acceptance semi-angle of  $\psi_a = 20^\circ$ , whereas the acceptance semi-angle of each side photodetector is restricted to  $35^\circ$ . Each photodetector is assumed to fit exactly into its

corresponding concentrator's exit area. Therefore, the detector facing up has a photosensitive area of  $0.28 \text{ cm}^2$ , whereas each side photodetector has a photosensitive area of  $0.8 \text{ cm}^2$ . These values are acceptable in the case of a mobile terminal.

## 5.4 Optical Wireless System Model

In order to study the impact of directive ambient light noise sources and multipath dispersion, as well as their effect on the received data flow, consideration was given to an unoccupied rectangular room that had no furnishings, with dimensions of  $8 \text{ m} \times 4 \text{ m} \times 3 \text{ m}$  (length  $\times$  width  $\times$  height), similar to those considered in the previous chapters. Previous research in [8], [16] has found that the power reflected by elements on either the wall or the ceiling is Lambertian in nature, having a reflectivity of 0.8 for walls and ceiling, and 0.3 for the floor. In this study, we regarded the reflections from the windows and doors to be identical to those coming from the walls. The reflecting elements can be modelled by subdividing the ceiling and walls into small square surfaces which operate as secondary small diffuse transmitters ( $n=1$ ). The effect of a realistic indoor office (windows, door, chairs, physical partitions and other objects) will be considered in Chapters 6 and 7. The accuracy of the impulse response profile is controlled by the size of the reflecting elements. Therefore, element sizes of  $5 \text{ cm} \times 5 \text{ cm}$  for the first order reflections and  $20 \text{ cm} \times 20 \text{ cm}$  for the second order reflections are employed for all arrangements. As discussed previously, reflections up to the second order are considered in our simulator (we have however evaluated the impact of third order reflections on our high bit rate systems and have shown that third order reflections have little impact on our adaptive (beam angle and beam power) systems).

Our simulation tool, comparable to the one created by Barry et al. [34], is employed to calculate the received optical power and generate the impulse

response. To compute the received optical power at the receiver, a ray-tracing algorithm was employed, which is explained in detail in Chapter 3. In order to study the functionality of our configuration under mobility, four arrangements were considered: pure CDS diffuse, non-adaptive LSMS, adaptive PA-LSMS and APA-LSMS multi-spot combined with different detection methods. The transmitter was positioned straight up in two different places on the communication plane (CP), i.e., (2m, 4m, 1m) and (2m, 7m, 1m) and radiated 1W optical power with a Lambertian pattern. CGHs can be employed to generate static multi-spot intensities. Power adaptation of the beam powers can be implemented by using LC devices. These LC devices can also vary the beam angle if they are used to produce the two-dimensional holograms. These devices have a response time of  $\mu s$  to  $ms$  [185]. A feedback signal can be made available by employing one of the beams at a low data rate.

In order to evaluate the benefits of having beam angle and beam power adaptation with angle diversity, eight spotlights are considered ('Philips PAR 38 Economic' (PAR 38)) in our configurations as described in Chapter 3. Three angle diversity detectors are employed in order to minimise the effect of background noise and multipath dispersion. Additional simulation parameters are provided in Table 5.1. Our simulation is comparable to the one created and implemented in Chapters 3 and 4 with additional alterations to address the beam angle adaptation. The simulation is employed to produce the channel impulse response and calculate delay spread, 3-dB channel bandwidth as well as SNR for all mobile adaptive and non-adaptive multi-spot OW systems.

## 5.5 Performance Evaluation

This section studies the impulse response, delay spread, 3-dB channel bandwidth and the SNR of our proposed OW systems under the impact of background noise sources, user mobility, receiver noise and multipath dispersion. The results are provided for two different positions when the

transmitter is placed on the CP at (2m, 4m, 1m) and (2m, 7m, 1m). In order to process the electrical signals, SC and MRC techniques are considered.

Table 5.1: Simulation Parameters.

Parameter	Configuration		
	UPLINKS TRANSMISSION		
Length	8 m		
Width	4 m		
Height	3 m		
$\rho$ x-z wall	0.8		
y-z wall	0.8		
x-z op wall	0.8		
y-z op wall	0.8		
Floor	0.3		
	Transmitter		
Quantity	1		
Location (x,y,z)	(2m, 4m, 1m)	(2m, 7m, 1m)	
Elevation	90°		
Azimuth	0°		
	Receiver		
Quantity	3		
Photodetector's area used at Mbit/s	0.8 cm <sup>2</sup>	0.28 cm <sup>2</sup>	0.8 cm <sup>2</sup>
Photodetector's area for wide FOV single receiver	2.445 cm <sup>2</sup>		
Photodetector's area used at Gbit/s	5 mm <sup>2</sup> 1 mm <sup>2</sup>	5 mm <sup>2</sup> 1 mm <sup>2</sup>	5 mm <sup>2</sup> 1 mm <sup>2</sup>
Acceptance semi-angle	35°	20°	35°
Location (x,y,z)	(1,1,1),(1,2,1),(1,3,1),(1,4,1),(1,5,1),(1,6,1),(1,7,1)		
Elevation	35°	90°	35°
Azimuth	0°	0°	180°
	Resolutions		
Time bin duration	0.5 ns	0.01 ns	
Bounces	1	2	
Surface elements	32000	2000	
Number-of-spot lamps	8		
Locations	(1,1,1), (1,3,1), (1,5,1), (1,7,1) (3,1,1), (3,3,1), (3,5,1),(3,7,1)		
Wavelength	850 nm		
Bandwidth (BW)	30 MHz	5 GHz	10 GHz
Bit rate	30 Mb/s	5 Gb/s	10 Gb/s

The SC impulse response results of the CDS, non-adaptive LSMS and adaptive PA-LSMS combined with narrow FOVs diversity receivers, when the transmitter is stationary at the room centre and the receiver is placed at one of the room corners, is plotted in Figure 5.4. The results show the optical received power profile ( $\mu W$ ) as a function of time (ns). Practically, the impulse response profile of the optical wireless system is continuous; nonetheless, the model subdivides reflective planes - the walls, floor and ceiling- into small square elements ( $dA$ ). In order to minimise the impact of discretization, we grouped and stored the received optical powers within a time bin interval (0.5 ns) into a single received power, hence the smoothness viewed in the shape of the impulse response. A time bin smaller than 0.5 ns, i.e. 0.01 ns was also taken into account for high bit rates, i.e., 5 Gb/s and 10 Gb/s. A time frame (time bin) with a small duration has to be used when a high data rate is considered. Reflective elements of 2.5 cm  $\times$  2.5 cm for first order reflections and 10 cm  $\times$  10 cm for second order reflections were used for higher data rates (5 Gb/s and 10 Gb/s).

Figure 5.4 shows that the adaptive multi-spot PA-LSMS transmitter combined with three-branched angle diversity receivers performs considerably better than both the pure diffuse wide CDS system and the non-adaptive angle diversity LSMS configuration. As shown in Figure 5.4, the adaptive PA-LSMS increases the direct power from around 4  $\mu W$  of the non-adaptive angle diversity LSMS system to about 15  $\mu W$ . This is as a result of assigning higher powers to the spots near to the receiver location, thereby increasing the direct LOS components. This factor can be further increased by employing beam delay and power adaptive multi-beam clustering method (BDPA-BCM) with a seven-branched diversity receiver, as seen in Chapter 4. Nonetheless, adapting delay and power between the beams may not offer much improvement in the OW system during mobility. Figure 5.5 shows the SC impulse response of the APA-LSMS and PA-LSMS in the worst possible link (6m separating the receiver and the transmitter). A considerable improvement in the received direct power level

is obtained by utilising beam angle and power adaptation methods. As can be seen in Figure 5.5, our proposed APA-LSMS significantly increased the power level by a factor of 27 compared with the adaptive PA-LSMS configuration.

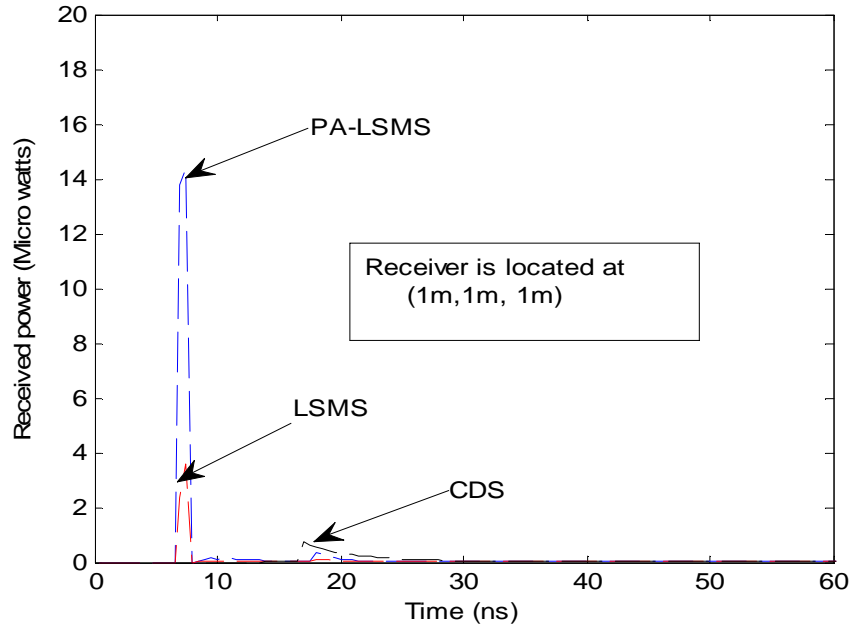


Figure 5.4: Impulse response of the three configurations: CDS, LSMS and PA-LSMS when the transmitter is placed at (2m, 4m, 1m) and the receiver is at (1m, 1m, 1m).

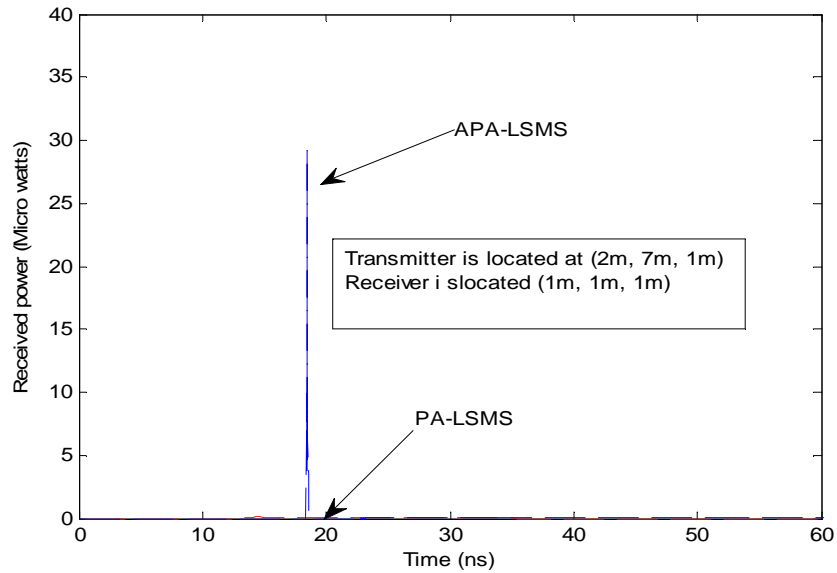
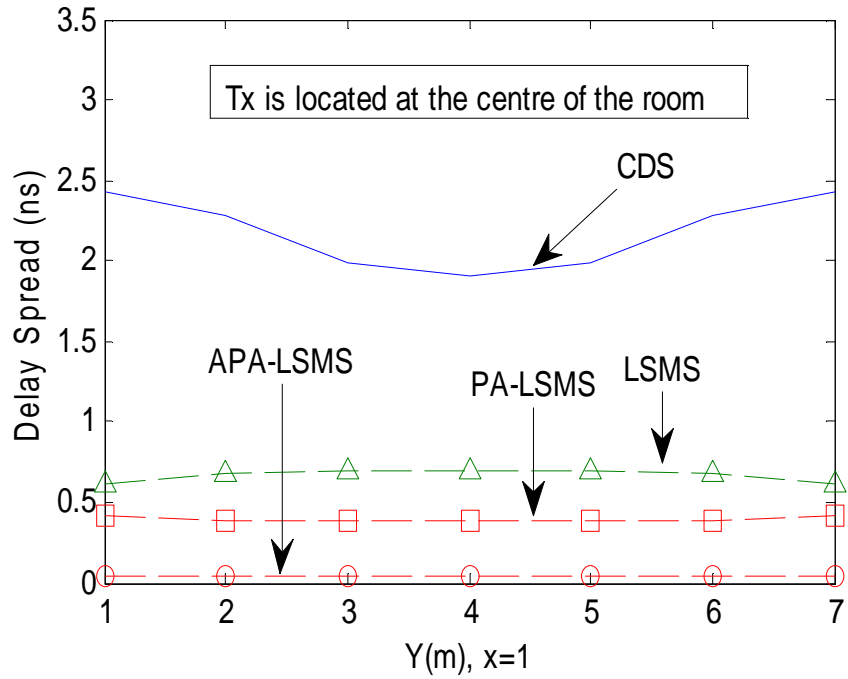
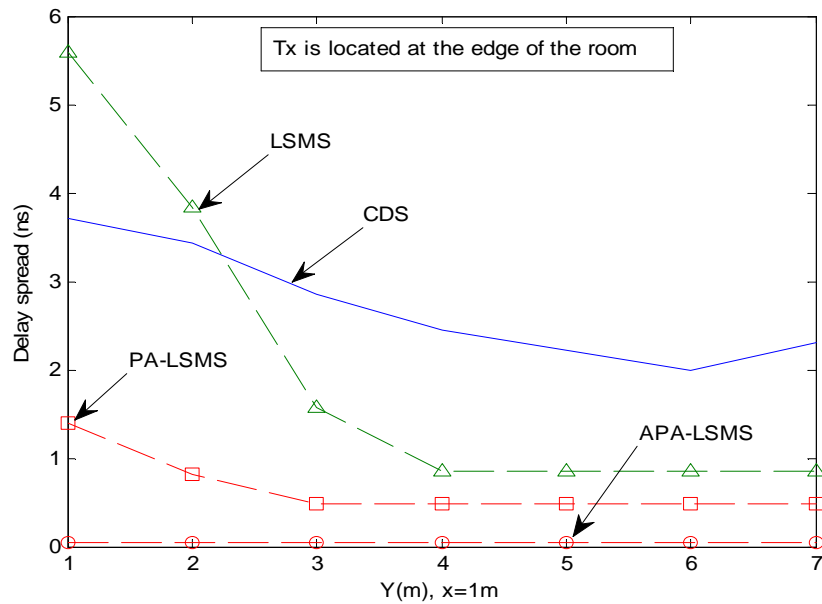


Figure 5.5: Impulse response of two configurations: PA-LSMS and APA-LSMS at a transmitter-receiver horizontal separation of 6m.

For delay spread analysis, Figure 5.6 (a) shows the delay spread of the CDS, LSMS, PA-LSMS and APA-LSMS, when the system is stationary in the middle of the room (2m, 4m, 1m) while the receiver is moved along the y-axis in a line of  $x = 1\text{m}$ . The pure diffuse CDS system shows much more signal delay spread due to diffuse transmission and the wide receiver FOV. There is a significant reduction in the signal spread for the APA-LSMS. The results show that the APA-LSMS can reduce the delay spread by a factor of 11 compared with the adaptive PA-LSMS system. Further, degradation in the delay spread result for diffuse CDS, LSMS and PA-LSMS can be induced due to the transmitter-receiver mobility; see Fig. 5.6 (b). At the poor communication path, the delay spread of non-adaptive LSMS and adaptive PA-LSMS reached 5.6 ns and 1.45 ns respectively. This is due to: (1) the large distance between the receiver and the multi-spot transmitter and (2) the physical structure of the three-branched angle diversity receivers. Significant improvement in the delay spread can be achieved in our adaptive APA-LSMS system. At a given receiver position, even with a large distance between the adaptive transmitter and the receiver, the spots are dynamically located near to the receiver based on the angle and power methods which can considerably reduce the delay spread at the receiver. The proposed APA-LSMS reduces the delay spread from almost 1.45 ns for the PA-LSMS to about 0.04 ns. Furthermore, the proposed system, with three-branched angle diversity receiver, can reduce the delay spread by a factor of 7 compared with the beam delay and power multi-beam clustering method (BDPA-BCM) coupled with seven-branched diversity receivers proposed in Chapter 4. The delay spread distribution is almost independent of the receiver-transmitter distance in our new APA-LSMS system as the angles and the powers of the beams are adapted to provide the best SNR. Additionally, a 0.01 ns time bin is taken into account when a high bit rate is considered. Figure 5.7 illustrates the delay spread distribution of our APA-LSMS with different time bins of 0.5 ns and 0.01 ns. A smaller time bin of 0.01 ns caused a slightly higher delay spread in comparison with 0.5 ns time bin interval.



(a) Transmitter is placed at the centre of the room.



(b) Transmitter is placed at the edge of the room

Figure 5.6: Delay spread of four configurations: CDS, LSMS, PA-LSMS and APA-LSMS when the transmitter is placed at (a) (2m, 4m, 1m) and (2m, 7m, 1m) while the receiver moves along the x=1m line.

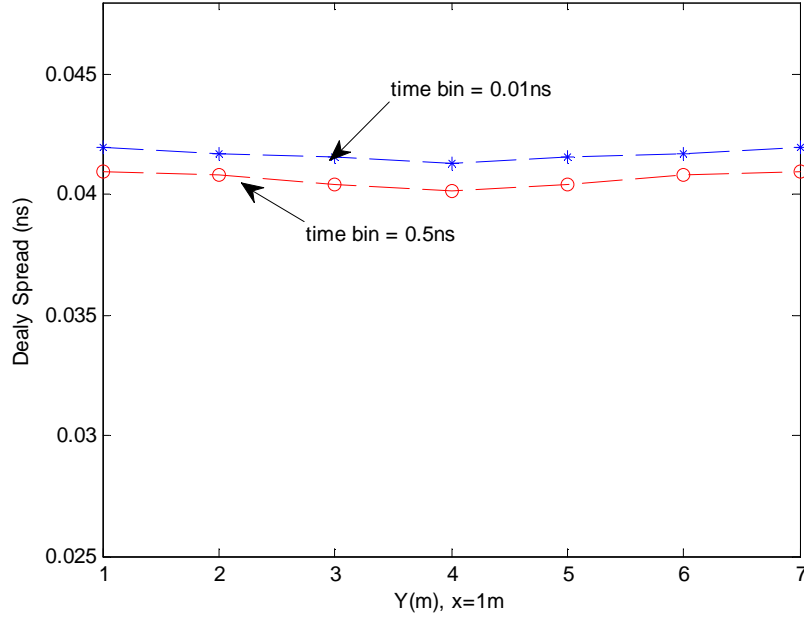


Figure 5.7: Delay spread of APA-LSMS using different time bins: 0.5ns and 0.01ns.

### 5.5.1 OW 3-dB Channel Bandwidth

The 3-dB channel bandwidth of the pure diffuse CDS, non-adaptive and adaptive multi-spot configurations (LSMS, PA-LSMS and APA-LSMS), when the system is stationary in the middle of the room and the receiver moves along the y-axis at the x=1m line, is given in Figure 5.8. The results show that in comparison with other systems, our proposed angle diversity APA-LSMS configuration provides the largest channel bandwidth. This is due to three factors: (1) optimisation of the spots positions in an area on the ceiling and/or walls, whereby the receiver can collect a strong signal through direct LOS components from the spots (2) allocation of a high power level to the spots nearest to the receiver, which results in a strong received power and (3) employment of a diversity receiver which significantly reduces the background noise collected. Our proposed APA-LSMS increases the bandwidth from the 25.5 MHz offered by the CDS (with wide FOV receiver) to almost 7.2 GHz, see Figure 5.9. Our simulation results show that the CDS with a wide FOV at a 6 m

transmitter-receiver separation achieves 25.5 MHz bandwidth, which is in good agreement with previous work [16], [34]. When the transmitter is placed at the centre of the room, the multi-spot configuration (spot-diffusing) combined with an angle diversity receiver increases the communication channel bandwidth up to 638 MHz, which corresponds with the level reported in [140], see Figure 5.8. Previous work [132] has shown that adopting a multi-beam transmitter coupled with  $7^\circ$  field of view angle diversity receivers can provide 3-dB channel bandwidths of more than 2.5 GHz. Furthermore, recent work has demonstrated an experimental 1.25 Gb/s OW line of sight system with an angle diversity receiver [75]. However these studies do not use angle and power adaptations in conjunction with the diversity receiver. When the PA-LSMS replaces the conventional LSMS, there is significant bandwidth improvement, from 638 MHz to approximately 4.2 GHz. This significant increase in channel bandwidth is due to assigning higher power to the spots nearest to the receiver, which results in high direct LOS components from the diffusing spots to the receiver, and is also due to limiting the rays accepted by employing a narrow FOV diversity receiver. Further improvement in channel bandwidth can be achieved when the beam delay adaptation is coupled with power adaptation, which increases channel bandwidth up to 5.2 GHz, as explained in Chapter 4. We assume that the journey of the beam from the transmitter to the spot location is a perfect journey where no power is lost and where the pulse width does not increase. This is reasonable, as the beams creating the spots are greatly collimated [9], [85]. It can be observed that distributing the power among the beams uniformly may cause misused power in the spots that are distant from the receiver, thereby reducing the receiver collected power, increasing reflections and reducing the 3-dB channel bandwidth. Therefore, beam angle and beam power adaptations help to identify the optimum locations of the spots and assign high powers to the spots nearest to the receiver, thus significantly increasing the channel bandwidth from 25.5 MHz (CDS with wide FOV) to 7.2 GHz in a worst case scenario with APA-LSMS, as shown in Figure 5.8. This significant increase in

channel bandwidth enables our proposed APA-LSMS system to operate at higher data rates, i.e., 5 Gb/s and 10 Gb/s. As previously mentioned in Chapter 4, the optimum receiver bandwidth is 0.7 times the bit rate. Therefore, a 10 Gb/s data rate requires a 7 GHz receiver bandwidth (the 0.7 figure is based on Personik's optical receiver design [77]). Our proposed APA-LSMS can already offer a bandwidth of more than 7 GHz, which enables it to support operation at 5 Gb/s and 10 Gb/s.

Third order reflections are also considered at two different receiver locations (1m, 1m, 1m) and (1m, 4m, 1m). Table 5.2 shows the delay spread and the channel bandwidth of the proposed APA-LSMS with and without third order reflections. As can be seen from Table 5.2, the reduction in receiver bandwidth is very small when third order reflections are included. This is attributed to beam angle and beam power adaptation which align the beam angle and power such

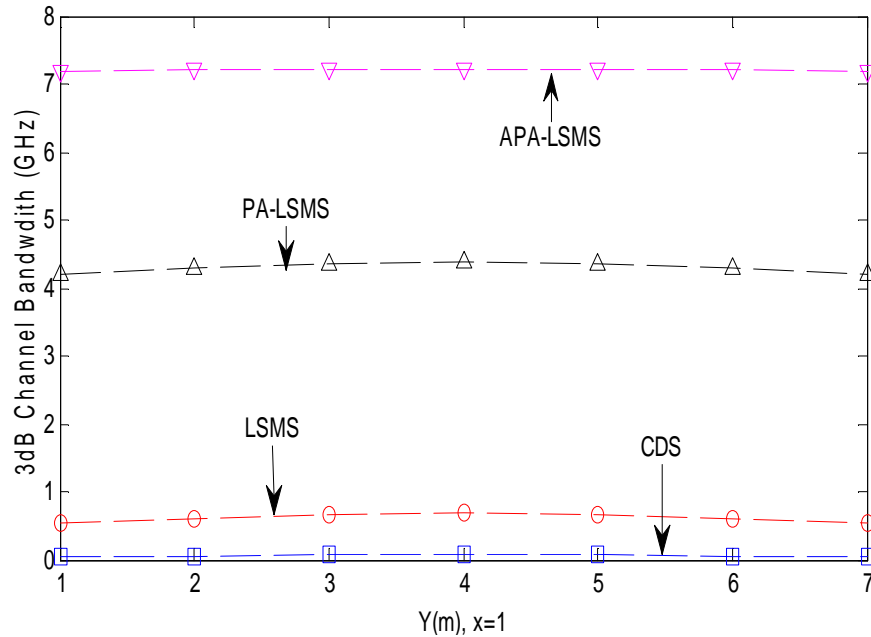


Figure 5.8: 3-dB channel bandwidth of four configurations: CDS, LSMS, PA-LSMS and APA-LSMS when the transmitter is placed at (2m, 4m, 1m) and the receiver moves along the x=1m line.

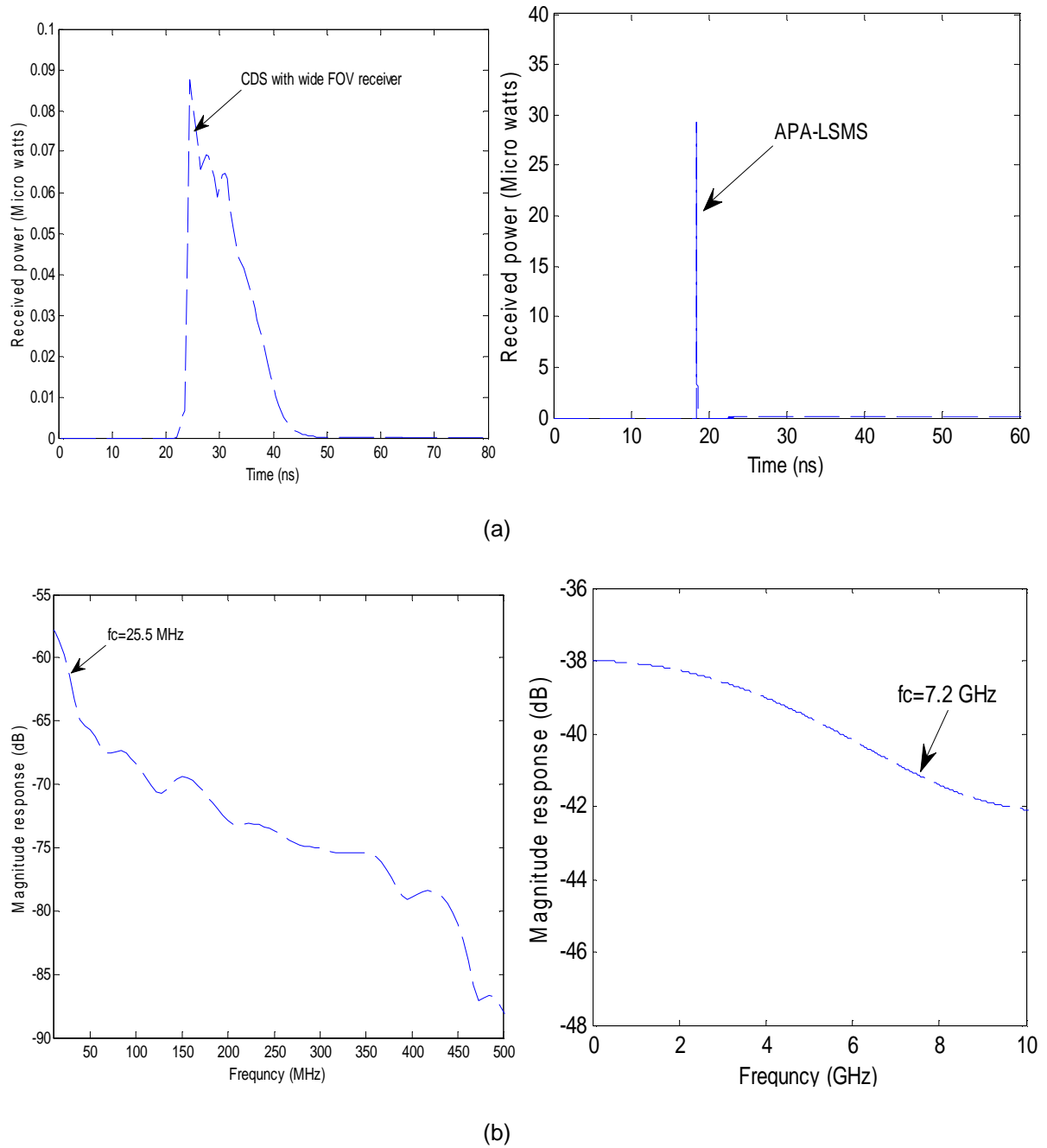


Figure 5.9: Impulse response and frequency response of CDS and APA-LSMS.

that the receiver receives a strong direct component directly from one or more diffusing spots. This is an important distinction between our proposed systems and conventional diffuse systems where in the latter third order reflections may play a significant role at high data rates.

Table 5.2: Delay spread and 3 dB Channel Bandwidth of our proposed APA-LSMS.

Transmitter (2m, 4m, 1m)	APA-LSMS up to Second reflections		APA-LSMS up to Third Reflections	
	Receiver (1m,1m,1m)	Receiver (1m,4m,1m)	Receiver (1m,1m,1m)	Receiver (1m,4m,1m)
Delay Spread (ns)	0.042	0.0409	0.053	0.0499
3dB Channel Bandwidth (GHz)	7.213	7.255	7.103	7.145

### 5.5.2 SNR Results of the APA-LSMS system

The MRC SNR results of the adaptive and non-adaptive multi-spot arrangements (PA-LSMS, APA-LSMS and LSMS) as well as the wide FOV CDS system, are evaluated under the influence of multipath dispersion, mobility, background noise and receiver noise. The transmitter is placed near to the room's centre and the room's edge at (2m, 4m, 1m) and (2m, 7m, 1m) respectively, and operates at 30 Mb/s. The preamplifier used in the 30 Mb/s OW systems is the PIN FET preamplifier proposed in [121]. The SNR calculations are carried out for 7-different receiver locations along the y-axis at a consistent  $x=1m$ , which scans the highs and lows of the directive background noise sources. The MRC SNR results are plotted in Figure 5.10 and 5.11. The results show that the non-adaptive multi-spot angle diversity LSMS configuration provides a 23 dB SNR gain over the CDS when the transmitter is stationary at the centre of the room. A significant improvement can be achieved by employing PA-LSMS, which assigns high powers to the spots nearest to the receiver, thus providing about 13 dB SNR gain over the LSMS SNR. Our proposed APA-LSMS achieved an approximately 16 dB SNR gain over PA-LSMS.

Degradation in the SNR result is observed in both the PA-LSMS and the LSMS when the transmitter is on the move (mobile), as illustrated in Figure 5.11 (the transmitter is moved near to the room's edge at (2m, 7m, 1m) and the receiver is relocated to the room corner at (1m, 1m, 1m)). This SNR degradation is due to the transmitter mobility. The non-adaptive and adaptive PA-LSMS can be replaced with our adaptive APA-LSMS in order to reduce the impact of the transmitter movement. Our proposed APA-LSMS with three diversity receivers achieves about 45 dB SNR gain over PA-LSMS and 60 dB SNR gain over the CDS. The SNR results in Figure 5.10 and 5.11 show that the APA-LSMS SNR is independent of the transmitter location. Therefore, a considerable enhancement in SNR is obtained at each transmitter and receiver location. It has to be observed that if one beam (single spot) is employed, the enhancement in the SNR and channel bandwidth may be favourable;

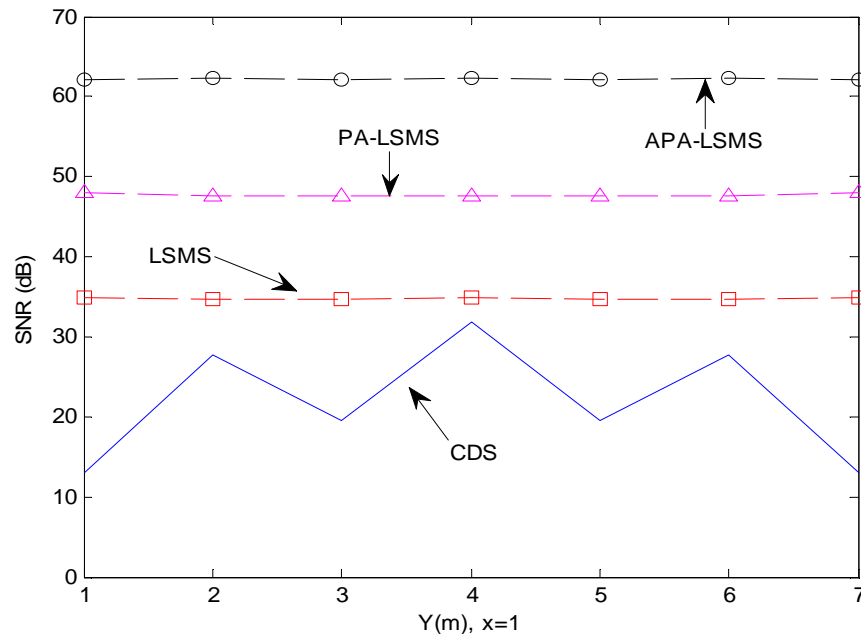


Figure 5.10: OW CDS, LSMS, PA-LSMS and APA-LSMS systems SNR at 30 Mb/s, when the transmitter is placed at (2m, 4m, 1m) and the receiver moves along the  $x=1$ m line, with a total transmit power of 1W.

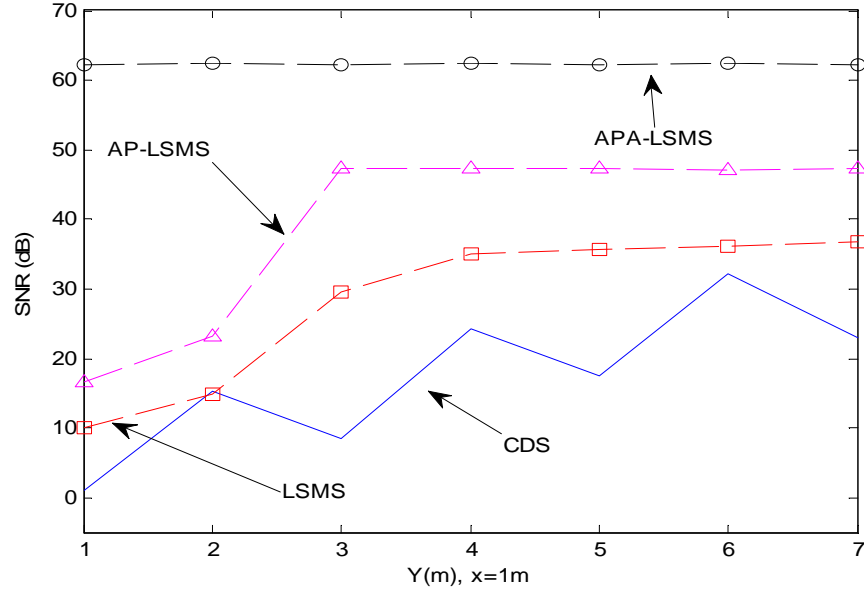


Figure 5.11: OW CDS, LSMS, PA-LSMS and APA-LSMS systems SNR at 30 Mb/s, when the transmitter-receiver separation is 6m, with a total transmit power of 1 W.

nonetheless, such a system can be affected by beam obstruction, as well as shadowing, and could violate regulations concerning eye safety if the total transmit power is assigned to a single beam. Other approaches can be adopted where, for example, three clusters of beams are used and are independently steered to areas in the ceiling near each of the receiver detectors; however, this is more complex. Further work in this area is however warranted.

It should also be noted that the beam power and angle adaptations are carried out at the rate at which the environment changes not at the system bit rate. The system design can allow an SNR margin, e.g. 3dB. This margin will ensure that the beam power and angle adaptations do not have to be repeated frequently. A 3 dB SNR margin corresponds to a distance of 1 m, see Figure 5.3. Hence adaptation has to be done every 1 second for a pedestrian speed of 1 m/s. Therefore the overhead of our proposed system is 0.8% as mentioned earlier if 8 ms are needed for the adaptation.

Significant enhancement in SNR is achieved coupled with high channel bandwidth, as shown in Figure 5.8, which allows operation at higher data rates. We used the PIN FET design proposed by Kimber et al. [186] for our proposed 5 Gb/s and 10 Gb/s APA-LSMS systems. This preamplifier has a noise current spectral density of  $10 \text{ pA}/\sqrt{\text{Hz}}$  and a bandwidth of 10 GHz. The preamplifier bandwidth can be limited to 3.5 GHz and 7 GHz through the use of appropriate filters. At a higher data rate our proposed system used photodetector areas of  $0.05 \text{ cm}^2$  and  $0.01 \text{ cm}^2$  with a  $7^\circ$  FOV instead of  $0.8 \text{ cm}^2$  ( $35^\circ$ FOV). The  $0.01 \text{ cm}^2$  detector will collect 19 dB less power than the  $0.8 \text{ cm}^2$  detector. This is however compensated for by increasing the concentrator gain from 9.4 dB for a  $35^\circ$  FOV to about 22.9 dB by reducing its FOV to  $7^\circ$ . The narrower receiver FOV is possible in our system since the beam angle adaptation method introduced is able to identify the optimum location of the spots as seen by the receiver. Our proposed system thus has a concentrator gain of 22.9 dB corresponding to a  $7^\circ$  FOV [50], [72]. Figure 5.12 shows the SNR of the PALSMS and APA-LSMS operating at 5 Gb/s and 10 Gb/s with photodetector areas of  $0.05 \text{ cm}^2$  and  $0.01 \text{ cm}^2$  when the systems operate under background noise and multipath dispersion impairments. The transmitter is placed at (2m, 7m, 1m) and the receiver moves at a constant  $x = 1 \text{ m}$  along the  $y$ -axis over the communication plane. Figure 5.12 shows that our APA-LSMS achieves a consistent 37 dB and 34.5 dB SNR at 5 Gb/s and 10 Gb/s, respectively, in the presence of background shot noise, multipath dispersion, receiver noise and mobility. At 10 Gb/s our APA-LSMS system with a photodetector area of  $0.01 \text{ cm}^2$  obtained about 21 dB SNR, still achieving a BER of  $10^{-9}$ , see Figure 5.12.

The SNR enhancement achieved through the combination of beam angle and power adaptations, multi-spot diffusing and angle diversity detections allows us to reduce the transmission power under the present 1 W level. To investigate our proposed system (with a photodetector area of  $0.05 \text{ cm}^2$ ) with respect to

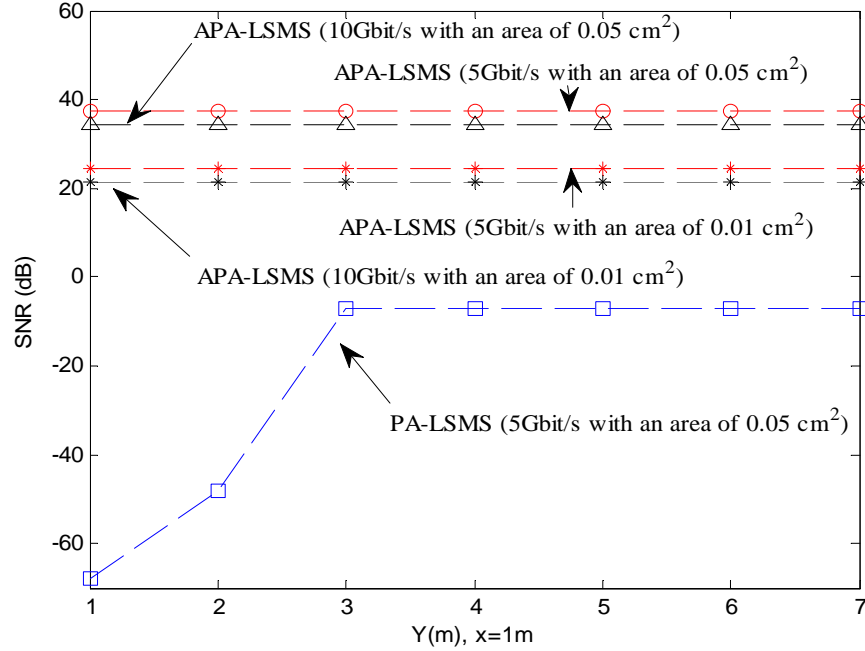


Figure 5.12: OW PA-LSMS and APA-LSMS systems SNR at 5 Gb/s and 10 Gb/s, with two detection areas ( $0.05 \text{ cm}^2$  and  $0.01 \text{ cm}^2$ ), when the transmitter-receiver separation is 6m, with a total transmit power of 1 W.

eye safety regulations, we used a total transmit power of 60 mW (0.75 mW per beam) and introduced a limitation in the power adaptation algorithm such that it was not allowed to increase the beam power more than 0.25 mW after power adaptation. We have also reduced the size of the spot from a diameter of 1 cm to 0.5 cm which allows more flexibility in clustering the spots closely if needed. The SNRs achieved in our proposed system in this case were about 13 dB and 10 dB at 5 Gb/s and 10 Gb/s, respectively, under the impact of background noise, multipath dispersion, receiver noise and mobility, see Figure 5.13. These degradations are due to the reduction in the total transmit power from 1 W to 60 mW, and also due to the 0.5 mW power restriction in our algorithm. At 10 Gb/s the SNR is still greater than 9.5 dB ( $\text{BER} < 10^{-3}$ ). Therefore forward error correction (FEC) can be used to further reduce the BER from  $10^{-3}$  to  $10^{-9}$  in our proposed system (10 Gb/s with an area of  $0.05 \text{ cm}^2$ , 60 mW transmit power). The shape and the size of the transmitter have to be considered, however, to determine whether the human eye can see more than one beam

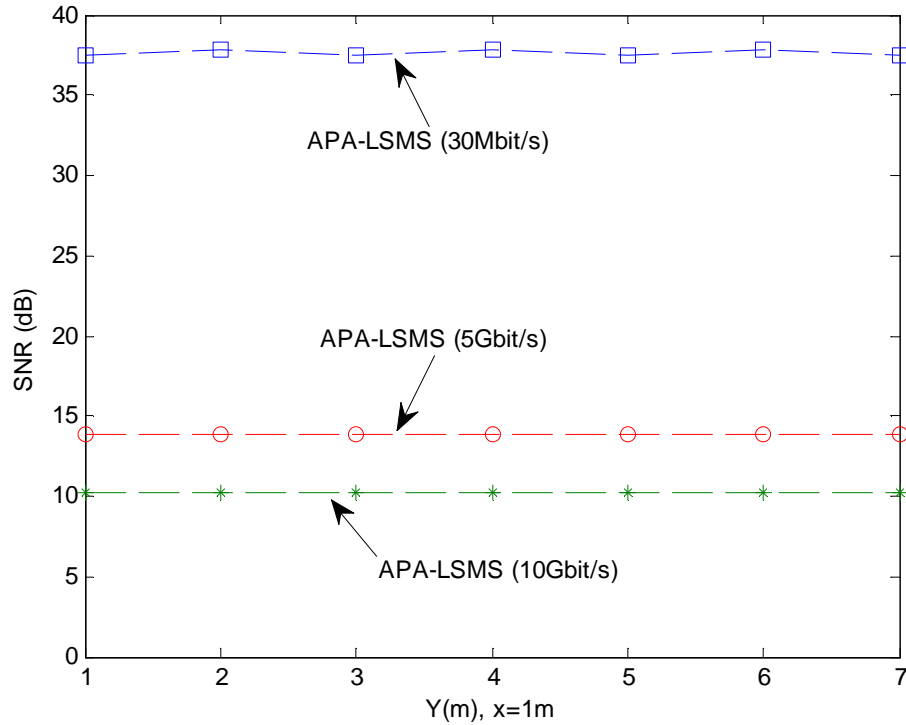


Figure 5.13: The SNR of our proposed system operating at 30 Mb/s, 5 Gb/s and 10 Gb/s, with a total transmit power of 60 mW and detection area of  $0.05 \text{ cm}^2$  for high data rates and  $0.8 \text{ cm}^2$  for 30 Mb/s.

simultaneously. The higher data rates of the PA-LSMS and the APA-LSMS are shown to be feasible through a combination of the methods of spot diffusion, beam angle and beam power adaptation. The APA-LSMS is able to achieve BER of  $10^{-9}$  while operating at 5 Gb/s and 10 Gb/s. We believe these are useful results for wireless communications.

## 5.6 Summary

User mobility can degrade the link functionality of the CDS, LSMS and PA-LSMS systems. In this chapter, we designed and evaluated an APA-LSMS coupled with three-branched angle diversity receivers in order to reduce the SNR degradation of a mobile OW system under the impact of background noise, user mobility, receiver noise and multipath dispersion. At a bit rate of 30

Mb/s, our proposed APA-LSMS offers SNR enhancement: 45 dB SNR gain over PA-LSMS and 60 dB SNR gain over CDS in a worst case scenario. This enhancement is obtained by introducing our techniques: beam power and beam angle adaptation as well as angle diversity receivers. Beam angle adaptation can help the transmitter guide and optimise its spots in the area where the receiver can achieve a good received signal, hence increasing SNR. Beam power adaptation can enable the transmitter to allocate more power to the spots closest to the receiver, thereby adding further enhancement in the SNR at the receiver. These techniques, coupled with angle diversity, are extremely useful in increasing the channel bandwidth from 25.5 MHz (conventional CDS) to 7.2 GHz (APA-LSMS with angle diversity receivers). Additionally, the proposed APA-LSMS offered a reduction in the delay spread by more than 60 compared with the pure diffuse CDS system. These considerable enhancements in SNR, delay spread and channel bandwidth of our proposed APA-LSMS system enable it to operate at high data rates. High data rates of 5 Gb/s and 10 Gb/s were shown to be feasible when our techniques - beam angle and power adaptation, multi-spot diffusing and angle diversity - are implemented in a mobile OW system.

# **6 Mobile Optical Wireless Systems Employing Beam Delay, Power and Angle Adaptation Methods with Imaging Detection in a Realistic Indoor Environment**

## **6.1 Introduction**

In this chapter, we propose and design a mobile OW system that employs beam delay, angle and power adaptation with a line strip multi-spot diffusing system (BDAPA-LSMS) coupled with an imaging receiver in a realistic indoor environment where the latter introduces shadowing, signal loss through windows) and generally more impairments. The ultimate goal of this study is to enhance the 3-dB channel bandwidth, minimise the impact of ISI, and increase the SNR when the transmitter operates at a high bit rate of 10 Gb/s under the effect of multiple dispersion, shadowing, mobility, background noise sources and receiver noise. An increase in channel bandwidth from 36 MHz (CDS) to about 9.8 GHz can be achieved when our methods of beam delay, angle and power adaptation coupled with an imaging receiver are employed. These improvements support our system to operate at data rates well beyond 10 Gb/s. Additionally, our proposed system is examined in a realistic indoor

communication scenario where physical partitions (shadowing), window availability, bookshelves, chairs, and cabinets are all present.

## 6.2 Simulation set-up

In order to study the benefit of our techniques (namely beam delay adaptation, beam angle adaptation, power adaptation, multi-spot diffusing and imaging reception) in indoor optical wireless configurations, simulation based on a ray-tracing algorithm (with modification to address our new adaptation techniques with imaging detection) was performed in an unoccupied middle sized room (empty) comparable to the one previously provided in Chapter 5, with 8m × 4m (length × width) floor dimensions and a height of 3m to the ceiling. A realistic setting, which is normally experienced in a realistic office arrangements where optical signal blockage (as a result of mini-cubicles), furniture, doors, windows, background noise and multipath propagation are all present, will be considered in Section 6.6. In an unoccupied room, we take into account ambient noise sources, user mobility, receiver noise and multipath propagation. Our results in Chapter 5 have shown that the reduction in receiver bandwidth is very small when third order reflections are included. Therefore, direct LOS with first and second order reflections are taken into account in our simulation.

The transmitter was positioned facing up in three different positions on the CP, at (2m, 4m, 1m), (2m, 7m, 1m) and (1m, 1m, 1m) and emitted 1 W optical power. CGHs can be mounted on the top emitter to generate static multiple beams in the form of LSMS. Beam delay, beam angle and beam power adaptation can be introduced with the use of an adaptive hologram. 2D liquid crystal (LC) devices are used to design an adaptive hologram. LC devices can be used to dynamically produce different spot powers at different locations on the walls and ceiling. These devices have  $\mu\text{s}$  to  $\text{ms}$  response time [185]. 2D spots on walls or a ceiling with the use of holograms have been experimentally validated in [85], [110], [111], [133], [189]. The 2D LC device can implement a

further 2D shutter stage which can be used for beam delay adaptation. The optimum spots distribution and their associated power levels and time delays that yield the best SNR at the imaging receiver can be chosen by our new adaptive BDAPA-LSMS system given in Section 6.4. It is believed that the holograms employed can produce a 1 W optical power. However, the high SNR results obtained by our new imaging BDAPA-LSMS system can be used to minimise the total transmission optical power to less than 1 W, while the system functions at a high data rate and complies with skin and eye safety regulations.

For the purpose of appraising our new adaptive OW configuration under the impact of surrounding light sources, eight halogen spotlights similar to the ones used in previous chapters were selected. These lamps generated a suitably lit environment. Furthermore, an imaging receiver, explained in Chapter 4, is employed to minimise the effect of surrounding light sources in addition to multipath dispersion. The imaging receiver is comprised of a single imaging lens and detector array that is divided/segmented into a large number of pixels. Each pixel is attached to a separate preamplifier. Therefore, the received signal in the pixels can be amplified individually and processed using suitable combining methods (MRC and SC). The reception area of each pixel is varied as the receiver terminal moves around the room over the CP. The calculation of the new reception area associated with each pixel is discussed in details in Chapter 4. Additional system parameters are provided in Table.6.1.

### **6.3 Transmitter Configuration (BDAPA-LSMS)**

In order to reduce the effect of a large distance between the receiver and the spots and to enhance the channel bandwidth at the receiver, we introduce beam angle, power and delay adaptation with line-strip multi-spot configuration (BDAPA-LSMS) combined with an imaging receiver. To help visualise our new adaptive BDAPA-LSMS transmitter, Figure 6.1 shows the OW communication architecture used in our proposed fully adaptive BDAPA-LSMS coupled with an

imaging receiver in an indoor environment. Beam angle and power adaptation help identify the best positions of spots and increase the power to the spots nearest to the receiver, thereby increasing the SNR. Even though the SNR is

Table 6.1: Simulation Parameters.

Parameter	Configuration		
	<b>UPLINKS TRANSMISSION</b>		
Length	8 m		
Width	4 m		
Height	3 m		
$\rho$ x-z wall	0.8		
y-z wall	0.8		
x-z op wall	0.8		
y-z op wall	0.8		
Floor	0.3		
	<b>Transmitter</b>		
Quantity	1		
Location ( $x, y, z$ )	(2m, 4m, 1m) (2m, 7m, 1m)		
Elevation	90°		
Azimuth	0°		
	<b>Imaging Receiver</b>		
Quantity	1		
Detector array's area	2 cm <sup>2</sup>		
Number of Pixels	200		
Area of pixels	1 mm <sup>2</sup>		
Elevation	90°		
Azimuth	0°		
Acceptance semi-angle	65°		
	<b>Modified Imaging Receiver for (BDAPA-LSMS)</b>		
Quantity	1		
Detector array's area	2.53 cm <sup>2</sup>		
Number of Pixels	256		
Area of pixels	0.99 mm <sup>2</sup>		
Elevation	90°		
Azimuth	0°		
Acceptance semi-angle	45°		
	<b>Resolutions</b>		
Time bin duration	0.5 ns , 0.01ns		
Bounces	1	2	
Surface elements	32000	2000	
Number-of-spot lamps	8		
Locations	(1,1,1), (1,3,1), (1,5,1), (1,7,1) (3,1,1), (3,3,1), (3,5,1), (3,7,1)		
Wavelength	850 nm		
Preamplifier design	PIN-FET		
Bandwidth (BW)	30 MHz	10 GHz	12.5 GHz
Bit rate	30 Mb/s	10 Gb/s	12.5Gb/s

maximised, limitations remain in channel bandwidth due to multipath dispersion as well as time delay between the signals from the spots within the selected receiver's FOV. Switching on all the beams at the same time increases the delay spread hence limiting the 3-dB channel bandwidth. Beam delay adaptation introduces a differential delay ( $\Delta t$ ) between the beams to ensure that all the beams reach the receiver at the same time. The beam delay, beam angle and beam power adaptations can be implemented using an adaptive hologram that produces spots whose locations and intensities can be varied with transmission angles ( $\delta_x, \delta_y$ ) in the  $x, y$  directions. Most of the adaptive holographic switches are LC-based [190]. A high switching speed is important for data applications with switching times reported down to  $10 \mu s$  [191]. The 2D liquid crystal device can implement a further 2D shutter stage which can be used for beam delay adaptation (however there are switching speed limitations, where the typical liquid crystal adaptation speeds are in the order of tens to hundredths of microseconds [185]). Other implementation approaches can also be considered, for example where the beams are produced by an array source. Here the delay adaptation is implemented through array element delayed switching (hence the switching speed limitations are reduced or removed) and beam power adaptation is achieved through varying the intensity per array element. The liquid crystal device in this case has the sole role of beam angle adaptation (beam steering). The implementation choices and their optimisation warrant further study and are beyond the scope of the current work.

The beam angles can be varied between  $(-90^\circ, 90^\circ)$  in both directions ( $x - y$ ) with respect to the transmitter normal. The 2D adaptive hologram firstly generates one spot, which is used to scan a number of locations along walls and ceiling to determine the best SNR position at the receiver. The received multipath profiles are stored for each spot at each given location. The total power profile is the sum of the powers as a result of the  $N_s$  impulse response

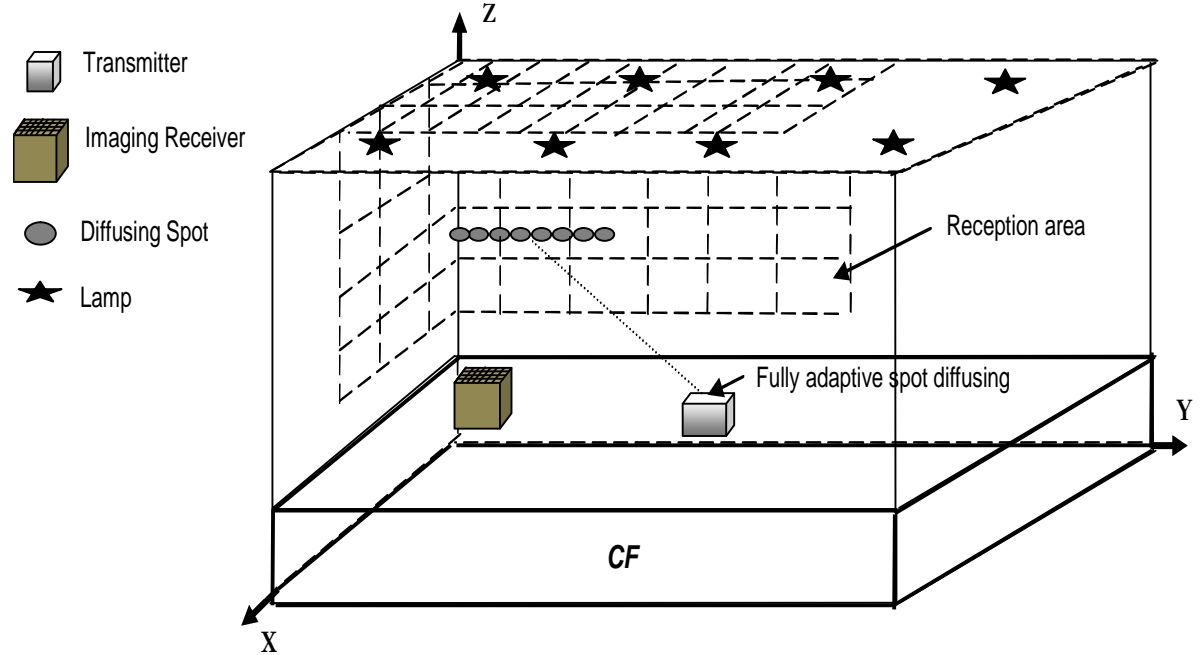


Figure 6.1: OW communication system architecture for our new fully adaptive BDAPA-LSMS with imaging receiver.

( $N_s=80$  in our case). Instead of switching on all the beams at the same time at (the optimum location) and increasing the delay spread, beam delay adaptation switches on the beam that has the longest journey to travel first, and then switches on the other beams with different differential delays ( $\Delta t$ ) so that all the beams reach the receiver at the same time. The block diagram for our proposed BDAPA-LSMS structure is shown in Figure 6.2. The BDAPA-LSMS algorithm, adapts the beam delays, angles and powers for a single transmitter and a single receiver as follows:

- 1- The adaptive hologram generates a single spot which scans the walls and ceiling by changing the beam angle associated with the spot between  $-90^\circ$  and  $90^\circ$  in steps of  $2.86^\circ$  (in each step the spot moves 10 cm which results in a total of 8000 possible locations ( $40 \times 80$  locations in the ceiling,  $40 \times 20$  locations in the wall  $xz_{y=0, y=8m}$  and  $80 \times 20$  locations in the wall  $yz_{x=0, x=4m}$ )).

- 2- The receiver computes the SNR at each step and sends a control feedback signal at a low rate to the transmitter about the SNR associated with each step.
- 3- The transmitter documents the transmission angles  $(\delta_{xc}, \delta_{yc})$  that achieved the highest SNR at the receiver, and determines the spot position  $(x_c, y_c, z_c)$ .
- 4- The transmitter produces a line strip ( $80 \times 1$ , with equal power among the beams) where its centre is at the position that optimised the SNR.
- 5- Commencing with a minimum angle of  $0.28^\circ$  between the beams, all the beams spots touch each other in the line strip, each beam spot has a diameter of 1cm.
- 6- The transmitter switches on each spot individually, the receiver calculates the received power, computes the SNR at each pixels ( $K=200$  pixels) and the SNR after combining the signals using MRC weights and also calculates the time delay of the maximum received power.
- 7- The receiver considers the time delay and the SNR in step 6 as the time delay and the SNR associated with the spot.
- 8- The transmitter and receiver repeat steps 6 and 7 for all the spots.
- 9- The receiver sends a control feedback signal at a low rate to the transmitter about the time delay and the SNR associated with each spot.
- 10- The transmitter redistributes the total transmission power among the beams according to the ratio of SNRs from equation (4.1).
- 11- The transmitter calculates a differential delay between the beams from equation (4.2) to compensate for the spread due to the differential beam arrival times as seen by the receiver. Note that most of the power is collected by the receiver through the line of sight with each spot

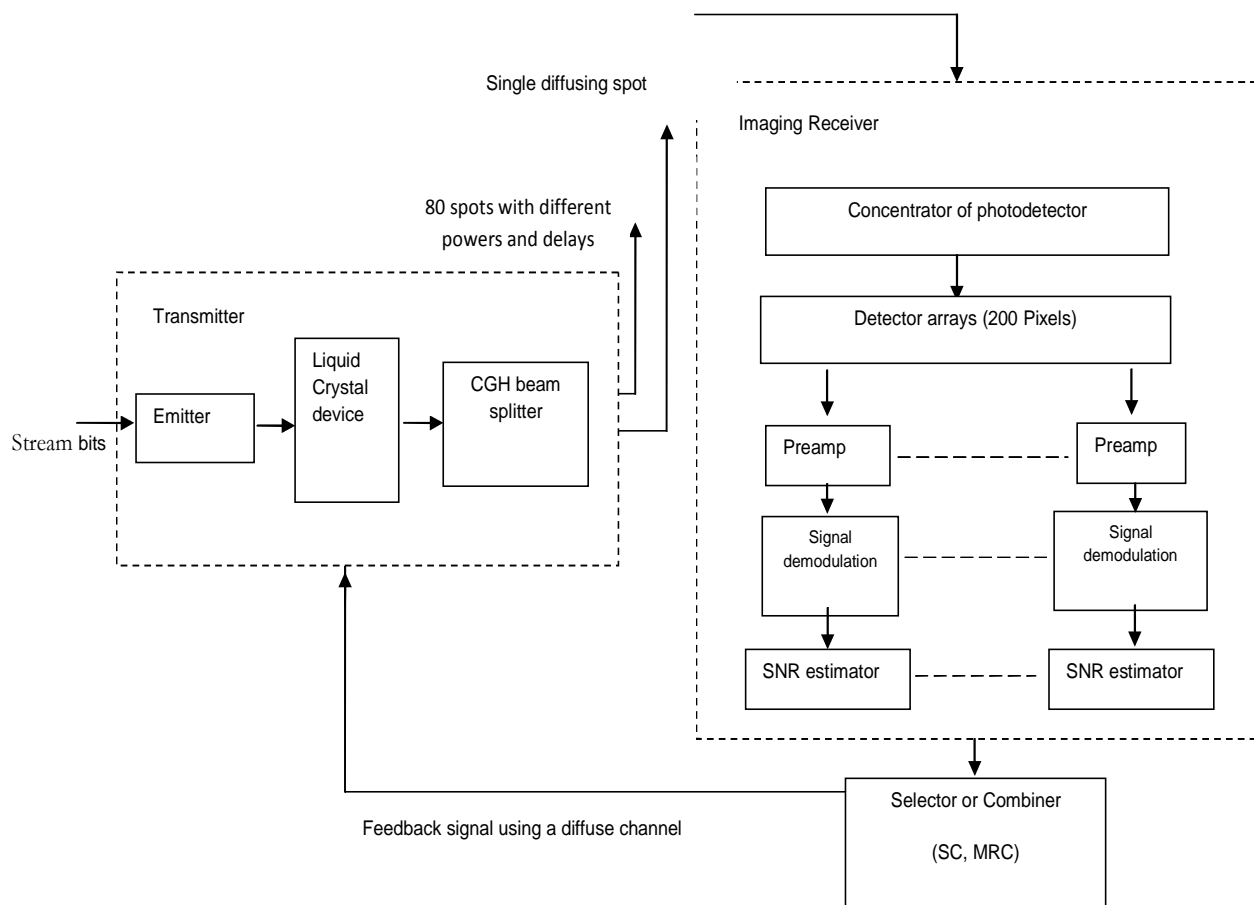


Figure 6.2: Block diagram of the beam delay, angle and power adaptation algorithm.

(significantly lower power through reflections). Therefore adjusting the differential beam delays helps reduce the delay spread at the receiver.

12- The transmitter switches on the beam with the longest journey first, and then switches on the other beams with differential delays so that all the beams reach the receiver at the same time. It should be noted that beams with the same delay (due to room symmetry) are switched on at the same time.

13- The transmitter increases the angle between the beams in steps of  $0.57^\circ$  (notice that the angles between the beams are equal), and steps 6 to 13 are repeated.

14- The algorithm ceases when the angle between the beams reaches to  $2.86^\circ$ .

- 15- The transmitter is specified so that it operates at the optimum beam delays, angles and powers.

Pedestrians move typically at a speed of 1m/sec. If each SNR computation is carried out in 10  $\mu$ s (considering high-speed imaging receiver (200 pixels) computation time), then the total adaption time when the receiver moves is 80 ms which is lower than the 1 second available. We propose that the receiver periodically (namely at 1 second intervals) re-evaluates its SNR and if this has changed significantly (compared to a threshold value) then this change initiates transmitter adaptation. As such the holograms can adapt every 1 second. The 80 ms adaptation time therefore represents an overhead of 8% in terms of transmission time. It should be noted that this adaptation has been done at the rate at which the environment changes for example the rate at which humans move not at the system's bit rate. Therefore when the system is stationary it can achieve 10 Gb/s, when it is on the move it can achieve 92% of this data rate, i.e. 9.2 Gb/s. Holograms based on LC devices capable of adapting within ms times are feasible. We estimated the power consumption if our algorithm is implemented in an embedded system. For example if the Microchips 32-bits microcontroller is used as processor (PIC32MX110F016B) [192], the power consumption is found to be 72 mW. Therefore the energy consumption is 5760  $\mu$  Joule in 80 ms.

The transmitter and receiver are synchronised, and at the start of a frame, the transmitter individually turns on each spot, and then the receiver calculates the SNR after combining signals using MRC and also computes the power received from the detector that has the highest SNR and calculates the delay,  $t_1$ , of the maximum received power with respect to the start of the frame. The transmitter turns on the second beam after a predetermined time delay  $T$ . The receiver receives this second pulse at time  $(t_1 + T + t_2)$  and hence determines  $t_2$ . The difference between  $t_2$  and  $t_1$ , i.e.  $\Delta t = t_2 - t_1$ , is the difference in delay the two beams experience in the channel. The individual receivers' varying response

times may add a jitter element to this value if their response is slow or if they are not implemented on a common integrated platform, the latter may reduce variability. The receiver sends the time delays associated with the beams back to the transmitter to help optimise the delay spread at the receiver. The adaptive BDAPA-LSMS transmitter switches on the beams at different times, starting with the beam that induces the maximum time delay. The rest of the beams propagate to the receiver, each at a certain time that is equal to the difference between its associated time delay and the maximum time delay.

The SNR measured by the receiver is conveyed back to the transmitter via a response channel at a low data rate for validation. This may be a diffuse channel, for instance, by employing a different source or by employing one of their beams. An important observation here is that the design of the holograms and their implementation through LC devices is not ideal. The input power may not be all allocated to spots but may partially leak through resulting in a form of noise where data is not directed at the correct spatial orientations desired (spots). The impact of such noise (a form of background noise) is of interest in the overall design and is not considered here.

## **6.4 Simulation Results**

### **6.4.1 Delay Spread Distribution**

For the channel delay spread evaluation, the transmitter is immobile in the middle of the room at (2m, 4m, 1m) and the receiver is moved along the  $x = 1\text{m}$  axis above the CP. At every position, the spots/beams are optimised through our techniques (beam delay, angle and power adaptation) to minimise the delay spread and enhance the SNR at the receiver. The delay spread result of CDS, non-adaptive LSMS and fully adaptive BDAPA-LSMS configurations coupled with imaging receiver, is plotted in Figure 6.3. The CDS non-imaging channel receiver is also taken into account. The CDS non-imaging receiver show a high

signal delay spread. However, when the imaging receiver substitutes the non-imaging receiver, the delay spread of the CDS system is improved from 2.4 ns to 0.35 ns. This improvement in delay spread is credited to the small field of view connected to each pixel, which limits the range of accepted signals, hence reducing the pulse spread. The multi-spot transmitter, LSMS, reduces the delay spread to almost 0.14 ns. There is a significant reduction in delay spread to almost 0.02 ns when beam angle and power adaptations are introduced (APA-LSMS). Our proposed BDAPA-LSMS reduces the delay spread by a factor of 10 compared with imaging APA-LSMS. A smaller time bin of 0.01 ns was also considered for higher data rates (5 Gb/s and 10 Gb/s) in our proposed systems which results in a slightly higher delay spread compared to that obtained using a 0.5 ns time bin. Note that if one ray dominates the impulse response (due to angle and power adaptation), then the impact of a smaller time bin is reduced. Figure 6.4 shows the delay spread of our proposed beam angle and power

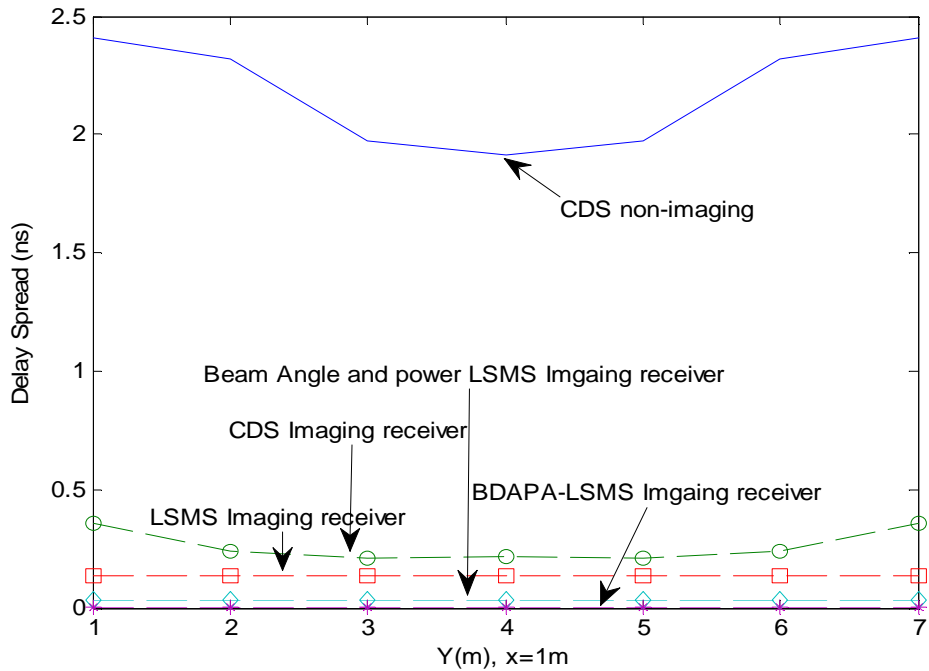


Figure 6.3: Delay spread of four configurations: CDS, LSMS, APA-LSMS and BDAPA-LSMS when the transmitter is placed at (2m, 4m, 1m) and the receiver moves along the x=1m line.

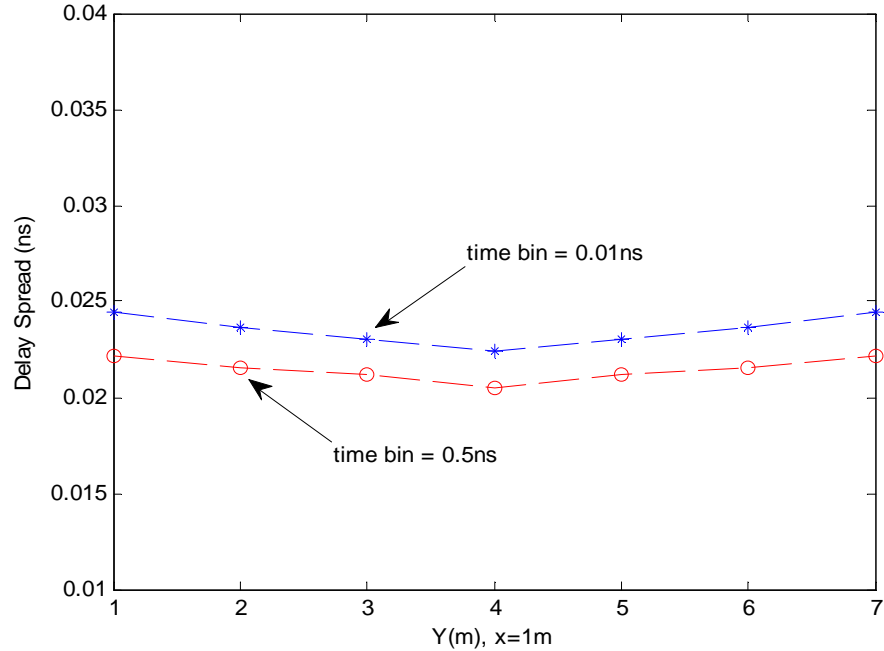


Figure 6.4: Delay spread of APA-LSMS using different time bins: 0.5ns and 0.01ns, when the transmitter is placed at (2m, 4m, 1m) and the receiver moves along the  $x=1m$  line.

adaptation LSMS (APA-LSMS) with different time bins of 0.5 ns and 0.01 ns. A smaller time bin (0.01 ns) resulted in a slightly higher delay spread compared with a time bin of 0.5 ns.

### 6.4.2 Impulse response and 3-dB Channel bandwidth

The 3-dB channel bandwidth of four configurations (non-imaging and imaging CDS, LSMS, BDPA-LSMS and BDAPA-LSMS coupled with imaging receiver), when the transmitter is stationary in the middle of the room and the receiver is mobile and moves along the  $x=1m$  line, is plotted in Figure 6.5. The results show that the proposed BDAPA-LSMS provides the largest bandwidth compared with the other systems. This is attributed to four factors: (1) introducing differential delay among the beams significantly reduces the delay spread, hence increasing the channel bandwidth, (2) through optimisation of the spot locations on a particular area of the walls and/or ceiling where the receiver

can collect strong signals through LOS components, (3) by allocating more power to the spots closest to the receiver, which results in strong received power, and (4) ultimately engaging an imaging receiver with small view pixels considerably reduces the effect of the background noise sources as well as multipath dispersion. Our simulation results show that the diffuse CDS system coupled with an imaging receiver increases the communication channel bandwidth from the 36 MHz offered by the CDS non imaging wide FOV receiver to almost 330 MHz, see Figure 6.6. The multi-spot transmitter coupled with an imaging receiver enhances the 3-dB channel bandwidth from the bandwidth offered by the CDS to almost 1.1 GHz, see Figure 6.5. Recent research has successfully demonstrated an experimental 2.5 Gb/s OW over a 1-2m distance (limited mobility) with a 45 degrees diffused beam in an indoor environment [66]. However these studies do not use beam delay, angle and power adaptations in conjunction with the imaging receiver. When beam power adaptation coupled with an angle diversity receiver replaces the conventional LSMS, there is significant bandwidth improvement to approximately 4.2 GHz (provided in Chapter 4). Moreover, beam angle and power adaptation in conjunction with an angle diversity receiver increases the channel bandwidth up to 7.2 GHz (provided in Chapter 5). Introducing beam delay with only power adaption and an imaging receiver increases the channel bandwidth to 7.9 GHz, see Figure 6.5. Our new proposed system, BDAPA-LSMS, increases the 3-dB channel bandwidth to 9.8 GHz as shown in Figure 6.5. This increase in channel bandwidth enables our proposed system to operate at higher data rates, i.e., 10 Gb/s and 12.5 Gb/s (to the best of our knowledge this is the highest data rate (feasibility) reported for an indoor *mobile* optical wireless system employing any method). In an optical direct detection system, the optimum receiver bandwidth

## 6.4 Simulation Results

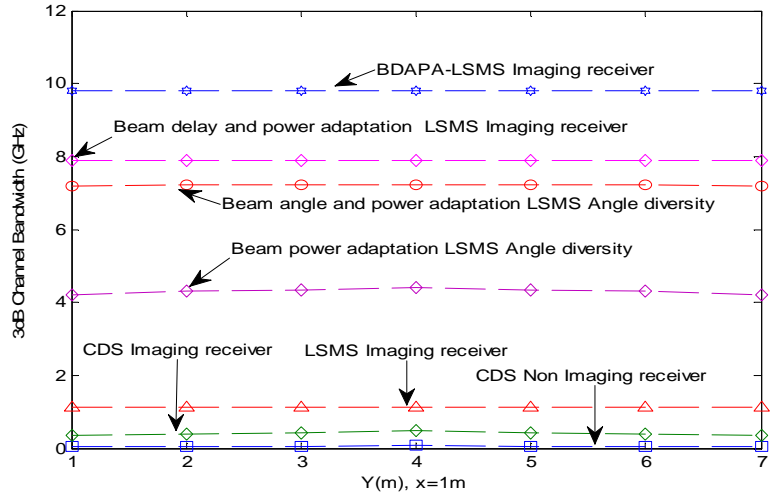
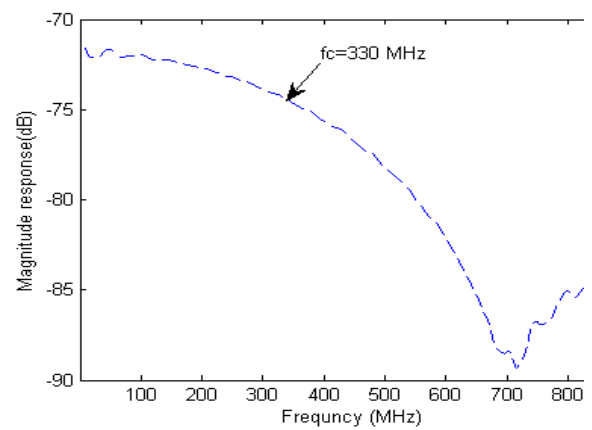
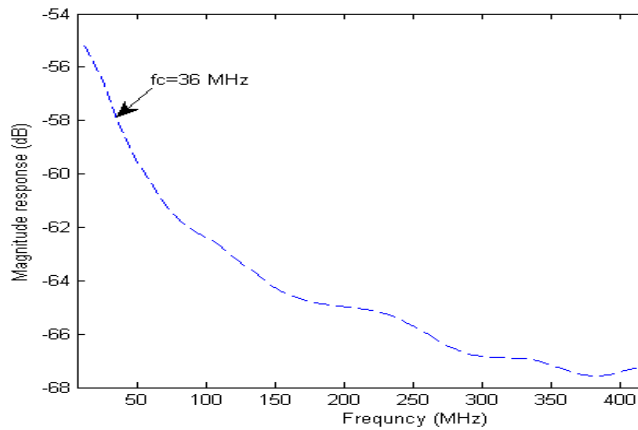
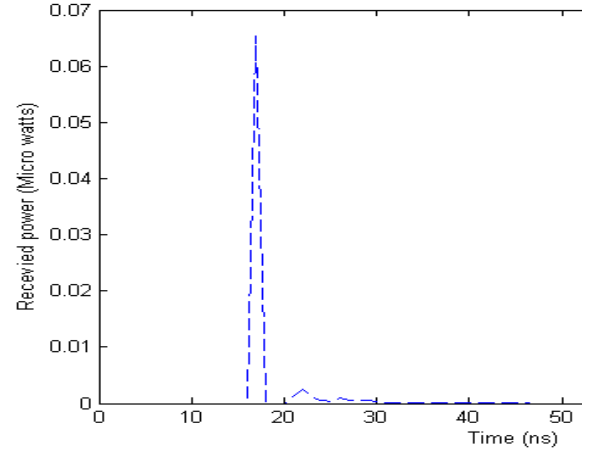
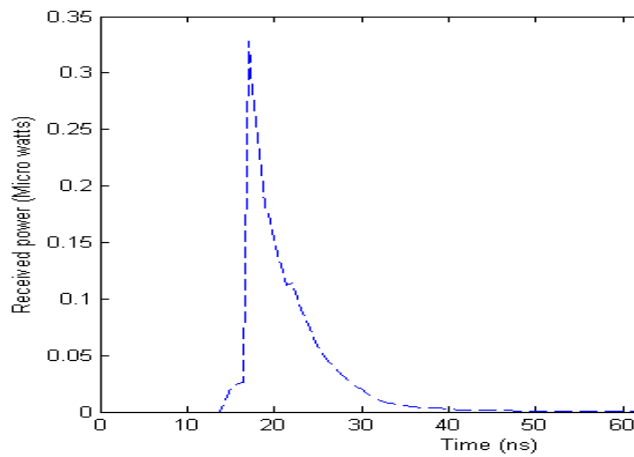
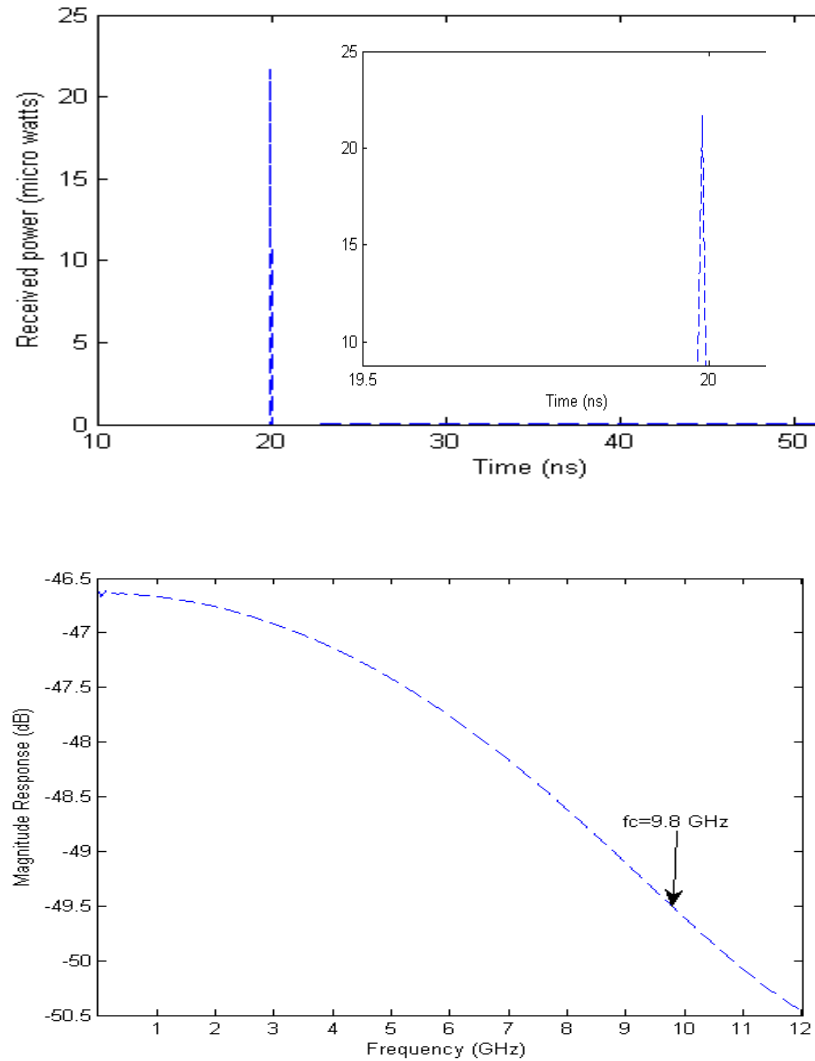


Figure 6.5: 3-dB channel bandwidth of three configurations: CDS, LSMS, BDAPA-LSMS when the transmitter is placed at (2m, 4m, 1m) and the receiver moves along the  $x=1m$  line.



(a) CDS wide FOV non-imaging receiver.

(b) CDS with 200 pixels imaging receiver



(c) BDAPA-LSMS with 200 pixels imaging receiver.

Figure 6.6: Impulse response and frequency response of CDS and BDAPA-LSMS when the transmitter is placed at (2m, 4m, 1m) and the receiver is at the corner of the room (1m, 1m, 1m).

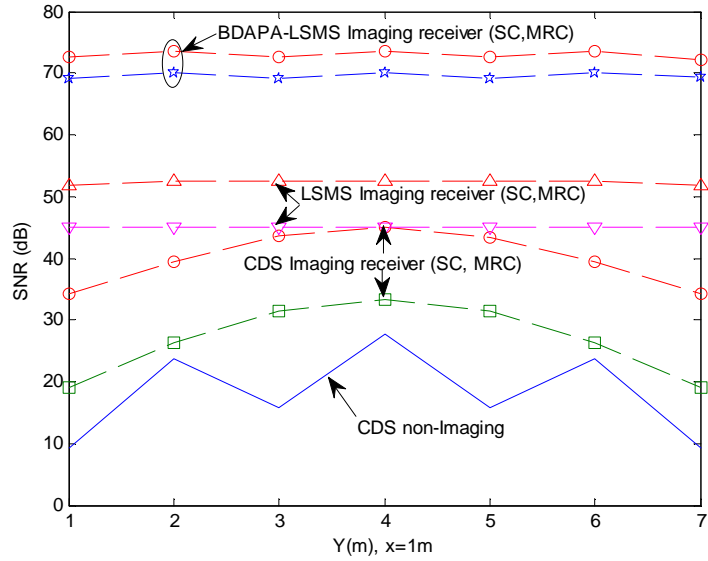
is 0.7 times the bit rate. As such a 12.5 Gb/s data rate requires an 8.75 GHz receiver bandwidth (the 0.7 figure is based on Personik's optical receiver design [77]). In our proposed systems unlike diffuse systems, the third order reflections are very small in comparison given that the first order reflections from the spots are very strong. Hence the impact of higher order reflections is very small when our adaptation techniques are introduced. This is an important observation

when comparing our proposed systems and conventional diffuse systems where in the latter third order reflections may play a significant role at high data rates.

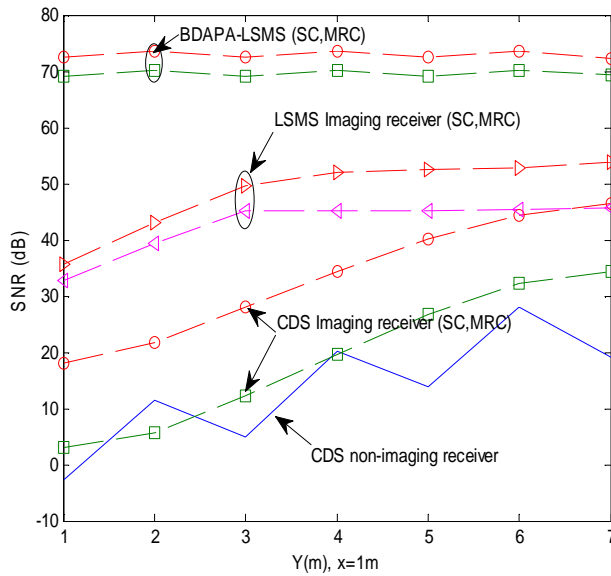
### 6.4.3 SNR Results

The SNR results of the proposed imaging configurations: CDS, LSMS and BDAPA-LSMS using SC and MRC techniques compared with the CDS non-imaging system, operating at 30 Mb/s, when the transmitter is positioned at (2m, 4m, 1m), (1m, 1m, 1m) and (2m,7m,1m) are given in Figure 6.7. The SNR computations were carried out for fourteen different locations when the receiver is moved along the y-axis at a constant  $x=1\text{m}$  and  $x=2\text{m}$ , which scans the highs and lows of surrounding light noise sources. At 30 Mb/s, we used the preamplifier design proposed in [121]. Our simulation findings illustrate that variation in the CDS SNR (due to background noises and multipath dispersion) is reduced by over 20 dB in the worst communication link, when the imaging receiver MRC substitutes the wide FOV non-imaging receiver. This result is well matched with the previous findings in the literature [121]. This considerable enhancement in the level of SNR is due to the capability of the imaging receiver to choose and combine the pixels that observe the minimum ambient noise. A considerable enhancement can be obtained by using the simple multi-spot LSMS configuration, which offers a 17 dB SNR advantage above the diffuse CDS imaging receiver. This enhancement in the SNR is due to the fact that the LSMS is capable of equally covering its environment through the use of a number of spots, when the transmitter is located in the middle of the room, which allows the receiver to collect the signal from the closest diffusing spot. Although the improvements were achieved in both the CDS and the LSMS imaging receiver, degradation in the SNR performance is noted when the transmitter is on the move (mobile), as illustrated in Figure 6.7 (b) and (c), in which the transmitter is shifted away from the receiver to the edge of the room at (2m, 7m, 1m) or to the room corner at (1m, 1m, 1m). This drop in the SNR

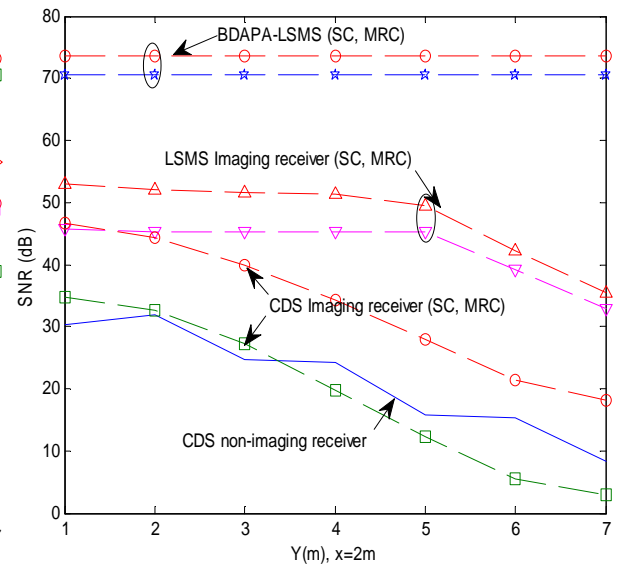
## 6.4 Simulation Results



(a) Transmitter at (2m, 4m, 1m)



(b) Transmitter at (2m, 7m, 1m)



(c) Transmitter at (1m, 1m, 1m)

Figure 6.7: OW CDS, LSMS and BDAPA-LSMS systems SNR with an imaging receiver at 30 Mb/s.

results is attributed to the user movement and can be reduced by replacing the CDS and the LSMS with our new fully imaging BDAPA-LSMS. The proposed imaging BDAPA-LSMS achieves around 55 dB SNR gain above the CDS imaging receiver in the worst case channel. Our results in Figure 6.7 prove that

the BDAPA-LSMS SNR is totally independent of the transmitter position. Therefore, a considerable enhancement in SNR is accomplished at each transmitter and receiver location. It has to be observed that if a single beam is employed the enhancement in the channel bandwidth and SNR may be desirable. However, this sort of structure may be affected by beam obstruction as well as shadowing, and may violate skin and eyes safety rules, if all of the transmission power is allocated to the single beam.

## 6.5 Effect of Realistic Indoor Environment

In this part, we extend the analysis and evaluation of diffuse CDS, non-adaptive LSMS and fully adaptive BDAPA-LSMS configurations, coupled with an imaging receiver, to realistic office arrangements where optical signal blockage (as a result of mini-cubicles), furniture, doors and windows, multipath propagation and ambient light sources are all present. The non-imaging CDS structure is additionally studied evaluated and compared with our new systems for two room scenarios (1) an unshadowed room and (2) a shadowed room environment. The simulation was conducted in a room comparable to that used in Section 6.2 with an  $8\text{m} \times 4\text{m} \times 3\text{m}$  room as an example. Figure 6.8 shows the room arrangements: (a) the unshadowed room in which there is a door, three large glass windows, and eight spotlights (background noise) and (b) the shadowed room which has the same items as the unshadowed room plus a number of rectangular cubicles that have surfaces parallel to the walls of the room (physical partitions, which create shadowing) and other furniture like filing cabinets, bookshelves and chairs. In Figure 6.8, the ceiling has a diffuse reflectivity of 0.8, while the floor has a diffuse reflectivity of 0.3. The three glass windows and the door are assumed to not reflect any signal, thus their diffuse reflectivities are set at zero. Moreover, the walls that encompass the ceiling and the wall segments around the windows have diffuse reflectivity of 0.8. Two of the walls at  $x=4\text{m}$  and  $y=8\text{m}$  (apart from the door) covered by filing cabinets and

bookshelves, have a reflectivity of 0.4. It is assumed that signals that get to the office physical barriers (cubical office partitions) are blocked or absorbed. Additionally, chairs and desk tables inside the room have a similar reflectivity to that of the floor (0.3). The complexity is apparent in the room in Figure 6.8 in which the physical partitions and the low reflective objects can create significant

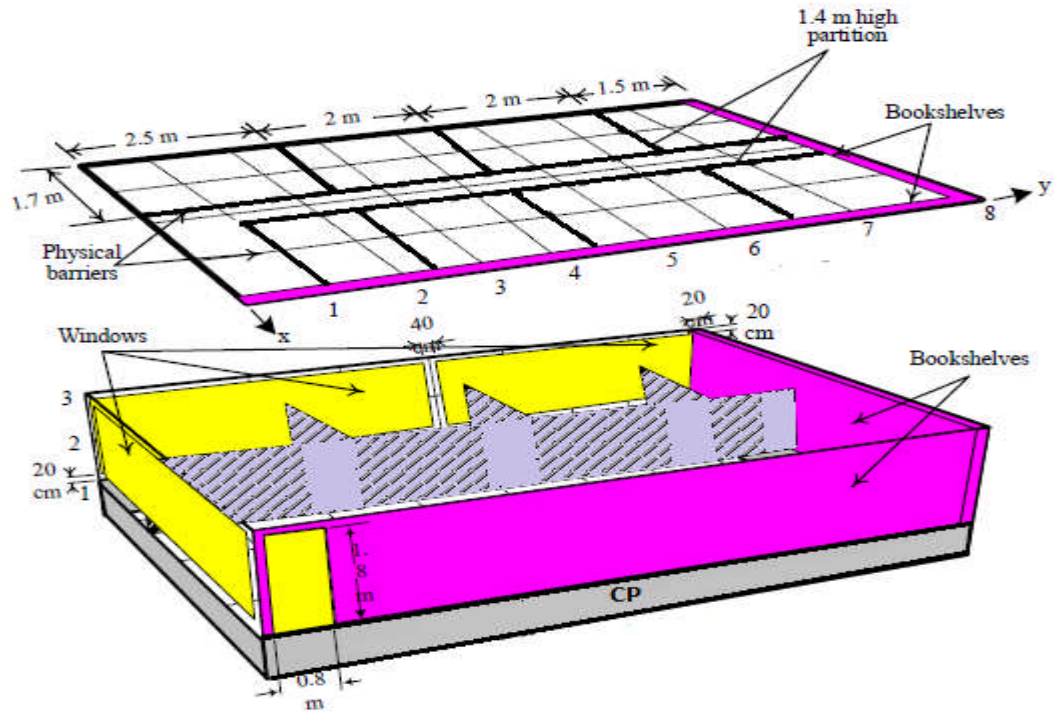


Figure 6.8: Schematic representation of a realistic indoor office environment with the potential of beam interruption (shadowing)

shadowing, beam blocking and reduce the received optical power at the receiver in the case of the diffuse transmitter. In a realistic indoor environment, a simulation package similar to the one explained in Section 6.2 (where beam delay, angle and power adaptation coupled with an imaging receiver are implemented) was developed in order to calculate the impulse response (received optical signals) and background noise signals and to compute the SNR at the receiver. In order to model the reflections in a realistic environment, the room surfaces were divided into small reflective elements similar to the

ones stated in previous chapters which are modelled as Lambertian reflectors. In this study, reflections up to the second order are considered.

Figure 6.9 shows the SNR results of our proposed configurations: non-imaging and imaging CDS, LSMS and BDAPA-LSMS combined with an imaging receiver in the two room arrangements: shadowed and unshadowed rooms, when the system operates at 30 Mb/s. The results are plotted when the transmitter is positioned in the room corner at (1m, 1m, 1m), while the imaging receiver moves across the line  $x=2m$ . In the case of the non-imaging CDS arrangement, at the worst communication channel, the SNR in the unshadowed is lower by 6.8 dB compared to an empty room. This is attributed to the reduction in the total optical received power where part of the signals is lost as a result of the three big glass windows in the two upright walls in addition to the door. Further degradation by 21 dB in the SNR of the non-imaging CDS took place in a shadowed room. This is due to the setup of the room where the physical partitions and low reflectivity (0.4) on two walls ( $x=4m$  and  $y=8m$ ) that are covered by filing cabinets and bookshelves in addition to the low reflectivity of other objects result in low received optical signals through reflection surfaces. This shadowing degradation may be decreased by 9.5 dB when a non-imaging receiver is substituted by an imaging MRC receiver. Table 6.2 shows the SNR degradation of the CDS imaging (MRC) and non-imaging systems in a shadowed and an unshadowed room compared with an empty room. Employing multi-spot LSMS configuration in conjunction with an imaging receiver (200 pixels) can help reduce the effect of shadowing. This is due to the fact that the multi-spot LSMS in conjunction with the 200 pixels imaging receiver is able to establish a direct LOS between the spots (on the ceiling where there is a suitable path) and the receiver during mobility, which can provide a strong connection in the presence shadowing. However, 15 dB SNR degradation is observed in the mobile imaging LSMS, when the transmitter is placed at (1m,

Table 6.2: SNR degradation of CDS imaging (MRC) and non-imaging systems in shadowed and unshadowed rooms compared with an empty room.

Tx (1m, 1m, 1m)	SNR degradation of CDS imaging (MRC) and non-imaging systems in shadowed and unshadowed rooms compared with an empty room.						
	Rx (x m, y m, 1m)	(2m,1m)	(2m,2m)	(2m,3m)	(2m,4m)	(2m,5m)	(2m,6m)
CDS non-imaging (unshadowed)	6.5dB	5.3dB	4.8dB	4.8dB	5.1dB	5.7dB	6.8dB
CDS non-imaging (shadowed)	9.1dB	8.8dB	10.9dB	13.9dB	16.5dB	18.7dB	21.5dB
CDS imaging (unshadowed)	2.7dB	1.7dB	1.6dB	1.7dB	1.9dB	2.3dB	4.6dB
CDS imaging (shadowed)	3.2dB	2.6dB	4dB	5.8dB	6.9dB	7.1dB	9.5dB

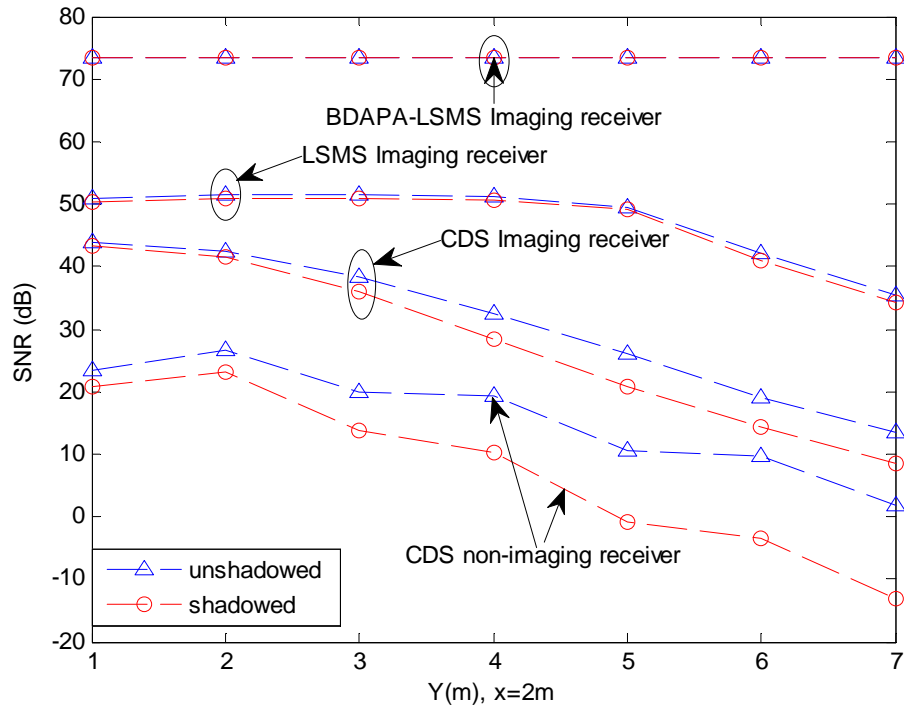


Figure 6.9: SNR of CDS, LSMS and BDAPA-LSMS systems at 30 Mbit/s, in a typical indoor office, when the transmitter is placed at (1m, 1m, 1m) and the imaging receiver moves along the x=2m line.

1m ,1m) and the receiver is moved to (2m, 7m, 1m) from (2m, 1m, 1m). Introducing our methods of beam delay, angle and power adaptive LSMS can considerably decrease the impact of the transmitter movement and the effect of the shadowing in a realistic office room. In the worst communication link considered, with the existence of shadowing, our fully adaptive imaging BDAPA-LSMS provides around 39 SNR enhancements over the non-adaptive multiple spot LSMS structure.

Considerable enhancement in the SNR and channel bandwidth is achieved as explained in Figure 6.6 (Section 6.5.2), which confirms that our new configuration is useful in increasing the data rate. The high data rates of 2.5 Gb/s and 5 Gb/s are seen to be viable in our previous systems: angle diversity BDPA-BCM and imaging BDPMA-BCM. Furthermore, 10 Gb/s is also studied with our angle diversity APA-LSMS multi-spot diffusing system (Chapter 5). Here, our new imaging BDAPA-LSMS shows significant enhancements in the link budget as well as the 3-dB channel bandwidth which enables the system to operate at 10 Gb/s and 12.5 Gb/s. The preamplifier used in the 10 Gb/s and 12.5 Gb/s OW systems is the PIN FET preamplifier proposed in [186]. Figure 6.10 shows the MRC SNR of the imaging beam delay and power adaptive LSMS (BDPA-LSMS), angle and power adaptive LSMS (APA-LSMS), and BDAPA-LSMS operating at 10 Gb/s and 12.5 Gb/s. The transmitter is positioned at (2m, 7m, 1m) and the receiver moves at a constant  $x=1m$  along the  $y$ -axis over the CP. Moreover, Figure 6.10 shows that BDPA-LSMS offers about 9 dB SNR gain in the worst case scenario over the LSMS that uses beam power adaptation only. This is due to the fact that beam delay and power adaptation helps increase the 3-dB channel bandwidth, hence increasing the SNR at the higher data rates (note that the SNR as defined in (3.27) takes into account the eye opening, hence dispersion). Furthermore, our proposed BDAPA-LSMS coupled with an imaging receiver (with a pixel FOV of  $11.3^\circ$ ) achieves a consistent 25 dB SNR (BER  $<10^{-9}$ ) at 10 Gb/s . Our proposed

system provides approximately 3 dB SNR gain over beam angle and power adaptation. Since our methods (beam delay, angle and power adaptation) are able to identify the optimum location of the spots as determined by the receiver, we reduce the acceptance semi angle of our imaging receiver to  $45^\circ$  and increase the number of pixels to 256 (our imaging receiver has a pixel FOV of  $7.1^\circ$  and a pixel area of  $0.99 \text{ mm}^2$ ), in order to enhance the link budget at higher data rates. Our proposed system, BDAPA-LSMS, coupled with an imaging receiver having a pixel's FOV of  $7.1^\circ$  provides 32.3 dB and 29.2 dB SNR at 10 Gb/s and 12.5 Gb/s, respectively, in the presence of background shot noise, multipath dispersion and mobility. The SNR improvement obtained through the combination of beam delay angle and power adaptations, spot-diffusing and imaging receiver allows us to reduce the transmit power below the current 1 W level. To investigate our proposed system with respect to eye safety regulations, we used a total transmit power of 80 mW (1 mW per beam) and introduced a limitation in the power adaptation algorithm so that the power per beam is not increased beyond 1.5 mW. We have also reduced the size of the spot from a diameter of 1 cm to 0.5 cm which allows more flexibility in clustering the spots closely if needed. The SNRs achieved in our proposed system in this case were about 12.5 dB and 9.5 dB at 10 Gb/s and 12.5 Gb/s, respectively, under the impact of background noise, multipath dispersion and mobility, see Figure 6.11. At 12.5 Gb/s the SNR is still greater than 9.5 dB ( $\text{BER} < 10^{-3}$ ). Therefore forward error correction (FEC) can be used to further reduce the BER from  $10^{-3}$  to  $10^{-9}$  in our proposed system. The higher data rates (12.5 Gb/s and 10 Gb/s) in our BDAPA-LSMS system are therefore shown to be feasible through the combination of multiple transmit beams, beam delay adaptation, beam angle adaptation, beam power adaptation and imaging receivers.

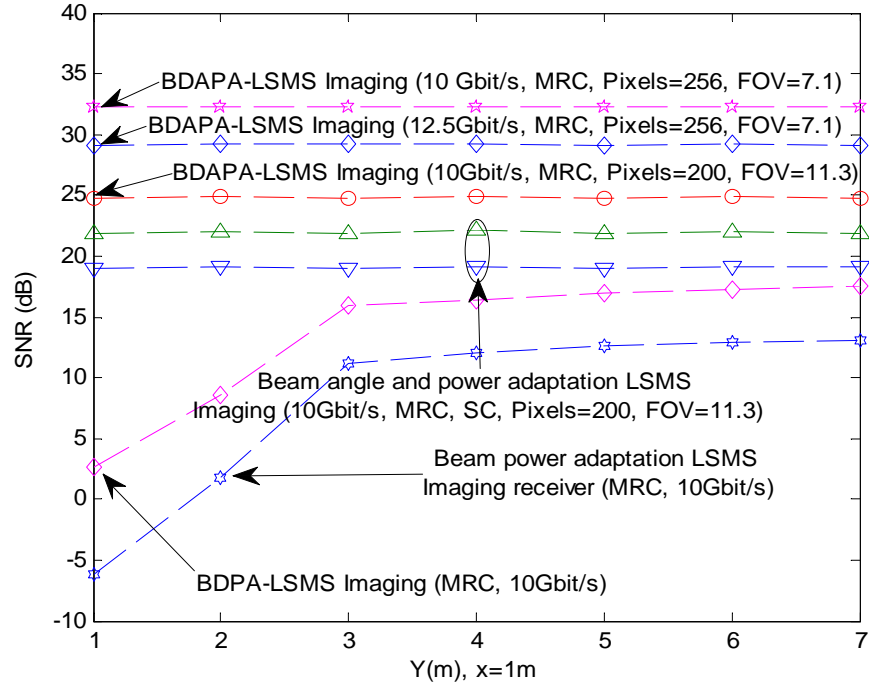


Figure 6.10: SNR of beam power adaptation LSMS, BDPA-LSMS, APA-LSMS, and BDAPA-LSMS systems at 10 Gbit/s and 12.5 Gbit/s, when the transmitter is placed at (2m, 7m, 1m) and the receiver moves along the x=1m line.

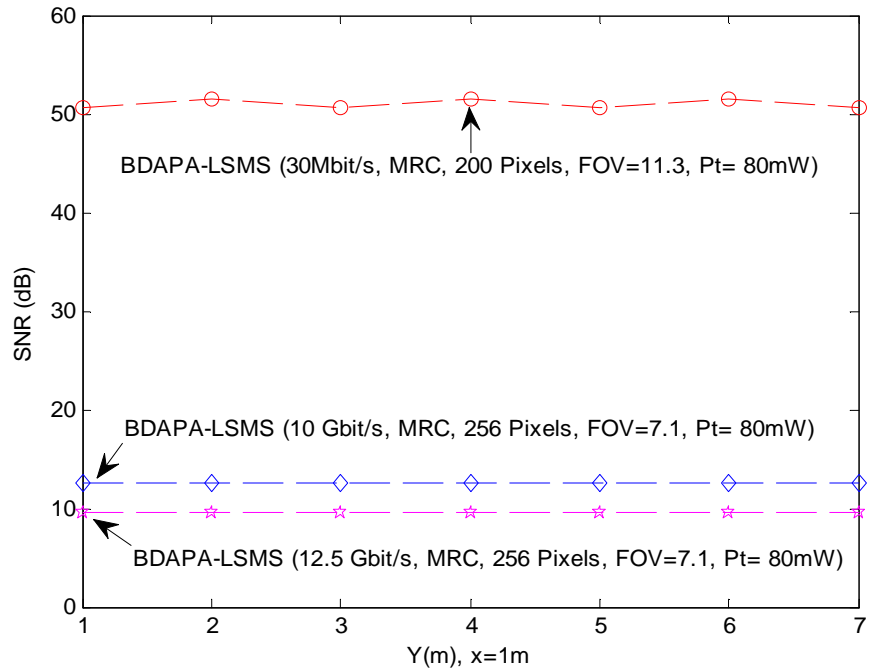


Figure 6.11: The SNR of our proposed system operating at 30Mbit/s, 10 Gbit/s and 12.5 Gbit/s, with a total transmit power of 80 mW.

## **6.6 High data rate OW communications challenges and possibilities**

Achieving high data rate OW communications is possible using our proposed system. Since the adaptive transmitter (tracking system) is able to track the receiver, even with small FOV imaging receivers, the link budget is increased. However, the fabrication and testing of a high speed OW receiver array are very challenging tasks. To the best of our knowledge, there is no commercial high-speed receiver to date that has specially been designed for indoor OW. At a data rate of 10 Gb/s, most of the components will probably be adopted from the optical fiber domain, which is not ideal for OW, thus making the receiver fabrication a challenging task. This is especially the case for custom OW components such as the concentrator (lens), the small detector size and its narrow field of view.

## **6.7 Summary**

User mobility as well as shadowing can significantly degrade the functionality of the CDS, LSMS and BDPA-LSMS in the indoor environment. In this chapter, we introduced beam delay adaptation and imaging detection approaches and examined their use with our two previously introduced methods provided in Chapter 5: beam angle adaptation and beam power adaptation. The SNR results show that beam delay, angle and power adaptation in conjunction with an imaging receiver can significantly help reduce the effect of background noise, shadowing, multipath dispersion and mobility. At a bit rate of 30 Mb/s our adaptive imaging BDAPA-LSMS provides SNR enhancements of 55 dB above CDS in the worst possible link. This enhancement is obtained by introducing five techniques: beam delay adaptation, beam angle adaptation, beam power adaptation, multi-spot transmitters and imaging receivers. Steering the beams' angles through an angle adaptation method can help the transmitter target its

spots at a position where the receiver can collect a robust signal from direct LOS components. Beam delay adaptation helps reduce the delay spread, and hence increases the 3-dB channel bandwidth and the SNR at high data rates. Beam power adaptation can enable the transmitter to allocate more power to the spots nearest to the receiver thus increasing the SNR at the receiver. Our proposed methods coupled with an imaging receiver are shown to be extremely effective in increasing the channel bandwidth from 36 MHz (CDS) to about 9.8 GHz (BDAPA-LSMS with an imaging receiver). The results show that the impact of signal blockage and shadowing can be adequately reduced through the use of these techniques. Our simulation results show that the imaging BDAPA-LSMS system achieves about 29.2 dB SNR level at 12.5 Gb/s. To investigate our proposed system with respect to eye safety regulations, we used a total transmit power of 80 mW (1mW per beam) and introduced a limitation in the power adaptation algorithm so that the power per beam is not increased beyond 0.5 mW. The SNRs achieved in our proposed system in this case were about 12.5 dB and 9.5 dB at 10 Gb/s and 12.5 Gb/s, respectively, under the impact of background noise, multipath dispersion and mobility, FEC can be used to further reduce the BER from  $10^{-3}$  (at these SNRs) to  $10^{-9}$  in our proposed system.

# **7 Indoor Optical Wireless Links**

## **Employing Fast Angle and**

## **Power Adaptive Finite**

## **Vocabulary of Holograms**

### **7.1 Introduction**

Simulation results in Chapters 5 and 6 proved that a significant enhancement was achieved in a mobile OW system that employs beam angle and beam power adaptation in a line strip multi-spot system (APA-LSMS) configuration [113], [123]. A cost has to be paid, however, in terms of the complex design of the beam power adaptive line strip multi-spot system (PA-LSMS), angle adaptive line strip multi-spot system (AA-LSMS) and APA-LSMS. The complexity is associated with the computation time required to identify the optimum spot location, as well as the time needed to compute and generate the hologram with optimum power and angle distribution. In order to solve this problem, we introduce a new adaptive finite hologram vocabulary approach using simulated annealing to generate multi-beam spots. The holograms are pre-calculated and stored in the proposed system (each hologram is suited for a given (range of) transmitter and receiver locations) and eliminate the need to calculate a real-time hologram at each transmitter and receiver location.

In this chapter we propose fast angle adaptive holograms (FAA-Holograms), fast power adaptive holograms (FPA-Holograms), and fast angle and power adaptive holograms (FAPA-Holograms) mobile OW systems, in conjunction with imaging reception. The simulation results show that adaptive hologram

systems can significantly improve the impulse response, SNR, as well as the delay spread in a typical indoor environment (mobility, ambient light noise and multipath propagation). A further improvement can be obtained by increasing the number of holograms in this system to try to approach the performance of the un-constrained (by finite number of choices) angle and power adaptive systems previously introduced. However, increasing the number of holograms leads to an increase in the computation time required to identify the optimum hologram. In order to reduce the number of holograms to be generated and speed-up the search for the best hologram from the finite hologram vocabulary (stored in the transmitter), we propose a fast divide-and-conquer (D&C) search algorithm and study the impact of having a finite hologram vocabulary as well as study the trade-offs between computation complexity and SNR penalty and compare the results to a range of systems.

The new proposed systems are compared with pure diffuse imaging and non-imaging systems as well as non-adaptive LSMS configuration. All the systems are simulated at 30 Mb/s to facilitate comparison with the results in the literature, for example [121]. High data rates of 1.25 Gb/s, 2.5 Gb/s and 5 Gb/s are also considered for the FAPA-Holograms system. The simulation results indicate that the proposed FAPA-Holograms system is able to achieve a consistent SNR at every transmitter and receiver location. The trade-off between complexity and performance of our proposed systems compared with beam power and angle adaptations proposed in previous chapters is of interest and is investigated. Moreover, the new method of adaptive finite holograms has also been introduced with angle diversity receivers. Nine narrow FOVs angle diversity receivers have been employed with our FAPA-Holograms. The proposed system has been examined in a realistic indoor office where doors, windows, a number of rectangular-shaped partitions (shadowing), and other furniture, like filing cabinets, bookshelves and chairs with low reflectivity surfaces are all present.

The rest of the chapter is organised as follows: Section 7.2 describes the imaging receiver design used in this study. The OW channel characteristics and the simulation model are given in Section 7.3. The new proposed systems based on fast adaptive finite vocabulary holograms (FPA-Holograms, AA-Holograms and FAPA-Holograms) are discussed in Section 7.4. The delay spread and the SNR results of mobile OW systems including: CDS, LSMS, FPA-Holograms, FAA-Holograms and FAPA-Holograms imaging receivers are given in Section 7.5 and 7.6, respectively. Section 7.7 investigates the trade-off between the SNR penalty and computational saving of our proposed system compared to the beam power and angle adaptations. A nine angle diversity receiver structure coupled with our FAPA-Hologram is provided in Section 7.8. The effect of shadowing in a realistic indoor office is given in Section 7.9. Finally, a summary is presented in Section 7.10.

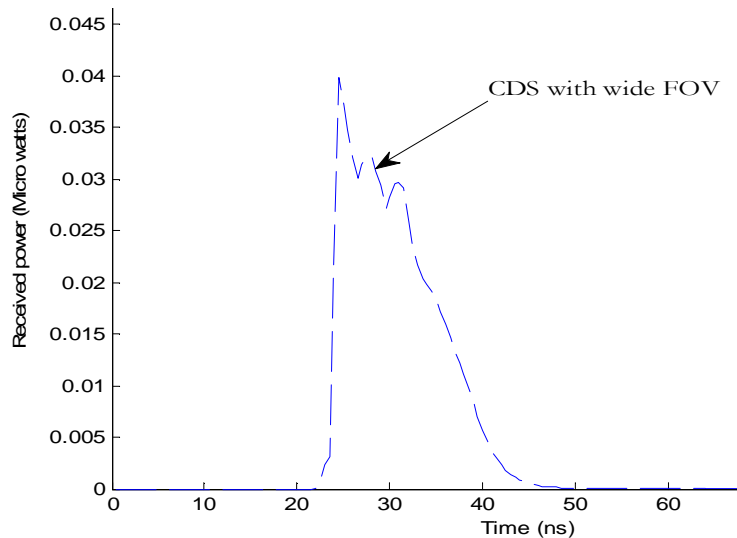
## **7.2 Simulation set-up**

The simulation tool used is similar to the ones used in previous chapters. The signal and noise modelling is performed in the same way in the previous chapters. Imaging receivers as well as multiple non-imaging angle diversity receivers are used to reduce the impact of directive noise sources as well as multipath dispersion. The imaging receiver design provided in Chapters 4 and 6 is used with our new finite adaptive holograms (FPA-Holograms, FAA-Holograms and FAPA-Holograms) configurations. Our previous results in Chapters 4 and 6 show that MRC offers better improvement compared with the SC technique. Nine narrow FOVs non-imaging angle diversity receivers will be explained in Section 7.7.

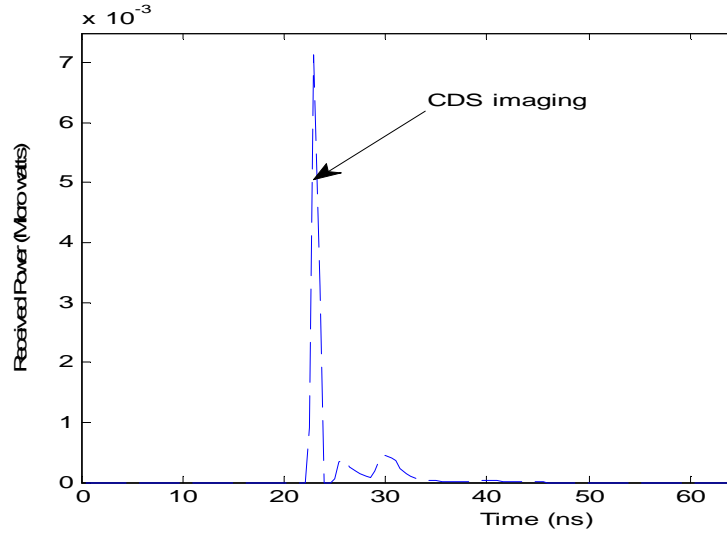
## 7.3 Transmitter Structures

### 7.3.1 Diffuse CDS and Non-adaptive LSMS Configurations

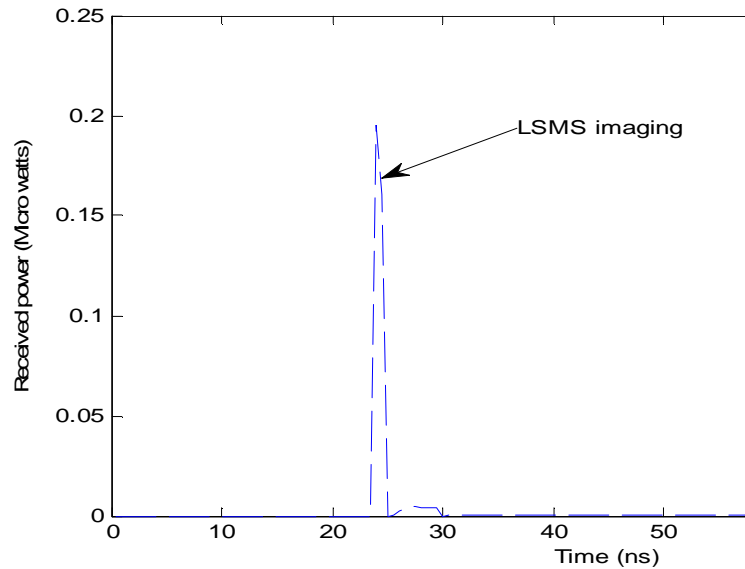
For impulse response assessment, the transmitter was located at the room corner (1m, 7m, 1m) above the communication plane (CP), while the receiver was placed on the opposite side of the room at (2m, 1m, 1m) (6m horizontal separation between the transmitter and the receiver). The impulse response of the CDS with a wide FOV receiver is depicted in Figure 7.1 (a). The spread in the channel impulse response is observed, which is due to diffuse transmission and the wide FOV detector, resulting in multiple reflecting elements being seen by the receiver; hence there is a restriction on the achievable bandwidth. The spread in diffuse channel can be reduced when an imaging receiver substitutes the wide FOV receiver, see Figure 7.1 (b). This improvement is due to the narrow FOV of the imaging receiver pixels which limit the range of rays accepts hence increasing the 3-dB channel bandwidth compared with the wide FOV non-imaging receiver. However, a significant reduction in the received power (imaging receiver) compared with CDS is observed. This reduction can be



(a) CDS wide FOV non-imaging receiver.



(b) CDS with 200 pixels imaging receiver.



(c) LSMS with 200 pixels imaging receiver.

Figure 7.1 : impulse response of (a) CDS with wide FOV receiver (b) CDS with imaging receiver (c) LSMS with imaging receiver, when transmitter is placed at (1m, 7m, 1m) and receiver is moved at (2m, 1m, 1m).

compensated when a multi-spot diffusing LSMS transmitter is employed instead of the diffuse transmitter as shown in Figure 7.1 (c). The result shows an increase in the total received power from  $15.66 \text{ nW}$  (CDS-imaging receiver) to  $0.39 \text{ } \mu\text{W}$  when a multi-spot diffusing transmitter is employed.

## 7.3.2 Adaptive Holograms Configurations

This section considers the design and configurations of adaptive holograms.

### 7.3.2.1 Fast Angle Adaptive finite vocabulary of Holograms (FAA-Holograms)

An angle adaptive OW system has been introduced in Chapter 5 and 6. In beam angle adaptation the transmitter first produces a single spot to scan the walls and ceiling at approximately 8000 possible locations (associated with a  $2.86^\circ$  beam angle increment [113], [123]) in order to identify the best location, then the transmitter generates a hologram that produces a line strip of diffusing spots (LSMS) at the optimum location. These processes require intensive calculations and time from a digital signal processor (DSP). In order to eliminate the need to compute the holograms at each step to determine the best location, a new adaptation approach is introduced where a finite vocabulary of stored holograms is used. The floor (or ceiling) is divided into regions i.e., eight regions ( $2\text{m} \times 2\text{m}$  per region), see Figure 7.2. In each region, the transmitter should possess a hologram that generates the optimum diffusing spots if the receiver is present in any one of the eight regions. These holograms can be pre-calculated so as to target the spots near the receiver (in whichever region the receiver may be) based on our angle adaptation algorithm proposed in Chapter 5 and 6.

Holograms generated by means of a computer can produce spots with any prescribed amplitude and phase distribution. For the fast angle adaptive holograms (FAA-Holograms), all the spots have the same weight (power), (but different phases). CGH's have many useful properties. Spot distributions can be computed on the basis of diffraction theory and encoded into a hologram.

Calculating a CGH means the calculation of its complex transmittance. The transmittance is expressed as:

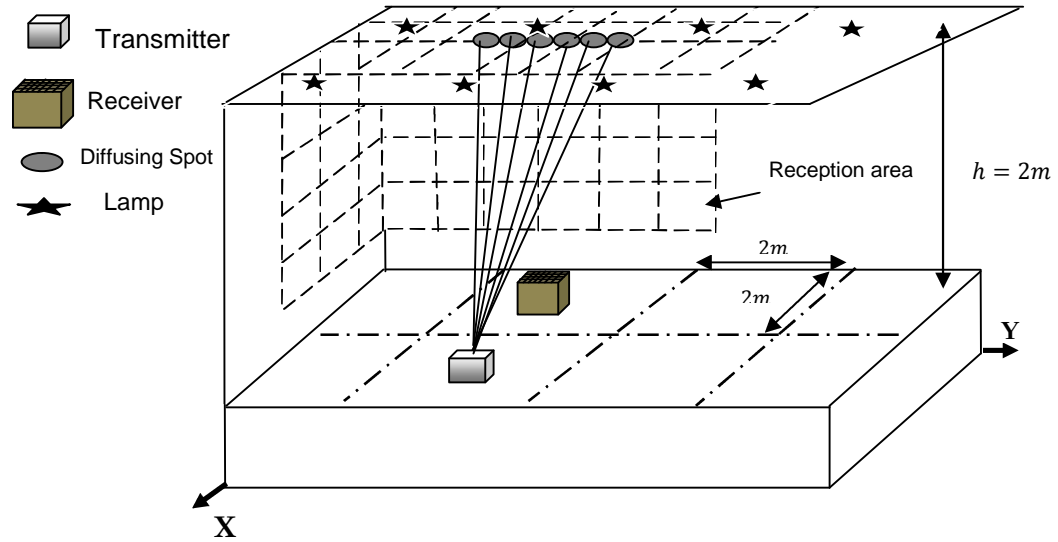


Figure 7.2: Our proposed OW communication system with adaptive holograms when the transmitter is placed at  $(3m, 3m, 1m)$  and the receiver is at  $(1m, 3m, 1m)$ .

$$H(u, v) = A(v, u) \cdot \exp[j\phi(u, v)], \quad (7.1)$$

where  $A(u, v)$  is its amplitude distribution,  $\phi(u, v)$  is its phase distribution, and  $(u, v)$  are coordinates in the frequency space. The relative phases of the generated spots are the objects of interest. The hologram is able to modulate only the phase of an incoming wavefront, the transmittance amplitude being equal to unity. The analysis used in [133], [193] – [194] has been employed for the design of the CGHs. The hologram  $H(u, v)$  is considered to be in the frequency domain and the observed diffraction pattern  $h(x, y)$  in the spatial domain. They are related by the continuous Fourier transform:

$$h(x, y) = \iint H(u, v) \exp[-i2\pi(ux + vy)] du dv \quad (7.2)$$

The hologram structure is an  $M \times N$  array of rectangular cells, with dimension  $R \times S$ . Each cell represents a complex transmittance value  $H_{kl}$ :  $-M/2 < k < M/2$  and  $-N/2 < l < N/2$ . If the hologram is placed in the frequency plane, the diffraction pattern is given by:

$$h(x, y) = RS \operatorname{sinc}(Rx, Sy) \sum_{k=-\frac{M}{2}}^{\frac{M}{2}-1} \sum_{l=-\frac{N}{2}}^{\frac{N}{2}-1} H_{kl} \exp[i2\pi(Rkx + Syl)] \quad (7.3)$$

where  $\operatorname{sinc}(a, b) = \sin(\pi a) \sin(\pi b) / \pi^2 ab$ . The hologram is designed such that the complex amplitude of the spots is proportional to some value of interest. However, because of the finite resolution of the output device and the complex transmittance of the resulting hologram, the reconstruction will be in error. This error can be considered to be a cost function. Simulated annealing (SA) was used to minimise the cost function [193], [195]. The amplitudes and phases of every spot are determined by the hologram pixels pattern and are given by its Fourier transform. The constraints considered in the hologram plane are to discretize the phase from 0 to  $2\pi$  and a constant unit amplitude for the phase only CGH.

Let the desired spots in the far field be  $f(x, y) = |f(x, y)| \exp(i\varphi(x, y))$ . The main goal in the design is to determine the CGH distribution  $g(v, u)$  that generates a reconstruction  $g(x, y)$  as close as possible to the desired distribution  $f(x, y)$ . The cost function (CF) is defined as a mean squared error which can be interpreted as the difference between the normalised desired object energy  $f''(x, y)$  and the scaled reconstruction energy  $g''(x, y)$ :

$$CF_k = \sqrt{\sum_{i=1}^M \sum_{j=1}^N (|f''(i, j)|^2 - |g''_k(i, j)|^2)^2}, \quad (7.4)$$

where  $f''(x, y)$  represents the normalised desired object energy and  $g''_k(i, j)$  represents the scaled reconstruction energy of the  $k^{\text{th}}$  iteration. Simulated annealing was used to optimise the phase of the holograms offline in order to minimise the cost function. The simulating annealing algorithm can help jump from local optima to close to a global optimum (minimising the cost function close to zero). The transition out of a local minima to global one is

accomplished by accepting hologram phases that increase the mean squared error of the reconstruction with a given probability. The probability of accepting these phases is  $\exp(-\Delta CF/T)$ , where  $\Delta CF$  is the change in error and  $T$  is a control parameter (the temperature of the annealing process). Firstly, we start with a high value of  $T$  so that all the change in the hologram phases are accepted and then slowly lower  $T$  at each iteration until the number of accepted changes is small. This method is similar to melting a metal at a high value of  $T$  and then reducing the  $T$  slowly until the metal crystals freezes at a minimum energy. The changes of hologram phases relate to a small perturbation of the physical system, and the resulting change in the mean squared error of the reconstruction corresponds to the resulting change in the energy of the system. Therefore, this technique finds a hologram configuration which has a minimum mean squared error (CF). For phase only CGHs the constraints are constant unit amplitude and a random phase distribution  $\varphi_0 (M \times N)$ . In the first iteration a random phase is applied to help in the convergence of the algorithm.

For a large room of  $8\text{m} \times 4\text{m}$ , the floor is divided into eight regions ( $2\text{m} \times 2\text{m}$  per region). A library which contains 64-holograms optimised offline using simulated annealing was established. Each hologram produces the optimum diffusing spots which were pre-calculated based on angle adaptation technique (provided in Chapter 5 and 6) in order to optimise spot locations at each particular area of  $2\text{m} \times 2\text{m}$ , see Figure 7.2. In each region, the transmitter should have eight holograms stored in a library in order to cover the eight possible receiver positions in the room. This results in 64 holograms in the case of eight regions in order to cover the entire room. The total number of holograms required is  $N^2$ , where  $N$  represents the number of regions into which the floor/ceiling is divided. An example of one hologram, when the transmitter is placed at  $(3\text{m}, 3\text{m}, 1\text{m})$  and the receiver is present in the second region, is shown in Figure 7.2. Simulated annealing was used to optimise the phase of the computer-generated hologram. The desired spots' intensities in the far field

are shown in Figure 7.3 (a). Figure 7.3 (b) shows four snapshots of hologram phase distributions and the reconstruction intensity of  $g(x, y)$  in the far field at different iterations. When the number of iteration increases, the reconstruction intensities are improved. This is attributed to the use of simulated annealing which attempts to reduce the cost function, hence improving phases in hologram, The cost function versus the number of iterations completed is shown Figure 7.4.

After generating 64 holograms using simulated annealing optimisation, the holograms are stored in the library of the proposed FAA-Holograms system. In the case of classic (i.e. not fast) angle adaptive holograms, the transmitter first sequentially tries all N holograms (64 holograms in this case) and the receiver computes the SNR associated with each hologram at the receiver and relays this information to the transmitter for the transmitter to identify the best hologram to use. This is an exhaustive search mechanism among the stored holograms.

The impulse response of the proposed angle adaptive holograms in conjugation with the imaging receiver is shown in Figure 7.5 (a) when the transmitter is

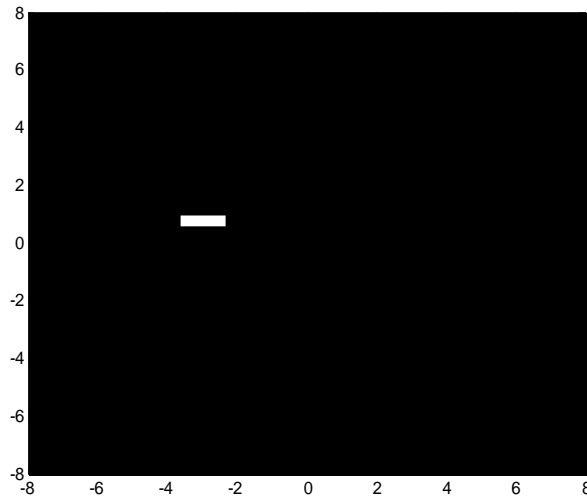


Figure 7.3 (a): The desired spots' intensities in the far field.

### 7.3 Transmitter Structures

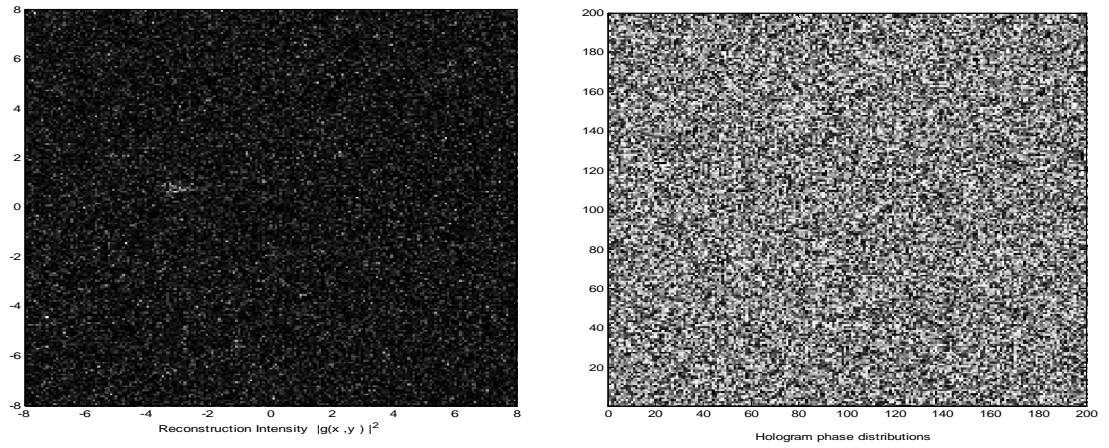


Figure 7.3 (b): Iteration.1

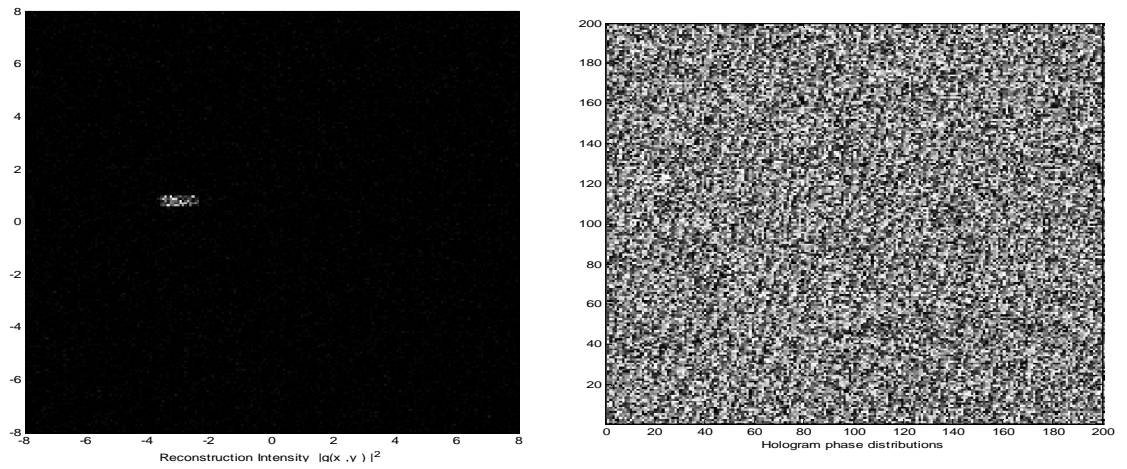


Figure 7.3 (b): Iteration.5

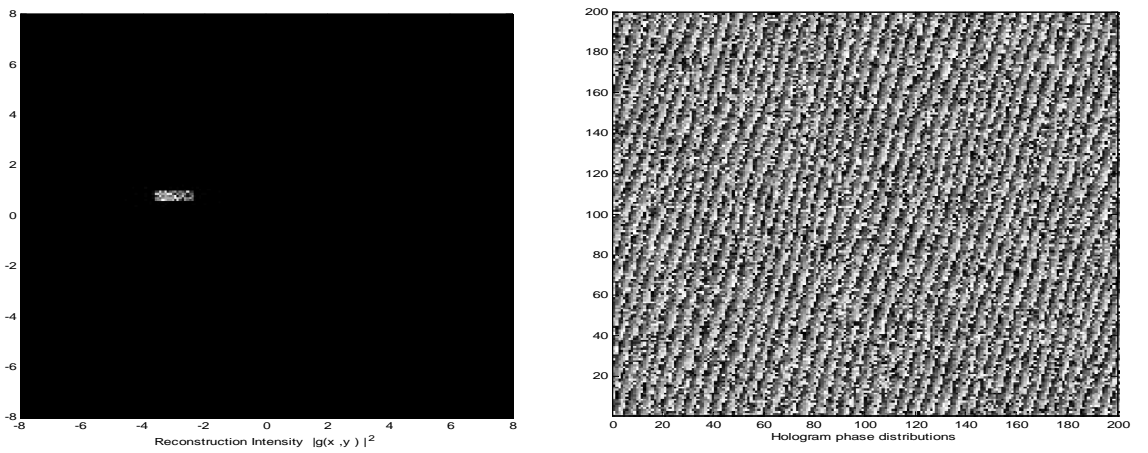


Figure 7.3 (b): Iteration.15

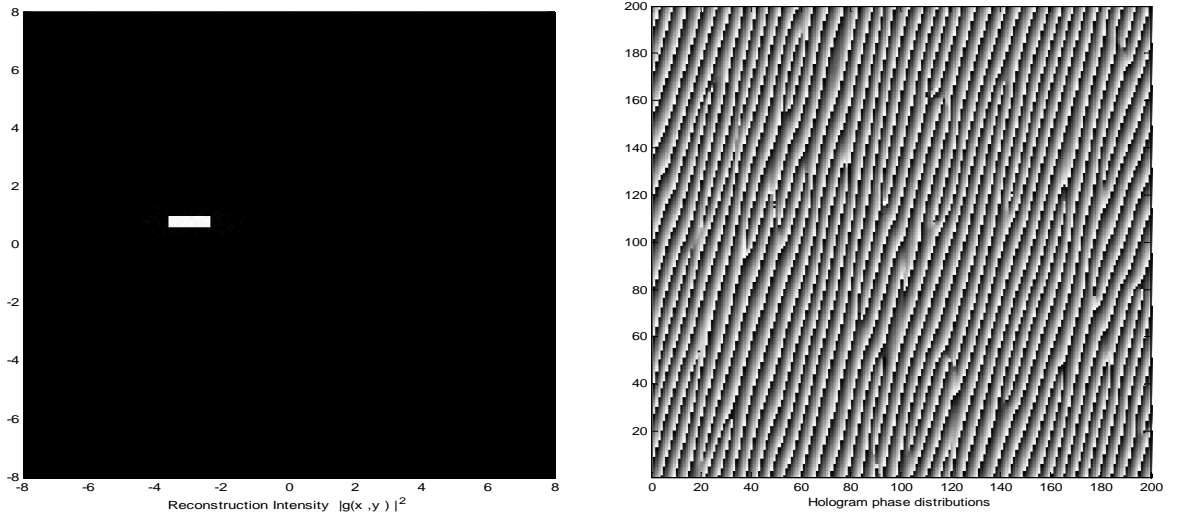


Figure 7.3 (b): Iteration.100

Figure 7.3: (a) the desired spots intensity in far field (b) hologram phase pattern and the reconstruction intensity in the far field at iterations 1, 5, 15 and 100 using simulated annealing optimisation. Different gray levels represent different phase levels ranging from 0 (black) to  $2\pi$  (white).

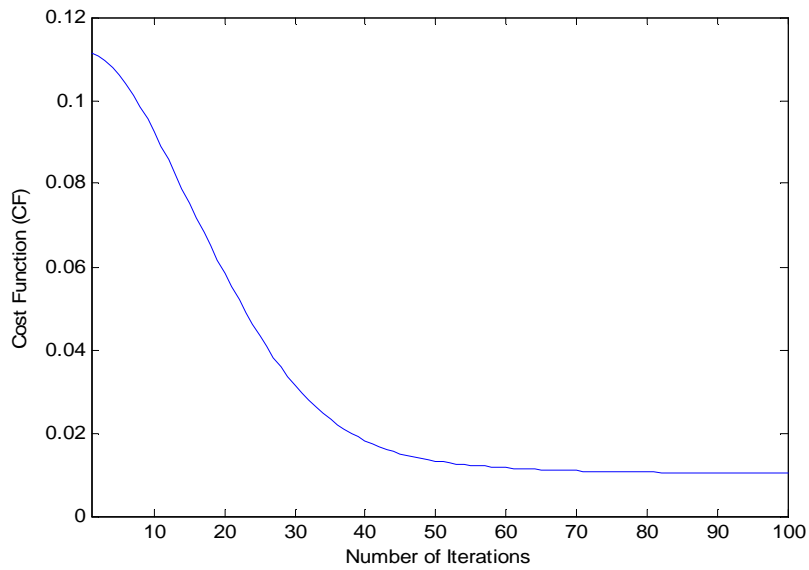


Figure 7.4: Cost function vs. the number of iterations.

placed in the room corner (1m, 7m, 1m) and the receiver is stationary at the room edge at (2m, 1m, 1m) and (2m, 2m, 1m). The results indicate that the adaptive holograms transmitters, coupled with an imaging receiver, offer

significantly better performance than both the CDS and the LSMS. This is due to selecting the best hologram whose spots are nearest the receiver, which increases the direct power components from  $0.2 \mu W$  offered by LSMS to  $6 \mu W$ .

The transmitter scans all the holograms, which results in a total of 64 holograms, in order to identify the best hologram. If each SNR computation is carried out in  $10 \mu s$ , then the total adaptation time when the receiver moves is  $640 \mu s$ . A further improvement in SNR can be achieved by increasing the number of regions on the floor which leads to smaller regions and improved spots locations, but a larger number of holograms to choose from leading to an increase in the time required to identify the best holograms. For example, increasing the number of regions from 8 to 16 will lead to an increase in the total number of holograms to 256. Hence the computation time required to identify the optimum holograms is increased to 2.56 ms. In order to overcome this problem, a fast angle adaptive hologram (FAA-Holograms) algorithm is introduced to effectively improve the SNR (through the use of more holograms) while reducing the computation time required to identify the optimum hologram. The fast algorithm determines the optimum hologram that yields the best receiver SNR based on a D&C algorithm. The transmitter divides the stored holograms into four quadrants with a boundary based on the hologram transmission angles  $(-\delta_{min} \text{ to } 0)$  and  $(0 \text{ to } \delta_{max})$  in both  $x, y$  axes. The transmitter first tries the middle hologram at each quadrant (four holograms will be first tried) to identify the sub-optimal quadrant; hence reducing the number of holograms that need to be tried by a factor of 4 in the first step. The receiver sends a feedback signal at a low rate, which informs the transmitter about the SNR associated with each hologram. The hologram that results in the best receiver SNR is identified as a sub-optimum hologram, and the quadrant that includes this sub-optimum hologram will be divided in the next step into four sub-quadrants. The transmitter again scans the middle hologram at four new sub-quadrants and identifies the second sub-optimal hologram; hence

identifying the second sub-optimal quadrant. The transmitter again divides the new second sub-optimal quadrant into four quadrants in a similar manner to the first and second sub-optimal quadrants to identify the third sub-optimal quadrant. The quadrant that is represented by the third sub-optimal hologram will be scanned. This technique helps to reduce the computation time required to identify the optimum hologram when a very large number of holograms is used. The proposed FAA-Holograms algorithm can be described for a single transmitter and receiver as follows:

- 1- The transmitter first divides the stored holograms into four main groups associated with quadrants based on the hologram transmission angles. The boundary angles associated with the first quadrant are  $\delta_{max-x}$  to 0 in the x-axis and  $\delta_{max-y}$  to 0 in y-axis.
- 2- The transmitter transmits using the middle hologram in each quadrant in order to determine the first sub-optimum hologram.
- 3- The receiver computes the SNR associated with each transmission (each hologram) and sends a feedback control signal at a low rate to inform the transmitter of the SNR associated with the hologram (four holograms will be tried first in order to find the first sub-optimal hologram / region).
- 4- The transmitter records (the transmission angles of) the hologram where the receiver SNR is sub-optimal.
- 5- The transmitter identifies the quadrant that includes the sub-optimal hologram from the hologram's transmission angles, for the next iteration.
- 6- The transmitter again divides the sub-optimal quadrant into four sub-quadrants and repeats steps 3 to 5 to identify the second sub-optimal quadrant.

- 7- The transmitter again divides the second sub-optimal quadrant in to four sub-quadrants and repeats steps 3 to 5 to identify the third sub-optimal quadrant.
- 8- The divide and conquer process continues and the transmitter determines the optimal hologram transmission angles that maximise the receiver's SNR.

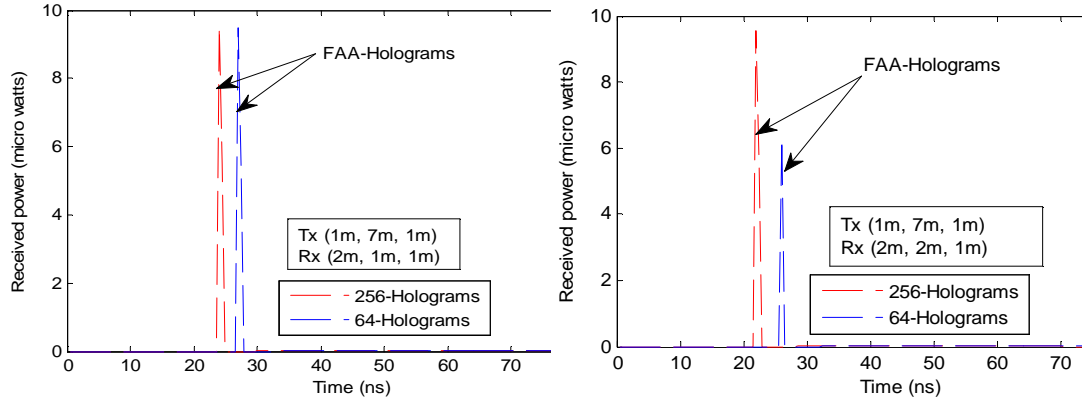
The proposed system, FAA-Holograms (with 256 holograms), reduces the computation time from 2.56 ms taken by the classic angle adaptive holograms to 160  $\mu$ s. Figure 7.5 (a) shows that the proposed FAA-Holograms with 256 holograms system increases the direct power component by a factor of 1.5 compared with angle adaptive 64 Holograms system (in some locations, and always better than or equal to 64 Holograms system); with a reduction in the amount of computation time required to identify the optimum holograms.

#### **7.3.2.2 Fast Power Adaptive finite vocabulary of Holograms (FPA-Holograms)**

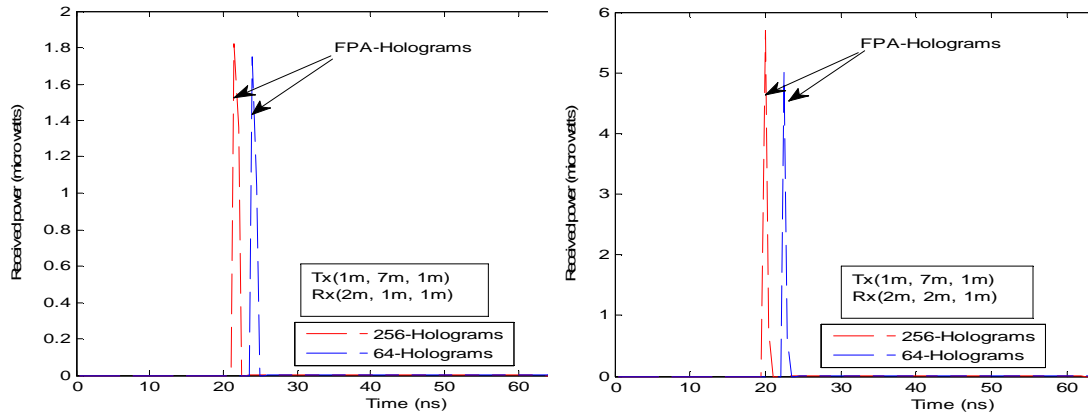
Beam power adaptation was introduced in our previous chapters with line strip multi-spot diffusing OW system (LSMS) to increase the power levels to the spots that are close to the receiver in order to optimise the SNR. The adaptive LSMS switches ON each spot individually and computes the SNR due to this spot at the receiver. The receiver then sends a control feedback signal at a low rate to inform the transmitter of the SNR associated with the beam (spot). The transmitter receives all the SNR weights associated with each spot (80 spots in our case). The transmitter then redistributes the transmit power ( $P_s$ ) among the beams according to the ratio of the SNRs given in (4.1), and then generates a hologram that produces spots with different intensities using liquid crystal devices. These steps require time and calculations to generate the hologram, which increases the transmitter complexity. The idea of beam power adaptation with the finite vocabulary holograms (FPA-Holograms) is to be compute

holograms (ready to be uploaded to the liquid crystal device) where each hologram represents the best power distribution among the spots using equation (4.1) for a given transmitter and receiver location. The floor is divided into regions similar to the FAA-Holograms. Instead of generating  $N^2$  holograms that represent different beam angles as in FAA-Holograms, here the spots are generated vertically above the transmitter, but the power is distributed among the spots to maximise the SNR for the given transmitter and receiver locations. This setting represents one of the  $N^2$  holograms generated and stored. The phase optimisation of holograms can be performed in similar fashion to FAA-Holograms using simulated annealing but with different spot intensities obtained from equation (4.1). A fast power adaptive holograms (FPA-Holograms) algorithm is introduced to reduce the time needed to find the best hologram. The fast algorithm is also based on a D&C algorithm that determines the optimum hologram that yields the best receiver SNR. Since the spots' angles in all holograms are equal, the algorithm divides holograms into two main groups based on the power distribution of spots (in the current case LSMS contains 80 spots). The holograms that increase the power level of spot 1 to spot 40 are listed in the first group and the second group represents holograms that increase the power level of spot 41 to spot 80. The transmitter first tries one hologram in each group. The receiver computes the SNR and informs the transmitter about the SNR weight associated with each hologram via a feedback signal. The transmitter determines the sub-optimal hologram that yields the best receiver SNR and the group that includes the sub-optimal hologram is divided into two sub-groups, whereby each sub-group contains the holograms that increase the power level of 20 spots. The transmitter and receiver carry on the calculations until the sub-group contains the holograms that increase the power level of five spots. This helps the transmitter to reduce the computation time required to identify the optimum holograms by a factor of 16.

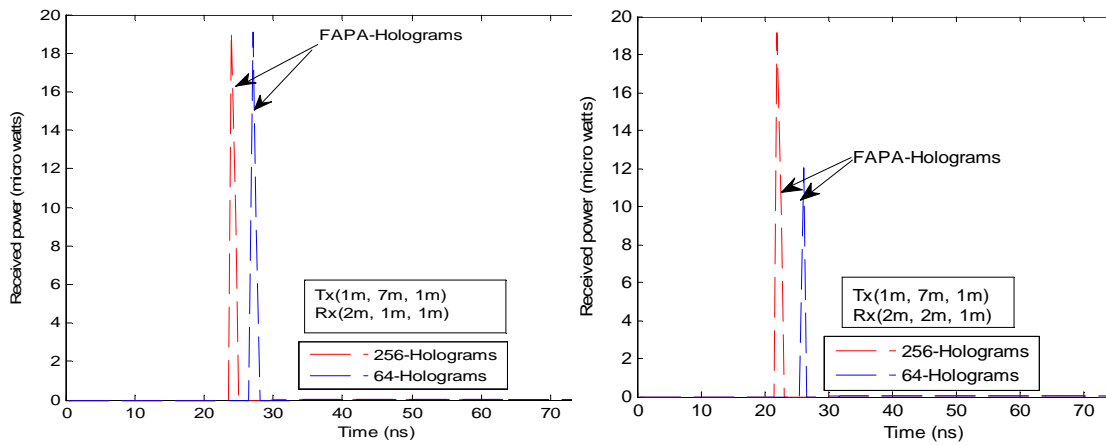
### 7.3 Transmitter Structures



(a) FAA-Holograms



(b) FPA-Holograms



(c) FAPA-Holograms

Figure 7.5: Impulse response of our proposed systems with 64 and 256 Holograms: (a) FAA-Holograms, (b) FPA-Holograms and (c) FAPA-Holograms with imaging receiver, when the transmitter is placed at (1m, 7m, 1m) and the receiver is at (2m, 1m, 1m) and (2m, 2m, 1m).

Figure 7.5 (b) shows the impulse response result of the proposed FPA-Holograms (with 64 and 256 holograms), when the transmitter produces power adaptive  $80 \times 1$ , diffusing spots at 6 m transmitter-receiver horizontal separation. The FPA-Holograms system increases the received power from  $0.2 \mu W$  of the LSMS to about  $1.81 \mu W$ . When the floor is divided into 16 regions, the fast proposed system only needs to scan/try 24 holograms to identify the optimum hologram.

### **7.3.2.3 Fast Angle and Power Adaptive finite vocabulary of Holograms (FAPA-Holograms)**

Although the FPA-Holograms system is better than LSMS, the fast angle adaptive hologram (FAA-Holograms) system still performs better. This is due the fact that the distance between the diffusing spots and the receiver is a main factor in mobile indoor multi-spot diffusing OW systems. The benefits of both systems are combined by introducing fast beam angle and power adaptation with a finite vocabulary of holograms (FAPA-Holograms), in order to further improve the system performance under the impact of background noise, receiver noise, mobility and multipath dispersion. The holograms are pre-calculated which can help the transmitter to target the spots near the receiver (in whichever region the receiver may be) based on our angle and power adaptation algorithm proposed in Chapter 5 and 6. The proposed FAPA-Holograms algorithm is similar to the fast angle adaptive algorithm explained above in the way that the optimum hologram is identified. The angles and power levels associated with the spots in each hologram are pre-calculated and stored in the library of the proposed system without adding any complexity at the transmitter when reproducing holograms. It should be noted that the two adaptation algorithms described (angle adaptation algorithm and power adaptation algorithm) apply to a single transmitter and a single receiver position. In a multi-user scenario, a number of different methods can be considered. For example, opportunistic scheduling [183] can be employed

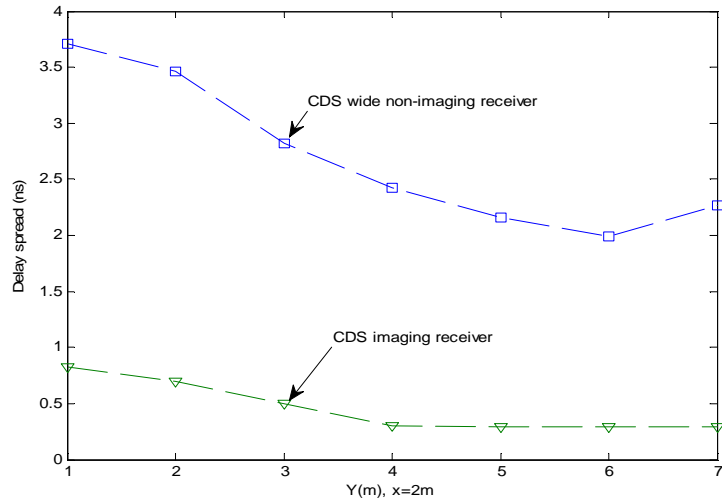
where the optimum hologram is chosen to maximise the SNR in a given region (set of users) for a given time period.

The impulse response of the FAPA-Holograms coupled with imaging receiver when the transmitter is placed near the room corner at (1m, 7m, 1m), and the receiver is close to the room edge at (2m, 1m, 1m) and (2m, 2m, 1m), is given in Figure 7.5 (c). The result shows that the proposed FAPA-Holograms (with 256-holograms) system can increase the direct received power by a factor of 2 and 10 over the FAA-Holograms and the FPA-Holograms systems respectively. This due to: (1) employing an angle adaptive holograms method which can help the transmitter to target its spots at an area on the ceiling where the imaging receiver can receive a strong signal through direct LOS components and through the shortest paths, and (2) introducing a power adaptation approach which can enable the transmitter to assign higher power levels to spots nearest to the receiver to produce further SNR improvement. Furthermore, a significant reduction in computation time is observed in the proposed FAPA-Holograms, based on a D&C search algorithm, when the total number of holograms is increased to 6400 (by dividing the floor into 80 regions) in order to enhance the system SNR (the SNR penalty as a result of using a finite number of holograms is investigated in Section 7.7). The computation time required to identify the optimum holograms is only about 1.12 ms instead of the 64 ms taken by the classic angle adaptive holograms, as shown in Section 7.7.

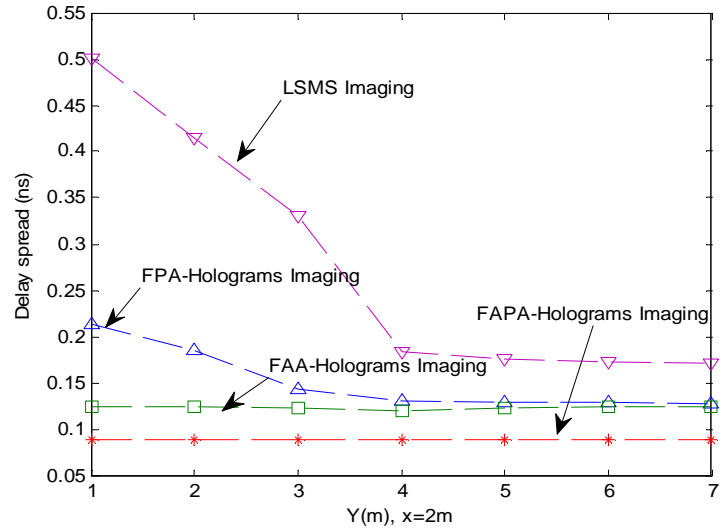
## 7.4 Delay Spread Assessment

The delay spread distribution of the CDS, LSMS, FAA-Holograms, FPA-Holograms and FAPA-Holograms (with 256-holograms) in conjunction with an imaging receiver when the transmitter is placed at one of the room corners (1m, 7m, 1m) and the receiver moves across the y-axis on the line  $x = 2\text{m}$ , is plotted in Figure 7.6. Comparison of the delay spread distribution between different regions, as well as the original beam power and angle adaptations, is discussed

in Section 7.7. The results here are quoted when the proposed imaging OW systems employ selection combining (SC) [123]. In the CDS system, the delay spread decreases from 3.7 ns to around 0.8 ns when an imaging receiver



(a) CDS imaging and non-imaging receiver.



(b) LSMS, FAA-Holograms, FPA-Holograms and FAPA-Holograms

Figure 7.6: Delay spread of four configurations : (a) CDS imaging and non-imaging receiver (b) LSMS, FAA-Holograms, FPA-Holograms and FAPA-Holograms, when the transmitter is placed at (1m, 7m, 1m) and the receiver moves along the x=2m line.

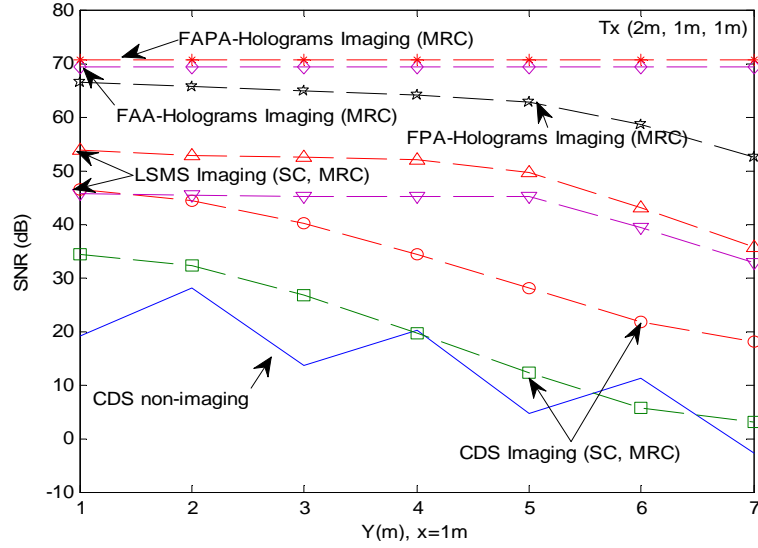
substitutes the non-imaging receiver at a 6 m horizontal separation between the transmitter and the receiver. Moreover, the imaging multi-spot LSMS configuration offers a reduction in the delay spread, from 0.8 ns associated with the imaging CDS system to almost 0.5 ns, see Figure 7.6. This reduction in the delay spread is attributed to adopting the spot-diffusing transmitter, as well as limiting the rays captured by utilising narrow FOV pixels (FOV=11.3°). A further reduction can be achieved when the power adaptation approach is introduced with an adaptive finite vocabulary of holograms (FPA-Holograms), which can reduce delay spread to 0.21 ns. The results for CDS (non-imaging and imaging receivers), LSMS and FPA-Holograms with imaging receiver show a direct relationship between the delay spread and the distance between the transmitter and the receiver. The delay spread increases as the separation between the transmitter and the receiver increases. However the delay spread is almost independent of the distance between the transmitter and the receiver when the new angle and power adaptive holograms (FAA-Holograms and FAPA-Holograms) are employed (due to beam steering). Figure 7.7 shows that a delay spread reduction, from 0.21 ns to 0.12 ns, is achieved when the FAA-Holograms system substitutes the FPA-Holograms. Furthermore, a reduction in the delay spread, from 0.12 ns (FAA-Holograms) to 0.088 ns, is obtained when the beam angle and power adaptation methods are implemented with adaptive holograms.

## 7.5 SNR Results

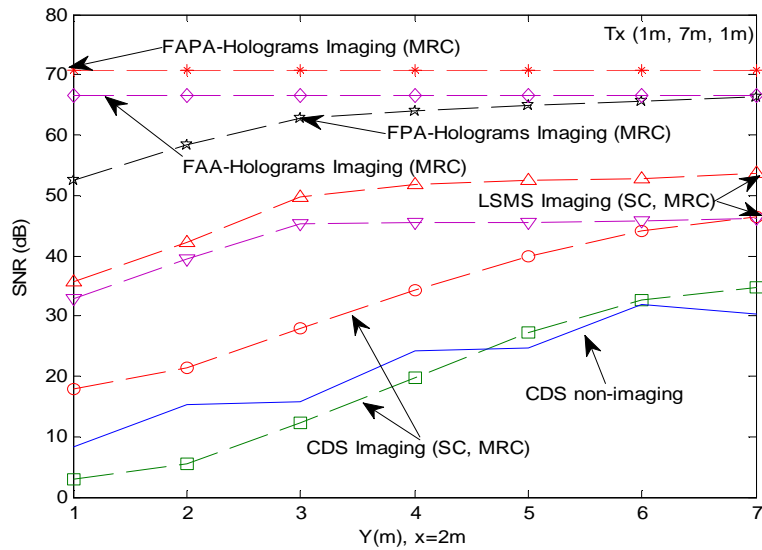
The SNR evaluation of imaging finite adaptive hologram (FAA-Holograms, FPA-Holograms and FAPA-Holograms) configurations is performed under the effect of surrounding noise sources, receiver noise, mobility and multipath propagation. All the proposed systems used 256 stored pre-calculated holograms, which is the case where the floor is divided into 16 regions. Comparison between different regions, as well as the original beam power and

angle adaptations, is discussed in the next section. For fair comparison with the baseline systems (30 Mb/s wide FOV non-imaging and imaging CDS, as well as the imaging LSMS system), the imaging adaptive hologram systems are operated at 30 Mb/s. The preamplifier used in the 30 Mb/s OW systems is the PIN FET preamplifier proposed in [121]. The SNR results are plotted in Figures 7.7 (a) and (b) when the transmitter is placed at (2m, 1m, 1m) and (1m, 7m, 1m) and the receiver moves across the y-axis at  $x=1\text{m}$  and  $x=2\text{m}$  lines, respectively. The receiver locations were selected in order to test our systems exactly under the directive light noise sources, across the  $y = 1, 3, 5,$  and  $7\text{m}$ , as well as at the location close to the room corner. Under all these circumstances, all the proposed systems are compared. The results show that the variations in the diffuse system (CDS) due to the directive light noise are reduced and the SNR is improved by 20 dB when the CDS MRC imaging receiver substitutes the non-imaging receiver. However, the small FOV ( $11.3^\circ$ ) associated with pixels leads to a reduction in the received optical power at the receiver. This reduction can be compensated for when a multi-spot diffusing transmitter (LSMS) is employed instead of the diffuse transmitter. The imaging multi-spot configuration LSMS offers 17 dB SNR gain over the CDS imaging receiver at the room corner, see Figure 7.7.

However, there is degradation in the SNR of the CDS and LSMS in a mobile OW system, as depicted in Figure 7.7 (a) and (b). This reduction in the SNR, which is attributed to the user mobility, can be reduced by employing our power adaptive holograms system. With an imaging receiver, the proposed FPA-hologram achieves about 17 dB SNR gain over LSMS and 34 dB SNR gain over the CDS imaging receiver in the worst case scenario. It should be noted that the SNR results of imaging CDS, LSMS and FPA-Holograms show inverse relationship between the SNR and the distance between the transmitter and the receiver. The SNR decreases as the transmitter-receiver distance increases. The effect of transmitter and receiver mobility can be reduced by employing our fast angle adaptive holograms system which can effectively guide the spots



(a)



(b)

Figure 7.7: SNR of OW CDS, LSMS, FPA-Holograms, FAA-Holograms and FAPA-Holograms with 256-Hologram at 30 Mb/s, when the transmitter is placed at (2m, 1m, 1m) and (1m, 7m, 1m) and the receiver moves along the x=1m and the x=2m lines.

nearer to the receiver location by using the best pre-calculated hologram stored in the system, as explained previously. In the case of the worst communication link considered, the proposed FAA-Holograms system achieved about 13 SNR gain over the power adaptive, see Figure 7.7 (b). Further improvement can be

obtained when beam angle and power adaptation methods are combined in our proposed FAPA-Holograms system. As seen in Figure 7.7 (b), at 6m transmitter-receiver horizontal separation, the FAPA-Holograms system provides 6 dB SNR improvements over the FAA-Holograms configuration. The proposed angle and power finite adaptive holograms system is able to achieve a consistent SNR at every transmitter and receiver location.

## 7.6 Finite Adaptive Holograms versus Original Beam Power and Angle Adaptations

Simulation results have shown that the beam angle and power adaptations, coupled with imaging receiver detection, can significantly improve performance in a multi-beam optical wireless system. However, a cost in terms of complexity in the design of PA-LSMS, AA-LSMS and APA-LSMS has to be paid. The complexity is associated with the computation time required to identify the optimum spot location, in addition to the time needed to generate the hologram with optimum spot powers and angles. As explained in Chapter 6, in a typical room with dimensions of 4m × 8m × 3m (width × length × height), the APA-LSMS system generates a single spot which scans the walls and ceiling by changing the beam angle associated with the spot between  $-90^\circ$  and  $90^\circ$  in steps of  $2.86^\circ$ , a total of 8000 possible locations, which requires 80 ms adaptation time in order to identify the optimum location. The time required to generate the hologram with optimum spot angles and powers can be estimated. If the APA-LSMS system uses the output plane phase optimisation (OPPO) algorithm proposed in [196], then the total computation is

$$t_{oppo} = 5 \times p \times S^2 + S \times M \times N, \quad (7.5)$$

where  $M \times N$  is the number of hologram pixels,  $S$  is the number of spots on the output plane (ceiling),  $p$  is the phase level. The first term ( $5 \times p \times S^2$ , complex

operations) represents the computations needed for designing the temporary hologram using direct binary search (DBS) and the second term ( $S \times M \times N$ , complex operations) represents the computation of the hologram using discrete Fourier transform (DFT). If  $M = N = 200$ ,  $S=80$  and  $p=8$ , then:

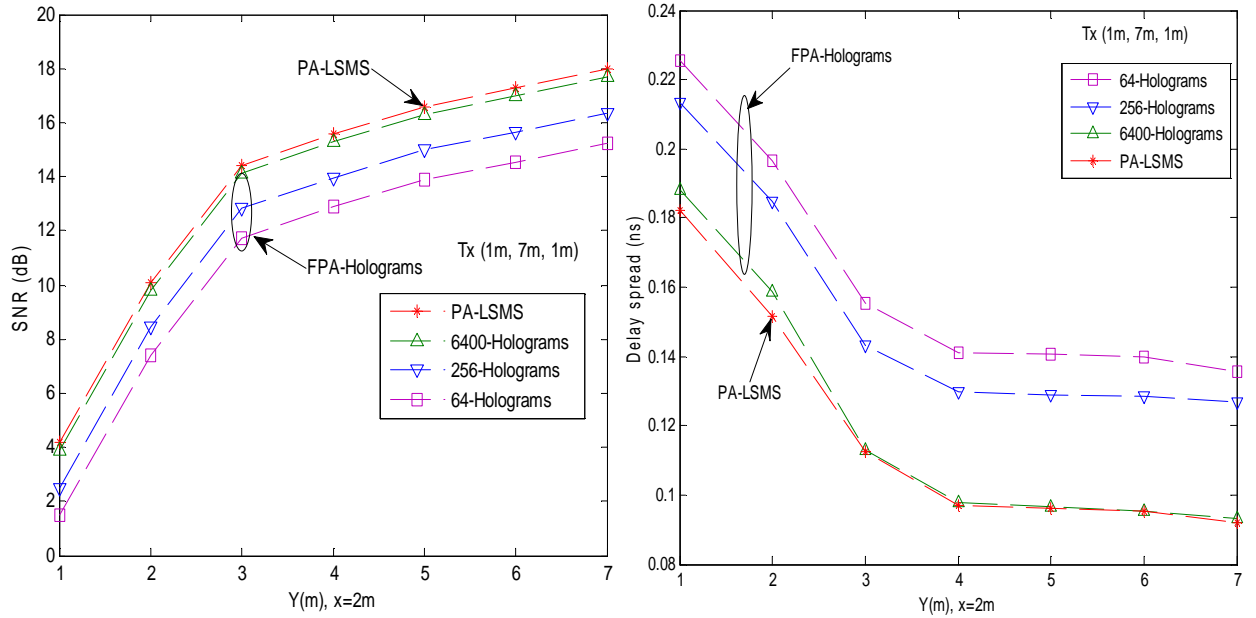
$$t_{oppo} = 0.2 \times 10^6 + 3.2 \times 10^6$$

The computation for designing the temporary hologram can be ignored based on the study in [196]. If each operation in the optimisation of the hologram is carried out at  $0.1 \mu s$  then the total time required to generate a hologram is 320 ms. Therefore, the time needed to find the optimum spots location plus the time to generate a hologram requires intensive calculations from a DSP.

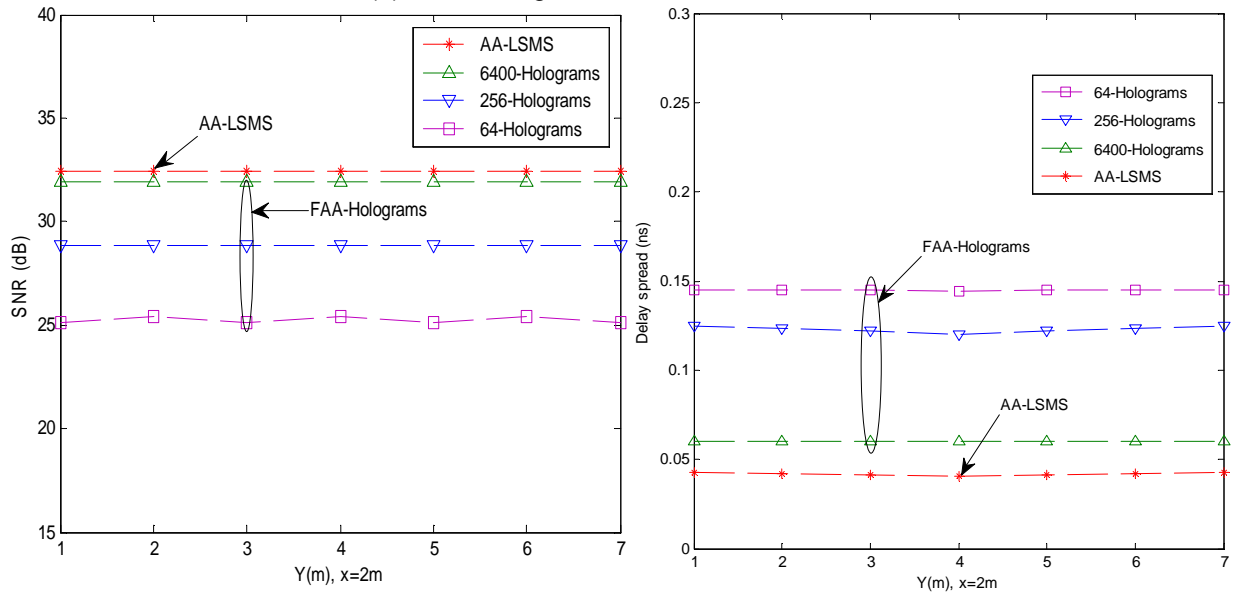
Adaptation based on a finite number of pre-calculated and stored holograms can reduce the computational burden and computation time as previously shown. It is however of interest to establish the penalty associated with the use of different finite vocabularies of holograms. The SNR and delay spread distributions of the fast finite adaptive holograms systems (FPA-Holograms, FAA-Holograms and FAPA-Holograms) are examined when the floor is divided into 8, 16 and 80 regions, see Figures 7.8 (a) and (b), (c). All the proposed systems operate at high data rate of 5 Gb/s. The preamplifier used in the 5 Gb/s OW system is the PIN-FET receiver design proposed in [187]. A reduction the total transmit power under eye safety regulations at high data rates of 1.25 Gb/s, 2.5 Gb/s and 5 Gb/s will be considered in the next section. The SNR penalty of the proposed systems compared with the original PA-LSMS, AA-LSMS and APA-LSMS configurations are shown in Figures 7.8. Improvements in the SNR and delay spread are observed in the proposed systems when the total number of regions increases. Increasing the number of regions helps the transmitter produce a hologram that more accurately matches each receiver's location, hence improving system performance for the given transmitter and receiver locations. Variations (relatively small) in the SNR and delay spread

might be present when a small number of holograms: (64 and 256 holograms) are used. This is due to the large size of regions ( $2\text{m} \times 2\text{m}$  and  $2\text{m} \times 1\text{m}$ ); therefore, the SNR and the delay spread results of FAA-Holograms and FAPA-Holograms (with 64 and 256 holograms) in Figures 7.8 (b) and (c) have been averaged when the transmitter moves in steps of 1m over the entire room while the receiver moves along the constant line  $x=2\text{m}$ . The improvements in the SNR and delay spread are achieved at the cost of computation time required to identify the optimum hologram due to the increase in the total number of holograms. However, the proposed systems use a D&C search algorithm which can help find the optimum hologram with less computational time compared with classic finite adaptive holograms systems. The SNR penalty of the proposed systems compared with the original adaptive OW systems (PA-LSMS, angle adaptive LSMS, and APA-LSMS) is reduced as the number of regions increases, see Figure 7.8. At the worst communication link, where the floor is divided into 80 regions (6400 holograms used), a significant computational saving in the proposed imaging FAPA-Holograms system, where only 112 holograms need to be scanned to identify the optimum hologram based on a D&C searching algorithm (computation time reduction from 80 ms required for APA-LSMS to 1.12 ms), can be achieved at the cost of an SNR penalty of less than 1 dB compared with an APA-LSMS system at each receiver location, see Figure 7.8. In addition, the proposed system eliminates the need to generate the hologram (320 ms) when the optimum location is found; all the holograms are pre-calculated and stored in the system, which can further simplify the design of the OW system. We suggest that the receiver periodically (namely at 0.1 second intervals) re-evaluates its SNR and if this has changed significantly (compared to a threshold value) then this change initiates transmitter adaptation. Therefore the 1.12 ms adaptation time represents an overhead of 1.12 % in terms of transmission time. It should be noted that this adaptation has been done at the rate at which the environment changes for example the rate at which humans move not at the system's bit rate. Therefore when the system is

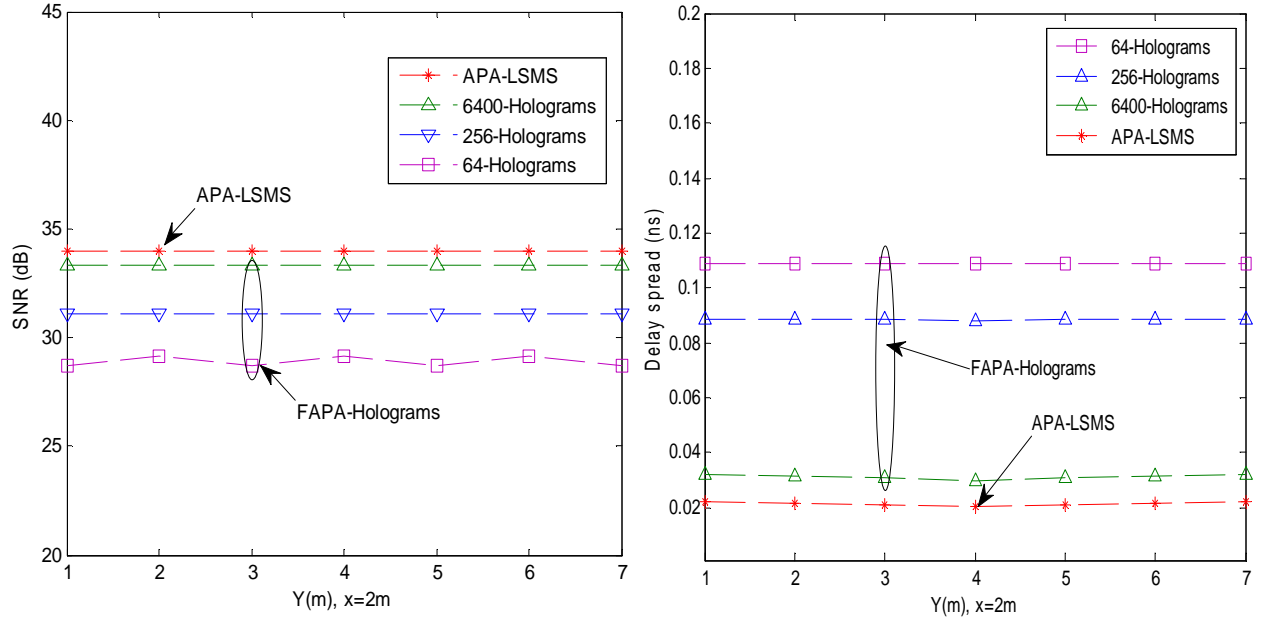
stationary it can achieve 5 Gb/s, when it is on the move it can achieve 98.8% of this data rate, i.e. 4.94 Gb/s. Note that when a small number of detectors are used at the receiver such as three or seven detectors, instead of 200 then the number of hologram to be scanned at each quadrant need to be increased.



(a) FPA-Holograms versus PA-LSMS.



(b) FAA-Holograms versus AA-LSMS.



(c) FAPA-Holograms versus APA-LSMS

Figure 7.8: The SNR and the delay spread of the adaptive finite holograms (FAPA-Holograms, FAA-Holograms and FAPA-Holograms) versus the original beam power and angle adaptive systems (PA-LSMS, AA-LSMS and APA-LSMS) when the transmitters operate at 5 Gb/s.

Furthermore, we have also examined the impact of designing a finite number of holograms based on a particular room size, and subsequently using the OW system in rooms with different sizes. The holograms were designed for our room with dimensions (4m × 8m × 3m) and the system was then evaluated in two empty rooms (without furnishings) with dimensions of (3m × 6m × 3m) and (5m × 10m × 3m) (width × length × height). The proposed FAPA-Holograms system is compared with the original beam power and angle adaptation (APA-LSMS) system. The latter fully adapts to any room of any size. Figure 7.9 (a) shows that in the case of a small room configuration (3m × 6m × 3m), the FAPA-Holograms system still has an SNR penalty of less than 1 dB compared with the APA-LSMS configuration. This is because with a small room size the FAPA-Holograms system, with 6400 stored holograms, is able to cover the entire room at each transmitter and receiver location (the choices available

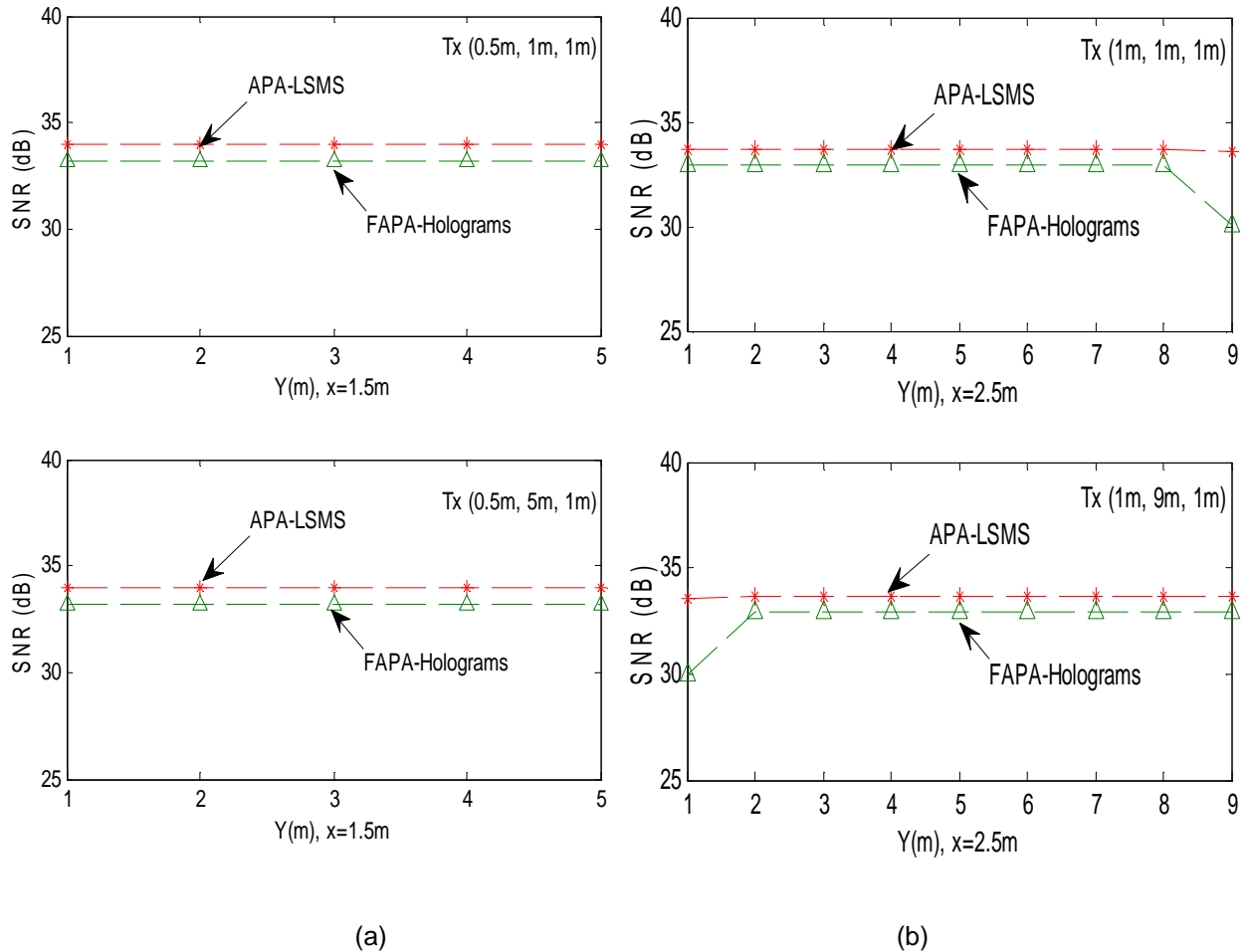


Figure 7.9: The SNR of APA-LSMS; and of FAPA-Holograms designed for (4m× 8m ×3m) room but used on rooms of dimensions (a) (3m× 6m ×3m) and (b) (5m×10m ×3m) when the transmitters operate at 5 Gb/s.

within the finite vocabulary are still good). However, with a large room size (5m × 10m × 3m), when the transmitter is near to the room corner at (1m, 1m, 1m), (1m, 9m, 1m) and the receiver is placed at the room edge at (2.5m, 9m, 1m), (2.5m, 1m, 1m), respectively, there is a differential SNR penalty of 2.8 dB. In order to reduce the SNR penalty, as well as mitigate the effect of the room configuration, finite adaptive holograms system (FAPA-Holograms) can be designed for a large room of (5m × 10m × 3m), where the floor is divided into 100 regions for example. In this case, 10,000 holograms need to be stored in the system. A D&C searching algorithm can be used to reduce the time required to identify the optimum hologram from 100 ms to around 1.7 ms.

### 7.6.1 High-speed Mobile OW communication systems

In conventional OOK systems, the SNR has to be 15.6 dB in order to achieve a BER of  $10^{-9}$ . The improvement in the SNR obtained as a result of our new system (FAPA-Holograms) can help the system reduce the total transmit power, while the systems operating at higher data rates of 1.25 Gb/s, 2.5 Gb/s and 5 Gb/s. To further increase the link budget at higher data rates, the number of holograms was increased to 6400 (which reduces the penalty due to the finite number of holograms) by dividing the floor into 80 regions. Note that a relatively small memory size is needed to store  $6400 \times (200 \times 200)$  complex numbers, where each complex number represents the phase of a pixel. At high data rates, we used preamplifier the PIN-FET receiver design in proposed in [187]. The bandwidth was limited to 0.875 GHz, 1.75 GHz and 3.5 GHz for 1.25 Gb/s, 2.5 Gb/s and 5 Gb/s, respectively via the use of appropriate filters. The fast algorithm based on D&C only needs to scan/try 112 holograms to identify the optimum hologram, which significantly reduces the computation time to 1.12 ms compared with the 64 ms needed in the case of classic angle and power adaptive hologram. To investigate the proposed system, FAPA-Holograms, with respect to eye safety regulations, we used a total transmit power of 80 mW (1 mW per beam). This limitation was introduced in our power adaptation which was not allowed to increase the power per spot beyond 0.5 mW. Again, all the holograms are pre-calculated and stored in the proposed system to eliminate the need to calculate a hologram at each step. This significantly reduces the transmitter complexity compared with adaptation techniques proposed in previous chapters. The SNRs achieved in the proposed system in this case were about 29 dB, 20 dB and 11 dB at 1.25 Gb/s, 2.5 Gb/s and 5 Gb/s respectively, under the impact of background noise, multipath dispersion and mobility, see Figure 7.10. The drop in the SNR result is attributed to the reduction in the total transmit power from 1 W to 80 mW, and also due to the power restriction per beam in our algorithm. At 1.25 Gb/s and 2.5 Gb/s the SNR

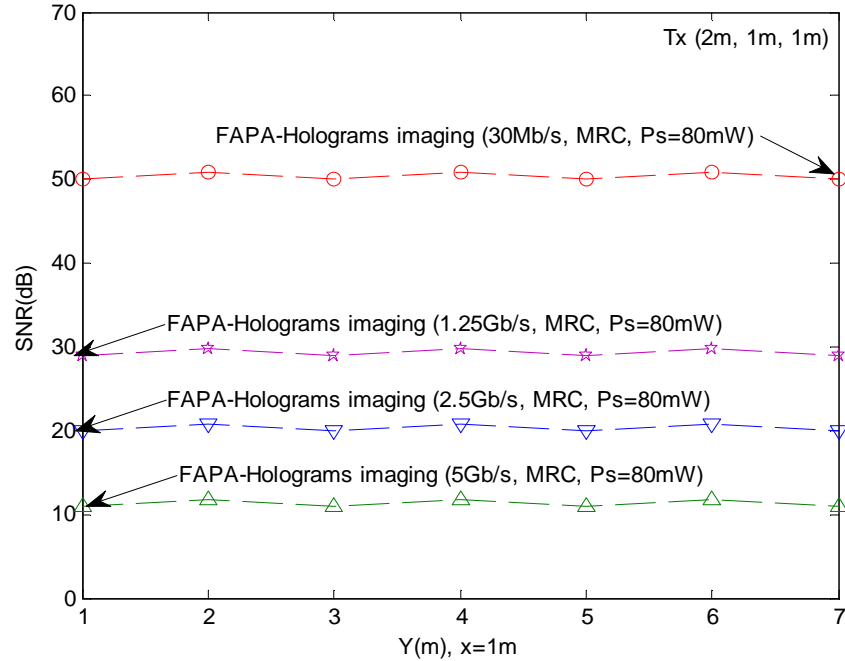


Figure 7.10: The SNR of our proposed FAPA-holograms system operating at 30 Mbit/s, 1.25 Gbit/s, 2.5 Gbit/s and 5 Gbit/s, with a total transmit power of 80 mW.

is still greater than 15.6 dB ( $\text{BER} < 10^{-9}$ ). Since the FAPA-Holograms system is able to identify the optimum hologram as determined by the receiver, it is possible to use the modified imaging receiver proposed in Chapter 6 [123] with our system at 5 Gb/s which can provide an SNR gain of round 7 dB. Furthermore, forward error correction (FEC) can be used with the proposed system at 5 Gb/s to reduce the BER from  $10^{-3}$  to  $10^{-9}$ . The higher data rates (1.25 Gb/s, 2.5 Gb/s and 5 Gb/s) in the FAPA-Holograms system are therefore shown to be feasible through a combination of angle and power adaptive holograms, and imaging receivers.

## 7.7 FAPA-Holograms with 9-Angle diversity receivers

The previous section has shown that the FAPA-Holograms system is a promising indoor mobile OW system in terms of complexity and system

performance. In this section, the proposed system (FAPA-Holograms with 6400 stored pre-calculated holograms) is evaluated with an angle diversity receiver. As previously stated in Chapter 4 and 5, the design of the angle diversity receivers uses multiple non-imaging detectors that are pointed in different directions. The narrow FOVs of these detectors are chosen to confine the optical signal and limit the background noise. The received signal in each detector can be processed and amplified separately, employing different methods such as SC and MRC in order to maximise the SNR of the system. As shown in Figure 7.11 the angle diversity receiver considered consists of nine detectors, mounted on the nine faces of octagon pyramidal planes. Each branch points in a certain direction which can be identified by two angles: elevation ( $El$ ) and azimuth ( $Az$ ). For the LSMS, the  $El$  angles of the nine detectors are fixed at:  $90^\circ$ ,  $65^\circ$ ,  $30^\circ$ ,  $30^\circ$ ,  $30^\circ$ ,  $65^\circ$ ,  $30^\circ$ ,  $30^\circ$ , and  $30^\circ$ , and the  $Az$  of all branches are set at:  $0^\circ$ ,  $30^\circ$ ,  $70^\circ$ ,  $110^\circ$ ,  $150^\circ$ ,  $210^\circ$ ,  $250^\circ$ ,  $290^\circ$  and  $330^\circ$ . In addition their FOVs are restricted to  $12^\circ$ . In the case of fast angle and power adaptive holograms, the  $El$  angle of the top detector was  $90^\circ$ , and the eight detectors remained at  $65^\circ$ . Their  $Az$  were set at:  $0^\circ$ ,  $0^\circ$ ,  $45^\circ$ ,  $90^\circ$ ,  $135^\circ$ ,  $180^\circ$ ,  $225^\circ$ ,  $270^\circ$  and  $315^\circ$  and the FOV of all detectors was  $12^\circ$ . The values of  $El$ ,  $Az$  and FOV have been selected in order to maintain the strong SNR during transmitter and receiver mobility in both LSMS and FAPA-Holograms transmitters based on an optimisation similar to that reported in [94], [95]. Furthermore, the FOV of each detector is chosen in order to view all the diffusing spots when the new proposed FAPA-Holograms system generates 80 diffusing spots in the form of line strips. An optical concentrator coupled with an optical band-pass filter are used in front of the detectors in the FAPA-LSMS and LSMS systems with a typical concentrator gain of 18.5 dB corresponding to  $12^\circ$  FOV [16], [72]. At 50 Mb/s, we used the preamplifier PIN-BJT design suggested by Elmighani *et al* [30] with a collection area of  $1 \text{ cm}^2$  in order to facilitate the comparison with our previous systems (CDS and LSMS). Higher data rates of 2.5 Gb/s and 5 Gb/s were also considered. The preamplifier proposed in [187]

with a small active area of  $10 \text{ mm}^2$  was considered when the system operates at high data rates. A small detector area helps to reduce the high capacitance, hence improving the receiver bandwidth. The receiver is always placed over the communication place (CP), a plane 1 m above the floor. Since the proposed FAPA-Holograms system (with 6400 stored holograms) coupled with only nine narrow FOVs angle diversity receivers, we increase the number of holograms that need to be scanned at each quarter to 100 holograms in our fast search algorithm in order to identify the receiver location. Therefore, a total of 1300 holograms will to be scanned in order to identify the best hologram based on a D&C search algorithm (computation time reduction from 64 ms required for classical angle and power adaptive hologram to 13 ms). If the adaptation has to be done every 0.1 second or more if an SNR lower than threshold value, then the proposed system represent an overhead time of approximately 13 % and as such the system can achieve 4.34 Gb/s when it is on the move.

### 7.7.1 Delay Spread Results

Figure 7.12 shows the delay spread of the CDS, LSMS and FAPA-Holograms (with 6400-holograms) in conjunction with nine non-imaging receivers when the transmitter is placed at one of the room corners (1m, 1m, 1m) and the receiver is moved across the y-axis at the line  $x = 2\text{m}$ . Moreover, the figure shows the result of the original beam power and angle adaptations with the line-strip multi-spot diffusing system (APA-LSMS). The delay spread result is almost independent of the receiver-transmitter separation distance in our fast adaptive hologram configuration (FAPA-Holograms) as the transmitter selects the best hologram with optimum beam angles and powers to achieve the highest SNR. Our proposed system achieves delay spread close to the original beam angle and power adaption system (APA-LSMS). This is attributed to the use of a very large number of holograms (6400) which helps the transmitter to accurately identify the receiver location over an indoor environment.

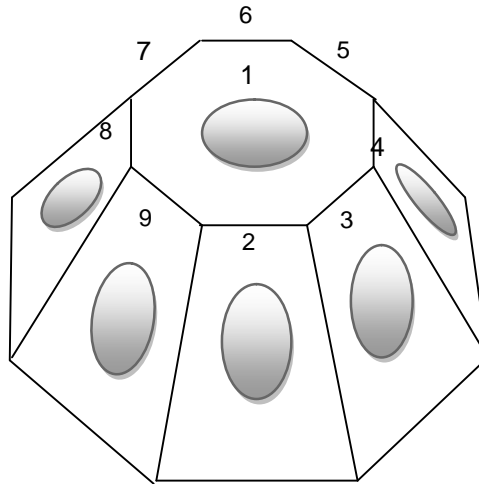


Figure 7.11: Physical structure of 9-angle diversity receivers placed on top of octagon pyramidal faces.

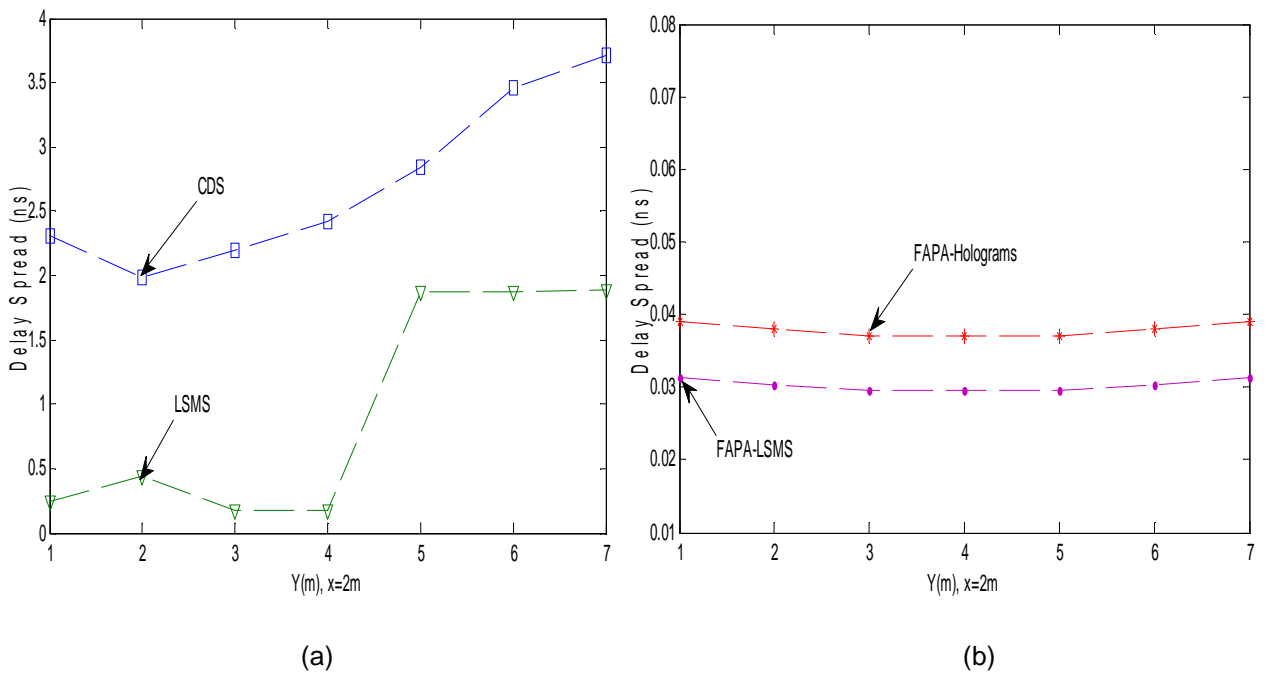


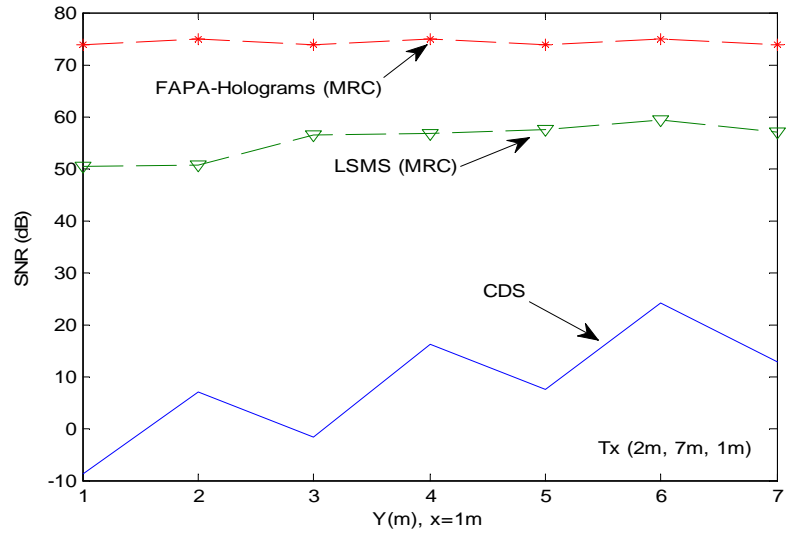
Figure 7.12: Delay spread of four configurations : (a) CDS and LSMS (b) FAPA-Holograms and APA-LSMS with angle diversity receiver, when the transmitter is placed at (1m, 1m, 1m) and the receiver moves along x=2m line.

### 7.7.2 SNR Results

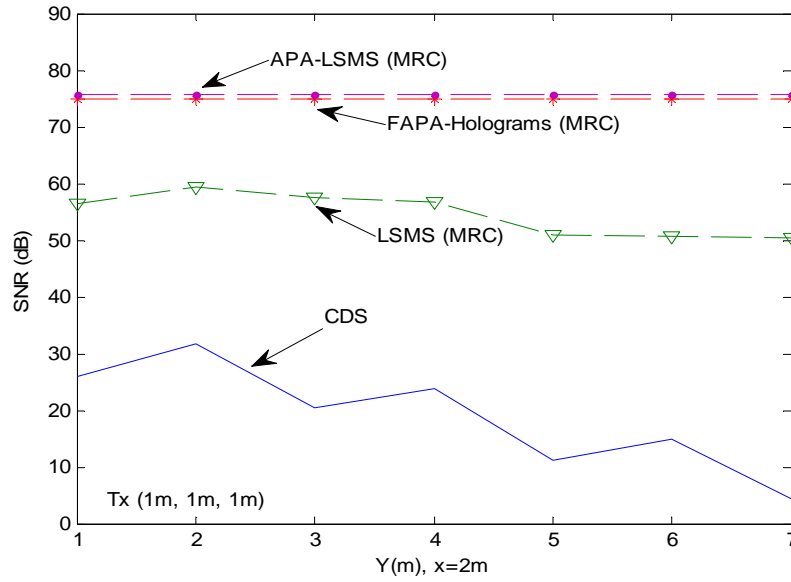
The performance of an angle diversity finite adaptive hologram (FAPA-Holograms) configuration operating at 50 Mb/s is evaluated under the impairments of ambient shot noise, receiver noise, multipath propagation, and mobility. The impact of a realistic environment including shadowing will be considered in the next section. The MRC SNR result of the proposed systems is given in Figure 7.13 and compared with a wide FOV CDS as well as the angle diversity non-adaptive LSMS system, when the transmitter is placed at (2m, 7m, 1m) and (1m, 1m, 1m) and the receiver moves a 1m step across the  $x = 1$  m and  $x=2$ m lines respectively. The mobile multi-spot diffusing transmitter (LSMS), coupled with angle diversity receivers, performs better than the wide FOV CDS system.

Even though enhancement was obtained through the use of diffusing spots and angle diversity receivers, degradation still remains in the receiver SNR when the transmitter is on the move (mobile), for example when the transmitter is moved towards the edge or the corner of the room at (2m, 7m, 1m) and (1m, 1m, 1m) while the receiver moves along the  $x=1$ m and  $x=2$ m lines, respectively, as seen in Figures 7.13 (a) and (b). This reduction in the SNR can be mitigated by employing our fast angle and power adaptive hologram system, which can automatically guide the spots closer to the receiver location by using the best pre-calculated hologram stored in the system, as explained previously. At the worst communication link considered, the proposed FAPA-Holograms system achieved about 24 SNR gain over the LSMS system: see Figure 7.13 (b). The SNR penalty of the proposed FAPA-Holograms system compared with the original angle diversity APA-LSMS OW system is plotted in Figure 7.13 (b). The proposed system (FAPA-Holograms) eliminates the need to calculate holograms as well as the time needed to identify the optimum hologram that produces the optimum angle and power level of diffusing spots at the cost of a

SNR penalty of less than 1 dB compared with an angle diversity APA-LSMS system, see Figure 7.13 (b).



(a)



(b)

Figure 7.13: SNR of OW CDS, LSMS, FAPA-Holograms with 6400-Hologram at 50 Mb/s, when the transmitter is placed at (2m, 7m, 1m) and (1m, 1m, 1m) and the receiver moves along  $x=1m$  and  $x=2m$  lines.

## 7.8 Effect of Shadowing and Realistic Indoor Office on the Proposed FAPA-Holograms

In this section, we expand the analysis of diffuse CDS, non-adaptive LSMS and fast adaptive FAPA-Hologram configurations combined with 9-angle diversity receivers in a realistic environment (realistic office arrangement) where optical signal blockage (due to mini-cubicles), furniture, doors and windows, multipath propagation and surrounding light sources are all present. The simulation model was created with room measurements, comparable to the one used in Section 7.2, of  $8\text{m} \times 4\text{m} \times 3\text{m}$ , as an example. We considered a typical real indoor office provided in Chapter 6 (Figure 6.8). The room has a door, three big glass windows, several rectangular cubicles (partitions) that have planes parallel to the walls of the room and eight lamps (background noise) as well as other furniture such as filing cabinets, bookshelves and chairs. The three glass windows and the door do not reflect any signal. Moreover, the reflectivity of the ceiling and walls around windows and floor are similar to those previously stated. Two of the walls on  $x=4\text{m}$  and  $y=8\text{m}$  (apart from the door) of the room are covered by cabinets and bookshelves, which have a reflectivity of 0.4. The mini-cubicle office partitions in the room are assumed to either block or absorb signals. Additionally, chairs and tables inside the room have a similar reflectivity to the floor (0.3).

The SNR of the proposed systems are given in Figure 7.14. The results are shown when the transmitter is placed in the corner at  $(1\text{m}, 1\text{m}, 1\text{m})$ , while the receiver moves across the  $y$ -axis at the line  $x=2\text{m}$ . In the case of CDS at the worst path considered, the SNR of unshadowing degrades by 6.8 dB compared to an empty room, as explained in Figure 7.13 (b). This degradation is due to the reduction in the total optical received power where part of the signals is lost as a result of the three big glass windows in the two upright walls in addition to the door. An additional degradation by 21 dB in the SNR of non-imaging CDS

took place in a shadowed room. This is attributed to the complexity of the room where the received optical signals through the reflections are blocked due to the physical obstructions (partitions) and other objects in addition to the low reflectivity on two walls ( $x=4\text{m}$  and  $y=8\text{m}$ ) that are covered by cabinets and bookshelves, which have a reflectivity of 0.4. Furthermore, the results show the weakness of the LSMS and the robustness of our new FAPA-Holograms against shadowing, signal blockage, and mobility. The effect of receiver mobility as well as shadowing on the LSMS performance can be observed and the SNR is reduced by 15 dB when the transmitter is at (1m, 1m, 1m) and the receiver moves from (2m, 1m, 1m) to (2m, 7m, 1m). This degradation is due to the fact that some spots are blocked by physical barriers and other objects and also due to the transmitter location at (1m, 1m, 1m) where some spots which fall on the glass windows are lost. In contrast, the SNR of our new fast adaptive FAPA-Holograms is independent of the transmitter position. The proposed FAPA-Holograms with an angle diversity receiver is more robust against shadowing and signal blockage, owing to its ability to select the best pre-calculated hologram with optimum angles and powers of diffusing spots located in the ceiling with the shortest path to the receiver. In shadowed communication links, our new proposed FAPA-Holograms coupled with angle diversity receivers offers about 35 dB SNR improvement over the traditional angle diversity LSMS configuration.

The improvement in the SNR achieved as a result of our new system (FAPA-Holograms) enables the system to reduce the total transmit power and operate at higher data rates of, 2.5 Gb/s and 5 Gb/s. A small detector area of  $10\text{ mm}^2$  is considered at high data rates in order to reduce the impact of high capacitance, hence improving receiver bandwidth. Our proposed system has a typical concentrator gain of 18.3 dB corresponding to a  $12^\circ$  FOV. In order to address

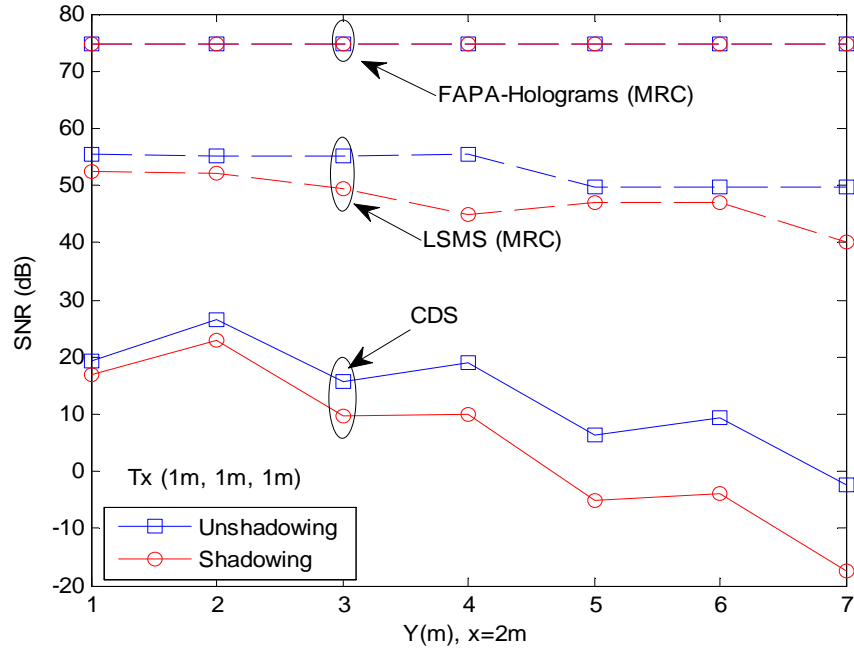


Figure 7.14: SNR of CDS, LSMS, FAPA-Holograms with 6400-Hologram at 50 Mb/s, when the transmitter is placed at (1m, 1m, 1m) and (1m, 7m, 1m) and the receiver moves along  $x=2m$ .

the eye safety regulations with our new system, FAPA-Holograms, we used a total transmit power of 80 mW (1 mW per beam) and introduced a limitation in the power adaptation algorithm so that the power per beam is not increased beyond 0.5 mW. Again, all the holograms are pre-calculated and stored in the proposed system to eliminate the need to calculate a hologram at each step. This significantly reduces the transmitter complexity. The SNRs achieved in the proposed system in this case were about 20.5 dB and 11 dB at 2.5 Gb/s and 5 Gb/s respectively, see Figure 7.15. At 5 Gb/s the SNR is still greater than 9.5 dB ( $BER < 10^{-6}$ ). Since the FAPA-Holograms system is able to identify the optimum hologram as determined by the receiver, it is possible to use the receiver with small FOV such  $7^\circ$  which can further increase the received signal and improve the SNR to around 9.3 dB. Furthermore, forward error correction (FEC) can be used with the proposed system at 5 Gb/s to reduce the BER

from  $10^{-3}$  to  $10^{-9}$ . These suggested enhancements can further help the receiver reduce its active area to less than  $10 \text{ mm}^2$ , such as  $5 \text{ mm}^2$ . The higher

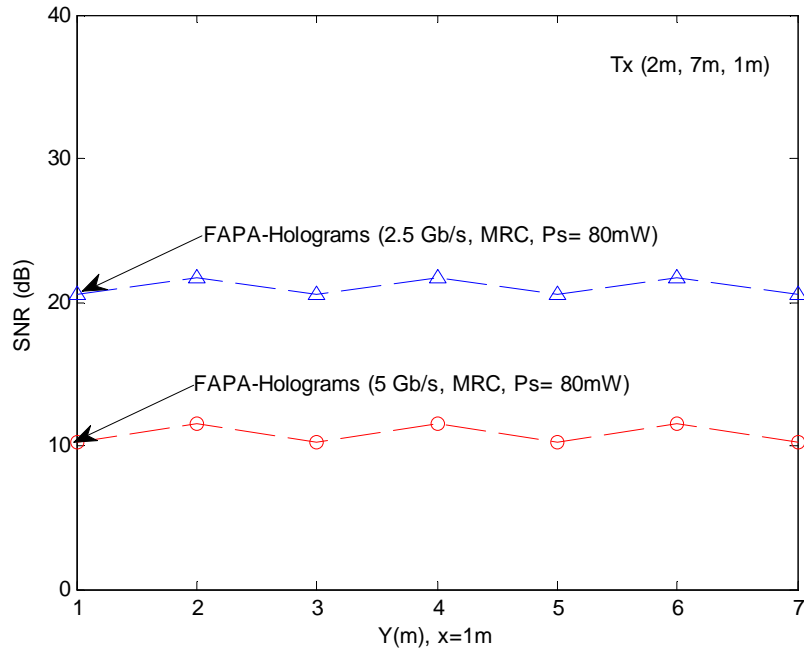


Figure 7.15: The SNR of our proposed FAPA-holograms system operating at 2.5 Gb/s and 5 Gb/s, with a total transmit power of 80 mW.

data rates (2.5 Gb/s and 5 Gb/s) in the FAPA-Holograms system are therefore shown to be feasible through a combination of angle and power adaptive holograms, and angle diversity receivers.

## 7.9 Summary

In this chapter, we introduced a new adaptive finite vocabulary of holograms that are pre-calculated and stored in our proposed system. We also introduced a new search algorithm based on D&C in order to reduce the time needed to select the best pre-calculated hologram. Our proposed systems are coupled with an imaging receiver to further improve the received optical signal at the receiver, as well as mitigate the impact of background noise and multipath dispersion. At 30 Mb/s, the results show that one of the proposed systems,

FPA-Holograms, offers an SNR improvement of 17 dB over the imaging receiver spot-diffusing system (LSMS) and almost 34 dB over the diffuse (CDS) imaging receiver system. Moreover, the FAA-Holograms can effectively guide the spots nearer to the receiver location, which provides an SNR gain of about 13 dB over the power adaptive holograms configuration. Further improvement was attained when the beam angle and power adaptation were combined in our proposed FAPA-Holograms system. The simulation results show that the proposed FAPA-Holograms system achieved 6 dB SNR improvement over the FAA-Holograms system at the worst communication link. It should be noted that the angles and power levels associated with the spots in each hologram are pre-calculated and stored in the proposed system without adding any complexity at the transmitter to reproduce (compute) the holograms. The improvements in the SNR and delay spread achieved as a result of the new system (FAPA-Holograms) enables the system to reduce the total transmit power, in addition to operating at high data rates. To investigate the proposed FAPA-Holograms system with respect to eye safety regulations, a total transmit power of 80 mW (1 mW per beam) was used. A limitation was introduced in the power adaptation which was not allowed to increase power per spot beyond 0.5 mW. The SNRs achieved in our proposed system in this case were about 29 dB, 20 dB and 11 dB at 1.25 Gb/s 2.5 Gb/s and 5 Gb/s respectively, under the impact of background noise, multipath dispersion and mobility. The ultimate goal of the proposed systems was to eliminate the need to calculate a hologram, as well as the need to identify the optimum hologram that produces the optimum angle and power level of diffusing spots compared with the original beam power and angle adaptations proposed previously in our work. The SNR and delay spread results of our proposed systems (FPA-Holograms, FAA-Holograms and FAPA-Holograms) were examined with the original OW adaptive systems (PA-LSMS, AA-LSMS and APA-LSMS) proposed in our previous chapters. Improvements in the SNR and the delay spread in the proposed systems were observed and found to be close to original adaptive

OW systems, when the total number of regions increases. Increasing the number of regions helps the transmitter to accurately identify the receiver's location, hence improving system performance. A search algorithm based on D&C was used in order to reduce the time needed to select the best pre-calculated hologram. In the case of the worst communication path considered, whereby the floor is divided into 80 regions (6400 holograms are pre-calculated and stored in the system), our proposed FAPA-Holograms system can significantly reduce the time required to identify the optimum hologram position from 80 ms for the APA-LSMS configuration to about 1.12 ms, at the cost of an SNR penalty of less than 1 dB at every transmitter and receiver location. In addition, the proposed systems eliminate the need to generate the hologram (320ms) when the optimum location is found. This fast algorithm is only required to scan 112 holograms to identify the best hologram based on a D&C algorithm.

Moreover, different room sizes are also considered to examine the performance of the adaptive finite vocabulary of hologram system when it is designed for a given room size and used in rooms with different sizes. The proposed system is less sensitive to room geometry (when the design is made for a large room (5m, 10m, 3m)), where the diffusing spots can be targeted at the optimum location that maximises the receiver SNR at each location. The system therefore operates in our case with an SNR penalty of less than 1 dB in all rooms equal to or smaller in size than the design room (which can be selected to be large); crucially though our system offers faster adaptation than previous systems.

Furthermore, the idea of fast angle and power adaptive finite vocabulary of holograms (FAPA-Hologram) is also studied with angle diversity receivers. Our proposed angle diversity FAPA-Holograms system improved the received optical signal in the presence of very directive noise sources, mobility and shadowing. In the shadowing link, at 50 Mb/s, the results show that the proposed system, FAPA-Holograms, offered an SNR improvement of 35 dB

over the angle diversity spot-diffusing system (LSMS). Moreover, high data rates of 2.5 Gb/s and 5 Gb/s were considered. A 5 Gb/s rate is shown to be feasible when our techniques: multi-spot, adaptive angle and power finite holograms with angle diversity detections are implemented in the OW configuration.

# 8 Conclusions and Future Work

## 8.1 Conclusions of Research Work

A major interest in OW is to understand and tackle the design challenges of indoor systems, such as ambient noise, multipath dispersion, photodetector high capacitance and eye and skin safety regulations. This thesis has presented a range of tools and mathematical and simulation methods to model the optical wireless link in the indoor environment and studied the effects of these challenges on the received data stream. The impact of these challenges can be mitigated when a narrow beam transmitter is aimed directly into a small FOV receiver. However, this type of system suffers from shadowing and is significantly degraded under user mobility. A pure diffuse link (CDS) is an alternative scheme that does not rely on a direct path link between transmitter and receiver. It is dependent on the diffuse reflections on the ceiling and walls. It allows the system to operate even when the receiver is obstructed from the transmitter. Nonetheless, a diffuse transmitter is subject to multipath dispersion, which may result in pulse spread and extreme ISI.

The CDS transmitter can be substituted by multi-spot diffusing transmitters, resulting in considerable improvement in the performance of the optical wireless system. The merits of both direct LOS and non-LOS are merged in multi-spot diffusing transmitters. Important enhancement can be attained through the use of a simple LSMS transmitter. Moreover, multipath dispersion and ambient light noise can be minimised through the use of angle diversity receivers. The LSMS system integrated with angle diversity receivers can achieve a significant performance improvement in OW links. However, transmitter/receiver mobility as well as shadowing can significantly degrade the functionality of the multi-spot LSMS configuration.

This thesis has focused on introducing new methods in multi-spot OW links that can overcome the impairments discussed as well as combat user mobility and shadowing. Moreover, it has designed a high-speed, power efficient system that can operate at high data rates (5 Gb/s, 10 Gb/s and beyond). All proposed systems were evaluated in a typical rectangular room with a size of (4m × 8m × 3m) (width × length × height). The simulation results were performed through the use of a light ray-tracing algorithm where the transmitted optical signal travels through various paths (direct, first or second order reflections) of different lengths before it reaches the receiver. Computations and ray-tracing algorithm in this thesis were implemented with the use of *Matlab*. The performance evaluation of the OW systems focused on the impulse response, delay spread distribution, 3-dB channel bandwidth and SNR. We compared the findings of our simulator with the CDS and multi-spot LSMS configurations coupled with wide FOV and angle diversity receivers published in the literature. Good agreement was observed, giving confidence in the ability of our simulator to assess new novel optical wireless systems.

In this thesis, a novel mobile OW system that uses beam delay and power adaptation in multi-spots (BDPA-LSMS) coupled with three and seven branched angle diversity receivers was introduced and investigated. The aim was to increase the received optical power and enhance the SNR when the transmitter operates under the effect of ambient noise sources, user mobility, receiver noise and multipath dispersion. At 50 Mb/s, the proposed adaptive multi-spot BDPA-LSMS obtained a 10 dB SNR gain over the non-adaptive LSMS system. Moreover, the idea of beam delay and power adaptation was extended and introduced with multi-beam clustering methods (BDPA-BCM) in order to alleviate the poor communication and increase the link budget at the weakest links. The proposed adaptive clustering system can significantly enhance the performance of mobile non-directed OW connections. It offered a 10 dB SNR gain over an adaptive multi-spot BDPA-LSMS system. The high SNR results

and 3-dB channel bandwidth allowed our BDPA-BCM system to operate at high bit rates (2.5 Gb/s and 5 Gb/s).

Furthermore, a custom design of an imaging receiver was introduced. The CDS, non-adaptive LSMS and adaptive BDPA-LSMS multi-spot configurations were studied with imaging diversity receivers (200 pixels) to enhance the mobile OW system performance. Imaging reception can significantly help mitigate the effect of the background noise sources by selecting or combining (SC or MRC) the pixels that receive the minimum noise level. A 20 dB SNR gain was achieved when a diffuse CDS system employed an imaging receiver (MRC) instead of a wide FOV receiver. Additionally, 17 dB SNR improvement was obtained over the CDS system when multiple spot diffusing coupled with an imaging receiver was employed. The directed LOS received signals can be further enhanced in our adaptive BDPA-LSMS configuration, by allocating high intensities to spots closest to the receiver as well as introducing differential delays between the beams. The adaptive BDPA-LSMS multi-spot configuration imaging receiver produces an SNR gain of 19 dB above the imaging non-adaptive LSMS system. Furthermore, the basic adaptive delay and power, beam clustering technique was extended and developed to design a new multiple adaptive beam clustering method (BDPMA-BCM) coupled with imaging diversity receivers in order to improve the system performance and enable it to provide high data rates (2.5 Gb/s and 5 Gb/s). In the worst communication path considered, the 5 Gb/s BDPMA-BCM combined with the imaging receiver obtained an SNR gain of 10 dB above the imaging BDPA-LSMS.

Angle and power adaptation methods in multi-spot configuration (APA-LSMS) coupled with three-branched angle diversity receivers have been proposed to design a low complexity, high-speed indoor OW system. The proposed APA-LSMS offered SNR enhancement: 45 dB SNR gain over PA-LSMS and 60 dB SNR gain over CDS in a worst case scenario. The APA-LSMS system, coupled with three-branched angle diversity receivers, was particularly efficient in

increasing the channel bandwidth from 25.5 MHz (conventional CDS) to about 7.2 GHz. The SNR and 3-dB channel bandwidth enhancements achieved through the combination of beam angle and power adaptations, multi-spot diffusing and angle diversity detections, allow the system to reduce the transmission power under the present 1 W level while operating at high data rates. The achieved SNRs of the proposed APA-LSMS (with a photodetector area of  $0.05 \text{ cm}^2$  and a total transmit power of 60 mW) were about 13 dB and 10 dB at 5 Gb/s and 10 Gb/s, respectively, under the impact of background noise, multipath dispersion, receiver noise and transmitter-receiver mobility. At 10 Gb/s, the SNR is still greater than 9.5 dB ( $\text{BER} < 10^{-3}$ ). Therefore FEC can be used to further reduce the BER from  $10^{-3}$  to  $10^{-9}$  in the proposed system.

Furthermore, beam delay, angle and power adaptation were implemented in a multi-spot indoor OW transmitter (BDAPA-LSMS) coupled with imaging diversity receivers. The ultimate goal was to design a fully adaptive high-speed OW system that was robust against shadowing, signal blockage and mobility. The BDAPA-LSMS system provided SNR enhancement of 55 dB above CDS in the worst possible link. All the adaptation methods implemented in the multi-spot diffusing transmitter coupled with an imaging receiver are shown to be extremely effective in increasing the channel bandwidth from 7.2 GHz (APA-LSMS with angle diversity) to about 9.8 GHz (BDAPA-LSMS with an imaging receiver). Additionally, BDAPA-LSMS system was examined in a realistic indoor office (where mini-cubicles (shadowing), window availability, bookshelves, chairs and cabinets all are present) with fully mobility and compared with the CDS and LSMS systems. In a realistic indoor setting, a 15 dB SNR degradation was observed in the mobile imaging LSMS, when the transmitter is placed at (1m, 1m, 1m) and the receiver is moved to (2m, 7m, 1m) from (2m, 1m, 1m). Introducing our beam delay, angle and power adaptive methods to LSMS can considerably decrease the impact of the transmitter movement and the effect of the shadowing in a realistic office room. In the worst communication link

considered, with the existence of shadowing, our fully adaptive imaging BDAPA-LSMS provides around 39 dB SNR enhancement over the non-adaptive multiple spot LSMS structure. High data rates of 10 Gb/s and 12.5 Gb/s were considered in our imaging BDAPA-LSMS system.

Finally, a novel adaptive OW system that employs a finite vocabulary of stored holograms is introduced. A fast adaptation approach based on a divide-and-conquer methodology, resulting in a number of adaptation algorithms - fast angle adaptive holograms (FAA-Holograms), fast power adaptive holograms (FPA-Holograms), and fast angle and power adaptive holograms (FAPA-Holograms) - was proposed. The ultimate goal of the proposed systems was to eliminate the need to calculate holograms repeatedly, as well as reduce the time needed to identify the best hologram that produces the optimum angle and power level of diffusing spots compared with the original beam power and angle adaptation methods. The proposed systems were coupled with nine-faced angle diversity receivers and 200 pixels imaging diversity receivers. Based on the simulation results, it is shown that one of the proposed imaging systems, FPA-Holograms, offered an SNR improvement of 17 dB over the imaging receiver spot-diffusing system (LSMS) and almost 34 dB over the diffuse (CDS) imaging receiver system. Moreover, the FAA-Holograms can effectively guide the spots nearer to the receiver location, which provided an SNR gain of about 13 dB over the power adaptive holograms configuration. Further improvement was attained when the beam angle and power adaptation were combined in our proposed FAPA-Holograms system. The simulation results show that the proposed FAPA-Holograms system achieved 6 dB SNR gain over the FAA-Holograms system at the worst communication link.

The fast adaptive holograms system (FAPA-Holograms) allows us to reduce the transmit power under eye safety regulations while operating at high data rate of 5 Gb/s. It has to be noted that the angles and power levels associated with the spots in each hologram are pre-calculated and stored in the proposed system

without adding any complexity at the transmitter to reproduce (compute) the holograms. The results have shown that the new introduced methods coupled with either angle diversity or imaging diversity reception can maximise the SNR at the receiver over the entire CP regardless of the transmitter position. This is due to the fact that angle and power adaptive finite holograms system is able to move the spots near to the receiver at each given location. The proposed system was also examined in different room sizes. The result shows that the proposed system is less sensitive to room geometry compared to CDS and non-adaptive LSMS configurations. Moreover, our new methods were also tested in a realistic environment with full mobility.

## 8.2 Areas of Further Investigation

The following is a list of new areas of research that deserve further investigation:

- 1- Equalisation techniques such as adaptive decision-feedback equalisation (DEF), maximum likelihood equalisation, and zero-forcing equalisation can be examined in the current configurations, which would enhance performance.
- 2- Forward error correction (FEC) codes can be studied in OW systems to further reduce the BER when the system operates at high data rates.
- 3- Beam delay, angle and power adaptation have been investigated for a single user scenario where the optimum spot distributions, power levels and delays are assigned to one receiver location. An open area of research is the use of these techniques in multi-user scenarios. In this case, opportunistic scheduling can be investigated where the optimum spot locations (angles), powers and delays can be chosen to maximise SNR to the users who experience lower ambient noise at particular time window.

- 4- Our OW system with multiple beams and multiple receivers (angle diversity or imaging pixels) is a MIMO system. The body of knowledge developed in MIMO systems can be used in our current systems.
- 5- The conventional diffuse system (CDS) uses a light source with a Lambertian pattern of radiation where the transmitted optical signal is reflected from all the surfaces in the room (walls, ceiling and floor). Further investigation can be applied by changing the Lambertian radiation pattern where the transmitted optical signals are only reflected from one surface, such as the ceiling (as a mirror). This could help to increase the received power with full mobility.
- 6- The 2-D adaptive beam clustering techniques can be extended to consider 3-D beams. The optimum number of spots and clusters in each plane deserves further investigation.
- 7- Further investigation can be carried out on the beam angle adaptation in order to find the optimum spot location. A direct binary search (DBS) algorithm can be applied to reduce the time needed to find the optimum location of the spot.
- 8- Finally experimental verification of the different systems introduced in this thesis will be very valuable and will open new avenues in optimum receiver and transmitter design.

# References

- [1] R. W. Burns, "Communications: An international history of the formative years," IET Publication, pp. 192-196, 2004.
- [2] A. G. Bell, "Selenium and the Photophone," in *Nature*, pp. 500-503, Sept. 23, 1880.
- [3] S. Arnon, "Optical wireless communication," chapter in the *Encyclopedia of Optical Engineering (EOE)*, R. G. Driggers ed., Marcel Dekker, pp. 1866-1886, Invited, 2003.
- [4] S. Arnon, D. M. Britz, A. C. Boucouvalas and M. Kavehard, "Optical wireless communications: introduction to the feature issue," *Optical Networking, Journal of*, vol. 5, no. 2, pp.79-81, Feb, 2006.
- [5] H. Manor and S. Arnon, "Performance of optical wireless communication as function of wavelength," *Applied Optics*, vol. 42, no. 2, pp. 4285-4294, Jul. 2003.
- [6] M. J. McCullagh, D. R. Wisely, P. L. Eardley, and P. P. Smyth, "A 50 Mbit/s optical wireless LAN link using novel optical and electronic enabling technologies," *International Seminar on Digital Communications*, pp. 298-309, 1994.
- [7] J. M. Kahn, J. R. Barry, M. D. Audeh, J. B. Carruthers, W. J. Krause, and G. W. Marsh, "Non-directed infrared links for high-capacity wireless LANs," *Personal Communications, IEEE*, vol. 1, pp. 12-25, 1994.
- [8] F. R. Gfeller, and U. Bapst, "Wireless in-house data communication via diffuse infrared radiation," *Proceedings of the IEEE*, vol. 67, pp. 1474-1486, 1979.
- [9] G. Yun, and M. Kavehrad, "Spot-diffusing and fly-eye receivers for indoor infrared wireless communications," in *Wireless Communications, 1992. Conference Proceedings., 1992 IEEE International Conference on Selected Topics in*, pp. 262-265, 1992.
- [10] V. Pohl, V. Jungnickel, and C. Helmolt, "A channel model for wireless infrared communication," in *Personal, Indoor and Mobile Radio Communications, 2000. PIMRC 2000. The 11th IEEE International Symposium on*, 2000, pp. 297-303.

- [11] A. G. Al-Ghamdi, and J. M. H. Elmirghani, "Performance evaluation of a triangular pyramidal fly-eye diversity detector for optical wireless communications," *Communications Magazine, IEEE*, vol. 41, pp. 80-86, 2003.
- [12] M. Kavehrad and S. Jivkova, "Indoor broadband optical wireless communications: optical subsystems designs and their impact on channel characteristics," *Wireless Communications, IEEE*, vol. 10, no. 2, pp. 30–35, Apr. 2003.
- [13] O. Gonzalez, R. Perez-Jimenez, S. Rodriguez, J. Rabadan, and A. Ayala, "OFDM over indoor wireless optical channel," *Optoelectronics, IEE Proceedings-*, vol. 152, pp. 199-204, 2005.
- [14] O. Gonzalez, S. Rodraguez, , R. Perez-Jimenez, F. Delgado, and A. Ayala, "Multi-user adaptive orthogonal frequency-division multiplexing system for indoor wireless optical communications," *Optoelectronics, IET*, vol. 1, pp. 68-76, 2007.
- [15] Z. Ghassemlooy, W. Popoola, and S. Rajbhandari, *Optical Wireless Communications: System and Channel Modelling* Press, 2012.
- [16] J. M. Kahn and J. R. Barry, "Wireless infrared communications," *Proceedings of the IEEE*, vol. 85, no. 2, pp. 265-298, Feb. 1997.
- [17] G. Einarsson, and M. Leeson, "Principles of Lightwave Communications," *Physics Today*, vol. 50, pp. 84-86, 1997.
- [18] J. Kahn, J. Barry, W. Krause, M. Audeh, J. Carruthers, G. Marsh, E. Lee, and D. Messerschmitt, "High-speed non-directional infrared communication for wireless local-area networks," in *Signals, Systems and Computers, 1992. 1992 Conference Record of The Twenty Sixth Asilomar Conference on*, Oct 1992, pp. 83-87.
- [19] A. M. Street, , P. N. Stavrinou, , D. C. O'Brien, and D. J Edwards, "Indoor optical wireless systems - a review," *Optical and Quantum Electronics*, vol. 29, pp. 349-378, 1997.
- [20] S. D. Greaves, P. J. Nichols, D. R. Wisely, and R. T. Unwin, "Optical wireless video distribution," in *Proceedings of the International Society for Optical Engineering Conference*, 1995, pp. 280-285.

- [21] P. P. Smyth, M. J. McCullagh, D. R. Wisely, D. Wood, S. Ritchie, P. L. Eardley and S. Cassidy, "Optical wireless local area networks-enabling technologies," *BT technology, Journal*, vol. 11, pp. 56-64, April 1993.
- [22] D. R. Pauluzzi, P. R. McConnell and R. L. Poulin,, "Free-space, undirected infrared (IR) voice and data communications with a comparison to RF systems," in *Wireless Communications, 1992. Conference Proceedings.,1992 IEEE International Conference on Selected Topics in*, 1992, pp. 279-285.
- [23] Office of Communication: <http://www.ofcom.org.uk>.
- [24] Federal Communications Commission: <http://www.fcc.gov>.
- [25] A. C. Boucouvalas, "IEC 825-1 Safety Classification of some consumer electronics products," *Colloquium on Optical Free Space Communication Links*, (1996), 13/1-13/6.
- [26] IrDA standard, "Serial infrared: Physical layer link specification," 1997, Version 1.2.
- [27] IrDA up-to-date standards and <http://www.irda.org>. The IrDA can be contacted at P.O. Box 3883, Walnut Creek, CA 94598, USA.
- [28] A. C. Boucouvalas, "Indoor ambient light noise and its effect on wireless optical links," *Optoelectronics, IEE Proceedings-*, vol. 143, pp. 334-338, 1996.
- [29] A. J. C. Moreira, , R. T. Valadas, and A. M. de Oliveira Duarte, "Performance of infrared transmission systems under ambient light interference," *Optoelectronics, IEE Proceedings-*, vol. 143, pp. 339-346, 1996.
- [30] J. M. H. Elmirghani, H. H. Chan, and R. A. Cryan, "Sensitivity evaluation of optical wireless PPM systems utilising PIN-BJT receivers," *Optoelectronics, IEE Proceedings-*, vol. 143, pp. 355-359, 1996.
- [31] S. Hranilovic, *Wireless Optical Communication Systems*. Springer, 2005.
- [32] M. Audeh and J. Kahn, "Performance evaluation of L-pulse-position modulation on non-directed indoor infrared channels," in *Communications, 1994. ICC 94, SUPERCOMM/ICC '94, Conference Record, Serving Humanity Through Communications.*' IEEE International Conference on, May 1994, pp. 660-664.

- [33] Z. Ghassemlooy, A. Hayes, "Indoor Optical Wireless Communications Systems- Part I: Review," School of Engineering, Northumbria University, 2003.
- [34] J. R. Barry, J. M. Kahn, W. J. Krause, E. A. Lee, and D. G. Messerschmitt, "Simulation of Multipath Impulse Response for Wireless Optical Channels," *Selected Areas in Communications, IEEE Journal on*, vol. 11, no. 3, April 1993, pp. 367-379.
- [35] C. Singh, J. John, Y. Singh, and K. Tripathi, "A Review on Indoor Optical Wireless Systems," *IETE Technical review*, vol. 19, pp. 3-18, 2002.
- [36] P. P. Smyth, D. Wood, S. Ritchie, and S. Cassidy, "Optical wireless: New enabling transmitter technologies," in *Communications, 1993. ICC 93. Geneva. Technical Program, Conference Record, IEEE International Conference on*, 1993, pp. 562-566 vol.1.
- [37] J. R. Barry, *Wireless Infrared Communications*. Boston: Kluwer, 1994.
- [38] T. Minami, K. Yano, T. Touge, H. Morikawa, and O. Takahashi, "Optical wireless modem for office communication," in *Proceedings of the May 16-19, 1983, national computer conference*, 1983, pp. 721-728.
- [39] Y. Nakata, J. Kashio, T. Kojima, and T. Noguchi, "In-house wireless communication system using infrared radiation," in *Proceedings of the International Conference on Computer Communication*, 1984, pp. 333-337.
- [40] F. M. Chow, and J. M. Kahn, "Effect of non-reciprocity on infrared wireless local-area networks," in *Global Telecommunications Conference, 1999. GLOBECOM '99*, 1999, pp. 330-338, vol.1.
- [41] F. Gfeller, and W. Hirt, "A robust wireless infrared system with channel reciprocity," *Communications Magazine, IEEE*, vol. 36, pp. 100-106, 1998.
- [42] R. Otte, L. P. De Jong, and A. H. M. Van Roermund, "Wireless optical PPM telemetry and the influence of lighting flicker," *Instrumentation and Measurement, IEEE Transactions on*, vol. 47, pp. 51-55, 1998.
- [43] R. Narasimhan, M. D. Audeh, and J. M. Kahn, "Effect of electronic-ballast fluorescent lighting on wireless infrared links," *Optoelectronics, IEE Proceedings-*, vol. 143, pp. 347-354, 1996.

- [44] D. Wisely, and I. Neild, "A 100 Mbit/s tracked optical wireless telepoint," in Personal, Indoor and Mobile Radio Communications, 1997. 'Waves of the Year 2000'. PIMRC '97., The 8th IEEE International Symposium on, 1997, pp. 964-968 vol.3.
- [45] R. Wisely, "A 1 Gbit/s optical wireless tracked architecture for ATM delivery," in Optical Free Space Communication Links, IEE Colloquium on, 1996, pp. 14/1-14/7.
- [46] J. B. Carruthers and J. Kahn, "Angle diversity for nondirected wireless infrared communication," in Communications, 1998. ICC 98. Conference Record.1998 IEEE International Conference on, vol. 3, June 1998, pp. 1665 –1670 vol.3.
- [47] J. B. Carruthers, and J. M., Kahn, "Modeling of nondirected wireless infrared channels," Communications, IEEE Transactions on, vol. 45, pp. 1260-1268, 1997.
- [48] G. W. Marsh, and J. M. Kahn, "50-Mb/s diffuse infrared free-space link using on-off keying with decision-feedback equalization," Photonics Technology Letters, IEEE, vol. 6, pp. 1268-1270, 1994.
- [49] G. W. Marsh, and J. M. Kahn, "Performance evaluation of experimental 50-Mb/s diffuse infrared wireless link using on-off keying with decision-feedback equalization," Communications, IEEE Transactions on, vol. 44, pp. 1496-1504, 1996.
- [50] X. Ning, R. Winston, and O. J. Gallagher, "Dielectric totally internally reflecting concentrators," Applied Optics, vol. 26, pp. 300-305, 1987.
- [51] R. L. Poulin, D. R. Pauluzzi, and M. R. Walker "A multi-channel infrared telephony demonstration system for public access applications," in Wireless Communications, 1992. Conference Proceedings., 1992 IEEE International Conference on Selected Topics in, 1992, pp. 286-291.
- [52] J. P. Savicki, and S. P. Morgan, "Hemispherical concentrators and spectral filters for planar sensors in diffuse radiation fields," Applied Optics, vol. 33, pp. 8057-8061, 1994.
- [53] K. P. Ho and J. M. Kahn, "Compound parabolic concentrators for narrow-band wireless infrared receivers," Optical Engineering, vol. 34, pp. 1385–1395, May 1995.

- [54] J. Fadlullah, and Mohsen Kavehrad, "Indoor High-Bandwidth Optical Wireless Links for Sensor Networks," *Lightwave Technology, Journal of*, vol. 28, pp. 3086-3094, 2010.
- [55] M. N. Sadiku, *Optical and wireless communications: next generation networks*: CRC Press, 2002.
- [56] A. Moreira, R. Valadas, and A. M. de Oliveira Duarte, "Optical interference produced by artificial light," *Wireless Networks*, vol. 3, pp. 131-140, 1997.
- [57] S. Zahedi, J. A. Salehi, and M. Nasiri-Kenari, "A photon counting approach to the performance analysis of indoors wireless infrared CDMA networks," in *Personal, Indoor and Mobile Radio Communications, 2000. PIMRC 2000. The 11th IEEE International Symposium on*, 2000, pp. 928-932 vol.2.
- [58] A. J. C. Moreira, , A. M. Tavares, R. J. M. T. Valadas, and A. M. de Oliveira Duarte, "Characterisation and modelling of artificial light interference in optical wireless communication systems," in *Personal, Indoor and Mobile Radio Communications, 1995. PIMRC'95. 'Wireless: Merging onto the Information Superhighway, Sixth IEEE International Symposium on*, 1995, pp. 326-331 vol.1.
- [59] A. J. C. Moreira, , A. M. Tavares, R. J. M. T. Valadas, and A. M. de Oliveira Duarte, "Reducing the effects of artificial light interference in wireless infrared transmission systems," in *Optical Free Space Communication Links, IEE Colloquium on*, 1996, pp. 501-510.
- [60] C. Hsun-Hung, K. L. Sterckx, J. M. H. Elmirghani, and R. A. Cryan, "Performance of optical wireless OOK and PPM systems under the constraints of ambient noise and multipath dispersion," *Communications Magazine, IEEE*, vol. 36, pp. 83-87, 1998.
- [61] A. Tavares, R. Valadas, and A. M. de Oliveira Duarte, "Performance of wireless infrared transmission systems considering both ambient light interference and intersymbol interference due to multipath dispersion," in *Optical Wireless Communications, Proc. SPIE, Boston, MA*, 1998, pp. 82-93.
- [62] A. J. C. Moreira, , A. M. Tavares, R. J. M. T. Valadas, and A. M. de Oliveira Duarte, "Modulation methods for wireless infrared transmission systems:

- performance under ambient light noise and interference,” in SPIE Proceedings. on Wireless Data Transmission, Philadelphia, PA, USA, 1995, pp. 226-237.
- [63] J. R. Barry and J. M. Kahn, “Link design for non-directed wireless infrared communications,” *Applied optics*, vol. 34, no. 19, pp. 3764–3776, July 1995.
- [64] J. M. Senior and M. Y. Jamro, *Optical fiber communications: principles and practice*: Pearson Education, 2009.
- [65] K. Wang, A. Nirmalathas, C. Lim, and E. Skafidas, “Indoor gigabit optical wireless communication system for personal area networks,” in *IEEE Photonics Society, 2010 23rd Annual Meeting of the*, 2010, pp. 224-225.
- [66] K. Wang, A. Nirmalathas, C. Lim, and E. Skafidas, “High speed duplex optical wireless communication system for indoor personal area networks,” *Optics Express*, vol. 18, no. 24, pp. 25199–25216, Nov. 2010.
- [67] T. Ozugur, J. A. Copeland, M. Naghshineh, and P. Kermani, “Next-generation indoor infrared LANs: issues and approaches,” *Personal Communications, IEEE*, vol. 6, pp. 6-19, 1999.
- [68] H. L. Minh, Z. Ghassemlooy, D. O'Brien, G. Faulkner, “Indoor Gigabit optical wireless communications: Challenges and possibilities,” in *Transparent Optical Networks (ICTON), 2010 12th International Conference on*, 2010, pp. 1-6.
- [69] D. C. O'Brien, G. Faulkner, H. Le-Minh, O. Bouchet, M. E. Tabach, M. Wolf, J. W. Walewski, S. Randel, S. Nerreter, M. Franke, K. D. Langer, J. Grubor, and T. Kamalakis, “Gigabit optical wireless for a home access network,” in *Personal, Indoor and Mobile Radio Communications, 2009 IEEE 20th International Symposium on*, 2009, pp. 1-5.
- [70] W. T. Welford and R. Winston, *High Collection Nonimaging Optics*. San Diego: Academic, 1989.
- [71] L. Zeng, D. C. O'Brien, H. Le-Minh, G. E. Faulkner, K. Lee, D. Jung, Y. Oh, and E. T. Won, “High data rate multiple input multiple output (MIMO) optical wireless communications using white LED lighting,” *Selected Areas in Communications, IEEE Journal on*, vol. 27, pp. 1654-1662, 2009.

- [72] R. Ramirez-Iniguez, S. M. Idrus, and Z. Sun, *Optical wireless communications: IR for wireless connectivity*: CRC Press, 2008.
- [73] M. E. Marhic, M. D. Kotzin, and A. P. van den Heuvel, "Reflectors and immersion lenses for detectors of diffuse radiation," *Optical Society of America, Journal*, vol. 72, no. 3, pp. 352–355, Mar. 1982.
- [74] D. C. O'Brien, "High data-rate infra-red optical wireless communications: Implementation challenges," in *GLOBECOM Workshops (GC Wkshps)*, 2010 IEEE, 2010, pp. 1047-1051.
- [75] H. L. Minh, D. C. O'Brien, G. Faulkner, O. Bouchet, M. Wolf, L. Grobe, and J. Li, "A 1.25 Gb/s indoor cellular optical wireless communications demonstrator," *Photonics Technology Letters, IEEE*, vol. 22, no. 21, pp. 1598–1600, Nov. 2010.
- [76] B. G. Streetman and S. Banerjee, *Solid state electronic devices*, 6th ed.: Prentice Hall, 2009.
- [77] S. D. Personick, "Receiver Design for Digital Fiber Optic Communication Systems, I and II", *Bell System Technical Journal*, vol. 52, no. 6, pp 843-886, July-August 1973.
- [78] M. J. McCullagh and D. R. Wisely, "155 Mbit/s optical wireless link using a bootstrapped silicon APD receiver," *Electronics Letters*, vol. 30, no. 5, pp. 430–432, 1994.
- [79] D. K. Borah, A. C. Boucouvalas, C. C. Davis, S. Hranilovic, and K. Yiannopoulos, "A review of communication-oriented optical wireless systems," *Wireless Communications and Networking, EURASIP Journal on*, vol. 2012, pp. 1-28, 2012.
- [80] T. D. Nguyen, M.S. "report", Univ. Calif., Berkeley, July 1995.
- [81] C. Lomba, R. Valadas and A. Duarte, *Safety Issues of the Baseband IR PHY*, Doc. IEEE P802.11- 94/174, 1994.
- [82] Int. Electrotech. Commission, *CEI/IEC825-1: Safety of Laser Products*, 1993. J. D. Rancourt, *Optical Thin Films*. New York: Macmillan, 1987.
- [83] IEC 60825-1, *Safety of Laser Products—Part 1: equipment classification, requirements, and user's guide*, edition 1.2. International Electrotechnical Commission, 2001.

- [84] Safety of Laser Products, AS/NZS 2211.1:2004 Standards Australia International Ltd., Melbourne, Australia and Standards New Zealand, Wellington, New Zealand, 2004.
- [85] S. Jivkova and M. Kavehrad, "Indoor wireless infrared local access, multi-spot diffusing with computer generated holographic beam-splitters," in Communications, 1999. ICC '99. 1999 IEEE International Conference on, 1999, vol.1, pp. 604-608.
- [86] K. Akhavan, M. Kavehrad, and S. Jivkova, "Wireless infrared in-house communications: how to achieve very high bit rates," in Wireless Communications and Networking Conference, 2000. WCNC. 2000 IEEE, 2000, pp. 698-703.
- [87] P. L. Eardley, D. R. Wisely, D. Wood, and P. McKee, "Holograms for optical wireless LANs," Optoelectronics, IEE Proceedings-, vol. 143, pp. 365-369, 1996.
- [88] M. R. Pakravan, E. Simova and M. Kavehrad, "Holographic diffusers for indoor infrared communication systems," International Journal of Wireless Information Networks, vol. 4, pp. 259-274, 1997.
- [89] E. Simova, M. Tai, and M. Kavehard, "Indoor wireless infrared link with a holographic multi-spot diffuser," Applications of Photonic Technology, Plenum Press, New York, vol. 2, pp. 223-228, 1996.
- [90] [http://www.lasernet.com/resources/classification\\_overview.php](http://www.lasernet.com/resources/classification_overview.php).
- [91] H. H. Chan, J.M.H. Elmirghani, and R.A. Cryan, "Simulation of IR channel impulse response for PPM-CDMA indoor Wireless LANs", Proc. Second Communication Networks Symposium, pp. 182-185, 10-11 July 1995, Manchester, UK.
- [92] C. J. Georgopoulos, "Suppressing background-light interference in an in-house infrared communication system by optical filtering," International Journal of Optoelectronics, vol. 3, pp. 247-256, 1988.
- [93] K. K. Wong, T. O'Farrell, and M. Kiatweerasakul, "Infrared wireless communication using spread spectrum techniques," Optoelectronics, IEE Proceedings-, vol. 147, pp. 308-314, 2000.
- [94] A. Al-Ghamdi, and J. M. H. Elmirghani, "Optimization of a triangular PFDR antenna in a fully diffuse OW system influenced by background noise and multipath

- propagation,” *Communications, IEEE Transactions on*, vol. 51, pp. 2103-2114, 2003.
- [95] A. G. Al-Ghamdi, and J. M. H. Elmirghani, “Triangular PFDR antenna optimisation under the restriction of background noise and multipath propagation in an optical wireless system,” in *Communications, 2003. ICC '03. IEEE International Conference on*, 2003, pp. 2013-2019 vol.3.
- [96] M. D. Higgins, R. J. Green, and M. S. Leeson, “Receiver alignment dependence of a GA controlled optical wireless transmitter,” *Journal of Optics A: Pure and Applied Optics*, vol. 11, no. 7, p. 075403, 2009.
- [97] J. B. Carruthers, and P. Kannan, “Iterative site-based modeling for wireless infrared channels,” *Antennas and Propagation, IEEE Transactions on*, vol. 50, pp. 759-765, 2002.
- [98] J. B. Carruthers, S. M. Carroll, and P. Kannan, “Propagation modelling for indoor optical wireless communications using fast multi-receiver channel estimation,” *Optoelectronics, IEE Proceedings-*, vol. 150, pp. 473-481, 2003.
- [99] M. D. Higgins, R. J. Green, and M. S. Leeson, “A genetic algorithm method for optical wireless channel control,” *Journal of Lightwave Technology*, vol. 27, no. 6, pp. 760–772, 2009.
- [100] J. B. Carruthers, and J. M. Kahn, “Multiple-subcarrier modulation for nondirected wireless infrared communication,” *Selected Areas in Communications, IEEE Journal on*, vol. 14, pp. 538-546, 1996.
- [101] C. Ta-Shing, and M. Gans, “High speed infrared local wireless communication,” *Communications Magazine, IEEE*, vol. 25, pp. 4-10, 1987.
- [102] F. E. Alsaadi and J. M. H. Elmirghani, “Adaptive mobile multicarrier code division multiple access optical wireless systems employing a beam clustering method and diversity detection,” *Optoelectronics, IET*, vol. 4, pp.95, June. 2010.
- [103] F. E. Alsaadi, and J. M. H. Elmirghani, “MC-CDMA Indoor Optical Wireless System,” in *Global Telecommunications Conference, 2007. GLOBECOM '07. IEEE*, 2007, pp. 2455-2460.

- [104] F. E. Alsaadi and J. M. H. Elmirghani, "Spot diffusing angle diversity MC-CDMA optical wireless system" *Optoelectronics, IET*, vol. 3, pp. 131–141, 2009.
- [105] J. M. Alattar and J. M. H. Elmirghani, "Multi-line multi-spot diffusing indoor OW channel with a 7-detectors diversity receiver," in *Proc. IEEE London Commun. Symp.*, Sep. 2006, pp. 37–40.
- [106] J. M. Alattar and J. M. H. Elmirghani, "Performance evaluation of an indoor optical wireless system based on multi-line multi-spot diffusing configurations and two angle diversity receivers," in *Proc. IEEE Opt. Netw. Des. Model*, May 2006.
- [107] J. M. Alattar and J. M. H. Elmirghani, "Adaptive mobile spot diffusing transmitter for an indoor optical wireless system," in *Proc. IEEE Opt. Netw. Des. Model.*, 2007, vol. 4534/2007, pp. 398–407.
- [108] A. G. Al-Ghamdi, and J. M. H. Elmirghani, "Performance evaluation of a pyramidal fly-eye diversity antenna in an indoor optical wireless multipath propagation environment under very directive noise sources," *Optoelectronics, IEE Proceedings -*, vol. 150, pp. 482-489, 2003.
- [109] G. Yun, M. Kavehrad, "Indoor Infrared Wireless Communications Using Spot Diffusing and Fly-Eye Receivers," *Electrical and Computer Engineering, Canadian Journal of*, vol. 18, No. 4, pp. 151-157, October 1993.
- [110] S. Jivkova, B. A. Hristov, and M. Kavehrad, "Power-efficient multispot-diffuse multiple-input-multiple-output approach to broad-band optical wireless communications," *Vehicular Technology, IEEE Transactions on*, vol. 53, pp. 882-889, 2004.
- [111] K. Akhavan, M. Kavehrad, and S. Jivkova, "High-speed power-efficient indoor wireless infrared communication using code combining .I," *Communications, IEEE Transactions on*, vol. 50, pp. 1098-1109, 2002.
- [112] J. Carruthers, J. Kahn, "Angle Diversity for Nondirected Wireless Infrared" *Communications, IEEE Transactions on*, vol. 48, No 6, pp. 960-969, Jun. 2000.
- [113] M.T. Alresheedi and J. M. H. Elmirghani, "Performance Evaluation of 5 Gbit/s and 10 Gbit/s Mobile Optical Wireless Systems Employing Beam Angle and Power

- Adaptation with Diversity Receivers,” Selected Areas in Communications, IEEE Journal on, vol. 29, no. 6, pp. 1328-1340, June 2011.
- [114] M.T. Alresheedi and J. M. H. Elmirghani, “Mobile optical wireless systems employing beam angle and power adaptation with diversity receivers” IEEE International on Wireless and optical communications Network (WOCN’10), September 2010.
- [115] M.T. Alresheedi and J. M. H. Elmirghani,” Angle and Power Adaptation in 10 Gbit/s Multibeam Mobile Optical Wireless Systems with Angle Diversity Detection”, in Proc. of the 15<sup>th</sup> IEEE International Conference on Optical Network Design and Modelling (ONDM’11), Bologna, February, 2011.
- [116] M.T. Alresheedi and J. M. H. Elmirghani, “Line Strip Multibeam Spot Diffusing Optical Wireless System employing Beam Delay and Power Adaptation with Angle Diversity Detection” Accepted IEEE conference, International wireless communication and Mobile computing Conference. IWCMC’11, July 2011.
- [117] M.T. Alresheedi and J. M. H. Elmirghani, “High-speed wireless infrared links with an adaptive multibeam clustering method and angle diversity detection” IEEE International on Transparent Optical Networks (ICTON’12), July 2012.
- [118] A. P. Tang, J. M. Kahn, and H. Keang-Po, “Wireless infrared communication links using multi-beam transmitters and imaging receivers,” in Communications, 1996. ICC 96, Conference Record, Converging Technologies for Tomorrow’s Applications. 1996 IEEE International Conference on, 1996, pp. 180-186 vol.1.
- [119] V. Jungnickel, T. Haustein, A. Forck, and C. Helmolt, “155 Mbit/s wireless transmission with imaging infrared receiver,” Electronics Letters, vol. 37, pp. 314-315, 2001.
- [120] M. Vazquez and A. Notario, “Single-Channel Imaging Receiver for Optical Wireless Communications,” Communications Letters, IEEE, vol. 9, pp. 897-899, 2005.
- [121] P. Djahani, and J. M. Kahn, “Analysis of infrared wireless links employing multibeam transmitters and imaging diversity receivers,” Communications, IEEE Transactions on, vol. 48, pp. 2077-2088, 2000.

- [122] J. M. Kahn, R. You, P. Djahani, A. G. Weisbin, T. Beh Kian, and A. Tang, "Imaging diversity receivers for high-speed infrared wireless communication," *Communications Magazine*, IEEE, vol. 36, pp. 88-94, 1998.
- [123] M.T. Alresheedi and J. M. H. Elmirghani, "10 Gb/s Indoor Optical Wireless Systems Employing Beam Delay, Angle and Power Adaptation Methods with Imaging Detection," *Lightwave Technology, Journal of*, vol. 30, no. 12, pp. 1843-1856, 2012.
- [124] M.T. Alresheedi and J. M. H. Elmirghani, "Adaptive 10 Gbit/s Mobile Optical Wireless Systems Employing Beam Delay, Angle and Power Adaptation with Imaging Receivers" *IEEE GLOBECOM* , December, 2011.
- [125] M.T. Alresheedi and J. M. H. Elmirghani, "Adaptive Multibeam Spot Diffusing Optical Wireless System with Imaging receivers" *IEEE International on Transparent Optical Networks (ICTON'11)*, July 2011.
- [126] M.T. Alresheedi and J. M. H. Elmirghani, "High-speed Indoor Optical Wireless Employing Fast angle and power adaptive computer generated holograms with Imaging Detection," to be submitted to *IEEE Journal of Optical Communications and Networking*.
- [127] K. L. Sterckx, J. M. H. Elmirghani, and R. A. Cryan, "Pyramidal fly-eye detection antenna for optical wireless systems," in *Optical Wireless Communications (Ref. No. 1999/128)*, IEE Colloquium on, 1999, pp. 5/1-5/6.
- [128] K. L. Sterckx, J. M. H. Elmirghani, and R. A. Cryan, "Sensitivity assessment of a three-segment pyramidal fly-eye detector in a semidisperse optical wireless communication link," *Optoelectronics, IEE Proceedings -*, vol. 147, pp. 286-294, 2000.
- [129] A. G. Al-Ghamdi, and J. M. H. Elmirghani, "Analysis of diffuse optical wireless channels employing spot-diffusing techniques, diversity receivers, and combining schemes," *Communications, IEEE Transactions on*, vol. 52, pp. 1622-1631, 2004.
- [130] A. G. Al-Ghamdi, and J. M. H. Elmirghani, "Line strip multibeam transmitter to combat the multipath dispersion and background noise of the indoor optical

- wireless links,” in Global Telecommunications Conference, 2004. GLOBECOM '04. IEEE, 2004, pp. 3630-3635 Vol.6.
- [131] A. G. Al-Ghamdi, and J. M. H. Elmirghani, “Optimization of a pyramidal fly-eye diversity receiver for optical wireless systems under the influence of multipath dispersion and background noise,” *Microwave and Optical Technology Letters*, vol. 36, pp. 401-406, 2003.
- [132] S. Jivkova, and M. Kavehrad, “Receiver designs and channel characterization for multi-spot high-bit-rate wireless infrared communications,” *Communications, IEEE Transactions on*, vol. 49, pp. 2145-2153, 2001.
- [133] S. Jivkova, and M. Kavehard, “Multispot diffusing configuration for wireless infrared access,” *Communications, IEEE Transactions on*, vol. 48, pp. 970-978, 2000.
- [134] S. Jivkova, and M. Kavehrad, “Multi-spot diffusing configuration for wireless infrared access: joint optimization of multi-beam transmitter and angle diversity receiver,” *Proc. of SPIE International Symposium on Voice, Video, and Data Communications, Photonics East'99*, Vol. 3850, pp. 72-77, Sep.1999.
- [135] A. G. Al-Ghamdi, and J. M. H. Elmirghani, “Spot diffusing technique and angle diversity performance for high speed indoor diffuse infra-red wireless transmission,” *Optoelectronics, IEE Proceedings -*, vol. 151, pp. 46-52, 2004.
- [136] A. G. Al-Ghamdi, and J. M. H. Elmirghani, “Performance analysis of line strip multispot diffusing system, fully diffuse, and hybrid optical wireless techniques in a real environment,” in Global Telecommunications Conference, 2004. GLOBECOM '04. IEEE, 2004, pp. 1213-1220, vol.2.
- [137] A. G. Al-Ghamdi, and J. M. H. Elmirghani, “Performance comparison of LSMS and conventional diffuse and hybrid optical wireless techniques in a real indoor environment,” *Optoelectronics, IEE Proceedings -*, vol. 152, pp. 230-238, 2005.
- [138] J. M. Alattar and Jaafar M. H. Elmirghani, “Evaluation of An Indoor OW Channel Employing A Mobile Multi-line Multi-Spot Diffusing Transmitter and A Seven Detectors Angle Diversity Receiver”, *Proceedings of the London Communications Symposium*, pp. 37- 40, Sept. 2006.

- [139] K. D. Dambul, D. O'Brien, and G. Faulkner, "Indoor Optical Wireless MIMO System with an Imaging Receiver," *Photonics Technology Letters, IEEE*, vol. 23, pp. 97-99, 2011.
- [140] A. G. Al-Ghamdi, and J.M.H. Elmirghani, "Line strip spot-diffusing transmitter configuration for optical wireless systems influenced by background noise and multipath dispersion," *Communications, IEEE Transactions on*, vol. 52, pp. 37-45, 2004.
- [141] J. R. Barry, J. M. Kahn, E. A. Lee, and D. G. Messerschmitt, "High-speed nondirective optical communication for wireless networks," *Network, IEEE*, vol. 5, pp. 44-54, 1991.
- [142] D. C. Lee, J. M. Kahn and M. D. Audeh, "Trellis-Coded Pulse-Position Modulation for Indoor Wireless Infrared Communications", *Communications, IEEE Transactions on*, vol. 45, no.9, pp. 1080-1087, 1997.
- [143] D .S. Shiu and J. M. Kahn, "Differential Pulse-Position Modulation for Power-Efficient Optical Communication", *Communications, IEEE Transactions on*, vol. 47, pp. 1201-1210, 1999.
- [144] Z. Ghassemlooy and A. R. Hayes, "Digital Pulse Interval Modulation for Optical communication," *Communications Magazine, IEEE*, vol. 36, pp. 95-99, 1998.
- [145] W. O. Popoola, Z. Ghassemlooy, J. I. H. Allen, E. Leitgeb, and S. Gao, "Free-space optical communication employing subcarrier modulation and spatial diversity in atmospheric turbulence channel," *Optoelectronics, IET*, vol. 2, pp. 16-23, 2008.
- [146] J. G. Proakis, *Digital Communications*, 3rd ed. New York: McGraw-Hill, 1995.
- [147] M. D. Audeh, and J. M. Kahn, "Performance evaluation of baseband OOK for wireless indoor infrared LAN's operating at 100 Mb/s," *Communications, IEEE Transactions on*, vol. 43, pp. 2085-2094, 1995.
- [148] U. N. Griner and S. Arnon, "Multiuser Diffuse Indoor Wireless Infrared Communication Using Equalized Synchronous CDMA," *Communications, IEEE Transactions on*, vol. 54, pp. 1654-1662, Sep. 2006.
- [149] S. Rajbhandari, Z. Ghassemlooy, and M. Angelova, "Effective denoising and adaptive equalization of indoor optical wireless channel with artificial light using the

- discrete wavelet transform and artificial neural network,” *Lightwave Technology, Journal of*, vol. 27, no. 20, pp. 4493–4500, Oct. 2009.
- [150] H. Chan, J. Elmirghani, and R. Cryan, “An equalization technique for indoor IR wireless LANs,” *Microwave Optical Technology Letters* vol. 10, no. 4, 1995.
- [151] G. Ntogari, T. Kamalakis, and T. Sphicopoulos, “Performance Analysis of Non Directed Equalized Indoor Optical Systems,” in *Communication Systems, Networks and Digital Signal Processing, 2008. CNSDSP 2008. 6th International Symposium on*, 2008.
- [152] H. Park, “Ph.D. Thesis, Coded Modulation and Equalization for wireless Infrared Communication,” *School of Electrical and Computer Engineering, Georgia Institute of Technology*, 1997, pp.135.
- [153] Z. Ghassemlooy, W. O. Popoola, S. Rajbhandari, M. Amiri, and S. Hashemi, “A synopsis of modulation techniques for wireless Infrared communication,” in *International conference on Transparent Optical Networks Rome, Italy IEEE*, pp. 1-6, 2007.
- [154] K. K. Wong, T. O’Farrell and M. Kiatweerasakul, “The performance of optical wireless OOK, 2-PPM and spread spectrum under the effects of multipath dispersion and artificial light interference,” *International Journal of Communication Systems*, vol. 13, no. 7 & 8, pp. 551-576, November-December 2000.
- [155] R. J. Green, H. Joshi, M. D. Higgins, and M. S. Leeson, “Recent Developments in Indoor Optical Wireless,” *Communications, IET*, vol. 2, no. 1, pp. 3–10, Jan. 2008.
- [156] D. C. Lee and J. M. Kahn, “Coding and equalisation for ppm on wireless infrared channels,” *Communications, IEEE Transactions on*, vol. 47, pp. 255-260, 1999.
- [157] M. D. Audeh, J. M. Kahn, and J. R. Barry, “Performance of pulse position modulation on measured non-directed indoor infrared channels,” *Communications, IEEE Transactions on*, vol. 44, pp. 654-659, 1996.
- [158] R. A. Cryn, R. T. Unwin, I. Garrett, M. J. N. Sibley, and N. M. Calvert, “Optical fibre digital pulse position modulation,” *Optoelectronics, IEE Proceeding*, vol. 137, no. 2, April. 1990, pp. 89-96.

- [159] H. Park, and J. R. Barry, "Performance of multiple pulse position modulation on multipath channels," *Optoelectronics, IEE Proceedings-*, vol. 143, no. 6, 1996, pp. 360-364.
- [160] J. M. H. Elmirghani, and R. A. Cryan, "New PPM-CDMA hybrid for indoor diffuse infrared channels," *Electronic Letters*, vol. 30, pp. 1646-1647, 1994.
- [161] J. M. H. Elmirghani, and R. A. Cryan, "Hybrid PPM-CDMA systems utilizing optical orthogonal codes for indoor wireless infrared communication," *Microwave and Optical Technology Letters*, vol. 8, pp. 44-47, 1995.
- [162] R. Perez-Jimenez, M. J. Betancor, and V. M. Melian, "Improved PPM schemes for IR-wireless LAN," *Electronics Letters*, vol. 32, pp. 885-887, 1996.
- [163] E. D. Kaluarachi, Z. Ghassemlooy, and B. Wilson, "Digital pulse interval modulation for optical free space communication links," in *Optical Free Space Communication Links, IEE Colloquium on*, 1996, pp. 3/1-3/5.
- [164] T. Ohtsuki, "Multiple-Subcarrier Modulation in Optical Wireless Communications," *Communications Magazine, IEEE*, vol. 41, pp. 74-79, 2003.
- [165] Association, I. D., [www.irda.org](http://www.irda.org).
- [166] W. Hirt, J. Petrilla, and Y. Yuuki, "Proposed changes to IrDA serial infrared physical layer link specification for 16 Mbps addition (VFIR) final proposal," adopted with status final by the IrDA Board of Directors, San Francisco, CA 1999.
- [167] W. Hirt, M. Hassner, and N. Heise, "IrDA-VFIR (16 Mb/s): modulation code and system design," *Personal Communications, IEEE*, vol. 8, pp. 58-71, 2001.
- [168] Association, I. D., "[www.irda.org/associations/2494/files/Giga-IR\\_General.pdf](http://www.irda.org/associations/2494/files/Giga-IR_General.pdf)," ed, 2009.
- [169] Photonics Corporation San Jose and CA. [www.Photonics.com](http://www.Photonics.com).
- [170] IBM Corporation, Armonk and NY. [www.ibm.com](http://www.ibm.com).
- [171] Spectrix Corporation, Evanston and IL. [www.spectrixcorp.com](http://www.spectrixcorp.com).
- [172] A. G. Al-Ghamdi, and J. M. H., Elmirghani, "Performance analysis of mobile optical wireless systems employing a novel beam clustering method and diversity detection," *Optoelectronics, IEE Proceedings -*, vol. 151, pp. 223-231, 2004.

- [173] A. G. Al-Ghamdi, and J. M. H. Elmirghani, "Analysis of optical wireless links employing a beam clustering method and diversity receivers," in Communications, 2004 IEEE International Conference on, 2004, pp. 3341-3347 Vol.6.
- [174] A. G. Al-Ghamdi, and J. M. H. Elmirghani, "Characterization of mobile spot diffusing optical wireless systems with diversity receiver," in Communications, 2004 IEEE International Conference on, 2004, pp. 133-138, vol.1.
- [175] J. R. Barry, "Wireless communication using non-directed infrared radiation," PhD thesis, Dept. of Electrical Engineering and Computer Science, University of California, Berkeley, 1992.
- [176] A. M. R. Tavares, R. J. M. T. Valadas, and A. M. de Oliveira Duarte, "Performance of an optical sectored receiver for indoor wireless communication systems in presence of artificial and natural noise sources," in Proc. SPIE Conf. on Wireless Data Transmission, vol. 2601, Philadelphia, PA, Oct. 23–25, 1995, pp. 264–273.
- [177] E. Desurvire, *Erbium-doped fiber amplifiers: principles and applications*. New York: John Wiley and Sons, 1994.
- [178] G. P. Agrawal, "Fibre-optic communication systems" Wiley, 4<sup>th</sup> edition, 2004.
- [179] V. Pohl, V. Jungnickel, and C. Helmolt, "Integrating-sphere diffuser for wireless infrared communication," Optoelectronics, IEE Proceedings -, vol. 147, pp. 281-285, 2000.
- [180] A. G. Al-Ghamdi, "Performance of Optical wireless Links Employing Diversity Detection and Spot Diffusing Techniques," PhD. Thesis, University of Swansea, 2004.
- [181] A. G. Al-Ghamdi, and J.M.H. Elmirghani, "Optical wireless multibeam transmitter with line strip, diamond and uniform geometries," Optical Engineering Journal, vol. 42, no. 11, Nov. 2003.
- [182] H. Yang, and C. Lu, "Infrared wireless LAN using multiple optical sources," Optoelectronics, IEE Proceedings -, vol. 147, no. 4, Aug. 2000, pp. 301-307.

- [183] P. Viswanath, D. N. C. Tse, and R. Laroia, "Opportunistic beamforming using dumb antennas," *Information Theory, IEEE Transactions on*, vol. 48, pp. 1277-1294, 2002.
- [184] S. Buzzi, E. Conte, A. De Maio, and M. Lops, "Minimum error-probability diversity detection over fading dispersive channels with non-Gaussian noise," *Proceedings IEEE International Conf. On Acoustics, Speech, and Signal Processing*, vol.1, 2000, pp. 281-284.
- [185] J. M. H. Elmirghani and H. T. Mouftah, "Technologies and architectures for scalable dynamic dense WDM networks," *Communication Magazine, IEEE*, vol. 38, No. 2, pp. 58-66, Feb. 2000.
- [186] E. Kimber, B. Patel, I. Hardcastle, and A. Hadjifotiou, "High performance 10 Gbit/s pin-FET optical receiver," *Electronics Letter*, vol. 28, No. 2, pp. 120-122, Jan. 1992.
- [187] B. Leskovar, "Optical receivers for wide band data transmission systems," *Nuclear Science, IEEE Transactions on*, vol. 36, pp. 787-793, 1989.
- [188] F. E. Alsaadi, and J. M. H. Elmirghani, "High-Speed Spot Diffusing Mobile Optical Wireless System Employing Beam Angle and power Adaptation and Imaging Receivers," *Lightwave Technology, Journal of*, vol. 28, pp. 2191-2206, 2010.
- [189] S. Jivkova, and M. Kavehrad, "Transceiver design concept for cellular and multispot diffusing regimes of transmission," *Wireless Communications Networking, EURASIP Journal on*, vol. 2005, pp. 30-38, 2005.
- [190] H. Xu, B. Davey, D. Timothy, D. Wilkinson, and W.A. Crossland, "A simple method for optically enhancing the small electro-optical effects of fast switching electroclinic liquid crystals," *Applied physics letter*, vol.74, pp. 3099-3101, 1999.
- [191] T. D. Wilkinson, W. A. Crossland, S. T. Warr, T. C. B. Yu, A. B. Davey, and R. J. Mears, "New applications for ferroelectric liquid crystals," *Liquid Crystals Today*, vol. 4, no. 3, pp. 1-6, 1994.
- [192] <http://www.microchip.com/ParamChartSearch/chart.aspx?branchID=211&mid=10&lang=en&pageId=74>

- [193] M. A. Seldowitz, J. P. Allebach, and D. E. Sweeney, "Synthesis of digital holograms by direct binary search," *Appl. Opt.*, vol. 26, pp. 2788–2798, 1987.
- [194] F. A. Ramirez, "Holography - Different Fields of Application," InTech, 2011.
- [195] P. Carnevali, L. Coletti, and S. Patarnello, "Image processing by simulated annealing," *IBM Journal of Research and Development*, vol. 29, pp. 569-579, 1985.
- [196] A. Georgiou, T. D. Wilkinson, N. Collings, and W. A. Crossland, "Algorithm for computing spot-generating holograms," *Journal of Optics: A pure and applied optics*, vol. 10, no. 1, 2008.
- [197] H. Xu, B. Davey, D. Timothy, D. Wilkinson, and W.A. Crossland, "Optically enhancing the small electro-optical effect of a fast-switching liquid-crystal mixture," *Optical Engineering*, vol.8, pp. 1568-1572, 2000.